

UNCLASSIFIED

AD NUMBER

AD835245

LIMITATION CHANGES

TO:

Approved for public release; distribution is unlimited.

FROM:

Distribution authorized to U.S. Gov't. agencies and their contractors; Critical Technology; MAR 1968. Other requests shall be referred to Air Force Cambridge Research Laboratory, CRDM, Hanscom AFB, MA 01730. This document contains export-controlled technical data.

AUTHORITY

afcr1 ltr, 22 dec 1971

THIS PAGE IS UNCLASSIFIED

**STUDY TO OBTAIN DESIGN DATA  
FOR REENTRY ECM ANTENNA SYSTEMS (U)**

AD835245

**Paul E. Bisbing, Daniel L. McMenamin,  
Arthur K. Jordan, and Paul M. Scherer**

**REENTRY SYSTEMS DEPARTMENT  
MISSILE AND SPACE DIVISION  
GENERAL ELECTRIC COMPANY  
P.O. BOX 8555, PHILA., PA. 19101**

**Contract No. F 19628-67-C-0210  
Project No. 8671**

**FINAL REPORT**

**covering the period 15 March 1967 through 15 March 1968**

**MARCH 1968**

**THIS DOCUMENT IS SUBJECT TO SPECIAL EXPORT CONTROLS AND EACH TRANSMITTAL  
TO FOREIGN GOVERNMENTS OR FOREIGN NATIONALS MAY BE MADE ONLY WITH PRIOR  
APPROVAL OF AFCRL (CRDM), L.G. HANSCOM FIELD, BEDFORD, MASSACHUSETTS, 01730.**

**CONTRACT MONITOR: WALTER ROTMAN  
MICROWAVE PHYSICS LABORATORY**

**GE Report No. 68SD591**

**Sponsored By**

**ADVANCED RESEARCH PROJECTS AGENCY  
DEPARTMENT OF DEFENSE  
PROJECT DEFENDER  
ARPA ORDER NO. 693, AMENDMENT NO.1**

**Prepared For**

**AIR FORCE CAMBRIDGE RESEARCH LABORATORIES  
OFFICE OF AEROSPACE RESEARCH  
UNITED STATES AIR FORCE  
BEDFORD, MASSACHUSETTS 01730**



**BEST  
AVAILABLE COPY**

**GENERAL  ELECTRIC  
COMPANY**

VALLEY FORGE SPACE TECHNOLOGY CENTER (MAIL: P. O. BOX 8555 PHILA., PA. 19101) . . TEL. 962-2000

MISSILE AND  
SPACE DIVISION  
RE-ENTRY SYSTEMS  
DEPARTMENT

**To: Distribution List (Attached)**

**Subject: Contract No. F19628-67-C-0210  
Final Report**

**Gentlemen:**

**In accordance with contract F19628-67-C-0210, we are  
forwarding the subject report.**

**Very truly yours,**

*R M Baylson*

**R. M. Baylson, Contract Specialist  
Advanced Development Contracts**

AFCRL-68-0226

**STUDY TO OBTAIN DESIGN DATA  
FOR REENTRY ECM ANTENNA SYSTEMS (U)**

**Paul E. Bisbing, Daniel L. McMenamin,  
Arthur K. Jordan, and Paul M. Scherer**

**REENTRY SYSTEMS DEPARTMENT  
MISSILE AND SPACE DIVISION  
GENERAL ELECTRIC COMPANY  
P.O. BOX 8555, PHILA., PA. 19101**

**Contract No. F 19628-67-C-0210  
Project No. 8671**

**FINAL REPORT**

**covering the period 15 March 1967 through 15 March 1968**

**MARCH 1968**

**THIS DOCUMENT IS SUBJECT TO SPECIAL EXPORT CONTROLS AND EACH TRANSMITTAL  
TO FOREIGN GOVERNMENTS OR FOREIGN NATIONALS MAY BE MADE ONLY WITH PRIOR  
APPROVAL OF AFCRL (CRDM), L.G. HANSCOM FIELD, BEDFORD, MASSACHUSETTS, 01730.**

**CONTRACT MONITOR: WALTER ROTMAN  
MICROWAVE PHYSICS LABORATORY**

**GE Report No. 68SD591**

**Sponsored By**

**ADVANCED RESEARCH PROJECTS AGENCY  
DEPARTMENT OF DEFENSE  
PROJECT DEFENDER  
ARPA ORDER NO. 693, AMENDMENT NO.1**

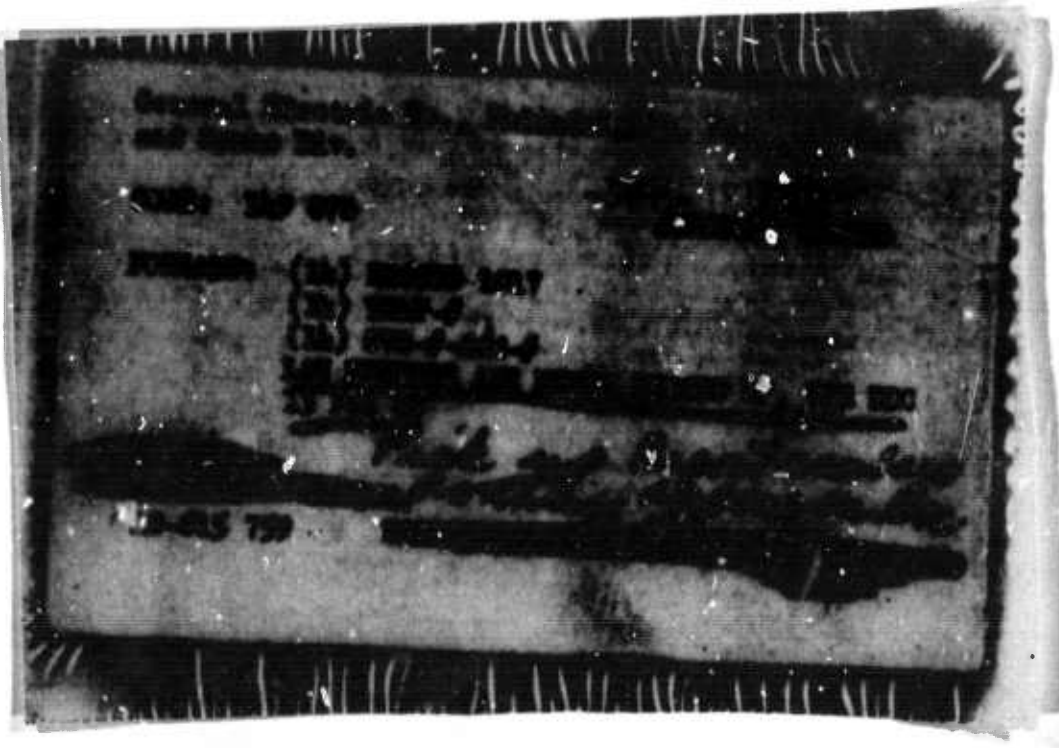
**Prepared For**

**AIR FORCE CAMBRIDGE RESEARCH LABORATORIES  
OFFICE OF AEROSPACE RESEARCH  
UNITED STATES AIR FORCE  
BEDFORD, MASSACHUSETTS 01730**

QUALIFIED REQUESTERS MAY OBTAIN ADDITIONAL COPIES FROM  
THE DEFENSE DOCUMENTATION CENTER.

# ACKNOWLEDGMENT

This research was supported by the Advanced Research Projects Agency, Project DEFENDER, and was monitored by the Air Force Cambridge Research Laboratories, under Contract No. F19628-67-C-0210.



## ABSTRACT

This is the first volume of the final report in a study of reentry effects on signal transmission from slender cone bodies at ICBM velocities. The report gives results of state of knowledge surveys of fluid mechanics methods and electromagnetic phenomena. Results of illustrative calculations are also given in many of these areas. Antenna breakdown is found to be the most important problem in reentry transmission effects, as well as the least well understood. Recommendations for needed research are given, including high gas temperature and convection experiments and theoretical analyses of temperature, convection, and flow field gradients effects. High altitude flow field development and studies of thermal nonequilibrium effects are recommended also.

**BLANK PAGE**

## TABLE OF CONTENTS

Section	Page
1 INTRODUCTION . . . . .	1-1
1.1 Objective of Study . . . . .	1-1
1.2 Background . . . . .	1-1
1.3 Format of Report . . . . .	1-3
2 SUMMARY . . . . .	2-1
3 FLOW FIELD ANALYSIS . . . . .	3-1
3.1 Survey of Flow Field Technology . . . . .	3-1
3.1.1 Introduction. . . . .	3-1
3.1.2 Review . . . . .	3-8
3.1.3 Flow Field Bibliography . . . . .	3-20
3.2 Flow Field Calculations . . . . .	3-45
3.2.1 Inviscid Flow Field Solutions . . . . .	3-45
3.2.2 Vibrational Nonequilibrium Calculations . . . . .	3-85
3.2.3 Stagnation Point Matched Inviscid-Boundary Layer Calculations. . . . .	3-92
3.2.4 Inviscid Layer-Boundary Layer Calculations. . . . .	3-103
4 ANTENNAS. . . . .	4-1
4.1 Survey of Field Distributions . . . . .	4-1
4.2 Illustrative Calculations . . . . .	4-3
5 LINEAR PLASMA EFFECTS . . . . .	5-1
5.1 Survey of Theory . . . . .	5-1
5.2 Illustrative Calculations . . . . .	5-6
6 ANTENNA BREAKDOWN . . . . .	6-1
6.1 Survey of Classical Breakdown Theory . . . . .	6-2
6.2 Survey of Reentry Effects . . . . .	6-10
6.2.1 Gas Density. . . . .	6-11
6.2.2 Ionization . . . . .	6-13
6.2.3 High Gas Temperature . . . . .	6-17
6.2.4 Convection . . . . .	6-22
6.2.5 Gradients of Gas Properties . . . . .	6-33
6.2.6 Effects of Gas Chemical Composition . . . . .	6-34
6.3 Illustrative Calculations . . . . .	6-34

## TABLE OF CONTENTS (Cont'd)

Section	Page
7    NONLINEAR INTERACTIONS. . . . .	7-1
7.1 Survey . . . . .	7-1
7.2 Broadband Signal Effects . . . . .	7-3
8    ALLEVIATION TECHNIQUES . . . . .	8-1
8.1 Plasma Alleviation. . . . .	8-1
8.2 Electromagnetic Techniques. . . . .	8-4
9    RECOMMENDATIONS . . . . .	9-1
9.1 Evaluation. . . . .	9-1
9.2 Research Recommendations. . . . .	9-3
9.2.1 High Gas Temperature . . . . .	9-3
9.2.2 Convection . . . . .	9-4
9.2.3 Gradients and Breakdown Criteria . . . . .	9-4
9.2.4 Flight Experiments . . . . .	9-5
10   CONCLUSION . . . . .	10-1
11   REFERENCES. . . . .	11-1

# LIST OF ILLUSTRATIONS

Figure		Page
3-1	Streamwise Variation of Normalized Pressure vs Normalized Coordinate Along Body Surface . . . . .	3-54
3-2	Streamwise Variation of Normalized Temperature vs Normalized Coordinate Along Body Surface . . . . .	3-55
3-3	Streamwise Variation of Normalized Density vs Normalized Coordinate Along Body Surface . . . . .	3-56
3-4	Streamwise Variation of Normalized Velocity Parallel to Surface vs Normalized Coordinate Along Body Surface. . . . .	3-57
3-5	Streamwise Variation of Molecular Oxygen Number Density vs Normalized Coordinate Along Body Surface. . . . .	3-58
3-6	Streamwise Variation of Molecular Nitrogen Number Density vs Normalized Coordinate Along Body Surface. . . . .	3-59
3-7	Streamwise Variation of Atomic Nitrogen Number Density vs Normalized Coordinate Along Body Surface. . . . .	3-60
3-8	Streamwise Variation of Atomic Oxygen Number Density vs Normalized Coordinate Along Body Surface. . . . .	3-61
3-9	Streamwise Variation of Nitric Oxide Number Density vs Normalized Coordinate Along Body Surface. . . . .	3-62
3-10	Streamwise Variation of Electron Number Density vs Normalized Coordinate Along Body Surface . . . . .	3-63
3-11	Normalized Pressure vs Shock Layer Thickness; $s_b/R_N = 4.962\sqrt{-1}$ ; Nonequilibrium . . . . .	3-64
3-12	Normalized Pressure vs Shock Layer Thickness; $s_b/R_N = 6.125\sqrt{-1}$ ; Nonequilibrium . . . . .	3-65
3-13	Normalized Pressure vs Shock Layer Thickness; $s_b/R_N = 2.433\sqrt{-2}$ ; Nonequilibrium . . . . .	3-66
3-14	Normalized Temperature vs Shock Layer Thickness; $s_b/R_N = 4.962\sqrt{-1}$ ; Nonequilibrium . . . . .	3-67
3-15	Normalized Temperature vs Shock Layer Thickness; $s_b/R_N = 6.125\sqrt{-1}$ ; Nonequilibrium . . . . .	3-68
3-16	Normalized Temperature vs Shock Layer Thickness; $s_b/R_N = 2.433\sqrt{-2}$ ; Nonequilibrium . . . . .	3-69
3-17	Normalized Density vs Shock Layer Thickness; $s_b/R_N = 4.962\sqrt{-1}$ . . . . .	3-70
3-18	Normalized Density vs Shock Layer Thickness; $s_b/R_N = 6.125\sqrt{-1}$ . . . . .	3-71
3-19	Normalized Density vs Shock Layer Thickness; $s_b/R_N = 2.433\sqrt{-2}$ . . . . .	3-72
3-20	Normalized Velocity Parallel to Surface vs Shock Layer Thickness; $s_b/R_N = 4.962\sqrt{-1}$ . . . . .	3-73
3-21	Normalized Velocity Parallel to Surface vs Shock Layer Thickness; $s_b/R_N = 6.125\sqrt{-1}$ . . . . .	3-74

# LIST OF ILLUSTRATIONS (Cont'd)

Figure		Page
3-22	Normalized Velocity Parallel to Surface vs Shock Layer Thickness; $s_b/R_N = 2.433\sqrt{2}$ . . . . .	3-75
3-23	Electron Number Density vs Shock Layer Thickness; $s_b/R_N = 4.962\sqrt{-1}$ . . . . .	3-76
3-24	Electron Number Density vs Shock Layer Thickness; $s_b/R_N = 6.125\sqrt{1}$ . . . . .	3-77
3-25	Electron Number Density vs Shock Layer Thickness; $s_b/R_N = 2.433\sqrt{2}$ . . . . .	3-78
3-26	$\int_0^{y_{SN}} N_e dy$ vs Normalized Coordinate Along Body Surface; Nonequilibrium . . . . .	3-79
3-27	Vibrational Nonequilibrium; Streamwise Variation of Temperature vs Normalized Coordinate Along Body Surface . . . . .	3-89
3-28	Vibrational Nonequilibrium; Streamwise Variation of Temperature vs Normalized Coordinate Along Body Surface . . . . .	3-90
3-29	Vibrational Nonequilibrium; Streamwise Variation of Temperature vs Normalized Coordinate Along Body Surface . . . . .	3-91
3-30	Matched Inviscid - Boundary Layer Solutions; Gas Temperature vs Normalized Distance From Shock Wave. . . . .	3-96
3-31	Matched Inviscid - Boundary Layer Solutions; Gas Temperature vs Normalized Distance From Shock Wave. . . . .	3-97
3-32	Matched Inviscid - Boundary Layer Solutions; Gas Density vs Normalized Distance from Shock Wave . . . . .	3-98
3-33	Matched Inviscid - Boundary Layer Solutions; Gas Density vs Normalized Distance From Shock Wave. . . . .	3-99
3-34	Matched Inviscid - Boundary Layer Solutions; Electron Density vs Normalized Distance From Shock Wave. . . . .	3-100
3-35	Matched Inviscid - Boundary Layer Solutions; Electron Density vs Normalized Distance From Shock Wave. . . . .	3-101
3-36	Matched Inviscid - Boundary Layer Solutions; Gas Pressure vs Normalized Distance From Shock Wave. . . . .	3-102
3-37	Normalized Temperature vs Shock Layer Thickness . . . . .	3-105
3-38	Normalized Velocity Parallel to Surface vs Shock Layer Thickness . . . . .	3-106
3-39	Normalized Density vs Shock Layer Thickness . . . . .	3-107
3-40	Electron Density vs Shock Layer Thickness . . . . .	3-108
3-41	Normalized Temperature vs Shock Layer Thickness . . . . .	3-109
3-42	Normalized Velocity Parallel to Surface vs Shock Layer Thickness . . . . .	3-110
3-43	Normalized Density vs Shock Layer Thickness . . . . .	3-111
3-44	Electron Density vs Shock Layer Thickness $s_b/R_N = 243.3$ . . . . .	3-112
3-45	Normalized Temperature vs Shock Layer Thickness . . . . .	3-113
3-46	Normalized Velocity Parallel To Surface vs Shock Layer Thickness . . . . .	3-114
3-47	Normalized Density vs Shock Layer Thickness . . . . .	3-115
3-48	Electron Density vs Shock Layer Thickness $s_b/R_N = 61.25$ . . . . .	3-116

# LIST OF ILLUSTRATIONS (Cont'd)

Figure		Page
4-1	Amplitude of Near Fields of a Conical Spiral Antenna Measured at 0.03 $\lambda$ from Surface . . . . .	4-6
5-1	Thin Plasma Attenuation . . . . .	5-8
5-2	Thin Plasma Attenuation at Large Values of Collision Frequency . . . . .	5-9
5-3	Typical Variation of Collision Frequency for a Slender Vehicle . . . . .	5-10
6-1	Breakdown Field as a Function of Pressure in Terms of Proper Variables. . . . .	6-8
6-2	High Gas Temperature Effects on Ionization Frequency . . . . .	6-19
6-3	Curve Fit to Ionization Frequency . . . . .	6-21
6-4	Electron Density at the Downstream Edge of a Uniform Field Region, Assuming Free Diffusion. . . . .	6-29
6-5	Ambipolar Diffusion Effect . . . . .	6-30
6-6	Space Charge Enhanced Convection Effect on Electron Density. . . . .	6-31
6-7	Comparison of Breakdown Field by the Theory of MacDonald and Scharfman . . . . .	6-35
6-8	Normalized Breakdown Power Versus $p\lambda$ Without Reentry Effects . . . . .	6-37
6-9	Normalized Breakdown Power Versus $p\lambda$ with Convection . . . . .	6-38
6-10	Normalized Breakdown Power Versus $p\lambda$ with Convection and Ionization . . . . .	6-39

## SECTION 1

### INTRODUCTION

This is the final report of a study of reentry effects on ECM antenna systems, in which data have been collected with the aim of aiding the antenna designer predict and, if possible, avoid such reentry effects. Much of these data are qualitative and some of it based on poorly understood phenomena in the present state of knowledge of the limiting technologies. Thus there is the need for critical evaluation and the formulation of recommendations for further study, as have been done.

#### 1.1 OBJECTIVE OF STUDY

The objective of this study is the preparation of a document to serve as a compendium of design data and principles for antennas compatible with slender body vehicles which reenter at ICBM velocity. This study gives consideration to flow field analysis, antennas, linear plasma effects, antenna breakdown, nonlinear attenuation, alleviation techniques, and the preliminary design of recommended flight experiments. In most of these areas the emphasis is placed on a survey of present knowledge and methods of prediction and control. Limited illustrative calculations have been carried out in many cases. The problem of reentry effects on antenna breakdown is stressed.

#### 1.2 BACKGROUND

The above objective is stated in terms of a technology problem, the solution of which has application to the design of antennas for reentry vehicles. The basic problem is the prediction and control of the effects of the reentry induced environment on the antenna performance. Attention is limited to the reentry flow field of a slender cone vehicle reentering the atmosphere with ICBM velocity. The aspects of the flow field which are important to the antenna performance are the profiles of gas species concentrations, including excited states, temperatures, velocities, and electron density in the body flow field (wake flow, except possibly base flow and near wake in rare cases, is unimportant). An important part of the problem of flow field characterization is the variation with altitude during reentry of each of the above quantities.

The presence of appreciable levels of ionization in the reentry flow field can lead to various linear plasma effects. Linear effects, which are defined as being independent of the antenna input power, can be expected at low input signal levels. They include but are not limited to attenuation, antenna input impedance changes, and antenna pattern distortion. These effects depend on the electron density, gas density, and temperature profiles over the body.

When the input signal level to the antenna cannot be assumed to be arbitrarily small, then it is possible for nonlinear plasma effects and breakdown to be important. Nonlinear plasma effects can take many more forms than linear effects, in that the signals which are input to the antenna can change the electromagnetic characteristics of the flow field in many different ways which depend on the nature of the signals as well as on the flow field properties. However the same basic flow field properties are important in nonlinear as in linear effects, provided breakdown has not yet been reached.

Antenna breakdown is reached when the input signal level becomes so strong that the antenna field ionizes the air around the antenna to the extent that signals can not propagate through to the receiver. This phenomenon takes place in a static cold air environment at a given altitude even without the effects of the reentry environment; however, the presence of hypersonic flow field conditions can change significantly the input signal level at which it takes place. Since cold air static breakdown can easily be measured in a laboratory vacuum chamber for a given antenna, the important thing to be determined about the effects of the reentry environment is just what change in the breakdown signal level versus altitude they will cause. Here the antenna field is a cause of electron sources and sinks as a function of the gas species concentrations, excitation levels, and velocity; thus these parameters as well as flow field ionization must be established to determine the reentry effects. In addition, the altitude region in which breakdown is important is so high (especially at the lower end of the frequency spectrum of reentry signal transmission systems) as to require study of the limits of the continuum regime of fluid mechanics.

### 1.3 FORMAT OF REPORT

After a short summary of the findings of this study, this report gives each technical problem area in the form of a survey, followed by a few illustrative calculations. The flow field section treats a limited number of calculations of importance in antenna breakdown for a typical vehicle configuration and velocity-altitude trajectory. The main emphasis on antennas is the estimation of diffusion length for use in breakdown calculations. In the section on linear plasma effects, the electron density levels which would be detrimental to the proper functioning of antennas on conical vehicles are indicated so that the vehicle designer can determine to what extent he should attempt to reduce the flow field plasma level. A complete survey of the theory of classical breakdown and of reentry effects is given, followed by illustrative calculations of normalized antenna breakdown power in a typical reentry environment. This section also presents a convenient closed form expression for breakdown power of an antenna. The section on nonlinear effects is concerned mainly with a survey intended to assess the relative importance of these effects without going into details of the theory, since this is a tremendously large and complicated subject. Alleviation techniques are surveyed with the purpose of indicating which might be useful. Recommendations are given on the importance of various aspects of the problem and on further research which is needed to provide definitive design data and systems limitations. Classified aspects are given in the second volume, including analyses of previous flight experiments and recommendations for future ones.

## SECTION 2

### SUMMARY

The electron density levels at which linear and nonlinear plasma effects on signal transmission from a slender cone reentry body become important are evaluated. Flow field technology and illustrative calculations show that these plasma effects can be avoided on a properly designed vehicle. A survey of reentry antenna breakdown brings out many important factors. The state of knowledge of antenna breakdown effects is such as to leave several important technology problems still to be solved. There is a need for more experimental and theoretical research in these areas. However, a closed form expression for reentry antenna breakdown power is given. This expression is sufficiently general to fit the available applicable experimental data, and it is probably accurate enough to give crude but conservative estimates of reentry effects.

**BLANK PAGE**

## SECTION 3

### FLOW FIELD ANALYSIS

#### 3.1 SURVEY OF FLOW FIELD TECHNOLOGY

A literature survey of theoretical techniques which are capable of describing the flow field environment about a body during atmospheric reentry is presented in the form of a categorized review and reference list. The survey was limited to within the United States, and the sources of information include the prominent journals and texts. In addition, thirty-seven organizations and individuals known to be involved in this type of work were solicited for inputs. However, because only seventeen of these requests were acknowledged, the survey, although extensive, cannot be considered complete. It is restricted in scope to axisymmetric or three-dimensional bodies within the continuum regime of reentry and to flows which are steady, compressible, and attached (as distinguished from separated boundary layer, shear layer, near or far wake flows). The material is divided into three main categories: the inviscid shock layer, the boundary layer, and the fully viscous and merged layers. These main categories are sub-divided under the headings of thermodynamic equilibrium/ideal gas and nonequilibrium gas, and the inviscid shock layer is farther divided into flows which are locally subsonic or supersonic. For the consideration of the reader who is not completely familiar with the reentry flow field problem, an introduction is presented which includes a discussion of the problem and definitions for many of the specialized terms.

##### 3.1.1 INTRODUCTION

In the reentry body flow field problem the word "reentry" is quite generally (and herein) taken to imply that the velocity of a body as it begins its descent into a planet's atmosphere is less than the velocity required to escape the planet's gravitational attraction. The escape velocity from earth is approximately 37,000 feet/second, and typical reentry velocities will range from 15,000 to 25,000 feet/second. This aspect is important in that, for reentry velocities, the energy losses within the flow field due to radiation are of a secondary nature and, as pointed out by Grusyczynski and Warren<sup>1</sup>, can be neglected; however, for entry velocities, radiation effects must be taken into account.

Another aspect of the problem which should be clarified is that the words "body flow field" denote the flow field about the forebody of the reentry body as distinguished from the flow field in the base region or the near or far wake regions.

The flow field environment which develops about a vehicle during atmospheric reentry has been divided into seven regimes by Probst<sup>2</sup> in an analysis based on the stagnation region of an approximately spherical body. With  $\lambda_{\infty}$  denoting the ambient mean free path,  $R_b$  the body radius, and  $\epsilon$  the ratio of the free stream density to the average density in the stagnation region, the four regimes within the continuum are defined by Probst as follows:

#### Fully Merged Layer Regime

$$R_b/10 < \lambda_{\infty} \leq R_b$$

#### Incipient Merged Layer Regime

$$\epsilon^{1/2} R_b/10 < \lambda_{\infty} \leq R_b/10$$

#### Viscous Layer Regime

$$\epsilon R_b/10 < \lambda_{\infty} \leq \epsilon^{1/2} R_b/10$$

#### Boundary Layer - Inviscid Layer Regime

$$\lambda_{\infty} \leq \epsilon R_b/10$$

For typical earth reentry, the average density ratio  $\epsilon$  will be about 1/10. For a nose radius of 1/2 inch and taking  $\lambda_\infty$  from the 1962 U.S. Standard Atmosphere Tables, the above four regimes in terms of altitude (kilofeet) are:

235 < Fully Merged Layer  $\leq$  285

210 < Incipient Merged Layer  $\leq$  235

175 < Viscous Layer  $\leq$  210

Boundary Layer - Inviscid Layer  $\leq$  175

Under the same conditions except for a nose radius of one foot, the above regimes will shift upwards by about 70 kilofeet.

In both of the merged layer regimes, the shock wave\* which envelops the reentry body is not a discontinuity but as Probstein points out is relatively thick, ranging from a value of about  $R_b/3$  at the upper limit of the fully merged layer regime to about  $R_b/90$  at the lower limit of the incipient merged layer regime. Throughout both of these regimes transport effects (thermal conductivity, viscosity and diffusion) are of primary importance, and must be included in the analysis of both the shock wave and the intervening shock layer between the back face of the shock wave and the body surface. For both of the merged layer regimes, Probstein recommends the solution of the Navier-Stokes equations (along with the continuity, energy, and state equations) including transport effects, with the boundary conditions determined by the body and free stream. However, Cheng<sup>199</sup> has pointed out that when the shock wave thickness can be neglected compared to the body radius (which on a 1/10 basis includes all of the incipient merged layer regime and about 70 percent of the fully merged layer regime), the shock wave thickness effects are secondary compared to the substantial changes\*\* in the

\* The shock wave is sometimes referred to as the shock transition zone, particularly when it is not of infinitesimal thickness.

\*\* For flow across an oblique shock wave of infinitesimal thickness bounding a flow field region in which transport effects (viscosity, conductivity and diffusion) can be neglected, i.e., for inviscid flow, the velocity component tangent to the shock wave and the stagnation enthalpy (total energy) remain unchanged across the shock wave. The value of this velocity component will depend on the shock wave angle, whereas the value of the stagnation enthalpy does not. The equations governing this type of flow can be found in Shapiro<sup>3</sup> and are generally referred to as the Rankine-Hugoniot relations.

tangential velocity component and the stagnation enthalpy across the shock wave caused by the transport processes. Cheng, therefore, maintains that the shock wave can be treated as a discontinuity whenever its thickness is negligible compared to the body radius and the flow across it adequately described by the Rankine-Hugoniot relations after they have been modified to account for transport effects. Thus, over a substantial part of the merged layer regimes, the modified Rankine-Hugoniot relations can be used to provide outer boundary conditions for the shock layer solution.

In the viscous layer regime, transport processes are of primary importance within the entire shock layer, but the shock wave is thin enough to be considered a discontinuity and the Rankine-Hugoniot relations provide the properties behind it to be used as boundary conditions for the shock layer solution.

In the boundary layer - inviscid layer regime, the shock wave thickness is on the order of several ambient mean free paths and is, therefore, a real physical discontinuity. Transport effects are important in the region of the shock layer adjacent to the body surface (the boundary layer), whereas they are negligible in the shock layer region adjacent to the shock wave (the inviscid layer\*). In this case the reentry body flow field problem can be solved separately in each of these regions by matching the flow properties at the interface, i.e., the boundary layer edge. This matching process is done as follows. An inviscid layer solution is obtained as if there existed no boundary layer on the body, i.e., the body surface is treated as the zero streamline. The distribution of flow properties along the inviscid zero streamline are then used to provide boundary layer edge conditions and a boundary layer solution is obtained which determine the actual mass flow within the boundary layer. By matching this mass flow to that contained within the appropriate streamline in the inviscid solution, a new distribution of properties for the boundary layer edge conditions is determined. If this distribution of properties differs significantly from the first distribution, the boundary layer must be recalculated using the new edge conditions until satisfactory agreement in the edge

---

\* Because the free stream is isoenergetic (constant stagnation enthalpy) and the flow across the shock wave is adiabatic, the inviscid layer is also isoenergetic.

conditions from one iteration to the next are obtained. (When this iteration process is required to match edge conditions, it is referred to as the vorticity interaction problem.) After the edge conditions are matched satisfactorily, the boundary layer solution is used to calculate the boundary layer displacement thickness, which is the distance the inviscid layer is displaced away from the body surface by the boundary layer. If the displacement thickness can be neglected compared to the shock layer thickness, then the matched inviscid layer - boundary layer solution has been obtained. However, if it cannot be neglected (which is referred to as the displacement thickness problem), then the displacement thickness must be added to the body surface and the inviscid shock layer recalculated treating the displaced "body" surface as the zero streamline. Starting with the boundary layer in which the edge conditions were matched for the original body, the matching process described above must be repeated for the displaced "body."

Due to the nature of the boundary layer problem, the coordinate system selected for the solution is always located on the body surface. In the axisymmetric case (as a simple example), the boundary layer equations in the surface coordinate system will involve both the transverse radius of curvature (the radial, or normal, distance from a local point in the boundary layer to the axis of symmetry) and the longitudinal body radius of curvature (the body surface radius of curvature in a meridional plane). If the boundary layer thickness is small compared to the transverse radius of curvature, the transverse radius of curvature can be approximated by the body radius, i.e., the radial distance from the body surface to the axis of symmetry.

If in addition the transverse curvature effect is neglected, the governing equations\* constitute what is known as first - order boundary layer theory. If either transverse or longitudinal curvature effects are taken into account, it is referred to as second - order boundary layer theory.

---

\* Within the boundary layer, neglecting the longitudinal curvature effect is equivalent to neglecting the transverse pressure gradient as shown, for example, in Cheng<sup>199</sup>.

To make the boundary layer problem more tractable, the longitudinal and traverse coordinates are usually recast to simplify the form of the governing equations. For compressible flows the Howarth - Dorodnitsyn transformation is often applied, which reduces the equations to the incompressible form by setting the transformed transverse coordinate proportional to the integral of the gas density over the physical transverse coordinate. In general, the boundary layer edge and wall (body surface) conditions will vary with the longitudinal coordinate. In some instances it is possible to recast the longitudinal coordinate and the dependent variables so that the transformed boundary conditions are constant and the wall and edge conditions appear in the governing conditions grouped as terms which are constant or which vary slowly with the transformed longitudinal coordinate. In the case when these terms are constant, it is called a similarity transformation, and the problem reduces to a two point boundary value problem because the dependent variables are functions only of the transverse coordinate. In the case when these terms vary slowly with the transformed longitudinal coordinate (so that they may be considered constant at any fixed value of the coordinate), the boundary layer problem again reduces to a two point boundary value problem, and the transformation is referred to as locally similar.

For the inviscid shock layer solution, the origin of the coordinate system is usually located at the apex or nose of the shock wave or nose of the shock wave or body, but is not necessarily made to coincide with the shock wave or body surface. If the reentry body has a sharp nose, the shock wave will be attached at the apex and the flow within the shock layer will be locally supersonic. If the reentry body has a blunt nose, the flow within the shock layer in the nose region is locally subsonic and becomes locally supersonic as it expands around the body. This fact complicates the blunt body problem because the governing partial differential equations are elliptic in the subsonic region, parabolic on the sonic surface and hyperbolic in the supersonic region. Where the flow is locally supersonic, the well established method of characteristics can be used. Where the flow is locally subsonic, the inviscid shock layer solution must be obtained by other methods such as finite difference methods, the method of integral relations, or Taylor series or other expansions. These methods are classified as either inverse or direct. In the inverse methods, the coordinate system is made to coincide with the shock wave, the contour of which is assumed. The blunt body problem is then solved

as an initial value problem, proceeding away from the specified shock wave contour until the body surface is determined by mass flow conservation requirements. By judiciously selecting the shock wave contour, the resulting body shape can be made to closely approximate the desired one. However, because the governing equations are elliptic, the initial value problem is not well posed and numerical techniques for its solution are inherently unstable. Although this presented serious difficulties in some of the first applications of the method, it has to a large extent been overcome by better integration techniques, coordinate transformations and other improvements. In the direct method the coordinate system is located on the body, and the inviscid blunt body problem is solved as a boundary value problem whether the position of one of the boundaries is unknown. The location and shape of the shock wave is, therefore, determined in the process.

A relatively new and very promising method of solving the steady reentry body flow field problem is the asymptotic time method proposed by Crocco<sup>4</sup> in which the steady flow field is recognized to be the state attained through any transient process after infinite time. The inclusion of the transient terms in the governing equations makes them hyperbolic and therefore amenable to solution as an initial value rather than as a boundary value problem. In theory the method is capable of solving the complete viscous shock layer problem as has been demonstrated by Scala and Gordon.<sup>5,6</sup>

At reentry velocities, the thermal environment within the shock layer is so high that the internal energy modes of the gas molecules (rotational, vibrational, and electronic states) become excited and chemical reactions, including dissociation and ionization, occur. In this case the shock layer properties cannot be accurately prescribed by treating the gas as ideal, i.e., as both thermally perfect (for which the pressure is proportional to the product of the gas density and temperature) and calorically perfect (for which the specific heat capacities are constant). At the lower altitudes (below approximately 100 kilofeet for typical earth reentry), this problem is rather easily resolved because the gas is in local thermodynamic

equilibrium.\* At the higher altitudes of the continuum regime, however, this problem is considerably more difficult because the gas is not in local thermal or chemical equilibrium throughout a substantial part of the flow field. In this case, to accurately describe the flow field properties, the finite rate processes for both thermal nonequilibrium and chemical nonequilibrium and their coupled effects must be taken into account.

### 3.1.2 REVIEW

In the following review the attempt has been made to identify each reference with enough clarity to enable the reader to determine whether or not the referenced work is pertinent to his particular interest. In most cases the method of solution, salient characteristics, and results are indicated. In certain cases where (in the author's opinion) a substantial contribution has been made which might not be extensively known, the work is discussed in more detail. It is by this aspect alone that the review is intended to be a critical one.

In the interest of brevity the following abbreviations have been employed:

MOC	-	method of characteristics
A/2D	-	axisymmetric or two-dimensional
3D	-	three-dimensional
E/IG	-	equilibrium or ideal gas
Le	-	Lewis number
Pr	-	Prandtl number

\* The word "local" is used in the macroscopic sense to denote a fluid element which contains enough gas particles to constitute an ensemble, i.e., its average properties are the most probable ones determined by statistical analysis of all possible quantum states of the gas. Thermodynamic equilibrium is defined to include mechanical, thermal and chemical equilibrium. For mechanical equilibrium, which is defined in the D'Alembert sense treating the fluid mass acceleration as an inertial body force, the sum of forces acting on a fluid element is zero. In thermal equilibrium the energy of each gas particle is partitioned equally per degree of freedom (equilibrated) among the energy modes. In chemical equilibrium the relative concentrations of the component species of the gas are established by the equilibrium of all possible chemical reactions. The concept of local thermodynamic (or mechanical, thermal or chemical) equilibrium in a flowing gas is applicable only when the effects of property gradients throughout a fluid element (ensemble) can be neglected. It is not applicable for example in strong shock wave flow for which some of the property gradients are appreciable.

### 3.1.2.1 Inviscid Shock Layer

#### 3.1.2.1.1 Equilibrium or Ideal Gas

3.1.2.1.1.1 Locally Supersonic Flow. The conical flow problem is treated in detail by Shapiro<sup>7</sup>. For an ideal diatomic gas tabulated results are presented by Kopal<sup>8</sup> and Wang et al.<sup>9</sup> and graphical results by Dailey and Wood<sup>10</sup> and the Ames Research Staff<sup>11</sup>. The method was extended to equilibrium air by Johnson<sup>12</sup> whose results show that at hypersonic speeds the conical solution is substantially affected by equilibrium gas properties being characterized by a thinner shock layer, lower pressure, significantly lower temperature, higher velocity, and significantly higher density than for an ideal diatomic gas.

The A/2D MOC solution for rotational flow of an ideal gas is treated at length by Ferri<sup>13</sup> and Isenberg and Lin<sup>14</sup>. The method has been extended to equilibrium air by Gravalos et al.<sup>69</sup> and many others (e.g., Powers<sup>15</sup>, Dresser<sup>16</sup>, Inouye et al.<sup>59</sup>). Edsall<sup>17</sup> improved the standard method by interpolating for the entropy of a streamline in a table constructed from the starting data and calculated shock points, thereby eliminating the necessity of using the projected velocity vector to linearly interpolate for the entropy at a grid point. Gravalos et al.<sup>18</sup> have expanded the method to provide for bodies with compression corners which result in secondary shock waves. Field and surface properties are furnished for a sphere-cone at Mach 10 for both equilibrium air and ideal gas. Davis<sup>19</sup> has developed an A/2D, E/IG solution which provides for expansion corners, compression corners, and shock wave intersections.

Flow over an axisymmetric body at small angle of attack can be determined by a limited application of the 3D MOC. The method is described in detail by Ferri<sup>13, 20</sup> and Whitham<sup>21</sup> and consists of solving the 3D characteristics equations by a perturbation technique, retaining only linear terms in angle of attack and obtaining the necessary zeroth order quantities from the axisymmetric MOC solution. Ideal gas results for cones are presented by Stone<sup>22</sup>

and Rakich<sup>23</sup> and for sphere cones by Rakich<sup>23</sup>, Ferri<sup>24</sup> and by Brong and Edelfelt<sup>25</sup> who also extended the method to equilibrium air. Rakich<sup>26</sup> broadened his previous work to equilibrium air and presents a comparison of equilibrium air and ideal gas results for cones, sphere cones and ogives.

The 3D MOC solution for steady rotational flow is treated by Holt<sup>27</sup> and Coburn<sup>28</sup>. Moretti et al.<sup>29</sup> have developed and applied the method to a variety of 3D and axisymmetric bodies at angle of attack for both equilibrium air and ideal gas. Pridmore Brown and Franks<sup>30</sup> have extended the method to provide for secondary shock waves; however, no applications are presented. C. W. Chu<sup>31</sup> has developed the method with an improved integration technique. Instead of satisfying the compatibility relation exactly along three arbitrarily selected bicharacteristics from the base of the Mach cone to the vertex, Chu approximately satisfies it for all (infinitely many) of the bicharacteristics on the Mach cone. He does this by minimizing the root mean square of the residual function determined from the compatibility relation which requires the evaluation of three contour integrals around the Mach cone base. Strom<sup>32</sup> has extended the method to provide for a gas which is frozen along streamlines but may have a different composition on each streamline.

Thommen and D'Attore<sup>33</sup> have shown that the finite difference scheme of Lax and Wendoroff can be applied successfully to the 3D supersonic inviscid flow problem.

3.1.2.1.1.2 Locally Subsonic Flow. The blunt body problem was first reviewed by Van Dyke<sup>34</sup>, who also developed an inverse numerical solution, and later extensively by Hays and Probst and Swigert<sup>36, 45</sup>. The work which was covered in these reviews will not be repeated here, and the reader is referred to Hays and Probst<sup>35</sup> for reviews on references 34 and 37 to 44, and to Swigert<sup>36, 45</sup> for reviews on references 45 to 53.

Maslen<sup>54</sup> and Cheng and Gaitatzes<sup>55</sup> have developed inverse blunt body solutions using the thin shock layer approximation which, considering their simplicity, show excellent agreement with results of exact solutions. Van Tuyl<sup>56</sup> has developed an approximate blunt body solution using Padé fractions (ratios of polynomials) to approximate the terms in the double power series expansion method and shows good agreement with exact solutions for spherical noses. Kao<sup>57</sup> has developed a direct series truncation blunt body solution for the zero angle case which is analogous to Swigert's<sup>34</sup> method for angle of attack.

Lomax and Inouye<sup>58</sup> have solved the inverse blunt body problem by numerical integration in physical coordinates using a predictor - corrector and a smoothing technique. Extensive tables for spheres in equilibrium air which include surface and field properties are presented at altitudes between 100 to 300 kft and free stream velocities between 10 and 45 kft /sec (a best buy). Inouye et al.<sup>57</sup> have coupled the solution of Lomax and Inouye with the method of characteristics. Ideal gas results for the surface and shock of a sphere-cone, an ellipsoid cylinder, and a sphere-cone-cylinder-flare are presented. Dresser and Anderson<sup>60</sup> have developed a numerical inverse axisymmetric solution and furnish results for a sphere-cone cylinder. Joss<sup>61</sup> has broadened the numerical inverse method to include axisymmetric bodies at angle of attack for ideal gas. Webb et al.<sup>62</sup> have produced a finite difference inverse solution similar to Joss<sup>61</sup> and furnish results for the Apollo body.

The axisymmetric direct blunt body problem using Dorodnitsyn's method of integral relations has been solved by Traugott<sup>63, 64</sup> for an ideal gas and by Feldman<sup>65</sup> and Kuby et al.<sup>64</sup> for equilibrium air and extended to angle of attack by Waldman<sup>47</sup>, Vaglio-Laurin<sup>67</sup> and Leigh and Rothrock<sup>68</sup>. However, Leigh and Rothrock found that when the entropy differential equation is properly treated the method of results in an overdetermined system of equations evidently caused by the boundary conditions of the shock. Gravalos et al.<sup>69</sup> have developed an axisymmetric direct finite difference method for the blunt body problem in which the body pressure distribution and shock wave are initially prescribed and the governing equations in intrinsic coordinates are solved. Based on the results of the solution, the shock wave and surface pressure are modified and the solution is repeated until the boundary conditions are satisfied to within a specified tolerance. Walter and Anderson<sup>70</sup> have also produced this type of solution.

The direct blunt body problem has also been solved using the asymptotic time approach. Bohachesky and Rubin<sup>48</sup> and Bohachesky and Mates<sup>49</sup> have developed this type of method in which the governing equations are solved by finite difference, with the free stream and body as initial conditions allowing the shock wave to develop and present ideal gas results for the Apollo body at angle of attack. Moretti et al.<sup>71,72</sup> have achieved a significant improvement in the finite difference asymptotic time method by treating the shock wave as a moving discontinuity, and furnish ideal gas results for different configurations. Webb and Dresser<sup>74</sup> have produced a solution similar to that of Moretti's. Sauerwein<sup>75,76</sup> and Boericke and Brong<sup>77</sup> have applied the asymptotic time approach to the blunt body problem using the unsteady three-dimensional method of characteristics. However, this method appears to be considerably less efficient and accurate than that of Moretti's method.

### 3.1.2.1.2 Nonequilibrium Gas

**3.1.2.1.2.1 Locally Supersonic Flow.** The two-dimensional axisymmetric method of characteristics was first extended to a nonequilibrium gas by Wood and Kirkwood<sup>78,79</sup> and B. T. Chu<sup>80</sup> who showed that, for gas in thermal or chemical nonequilibrium, the characteristics waves are propagated at the local frozen acoustic speed. Sidney et al<sup>81, 82, 83, 84</sup> have applied the nonequilibrium method of characteristics to wedges and cones for the vibrational relaxation of an ideal diatomic gas using the harmonic oscillator as a model. Their results show that vibrational nonequilibrium causes curvature in the shock wave and the surface pressure overexpands from the frozen value at the cone tip (which is larger than the equilibrium value because of the larger shock angle at the tip) to below the equilibrium value and asymptotically approaches from below, whereas the gas temperature asymptotically approaches the equilibrium value from above. Spurk et al.<sup>85,86</sup> have developed a thermal equilibrium chemical nonequilibrium characteristics solution for a 5 species - 10 reactions air system and furnish results for the distribution of surface properties and the shock wave shape for both cones and wedges. Gravalos<sup>87,88,89</sup> et al. have developed a thermal equilibrium chemical nonequilibrium characteristics solution for a 7 species - 7 reactions air system which provides for an expansion corner on the

body. Results are presented (in reference 87) for a  $45^\circ$  cone with a  $39^\circ$  expansion corner. Wood et al.<sup>90</sup> have developed a characteristics solution with both vibrational nonequilibrium and chemical nonequilibrium for a 7 species - 7 reaction air system. The harmonic oscillator model is used for the vibrational relaxation of molecular oxygen and nitrogen and the effect of vibration on their nonequilibrium dissociation rates are taken into account. Thermal equilibrium results are presented for a sphere - cone, and both vibrational and chemical nonequilibrium results for an ogive. Their sphere-cone results also show that the nonequilibrium streamtube gives excellent results for the electron density distributions. Kliegel et al.<sup>91</sup> have developed a characteristics solution for chemical nonequilibrium (6 species-6 reactions air system) with the provision for treating vibrational relaxation (without vibrational - dissociation coupling) using the anharmonic oscillator model. Thermal equilibrium results are presented for the surface profiles of a cone-cylinder. South<sup>92, 93</sup> and South and Newman<sup>94</sup> have applied Dorodnitsyn's method of integral relations to flow over pointed bodies (locally supersonic flow) of a vibrationally relaxing ideal diatomic gas and found that the method did not give the proper asymptotic behavior because of the improper weighting of the frozen flow boundary condition at the shock wave. This difficulty was overcome (in reference 94) by weighting the shock wave boundary condition and their results for a two strip approximation agree well with the characteristics solution of Sedney and Gerber<sup>83</sup>.

3.1.2.1.2.2 Locally Subsonic Flow. The blunt body problem for a nonequilibrium gas was first solved by Lick<sup>95, 96</sup> using a numerical inverse method for the subsonic region and the method of characteristics for the supersonic region. His results are for thermal equilibrium and although necessarily based on poor reaction rates show that nonequilibrium effects do not significantly affect the static pressure in blunt body flows. Hall<sup>97</sup> et al. have also used a numerical inverse method to solve the blunt body problem for a thermal equilibrium chemical nonequilibrium 7 species - 7 reactions air system. Results are furnished for body surface and field properties for a spherical nose and binary scaling is demonstrated. Additional results which have been obtained from this solution are presented by Gibson and Marrone<sup>98, 99, 100</sup> and by Wurster and Marrone<sup>101, 102</sup>. Based on the work of Treanor and Marrone<sup>103, 104, 105</sup>, Marrone<sup>106</sup> expanded the solution of Hall et al.<sup>97</sup> to include vibrational nonequilibrium which

treats both coupled vibration - dissociation and dissociation - vibration effects. The vibrational energy levels are prescribed from spectroscopic data and "preferred" dissociation from the upper vibrational levels is allowed by an arbitrary exponential probability. A Boltzman distribution is assumed for the vibrational level populations. Vibrational chemical nonequilibrium results are presented for the hypersonic flow of oxygen over a spherical nose. Lee and Chu<sup>107</sup> have produced a numerical inverse blunt body solution for thermal equilibrium chemical nonequilibrium (5 species - 6 reactions air system) and furnish a detailed comparison of their results with those of Hall et al.<sup>97</sup> Shih et al.<sup>108,109</sup> have applied Dorodnitsyn's method of integral relations to the direct blunt body problem for thermal equilibrium chemical nonequilibrium (5 species - 6 reactions air system). Results using the one strip approximation are furnished and frozen and equilibrium air results compared for a sphere.

The nonequilibrium streamtube method is an approximation technique which can be applied to either locally subsonic or supersonic flows. Thermal equilibrium chemical nonequilibrium streamtube solutions for air have been developed by Bloom et al.<sup>110,111,112</sup>, Lin and Teare<sup>113</sup>, Eschenroeder et al.<sup>114,115,116</sup> and Lordi et al.<sup>117</sup> and superimposed on ideal gas or equilibrium air flow field solutions by McMenamin and O'Brien<sup>118</sup> and Karydas<sup>119</sup>. Chen and Eschenroeder<sup>120</sup> have developed a streamtube solution which provides for vibrational relaxation using the harmonic oscillator model. Dresser et al.<sup>121</sup> have produced a streamtube solution which allows for both vibrational and electronic relaxation.

### 3.1.2.2 Boundary Layer

#### 3.1.2.2.1 Equilibrium/Ideal Gas

3.1.2.2.1.1 First Order. The similar boundary layer solution for this category is treated by Hayes and Probst<sup>122</sup> and the stagnation point boundary layer is an important case of its application. Libby<sup>123</sup> has developed a low temperature air solution with air injection or suction. He solves the two point boundary value problem after a transformation to the Crocco variables

numerically by the "shooting through" or initial value method determining the necessary initial slopes at the edge by means of an asymptotic expansion which is valid at the edge. Tabulated and graphical results are presented for a wide range of wall conditions and a comparison with an approximate integral method is made. Weston<sup>124</sup> has produced a high temperature equilibrium air solution with air injection or suction. He uses the shooting through method to obtain the numerical solution by assuming velocity and enthalpy slopes at the wall and iterating until the boundary conditions at the edge are satisfied. Tabulated profiles for an axisymmetric stagnation point are provided for a variety of wall conditions. Axisymmetric stagnation point boundary layers for air have also been developed by Herring<sup>125</sup> (without mass transfer) and by Hoshezaki and Smith<sup>126</sup> and Howe and Mersman<sup>127</sup> (with mass transfer). Strom<sup>128</sup> has developed a three-dimensional stagnation point finite difference solution with mass transfer. Axisymmetric similar solutions for other than the stagnation point have been produced by Waiter and Anderson<sup>129</sup> and Grabow<sup>130</sup>. Brant and Burke<sup>131</sup> have developed an axisymmetric locally similar solution for an arbitrary equilibrium gas which may contain many species. Locally similar three-dimensional (with linearized secondary flow) boundary layers have been developed by Beckwith<sup>132</sup> and Beckwith and Cohen<sup>133</sup> for equilibrium air or ideal gas with no mass transfer, by Polak and Li<sup>134</sup> for an ideal gas with no mass transfer, and by Hang et al.<sup>135, 136</sup> with mass addition for frozen chemistry.

Integral solutions for the axisymmetric boundary layer have been developed by Moran<sup>137</sup> and Carlson<sup>138</sup> for a binary gas and by Liu and Kuby<sup>139</sup> for the combustion of a graphite surface with frozen chemistry in the boundary layer. Kang<sup>140</sup> has produced a three-dimensional integral solution for ideal gas with mass transfer.

Li<sup>141</sup> has solved the axisymmetric boundary layer in the stagnation region by a series expansion method in which, after a transformation to the similarity variables, the velocity, enthalpy and stream function are expanded in a power series for which the coefficients are functions only of the transverse coordinate. Parr<sup>142</sup>, Krause<sup>143, 144</sup> and Waiter and Anderson<sup>145</sup> have developed A/2D, E/IG boundary layer solutions based on an implicit finite difference method developed by Flugge-Lotz and Blottner<sup>146</sup>. In this method the momentum

equation is linearized and the boundary layer is solved step wise in the longitudinal coordinate by inverting a tri-diagonal matrix at each step. Flannelop<sup>147</sup> has expanded the method to three-dimensional boundary layers. Raetz<sup>148</sup> and Der and Raetz<sup>149</sup> have also developed numerical solutions for the three-dimensional boundary layer.

The turbulent boundary layer problem has been treated by Crocco<sup>150</sup>. Denison<sup>151</sup> has produced results for turbulent boundary layer for equilibrium air on an ablating graphite surface using the Crocco solution (total enthalpy and species cross fractions linear function of velocity) with the Van Driest velocity profile.

**3.1.2.2.1.2 Second Order.** The second-order axisymmetric/two-dimensional boundary layer problem has been treated and reviewed by Van Dyke<sup>152,153,154</sup>. Lewis and co-workers<sup>155,156</sup> and Adams<sup>157</sup> have applied the second order theory of Van Dyke using the numerical method developed by Davis and Flugge-Lotz<sup>158</sup> for a perfect gas. Smith and co-workers<sup>159,160,161,162</sup> have solved the second order (transverse curvature) boundary layer problem as a sequence of two point boundary value problems by converting the governing equation to ordinary equations through the process of replacing the longitudinal derivatives by their finite difference approximations. The two point boundary value problem is then solved at each longitudinal station by the shooting through (or initial value) technique. This method has been applied to equilibrium air flow on a sphere-cone by Lewis and Whitfield<sup>163</sup> and Mayne et al.<sup>164</sup> for a binary gas on a sharp cone. Using the implicit finite difference technique of Flugge-Lotz and Blottner<sup>146</sup>, Levine<sup>165</sup> has developed an A/2D, E/IG second order boundary layer solution which includes transverse curvature and mass addition.

Similar second-order solutions have been developed for an ideal gas by Maslen<sup>166</sup>, Yasuhara<sup>167</sup> and Probstein and Elliot<sup>168</sup> and for equilibrium air or a mixture of ideal gases (binary diffusion) by Sagendorph<sup>169</sup>. Maslen includes both transverse and longitudinal curvature, whereas the others include transverse curvature.

### 3.1.2.2.2 Nonequilibrium Gas

3.1.2.2.2.1 First Order Theory. The similar nonequilibrium gas A/2D boundary layer problem is treated by Dorrance<sup>170</sup>. Finite difference solutions have been developed and applied at the stagnation point by Fay and Riddell<sup>171</sup> and Fay and Kaye<sup>172</sup>. Fay and Riddell used the shooting through or initial value technique and present catalytic and noncatalytic wall results for air with  $P=0.71$ , a Sutherland viscosity law and  $Le = 1, 1.4$  and  $2$ . Fay and Kaye used the implicit method for nitrogen dissociation treating the chemical production term as a parameter. Other similar solutions have been developed by Moore and Pallone<sup>173</sup> for air, Libby and Pierucci<sup>174</sup> for air plus hydrogen, and by Libby and Liu<sup>175</sup>. Locally similar solutions for trace contaminants in air have been obtained by Lenard<sup>176, 177</sup>.

Pallone et al.<sup>178</sup> have applied Doroditsyn's method of integral relations to the nonequilibrium air boundary layer problem. Property profiles at three stations on an  $8^\circ$  cone for three free stream conditions and a comparison of the effects of diffusion is made. Smith and Jaffe<sup>179</sup> have extended their previous finite difference method to the nonequilibrium gas boundary layer. Results are presented for a binary dissociating gas. Blottner<sup>180, 181, 182</sup> has developed an implicit finite difference solution for the nonequilibrium gas boundary layer based on the work of Flugge-Lotz and Blottner. His solution is capable of treating catalytic (recombined) or noncatalytic wall, mass transfer, and multicomponent diffusion for arbitrary (25 species - 40 reactions) chemical system. Air results are presented for a sphere-cone, cone and hemisphere-cylinder (binary gas). Additional applications of Blottner's solution have been presented by Lew<sup>183</sup>. Moore and Lee<sup>184</sup> have developed a solution analogous to Blottner's.

Approximate solutions for the nonequilibrium gas boundary layer have been produced by Fox<sup>185</sup> and Hayday<sup>186</sup>. Fox solves the problem in terms of the eigenfunctions of the basic boundary layer operator for a ideal dissociating gas. A particular solution is required for the species equation and, hence, the method is not applicable to multicomponent-multireaction system. Hayday uses an asymptotic series expansion method in which the coefficients are evaluated by approximately integrating the governing equations. Results are present only for an equilibrium air stagnation point.

Binary scaling laws have been developed by Lee and Levinsky<sup>187</sup> and Levinsky<sup>188</sup> for cones in pure air and will be extended to cones at angle of attack by Lee and Baker<sup>189</sup>.

3.1.2.2.2.2 Second Order Theory. No publications available in this category.

### 3.1.2.2 Viscous Layer - Merged Layer

#### 3.1.2.3.1 Equilibrium or Ideal Gas

The fully viscous layer and merged layer problems are treated by Hayes and Probstein<sup>190</sup>. Chen et al.<sup>191</sup> have solved the viscous layer stagnation region problem for an ideal gas with mass transfer. Modified Rankine-Hugoniot relations and a linear viscosity are employed. Results are presented for the axisymmetric stagnation point. Goldberg<sup>192</sup> and Goldberg and Scala<sup>193</sup> have developed a series expansion solution for the viscous layer stagnation region for equilibrium air with mass transfer. A Sutherland viscosity law is used and Lewis and Prandtl number are constant. Results are presented for a variety of wall conditions and Reynolds numbers.

Kao<sup>195</sup> has done a comparison of inviscid, viscous layer and third-order boundary layer theory for the stagnation region. Results are presented for Reynolds numbers (based on shock viscosity) of 10, 100 and 1,000. Probstein and Kemp<sup>195</sup> have used the constant density assumption to obtain the viscous layer stagnation region solution for an ideal gas. Lenard<sup>196</sup> has developed a merged layer stagnation point solution for an ideal gas. Wei<sup>197</sup> has used the method of inner and outer expansions to obtain the viscous layer solution on a slender body for an ideal gas. Waldron<sup>198</sup> has used a perturbation technique to obtain the viscous layer solution for an ideal gas on a slender body. Heat transfer results are presented.

#### 3.1.2.3.2 Nonequilibrium Gas

The viscous layer merged layer problem for a nonequilibrium gas is treated by Cheng<sup>199</sup>. Cheng also developed a numerical solution for the stagnation region and presents results for a binary gas.

Shih and Krupp<sup>200</sup> have solved the viscous layer stagnation region problem for an ideal dissociating gas using the series expansion method and numerically integrating the ordinary differential equations.

Chung<sup>201</sup> has developed a viscous layer stagnation region solution for a binary gas and Chung et al.<sup>202</sup> have developed a merged layer stagnation region solution for a binary gas. Lee and Zierten<sup>203</sup> have developed a merged layer stagnation region solution for air by superimposing on frozen flow field as calculated by Chung's method.

### 3.1.3 FLOW FIELD BIBLIOGRAPHY

1. Gruscynski, J.S. and Warren, W.R., Jr.: "Study of Equilibrium Air Total Radiation," AIAA Paper No. 66-103, January 1966; also AIAA Journal Vol. 5, No. 3, pp. 517-525, March 1967.
2. Probst, R.F.: "Shock Wave and Flow Field Development in Hypersonic Re-Entry," ARS Journal Vol. 31, No. 2, pp. 185-194, February 1961.
3. Shapiro, A.H.: The Dynamics and Thermodynamics of Compressible Fluid Flow, Vol. I, pp. 532-534, The Ronald Press Co., New York, 1953.
4. Crocco, L.: "A Suggestion for the Numerical Solution of the Steady Navier-Stokes Equations," AIAA Paper No. 65-1, January 1965.
5. Scala, S.M. and Gordon, P.: "Solution of the Time-Dependent Navier-Stokes Equations for the Flow around a Circulation Cylinder," AIAA Paper No. 67-221, January 1967.
6. Scala, S.M. and Gordon, P.: "Solution of the Time-Dependent Navier-Stokes Equations for the Flow of Dissociating Gas Over a Circular Cylinder," General Electric Co., TIS R67SD56, May 1967.

#### 3.1.3.1 Inviscid Shock Layer

##### 3.1.3.1.1 Equilibrium or Ideal Gas

##### 3.1.3.1.1.1 Locally Supersonic Flow.

7. Shapiro, A.H.: The Dynamics and Thermodynamics of Compressible Fluid Flow, Vol. II, pp. 653-663 and 676-684, The Ronald Press Co., New York, 1953.
8. Kopal, Z.: "Tables of Supersonic Flow Around Cones," Massachusetts Institute of Technology, TR No. 1, 1947.

9. Wang, C. J., Goebel, T. P. and Farnell, A. B.: "Conical Flow Tables," North American Aviation Inc., Rpt. No. NA-55-671, June 1955.
10. Dailey, C. L. and Wood, F. C.: Computation Curves for Compressible Fluid Problems, John Wiley and Sons, Inc., New York, 1949.
11. Ames Research Staff: "Equations, Tables and Charts for Compressible Flow," NACA Rpt. No. 1135, 1952.
12. Johnson, C.: "The Flow Field About a Right Circular Cone at Zero Yaw," General Electric Co., TIS 62SD211, November 1962.
13. Ferri, A.: "The Method of Characteristics," General Theory of High Speed Aerodynamics (W.R. Sears, ed.) Sect. 6, pp. 583-669, Princeton Univ. Press, Princeton, 1954.
14. Isenberg, J.S. and Lin, C.C.: "The Method of Characteristics in Compressible Flow," Part I Steady Supersonic Flow, Wright-Patterson Air Force Base Air Material Command, Rpt. No. F-TR-1173A-ND, December 1947.
15. Powers, S. A.: "Hypersonic Studies - Equilibrium Real Gas Flow Fields for Blunt Bodies," Northrop Corp., NB-62-14, January 1962.
16. Dresser, H.S.: "Method of Characteristics Program for Real Gas Equilibrium Flow," North American Aviation Inc. SID64-633, March 1964.
17. Edsall, R.H.: "A Modified Method of Characteristics for Calculating Inviscid Flow Fields," General Electric Co., FM-101, March 1963.

18. Gravalos, F.G., Brong, E. and Edelfelt, I.H.: "The Calculation of Flow Fields with Secondary Shocks for Real Gases at Chemical Equilibrium," General Electric Co., TIS R59SD419, May 1960.
19. Davis, R.S.: "Analysis and Programming of Supersonic Field with Shock Intersection," General Electric Co., TIS 62SD105, April 1962.
20. Ferri, A.: "The Method of Characteristics for the Determination of Supersonic Flow Over Bodies of Revolution at Small Angles of Attack," NACA Rpt. 1044, 1951.
21. Witham, G.B.: "Steady High Speed Flow Past an Axisymmetric Body at Incidence to the Stream," General Applied Sciences Laboratories Inc., Rpt. TR 41, November 1957.
22. Stone, A.H.: "On Supersonic Flow Past a Slightly Yawing Cone," Journal of Mathematics and Physics, Vol. XXVII, No. 1, pp. 67-81, April 1948.
23. Rakich, J.V.: "Numerical Calculation of Supersonic Flows of a Perfect Gas Over Bodies of Revolution at Small Angles of Yaw," NASA TN D 2390, July, 1964.
24. Ferri, A.: "The Linearized Characteristics Method and Its Application to Practical Nonlinear Supersonic Problems," NACA Rpt. 1102, 1952.
25. Brong, E.A. and Edelfelt, I.H.: "The Flow Field about a Slightly Yawed Blunt Body of Revolution in a Supersonic Stream," General Electric Co., TIS R62SD111, March 1962.
26. Rakich, J.V.: "Calculation of Hypersonic Flow over Bodies of Revolution at Small Angles of Attack," AIAA Journal, Vol. 3, No. 3, pp. 458-464, March 1965.

27. Holt, M.: "The Method of Characteristics for Steady Supersonic Rotational Flow in Three-Dimensions," *Journal of Fluid Mechanics*, Vol. 1, pp. 409-423, 1956.
28. Coburn, N.: "Intrinsic Form of the Characteristic Relations in the Steady Supersonic Flow of a Compressible Fluid," *Quarterly of Applied Mathematics*, Vol. 15, pp. 237-248, 1957.
29. Mcretti, G., Sanlorenzo, E. A., Magnus, D. E. and Welberstein, G.: "Flow Field Analysis of Re-entry Configurations by a General Three-Dimensional Method of Characteristics," Air Force Systems Command, A.S. Div. TR-61-727, Vol. III, February 1962.
30. Pridmore-Brown, B. N. and Frank, W. J.: "A Method of Characteristics Solution in Three Independent Variables," Aerospace Research Laboratories, ARL 65-124, June 1965.
31. Chu, C. W.: "Compatibility Relations and a Generalized Finite-Difference Approximation for Three-Dimensional Steady Supersonic Flow," *AIAA Journal* Vol. 5, No. 3, pp. 493-501, March 1967.
32. Strom, C. R.: "The Method of Characteristics for Three-Dimensional Real Gas Flows," Air Force Flight Dynamics Laboratory, TR-67-47, July 1967.
33. Thommen, H. U., D'Attorre, L.: "Calculation of Steady Three-Dimensional Supersonic Flow Fields by a Finite Difference Method," *AIAA Paper No. 65-26*, January 1965.
- 3.1.3.1.1.2 Locally Subsonic Flow.
34. Van Dyke, M. D.: "The Supersonic Blunt Body Problem - Review and Extension," *Journal of Aerospace Sciences*, Vol. 25, No. 8, pp. 485-496, August 1958.
35. Hayes, W. D. and Probstein, R. F.: Hypersonic Flow Theory, pp. 210-252, Academic Press Inc., New York, 1959.

36. Swigart, R.J.: "The Direct Asymmetric Hypersonic Blunt Body Problem," AIAA Paper No. 66-411, June 1966.
37. Maslen, S.H. and Moeckel, W.E.: "Inviscid Hypersonic Flow Past Blunt Bodies," *Journal of Aerospace Sciences*, Volume 24, No. 9, pp. 683-693, September 1957.
38. Uchida, S. and Yasuhara, M.: "The Rotational Field Behind a Curved Shock Wave Calculated by the Method of Flux Analysis," *Journal of Aeronautical Sciences*, Vol. 23, No. 9, pp. 830-845, September 1956.
39. Mitchell, A.R.: "Application of Relaxation to the Rotational Field of Flow Behind a Bow Shock Wave," *Quarterly Journal of Mechanics and Applied Mathematics*, Vol. 4, pp. 371-383, 1951.
40. Lin, C.C. and Rubinov, S.I.: "On the Flow Behind Curved Shocks," *Journal of Mathematics and Physics*, Vol. 27, No. 2, pp. 105-129, July 1948.
41. Lin, C.C. and Shen, S.F.: "An Analytic Determination of the Flow Behind a Symmetrical Curved Shock in a Uniform Stream," NACA TN-2506, 1951.
42. Zlotnick, M. and Newman, D.J.: "Theoretical Calculation of the Flow on Blunt-Nosed Axisymmetric Bodies in a Hypersonic Stream," AVCO Manufacturing Co., Rpt. RAD-TR-2-57-29, September 1957.
43. Garabedian, P.R. and Lieberstein, H.M.: "On the Numerical Calculation of Detached Bow Shock Waves in Hypersonic Flow," *Journal of Aeronautical Sciences*, Vol. 25, No. 2, pp. 109-118, February 1958.

44. Vaglio-Laurin, R. and Ferri, A.: "Theoretical Investigation of the Flow Field about Blunt-Nosed Bodies in Supersonic Flight," *Journal of Aerospace Sciences*, Vol. 25, No. 12, pp. 761-770, December 1958.
45. Swigart, R.J.: "A Theory of Asymmetric Hypersonic Blunt-Body Flows," *AIAA Journal*, Vol. 1, No. 5, pp. 1034-1042, May 1963; also Stanford University, Rpt. No. 120, AFOSR-TN-62-2232, 1962; also preprint 62-98, 1962.
46. Vaglio-Laurin, R.: "On the PLK Method and the Supersonic Blunt Body Problem," *Journal of Aerospace Sciences*, Vol. 29, No. 2, pp. 185-206, February 1962.
47. Waldman, G.D.: "Integral Approach to the Yawed Blunt Body Problem," *AIAA Paper* No. 65-28, January 1965.
48. Bohachevsky, I.O. and Rubin, E.I.: "A Direct Method for Computation of Nonequilibrium Flows with Detached Shock Waves," *AIAA Journal*, Vol. 4, No. 4, pp. 600-607, April 1966; also *AIAA Paper* No. 65-24, January 1965.
49. Bohachevsky, I.O. and Mates, R.E.: "A Direct Method for Calculation of the Flow about an Axisymmetric Blunt Body at Angle of Attack," *AIAA Journal*, Vol. 4, No. 5, pp. 776-782, May 1966; also *AIAA Paper* No. 65-24, January 1965.
50. Yeh, H. and Doby, R.: "On Detached Shocks for Blunt Bodies at Small Angles of Attack," *ASME Paper* No. 65-APM-7, 1965.
51. Garabedian, P.R.: "Numerical Construction of Detached Shock Waves," *Journal of Mathematics and Physics*, Vol. 36, No. 3, pp. 192-205, 1957.
52. Van Dyke, M.D. and Gordon, H.D.: "Supersonic Flow Past a Family of Blunt Axisymmetric Bodies," *NASA TR R-1*, 1959.

53. Fuller, F. B.: "Numerical Solutions for Supersonic Flow of an Ideal Gas Around Blunt Two-Dimensional Bodies," NASA TND-791, July 1961.
54. Maslen, S. H.: "Inviscid Hypersonic Flow Past Smooth Symmetric Bodies," AIAA Journal, Vol. 2, No. 6, pp. 1055-1061, June 1964.
55. Cheng, H. K. and Gaitatzes, G. A.: "Use of the Shock-Layer Approximation in the Inverse Hypersonic Blunt Body Problem," AIAA Journal, Vol. 4, No. 3, pp. 406-413, March 1966.
56. Van Tuyl, A. H.: "Use of Rational Approximations in the Calculation of Flows Past Blunt Bodies," AIAA Journal, Vol. 5, No. 2, pp. 218-225, February 1967; also U.S. Naval Ordnance Laboratory, NOLTR 66-14, February 1966.
57. Kao, H. C.: "An Analytic Approach to the Method of Series Truncation for the Supersonic Blunt Body Problem," Journal of Fluid Mechanics, Vol. 27, pt. 4, pp. 789-813, 1967.
58. Lomax, H. and Inouye, M.: "Numerical Analysis of Flow Properties about Blunt Bodies Moving at Supersonic Speeds in an Equilibrium Gas," NASA TR R-204, July 1964.
59. Inouye, M., Rakich, J. V. and Lomax, H.: "A Description of Numerical Methods and Computer Programs for Two-Dimensional and Axisymmetric Supersonic Flow over Blunt Nosed and Flared Bodies," NASA TN D-2970, August 1965.
60. Dresser, H. S. and Anderson, R. B.: "Inverse Blunt Body Computer Program for Axisymmetric Body Shapes at Zero Angle of Attack," North American Aviation Inc., SID66-1541, October 1966.

61. Joss, W.W.: "Application of the Inverse Technique to Flow over a Blunt Body at Angle of Attack," Cornell Aeronautical Laboratories Inc., Rpt. No. AG-1729-A-6, December 1965.
62. Webb, H.G., Jr., Dresser, H.S., Adler, B.K. and Waiter, S.A.: "An Inverse Solution for the Determination of Flow Fields about Axisymmetric Blunt Bodies at Large Angle of Attack," AIAA Paper No. 66-413, June 1966; also AIAA Journal, Vol. 5, No. 6, June 1967.
63. Traugott, S.C.: "An Approximate Solution of the Direct Supersonic Blunt Body Problem for Arbitrary Axisymmetric Shapes," Journal of Aerospace Sciences, Vol. 27, No. 5, pp. 361-370, May 1960.
64. Traugott, S.C.: "Some Features of Supersonic and Hypersonic Flow About Blunted Cones," Journal of Aerospace Sciences, Vol. 29, No. 4, pp. 395-399, April 1962.
65. Feldman, S.: "Numerical Comparison Between Exact and Approximate Theories of Hypersonic Inviscid Flow Past Slender Blunt Nosed Bodies," ARS Journal, Vol. 30, No. 5, pp. 463-468, May 1960.
66. Kuby, W., Foster, R.M., Byron, S.R. and Holt, M.: "Symmetrical Equilibrium Flow Past a Blunt Body at Superorbital Re-Entry Speeds," AIAA Journal, Vol. 5, No. 4, pp. 610-617, April 1967.
67. Vaglio-Laurin, R.: "Inviscid Supersonic Flow About General Three-Dimensional Blunt Bodies," Flight Dynamics Laboratory, TR ASD-TR-61-727, October 1962.
68. Leigh, D.C. and Rothrock, D.A.: "The Method of Integral Relations and Blunt Body Flows," General Electric Co., TIS 65SD227, April 1965.

69. Gravalos, F.G., Edelfelt, I.H. and Emmons, H.W.: "The Supersonic Flow About a Blunt Body of Revolution for Gases at Chemical Equilibrium," General Electric Co., TIS R58SD245, June 1958.
70. Waiter, S.A. and Anderson, R.B.: "Determination of the Transonic Flow Field Around a Blunt Body," North American Aviation Inc. SID64-634, February 1964.
71. Abbett, M. and Moretti, G.: "A Fast, Direct, and Accurate Technique for the Blunt Body Problem Part I - Analysis," General Applied Sciences Laboratory Inc., TR-583, January 1966; also AD-478119L.
72. Moretti, G. and Abbett, M.: "A Time-Dependent Computational Method for Blunt Body Flows," AIAA Journal, Vol. 4, No. 12, pp. 2136-2141, December 1966.
73. Moretti, G. and Bleich, G.: "Three-Dimensional Flow around Blunt Bodies," AIAA Journal, Vol. 5, No. 9, pp. 1557-1562, September 1967.
74. Webb, H.G., Jr. and Dresser, H.S.: "Unsteady Flow over Axisymmetric Blunt Bodies at Zero Angle of Attack," North American Rockwell Corp., SD67-881, September 1967.
75. Sauerwein, H.: "A General Numerical Method of Characteristics," AIAA Paper No. 65-25, January 1965.
76. Sauerwein, H.: "Numerical Calculations of Arbitrary Multidimensional and Unsteady Flows by the Method of Characteristics," Aerospace Rpt. TR-669 (S6815-71)-2, May 1966; also AD633 958; also AIAA Paper No. 66-412, June 1966.
77. Boericke, R.R. and Brong, E.A.: "A Method of Characteristics for Three-Dimensional Unsteady Flow Fields," General Electric Co., TIS 67SD362, November 1967.

### 3.1.3.1.2 Nonequilibrium Gas

#### 3.1.3.1.2.1 Locally Supersonic Flow.

78. Wood, W.W. and Kirkwood, J.G.: "Hydrodynamics of a Reacting and Relaxing Fluid," Journal of Applied Physics, Vol. 28, No. 4, pp. 395-398, April 1957.
79. Wood, W.W. and Kirkwood, J.G.: "Characteristic Equations for Reactive Flow," Journal of Chemical Physics, Vol. 27, No. 2, p. 596, August 1957.
80. Chu, B.T.: "Wave Propagation and the Method of Characteristics in Reacting Gas Mixtures with Applications to Hypersonic Flow," Wright Air Development Center, TN 57-213, May 1957; also AD 118 350.
81. Sedney, R.: "Some Aspects of Nonequilibrium Flows," Journal of Aerospace Sciences, Vol. 28, No. 3, pp. 189-196, March 1961.
82. Sedney, R., South, J.C. and Gerber, N.: "Characteristic Calculations of Nonequilibrium Flows," AGARD Monograph 68 (High Temperature Aspects of Hypersonic Flow), April 1962.
83. Sedney, R. and Gerber, N.: "Nonequilibrium Flow over a Cone," Ballistic Research Laboratories, Rpt. No. 1203, May 1963; also AIAA Journal, Vol. 1, No. 11, pp. 2482-2486, November 1963.
84. Sedney, R. and Gerber, N.: "Shock Curvature and Gradients at the Tip of Pointed Axisymmetric Bodies in Nonequilibrium Flow," Journal of Fluid Mechanics, Vol. 29, pt. 4, pp. 765-779, 1967; also Ballistic Research Laboratories, Rpt. No. 1350, December 1966.
85. Spurk, J.H., Gerber, N. and Sedney, R.: "Characteristic Calculation of Flow Fields with Chemical Reactions," AIAA Journal, Vol. 4, No. 1, pp. 30-37, January 1966.

86. Spurk, J.H., Knauss, D.T. and Bartos, J.M.: "Interferometric Measurement of Nonequilibrium Flow Fields around Cones and Comparison with Characteristics Calculations," AGARD Conference Proceedings No. 12 (Recent Advances in Aerothermochemistry), Vol. 2, 1967.
87. Gravalos, F.G.: "The Flow of a Chemically Reacting Gas Mixture," General Electric Co., TIS 63SD200, Vol. I and II, February 1963.
88. Gravalos, F.G.: "Analytical Foundations of Aerothermochemistry," General Electric Co., TIS 66SD259, September 1966.
89. Gravalos, F.G., Studerus, C.J. and Edelfelt, I.H.: "The Hypersonic Flow of a Chemically Reacting Gas Mixture about a Cone with an Expansion Corner," General Electric Co., TIS 67SD345, November 1967.
90. Wood, A.D., Springfield, J.F. and Pallone, A.J.: "Chemical and Vibrational Relaxation of an Irviscid Hypersonic Flow," AIAA Journal, Vol. 2, No. 10, pp. 1697-1705, October 1964; also AIAA Paper No. 63-441.
91. Kllegel, J.R., Peters, R.L. and Lee, J.T. Jr.: "Characteristics Solution for Nonequilibrium Flow Fields about Axisymmetric Bodies, Vol. 1 Analysis and Results," Thompson Ramo Wooldridge Inc., Rpt. No. 6453-6001-KU-000, July 1964.
92. South, J.C., Jr.: "Application of Dorodnitsyn's Integral Method to Nonequilibrium Flows Over Pointed Bodies," NASA TND-1942, 1963.
93. South, J.C., Jr.: "Applications of the Method of Integral Relations to Supersonic Nonequilibrium Flow Past Wedges and Cones," NASA TR R-205, 1964.

94. South, J.C. and Newman, P.A.: "Application of the Method of Integral Relations to Real-Gas Flows Past Pointed Bodies," AIAA Journal, Vol. 3, No. 9, pp. 1645-1652, September 1965.

**3.1.3.1.2.2 Locally Subsonic Flow.**

95. Lick, W.: "Inviscid Flow Around a Blunt Body of a Reacting Mixture of Gases, Part A - General Analysis," Rensselaer Polytechnic Institute, TR AE 5810, May 1958; also AD 158 335.
96. Lick, W.: "Inviscid Flow Around Blunt Body of a Reacting Mixture of Gases, Part B - Numerical Solutions," Rensselaer Polytechnic Institute, TR AE 5814, December 1958; also AD 207 833.
97. Hall, J., Eschenroeder, A. and Marrone, P.: "Blunt Body Nose Inviscid Airflows with Coupled Nonequilibrium Processes," Journal of Aerospace Sciences, Vol. 29, No. 9, pp. 1038-1051, September 1962.
98. Gibson, W.E. and Marrone, P.V.: "A Similitude for Nonequilibrium Phenomena in Hypersonic Flight," Paper presented at AGARD Conference on High Temperature Aspects of Hypersonic Flow, Brussels, Belgium, April 1962.
99. Gibson, M.E. and Marrone, P.V.: "Nonequilibrium Scaling Criterion for Inviscid Hypersonic Airflows," Cornell Aeronautical Laboratories, Rpt. No. QM-1626-A-8, November 1967.
100. Gibson, W.E. and Marrone, P.V.: "Correspondence Between Normal Shock and Blunt Body Flows," Physics of Fluids, Vol. 5, No. 12, December 1962.
101. Wurster, W.H. and Marrone, P.V.: "Study of Infrared Emission in Heated Air," Cornell Aeronautical Laboratories, Rpt. No. QM-1373-A-2, June 1960.

102. Wurster, W.H. and Marrone, P.V.: "Study of Infrared Emission in Heated Air," Cornell Aeronautical Laboratories, Rpt. No. QM-1373-A-A, July 1961.
103. Treanor, C.E. and Marrone, P.V.: "Vibration and Dissociation Coupling Behind Strong Shock Waves," Paper presented at AFOSR-GE Symposium on Dynamics of Manned Lifting Planetary Entry, Philadelphia, Pa., October 1962.
104. Treanor, C.E. and Marrone, P.V.: "Effect of Dissociation on the Rate of Vibrational Relaxation," Physics of Fluids, Vol. 5, No. 9, September 1962.
105. Marrone, P.V. and Treanor, C.E.: "Chemical Relaxation with Preferential Dissociation from Excited Vibrational Levels," Cornell Aeronautical Laboratories, Rpt. No. QM-1626-A-10, February 1963.
106. Maronne, P.V.: "Inviscid Nonequilibrium Flow Behind Bow and Normal Shock Waves, Part I - General Analysis and Numerical Examples," Cornell Aeronautical Laboratories, Rpt. No. QM-1626-A-12 (I), May 1963.
107. Lee, R.H. and Chu, S.T.: "Nonequilibrium Inviscid Flow about Blunt Bodies," Aerospace Corp., Rpt. No. TDR-269 (4560-10)-2, January 1964.
108. Shih, W.C.L., Baron, J.R., Krupp, R.S. and Towle, W.J.: "Nonequilibrium Blunt Body Flow Using the Method of Integral Relations," Massachusetts Institute of Technology, TR-66, May 1966.
109. Shih, W.C.L. and Baron, J.R.: "Nonequilibrium Blunt Body Flow Using the Method of Integral Relations," AIAA Journal, Vol. 2, No. 6, pp. 1062-1071, June 1964.
110. Bloom, M.H. and Ting, L.: "On Near Equilibrium and Near Frozen Behavior of One-Dimensional Flow," Polytechnic Institute of Brooklyn, PIBAL R-525, July 1960.

111. Bloom, M.H. and Steiger, M.H.: "Inviscid Flow with Nonequilibrium Molecular Dissociation for Pressure Distributions Encountered in Hypersonic Flight," *Journal of Aerospace Sciences*, Vol. 27, No. 11, pp. 821-835, November 1960.
112. Vaglio-Laurin, R. and Bloom, M.H.: "Chemical Effects in External Hypersonic Flows," *Hypersonic Flow Research*, Vol. 7, pp. 205-254, Academic Press, New York, 1962.
113. Lin, S.C. and Teare, J.D.: "A Streamtube Approximation for Calculations of Reaction Rates in the Inviscid Flow Field of Hypersonic Objects," AVCO Corp. Res. Note 223, August 1961; also Proceedings of AF/Aerospace Corp. Symposium on Ballistic Missile and Aerospace Technology, 1961.
114. Eschenroeder, A.G.: "Ionization Nonequilibrium in Expanding Flows," *ARS Journal*, Vol. 32, No. 2, February 1962.
115. Eschenroeder, A.G., Boyer, D.W. and Hall, J.G.: "Nonequilibrium Expansions of Air with Coupled Chemical Reactions," *Cornell Aeronautical Laboratories*, Rpt. AF-1413-A-1, May 1961; also *Physics of Fluids Journal*, Vol. 5, No. 5, May 1962.
116. Hall, J.G., Eschenroeder, A.G. and Marrone, P.V.: "Inviscid Hypersonic Airflows with Coupled Nonequilibrium Processes," *Cornell Aeronautical Laboratories*, Rpt. AF-1413-A-2, May 1962; also *IAS Paper No. 62-67*, January 1962.
117. Lordi, J.A., Mates, R.E. and Moselle, J.R.: "Computer Program for the Numerical Solution of Nonequilibrium Expansions of Reacting Gas Mixtures," *NASA CR-472*, May 1966; *Cornell Aeronautical Laboratories*, Rpt. No. AD-1689-A-6, October 1965.

118. McMennamin, D. and O'Brien, M.: "The Finite Difference Solution of Multicomponent Nonequilibrium Steady Inviscid Streamtube Flows Using a Novel Stepping Technique, Part I - Analysis and Applications," General Electric Co., TIS 67SD241, April 1967.
119. Karydas, A.D.: "Computer Program for the Inviscid Flow Field about Bodies Traveling at Supersonic Speeds - Air in Chemical Equilibrium, Frozen Flow Chemistry and One-Dimensional Nonequilibrium Chemistry along Streamlines," Philco-Ford, SRS/NBO Rpt. METN 119, December 1967.
120. Chem, T. and Eschenroeder, A.G.: "A Fortran Computer Code for Inviscid Nonequilibrium Streamtube Flow," General Motors Corp., TR65-01P, December 1965; also AD 476-192.
121. Dresser, H.S., French, E.P. and Webb, H.G., Jr.: "Computer-Program for One-Dimensional Nonequilibrium Reacting Gas Flow," Air Force Flight Dynamics Laboratory, TR-67-75, June 1967.

### 3.1.3.2 Boundary Layer

#### 3.1.3.2.1 Equilibrium or Ideal Gas

##### 3.1.3.2.1.1 First Order Theory.

122. Hayes, W.D. and Probstein, R.F.: Hypersonic Flow Theory, pp. 284-306, Academic Press Inc., New York, 1959.
123. Libby, P.A.: "The Homogeneous Boundary Layer at an Axisymmetric Stagnation Point with Large Rates of Injection," *Journal of Aerospace Sciences*, Vol. 29, No. 1, pp. 48-60, January 1962.
124. Weston, K.C.: "The Stagnation Point Boundary Layer with Suction and Injection in Equilibrium Dissociating Air," NASA TND-3889, March 1967.

125. Herring, T. K.: "The Boundary Layer Near the Stagnation Point in Hypersonic Flow Past a Sphere," *Journal of Fluid Mechanics*, Vol. 7, pp. 257-272, 1959
126. Hoshizaki, H. and Smith, H. J.: "Axisymmetric Stagnation Point Mass - Transfer Cooling," *Lockheed Aircraft Corp.*, LMSD-48379, December 1958.
127. Howe, J. T. and Mersman, W. A.: "Solutions to the Laminar Compressible Boundary Layer Equations with Transpiration which are Applicable to the Stagnation Regions of Axisymmetric Blunt Bodies," *NASA TND-12*, August 1959.
128. Strom, C. R.: "Heat and Mass Transfer at a Three-Dimensional Stagnation Point," *General Electric Co.*, TIS 67SD363, December 1967.
129. Walter, S. A. and Anderson, R. B.: "Determination of the Aerodynamic Parameters in a Laminar Dissociated Boundary Layer," *North American Aviation Inc.*, SID 64-636, February 1964.
130. Grabow, R. M.: "Boundary Layer Analysis of a Slightly Blunted Ablating Cone," *Philco-Ford*, SR3/NBO 4462-37-36, October 1967.
131. Brant, D. N. and Burke, A. F.: "Ablative Effects on the Turbulent Boundary Layer of Conical Bodies," *Cornell Aeronautical Laboratories*, Rpt. No. UB-1376-S-123, August 1965.
132. Beckwith, I. E.: "Similarity Solutions for Small Cross Flows in Laminar Compressible Boundary Layers," *NASA TR R-107*, 1961.
133. Beckwith, I. E. and Cohen, N. B.: "Application of Similar Solutions to Calculation of Laminar Heat Transfer on Bodies with Yaw and Large Pressure Gradient in High Speed Flow," *NASA TND-625*, January 1961.

134. Polak, A. and Li, T. Y.: "The Three-Dimensional Boundary Layer Flow Over a Flat Delta Wing at a Moderate Angle of Attack," AIAA Journal, Vol. 5, No. 2, pp. 233-240, February 1967.
135. Kang, S. W., Rae, W. J. and Dunn, M. G.: "Effects of Mass Injection on Compressible, Three Dimensional, Laminar Boundary Layers with Small Secondary Flow," Cornell Aeronautical Laboratories, Rpt. No. AI-2187-A-2, August 1966.
136. Kang, S. W., Rae, W. J. and Dunn, M. G.: "Effects of Mass Injection on Compressible, Three-Dimensional, Laminar Boundary Layers," AIAA Journal, Vol. 5, No. 10, pp. 1738-1745, October 1967.
137. Moran, J. P.: "Application of Coverts Approximations for the Binary Boundary Layer to a Porous Cone with a Solid Tip," Massachusetts Institute of Technology, NSL Rpt. 442, June 1960.
138. Carlson, W. O.: "Integral Solutions for Compressible Binary Gas Laminar Boundary Layers," General Electric Co. Aerophysics Laboratory, TM No. 90, July 1958.
139. Liu, S. W. and Kuby, G. H.: "Interaction of Surface Chemistry and Mass Transfer in Nonsimilar Boundary Layer Flows," AIAA Journal, Vol. 5, No. 2, pp. 527-534, March 1967.
140. Kang, S. W.: "An Integral Method for Three Dimensional Compressible Laminar Boundary Layers with Mass Injection," Cornell Aeronautical Laboratories, Rpt. No. AI-2187-A-5, May 1967.
141. Li, T. Y.: "Laminar Boundary Layer on the Frontal Portion of a Blunt Body of Revolution at Hypersonic Speeds," General Electric Co. Advanced Aerodynamics, TM No. 10, December 1956.

142. Parr, W.: "Laminar Boundary Layer Calculations by Finite Differences," U.S. Naval Ordnance Laboratory, NOLTR 63-261, March 1964.
143. Krause, E.: "On the Numerical Solution of the Boundary Layer Equations," New York University, Rpt. NYU-AA-66-57, June 1966; also AD 637-851 and AIAA Journal, Vol. 5, No. 7, pp. 1231-1237, July 1967.
144. Krause, E.: "On Investigation of the Vorticity Interaction by Perturbation Techniques," New York University, Rpt. NYU-AA-66-64, October 1966; also AD 644 026.
145. Waiter, S.A. and Anderson, R.B.: "Solution of the Laminar Boundary Layer Equations by an Implicit Finite Difference Method," North American Rockwell Corp., SD 67-587, November 1967.
146. Flugge-Lotz, I. and Blottner, F.G.: "Computation of the Compressible Laminar Boundary Layer Flow Including Displacement Thickness Interaction Using Finite Difference Methods," Stanford University, Rpt. No. 131, 1962.
147. Fannelop, T.K.: "A Method of Solving the Three-Dimensional Laminar Boundary Layer Equations with Application to a Lifting Re-entry Body," AVCO Corp., AVMSD-0209-66-RM, August 1966; also AD 637 679.
148. Raetz, G.S.: "A Method of Calculating Three-Dimensional Laminar Boundary Layers of Steady Compressible Flows," Northrop Aircraft Inc., Rpt. No. NAI-58-73-BLC-114, December 1957.
149. Der, J., Jr. and Raetz, G.S.: "Solution of General Three-Dimensional Laminar Boundary Layer Problems by an Exact Numerical Method," IAS Paper No. 62-70, January 1962.

150. Crocco, L.: "Transformations of the Compressible Turbulent Boundary Layer with Heat Exchange," AIAA Journal, Vol. 1, No. 12, pp. 2723-2731, December 1963.
151. Denison, M.R.: "The Turbulent Boundary Layer on Chemically Active Ablating Surface," Journal of Aerospace Sciences, Vol. 28, No. 6, pp. 471-479, June 1961.

3.1.3.2.1.2 Second Order Theory.

152. Van Dyke, M.: "Second-Order Compressible Boundary Layer Theory with Application to Blunt Bodies in Hypersonic Flow," Hypersonic Flow Research, Academic Press Inc., New York, pp. 37-76, 1962; also Stanford University, Rpt. AFOSR-TN-61-1270, July 1961.
153. Van Dyke, M.: "Higher Approximations in Boundary Layer Theory, Part I," Journal of Fluid Mechanics, Vol. 14, pp. 161-177, 1962.
154. Van Dyke, M.: "A Review and Extension of Second-Order Hypersonic Boundary Layer Theory," Rarefied Gas Dynamics Vol. II, Supplement 2, Academic Press Inc., New York, pp. 212-227, 1963.
155. Lewis, C.H.: "First and Second Order Boundary Layer Effects at Hypersonic Conditions," Presented at the AGARD Seminar on Numerical Methods for Viscous Flows, September 1967.
156. Marchand, E.O., Lewis, C.H., and Davis, R.T.: "Second-Order Boundary Layer Effects on a Slender Blunt Cone at Hypersonic Conditions," AIAA Paper No. 68-54, January 1968.
157. Adams, J.C., Jr.: "Higher Order Boundary Layer Effects on Analytical Bodies of Revolution," Presented at the AGARD Seminar on Numerical Methods for Viscous Flows, September 1967.

158. Davis, R. T. and Flugg-Lotz, I.: "Laminar Compressible Flow Past Axisymmetric Blunt Bodies (Results of Second-Order Theory)," Stanford University, TR-143, 1963.
159. Smith, A. M. O. and Clutter, D. W.: "Solution of Prandtl's Boundary Layer Equations," Douglas Aircraft Co., Paper 1530, February 1963.
160. Clutter, D. W. and Smith, A. M. O.: "Solution of the General Boundary Layer Equations for Compressible Laminar Flow, Including Transverse Curvature," Douglas Aircraft Co., Rpt. LB31088, February 1963.
161. Smith, A. M. O. and Clutter, D. W.: "Machine Calculation of Compressible Laminar Boundary Layers," AIAA Journal, Vol. 3, No. 4, pp. 639-647, April 1965.
162. Jaffe, N. A., Lind, R. C. and Smith, A. M. O.: "Solution to the Binary Diffusion Laminar Boundary Layer Equations with Second-Order Transverse Curvature," AIAA Journal, Vol. 5, No. 9, pp. 1563-1569, September 1967.
1663. Lewis, C. H. and Whitfield, J. D.: "Theoretical and Experimental Studies of Hypersonic Viscous Effects," AFARD Monograph 97 (Recent Developments in Boundary Layer Research) Part III, May 1965; also AEDC-TR-65-100, May 1965.
164. Mayne, A. W., Jr., Gilley, G. E. and Lewis, C. H.: "Binary Boundary Layers on Sharp Cones in Low Density Supersonic and Hypersonic Flow," AIAA Paper No. 68-66, January 1968.
165. Levine, J. N.: "Finite Difference Solution of the Laminar Boundary Layer Equations Including the Effects of Transverse Curvature, Vorticity and Displacement Thickness," General Electric Co., TIS 66SD349, December 1966.

166. Maslen, S.H.: "Second-Order Effects in Laminar Boundary Layers," AIAA Journal Vol. 1, No. 1, pp. 33-40, January 1963.
167. Yasuhara, M.: "Axisymmetric Viscous Flow Past Very Slender Bodies of Revolution," Journal of Aerospace Sciences, Vol. 29, No. 6, pp. 667-679, June 1962.
168. Probst, R.F. and Elliot, D.: "Transverse Curvature Effects in Compressible Axisymmetric Laminar Boundary Layer Flow," Journal of Aeronautical Sciences, Vol. 23, No. 3, pp. 208-224, March 1956.
169. Sagendorph, F.E.: "Hypersonic Flow Over a Slender Axisymmetric Body with Mass Addition," General Electric Co., ATFM 65-9, July 1965.

#### 3.1.3.2.2 Nonequilibrium Gas

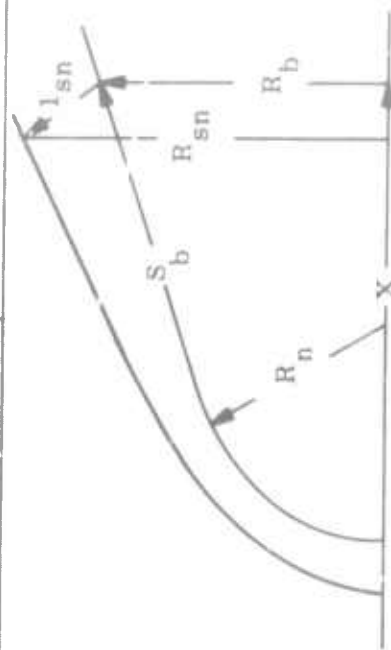
##### 3.1.3.2.2.1 First Order Theory.

170. Dorrance, W.H.: Viscous Hypersonic Flow, pp. 22-38, McGraw-Hill Book Co., Inc., New York, 1962.
171. Fay, J.A. and Riddell, F.R.: "Theory of Stagnation Point Heat Transfer in Dissociated Air," Journal of Aerospace Sciences, Vol. 25, No. 2, pp. 73-85, February 1958.
172. Fay, J.A. and Kaye, H.: "A Finite-Difference Solution of Similar Nonequilibrium Boundary Layers," AIAA Journal, Vol. 5, No. 11, pp. 1949-1954, November 1967; also AIAA Paper No. 67-219.
173. Moore, J.A. and Pallone, A.: "Similar Solutions to the Laminar Boundary Layer Equations for Nonequilibrium Air," AVCO Corp., Rpt. No. RAD-TR-62-59, July 1962.
174. Libby, P.A. and Pierucci, M.: "Laminar Boundary Layer with Hydrogen Injection Including Multicomponent Diffusion," AIAA Journal, Vol. 2, No. 12, pp. 2118-2126, December 1964.

175. Libby, P.A. and Liu, T.: "Laminar Boundary Layers with Surface Catalyzed Reactions," *Physics of Fluids*, Vol. 9, No. 3, pp. 436-445, March 1966.
176. Lenard, M.: "Chemically Reacting Boundary Layers," General Electric Co., Space Sciences Lab., TIS R64SD14, March 1964.
177. Lenard, M.: "Ionization of Cesium and Sodium Contaminated Air in the Hypersonic Slender Body Boundary Layer," General Electric Co., Space Sciences Lab., TIS R64SD22, August 1964.
178. Pallone, A.J., Moore, J.A. and Erdos, J.I.: "Nonequilibrium, Nonsimilar Solutions of the Laminar Boundary Layer Equations," *AIAA Journal*, Vol. 2, No. 10, pp. 1706-1713, October 1964; also AIAA Paper No. 64-50, January 1964.
179. Smith, A.M.O. and Jaffe, N.A.: "General Method for Solving the Nonequilibrium Boundary Layer Equations of a Dissociating Gas," *AIAA Journal*, Vol. 4, No. 4, pp. 611-620, April 1966; also AIAA Paper No. 65-129.
180. Blottner, F.G.: "Nonequilibrium Laminar Boundary Layer Flow of a Binary Gas," General Electric Co., Space Sciences Lab., TIS R63SD17, June 1963; also *AIAA Journal*, Vol. 2, No. 2, pp. 232-240, February 1964.
181. Blottner, F.G.: "Nonequilibrium Laminar Boundary Layer Flow of Ionized Air," General Electric Co., Space Sciences Lab., TIS R64SD56, November 1964; also AIAA Paper No. 64-41.
182. Blottner, F.G.: "Chemically Reacting Boundary Layers with Ablation Products and Nose Bluntness Effects," General Electric Co., TIS 67SD468, June 1967 (Confidential); also AD 382-026.

Table 3-3. Summary of Geometric Variables for Selected Body Surface Normals

$s_b/R_N$	$X/R_n$ $Y = 0$	$R_b/R_n$	Altitude (kilo feet)	$(Y_{sn}/R_n)$ nonequilibrium	$(R_{sn}/R_n)$ eq or fr	$(R_{sn}/R_n)$ nonequilibrium
$4.962 \sqrt{-1}$	$1.206 \sqrt{-1}$	$4.761 \sqrt{-1}$	$5.000 \sqrt{1}$	$8.529 \sqrt{-2}$	$5.164 \sqrt{-1}$	$5.167 \sqrt{-1}$
			$1.000 \sqrt{2}$	7.989	5.133	5.141
			1.500	8.596	5.106	5.170
			2.000	$9.352 \sqrt{-1}$	5.093	5.206
			2.500	1.103	5.459	5.286
$6.125 \sqrt{1}$	$6.000 \sqrt{1}$	$9.934 \sqrt{0}$	$5.000 \sqrt{1}$	$1.706 \sqrt{0}$	$1.141 \sqrt{1}$	$1.162 \sqrt{1}$
			$1.000 \sqrt{2}$	1.440	1.130	1.136
			1.500	1.625	1.134	1.154
			2.000	1.598	1.131	1.151
			2.500	1.492	1.132	1.121
$2.432 \sqrt{2}$	$2.400 \sqrt{2}$	$2.716 \sqrt{1}$	$5.000 \sqrt{1}$	$5.352 \sqrt{0}$	$4.225 \sqrt{1}$	$4.245 \sqrt{1}$
			$1.000 \sqrt{2}$	4.800	4.191	4.196
			1.500	5.140	4.206	4.224
			2.000	5.154	4.241	4.225
			2.500	4.606	4.181	4.171



In Figures 3-1 through 3-10 the contrast between equilibrium and nonequilibrium effects at an altitude of 150 kilofeet is demonstrated by plotting the streamwise variation of the flow properties against the distance along the body surface for three streamlines which intersect the bow shock at angles of approximately 50, 70, and 89 degrees. In sequence, these plots show this variation for the pressure, temperature, density, velocity component parallel to the surface (all normalized by the corresponding free stream quantities), and the number densities of molecular oxygen, molecular nitrogen, atomic nitrogen, atomic oxygen, nitric oxide, and electrons. Before proceeding to a brief discussion of some of the more interesting aspects of these results, it should be pointed out that in Figure 3-1, due to the positive normal pressure gradient in the nose region, the higher shock angle streamlines initially expand more rapidly; however, in the over-expansion region this trend is reversed prior to converging at the cone surface pressure value.

For the nonequilibrium results shown in Figures 3-1 through 3-10, it may be noted that the flow on the 89 degree streamline is almost in equilibrium at the first normal. This is caused by its passage through the near stagnation region. At this point oxygen is almost entirely dissociated. As the flow continues to expand over the nose, atomic oxygen freezes in the nonequilibrium case, whereas for equilibrium it begins to recombine. This single feature, more than any other, determines the nonequilibrium effects which are indicated in these results.

In Figures 3-11 through 3-25, nose bluntness and altitude effects on the nonequilibrium flow properties are shown by plotting the flow properties against shock layer thickness, with altitude as a parameter, for three selected normals located along the body surface at  $s_b/R_N$  equal to 0.4962, 61.25, and 245.3. Sequentially in groups of three, the normal profiles are given for the pressure, temperature, density, and velocity parallel to the surface (all normalized by the corresponding free stream quantity) and the electron number density. Profiles of the remaining species number densities are presented in Table 3-4, 3-5, and 3-6 for the different altitudes at the selected normals. In Figure 3-26 the integral of the electron density across the shock layer is plotted against the normalized coordinate along the body surface with altitude as a parameter. Some of the more noteworthy aspects of the results are discussed in the following paragraphs.

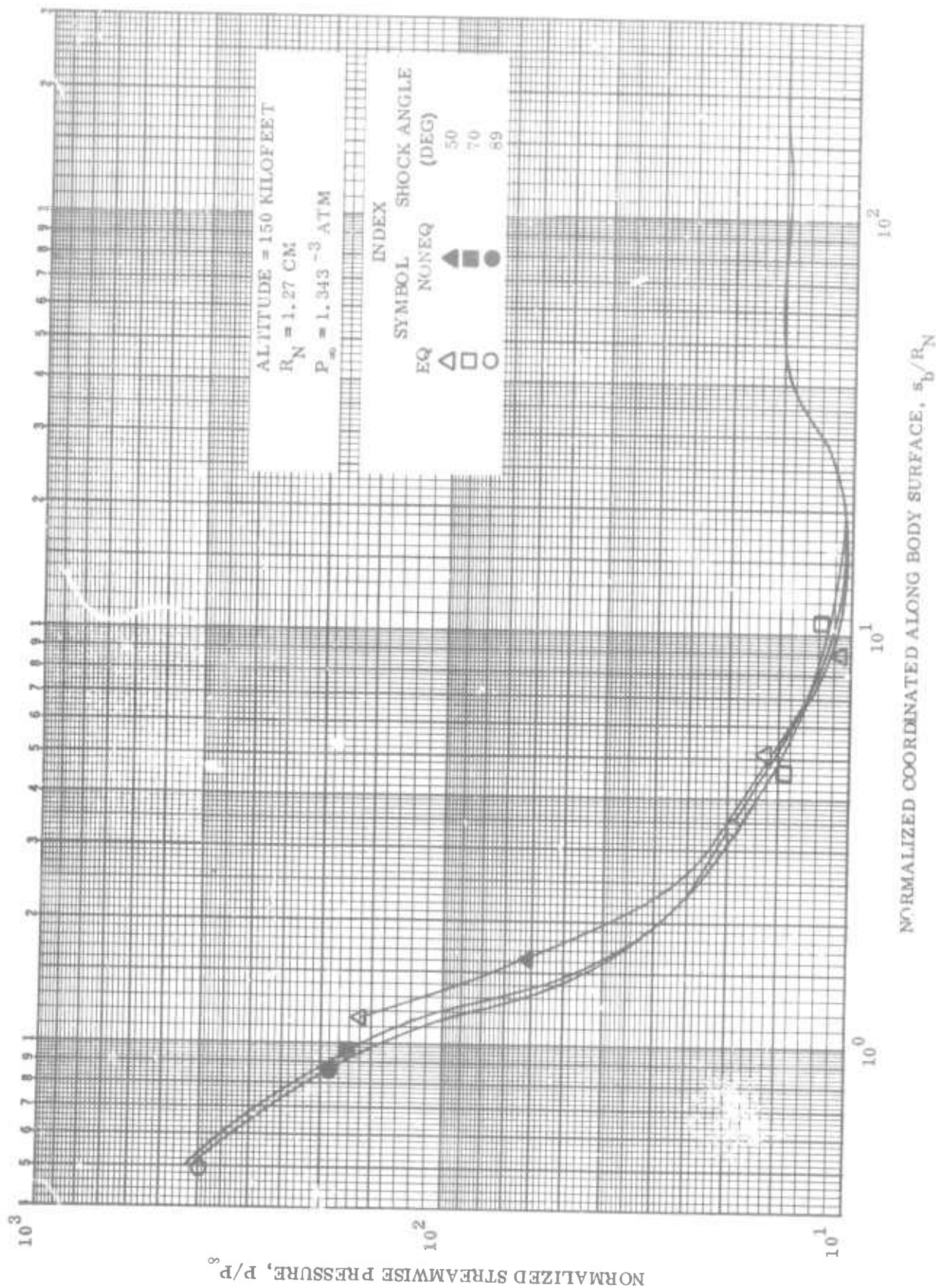


Figure 3-1. Streamwise Variation of Normalized Pressure vs. Normalized Coordinate Along Body Surface

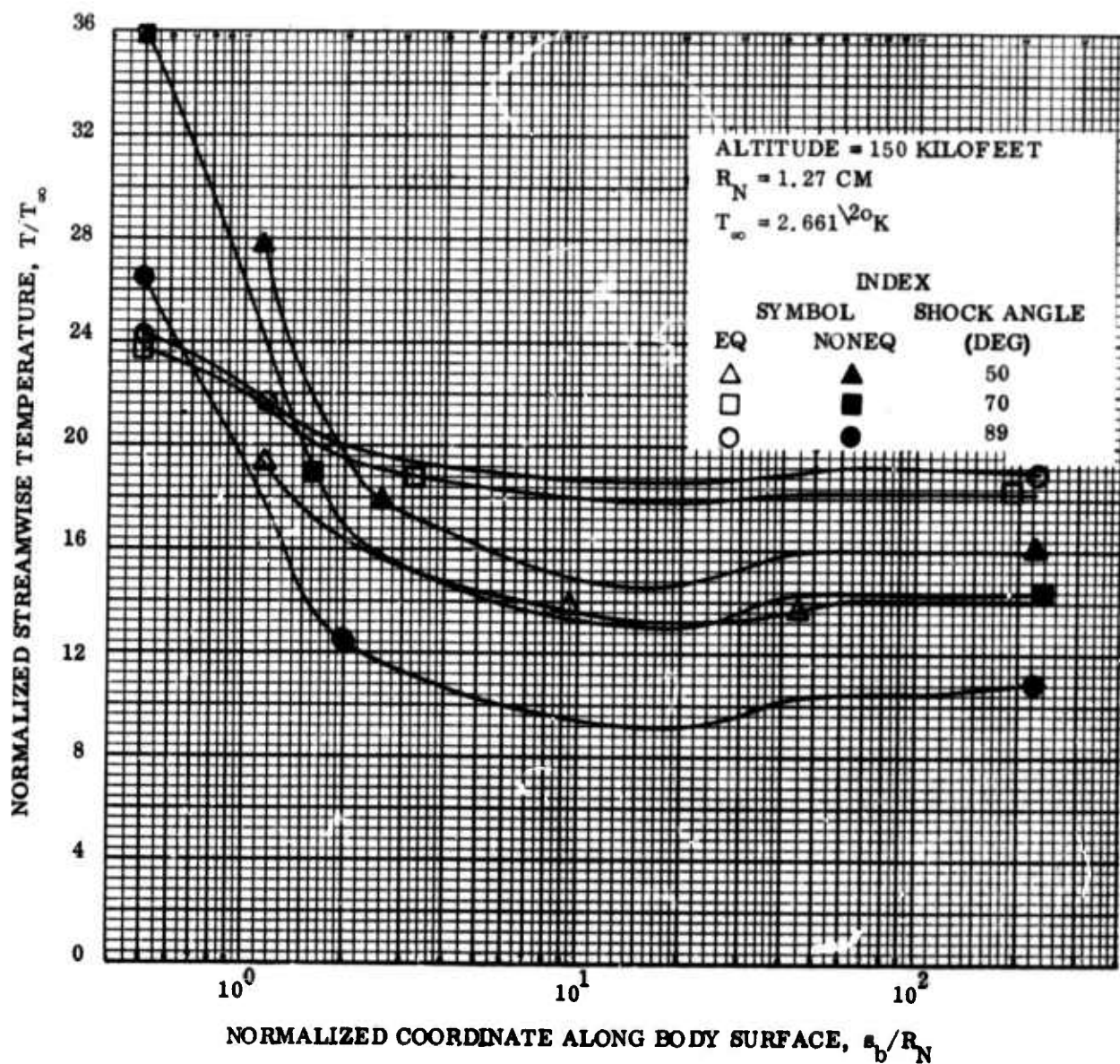


Figure 3-2. Streamwise Variation of Normalized Temperature vs. Normalized Coordinate Along Body Surface

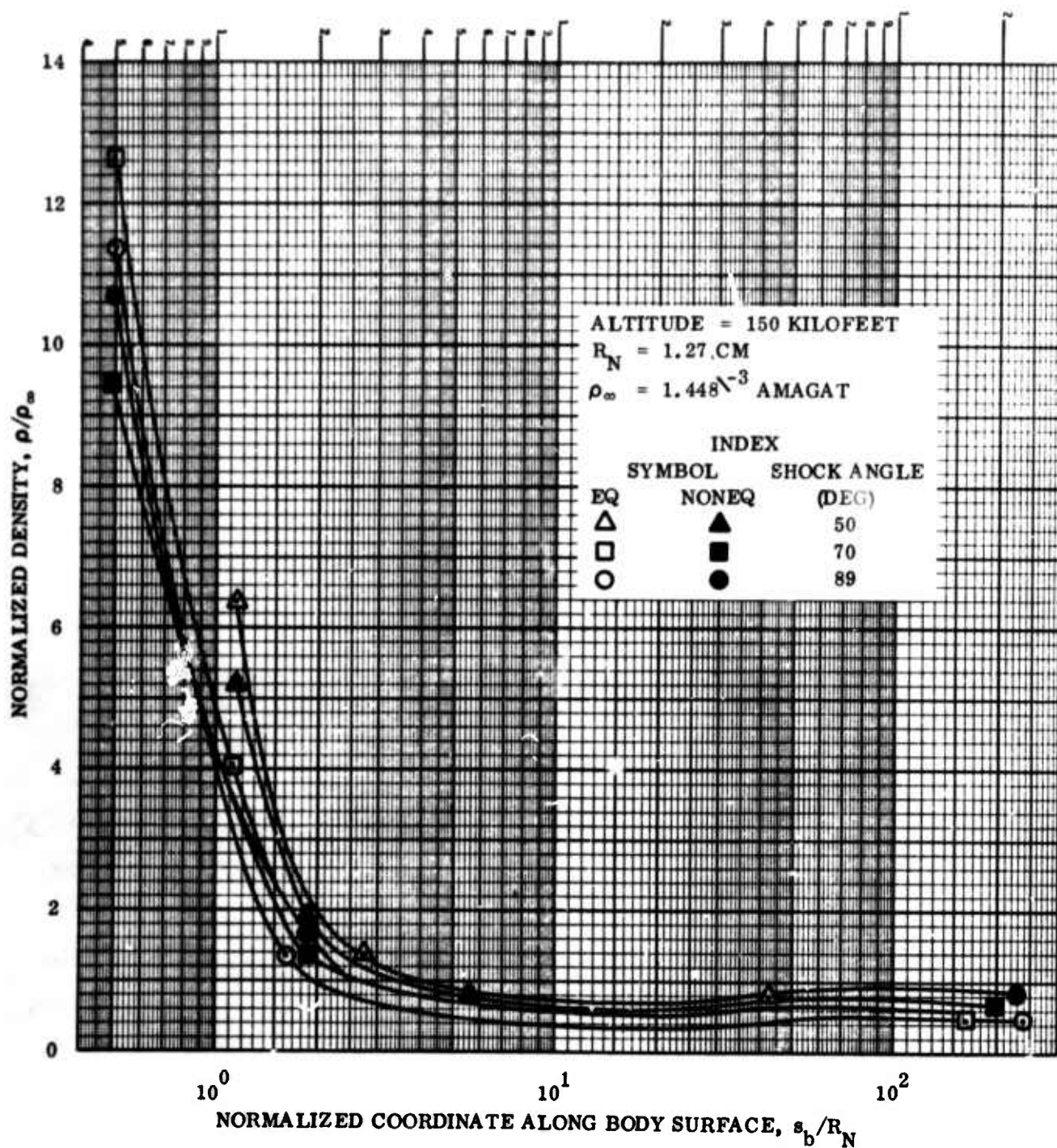


Figure 3-3. Streamwise Variation of Normalized Density vs. Normalized Coordinate Along Body Surface

NORMALIZED VELOCITY PARALLEL TO SURFACE

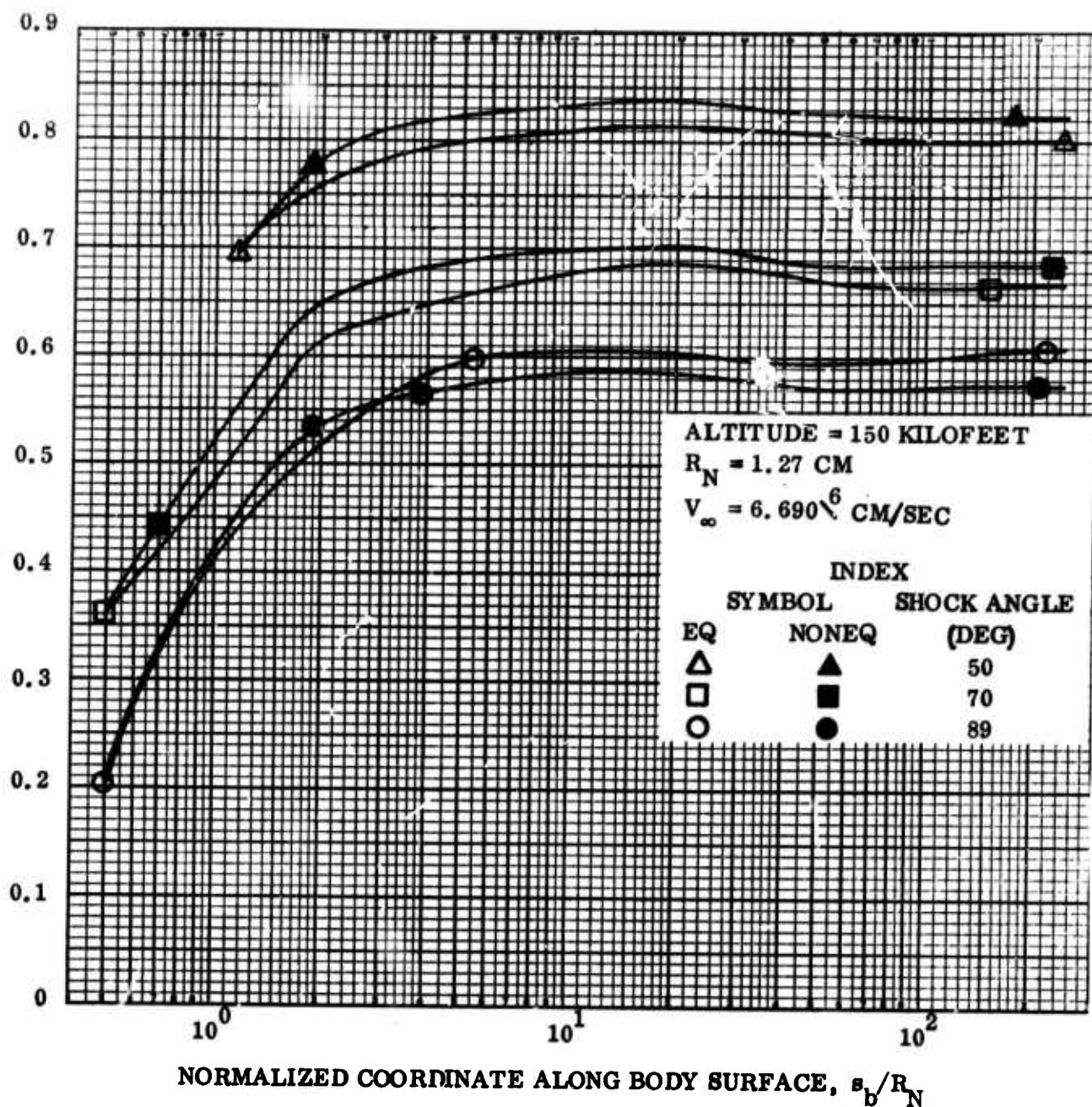


Figure 3-4. Streamwise Variation of Normalized Velocity Parallel to Surface vs. Normalized Coordinate Along Body Surface

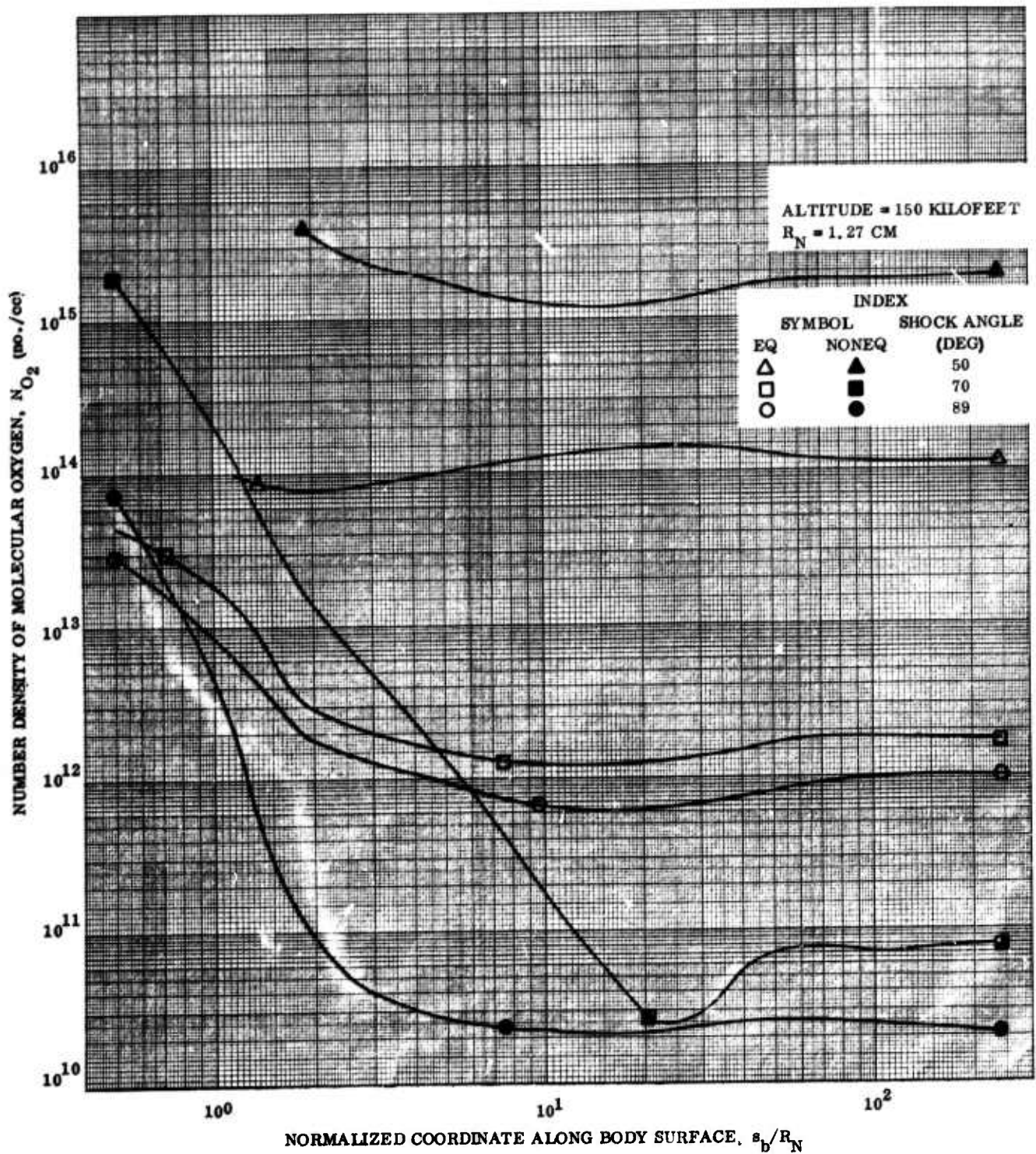


Figure 3-5. Streamwise Variation of Molecular Oxygen Number Density vs. Normalized Coordinate Along Body Surface

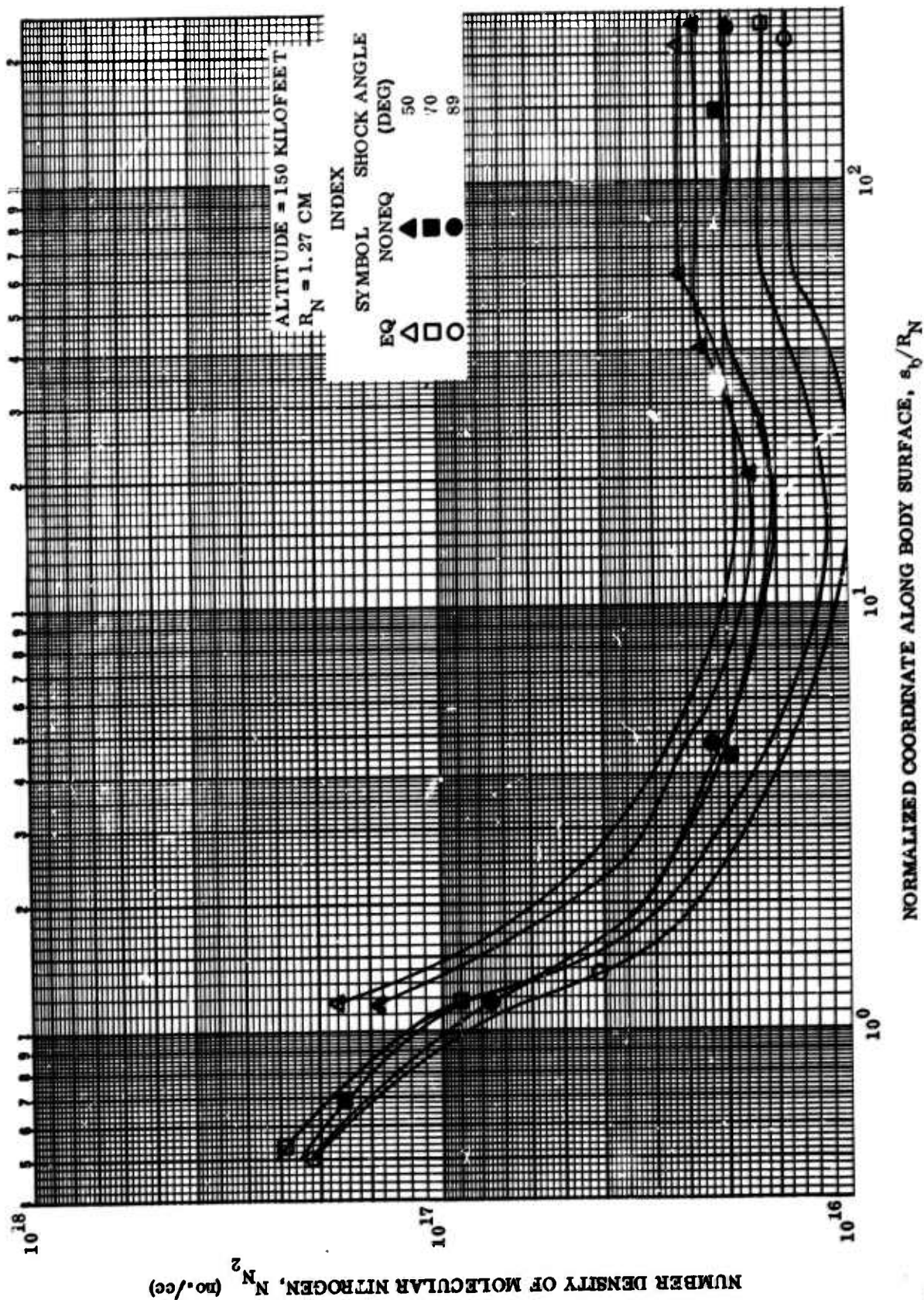


Figure 3-6. Streamwise Variation of Molecular Nitrogen Number Density vs. Normalized Coordinate Along Body Surface

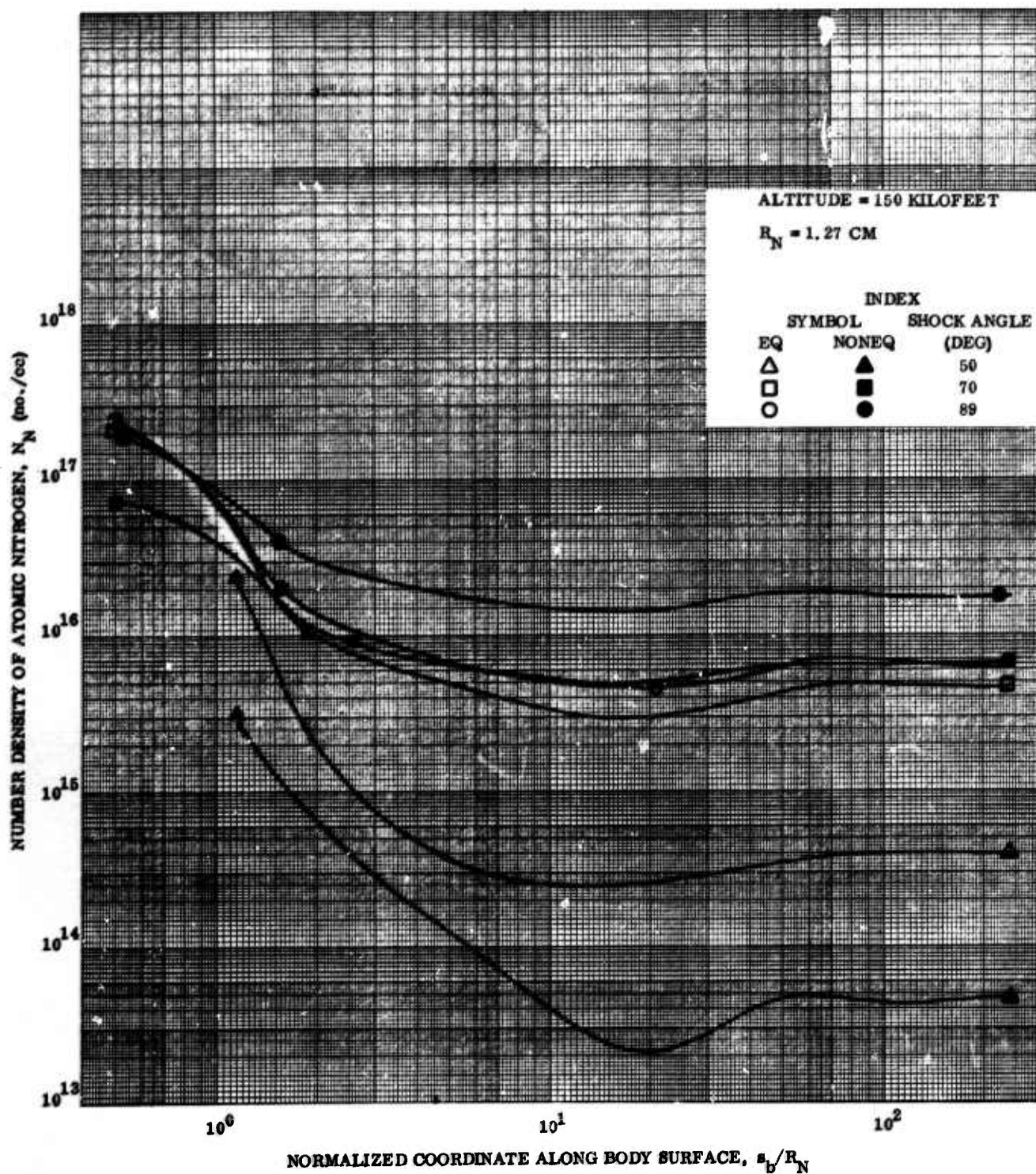


Figure 3-7. Streamwise Variation of Atomic Nitrogen Number Density vs. Normalized Coordinate Along Body Surface

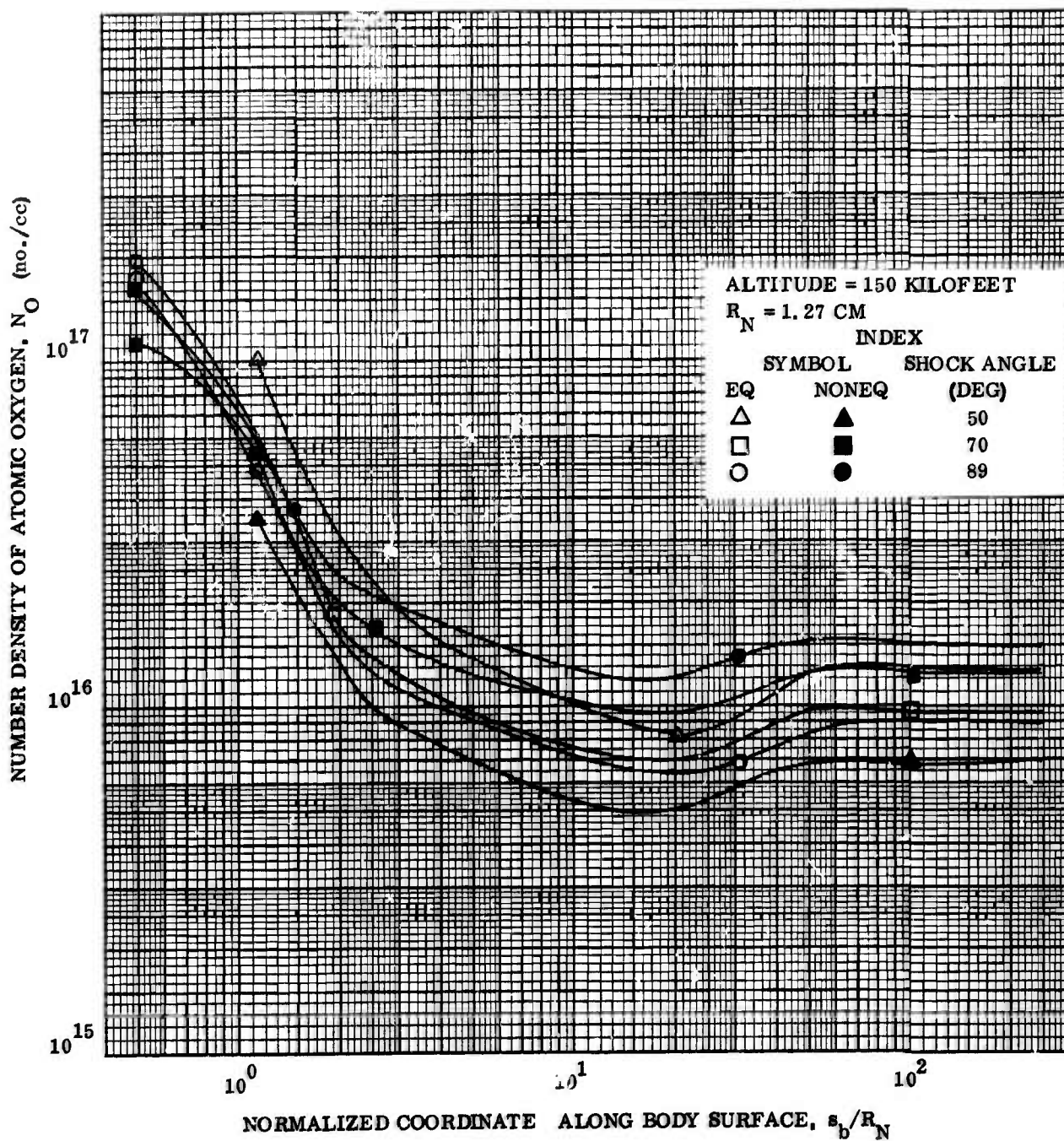


Figure 3-8. Streamwise Variation of Atomic Oxygen Number Density vs. Normalized Coordinate Along Body Surface

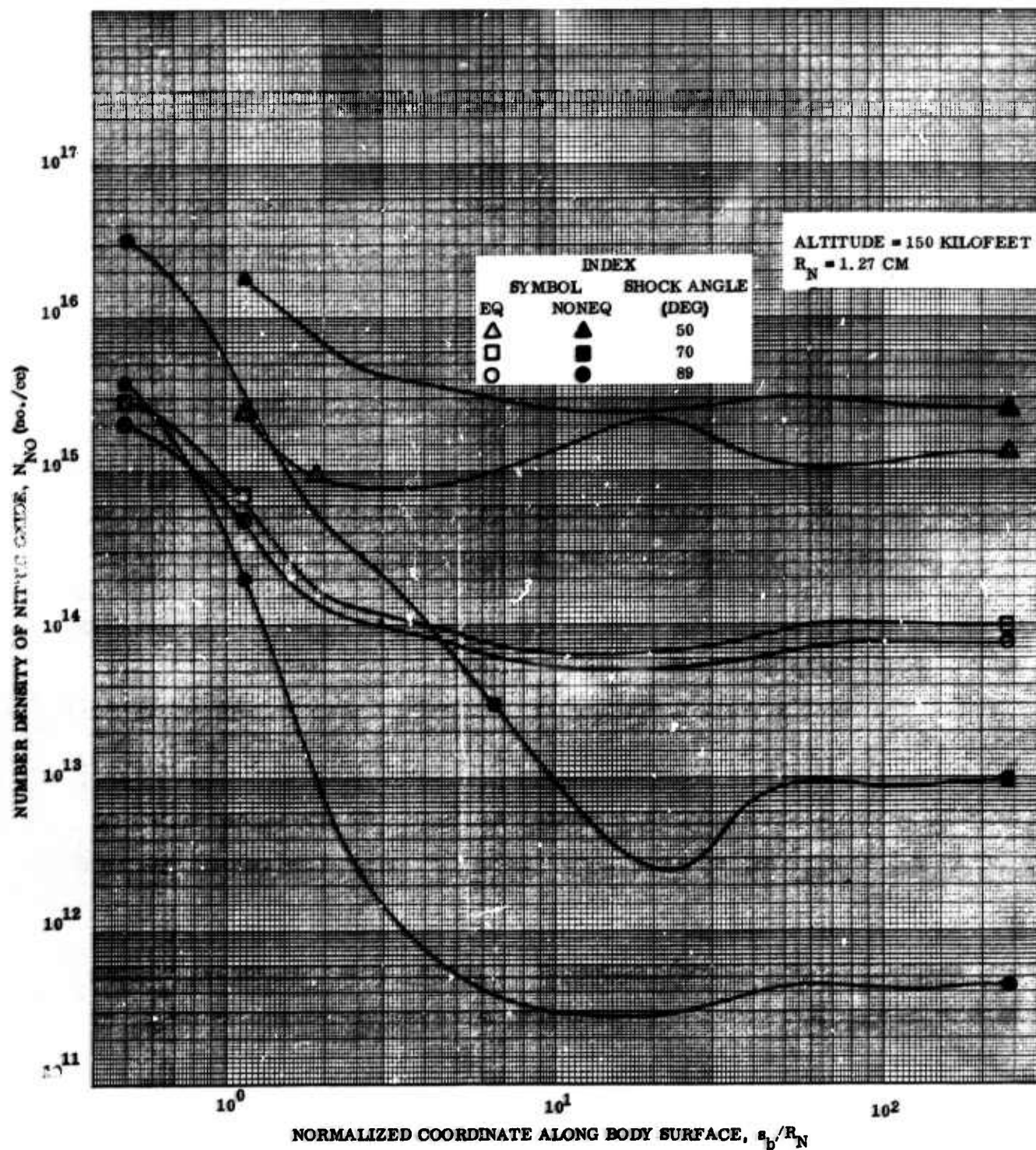


Figure 3-9. Streamwise Variation of Nitric Oxide Number Density vs. Normalized Coordinate Along Body Surface

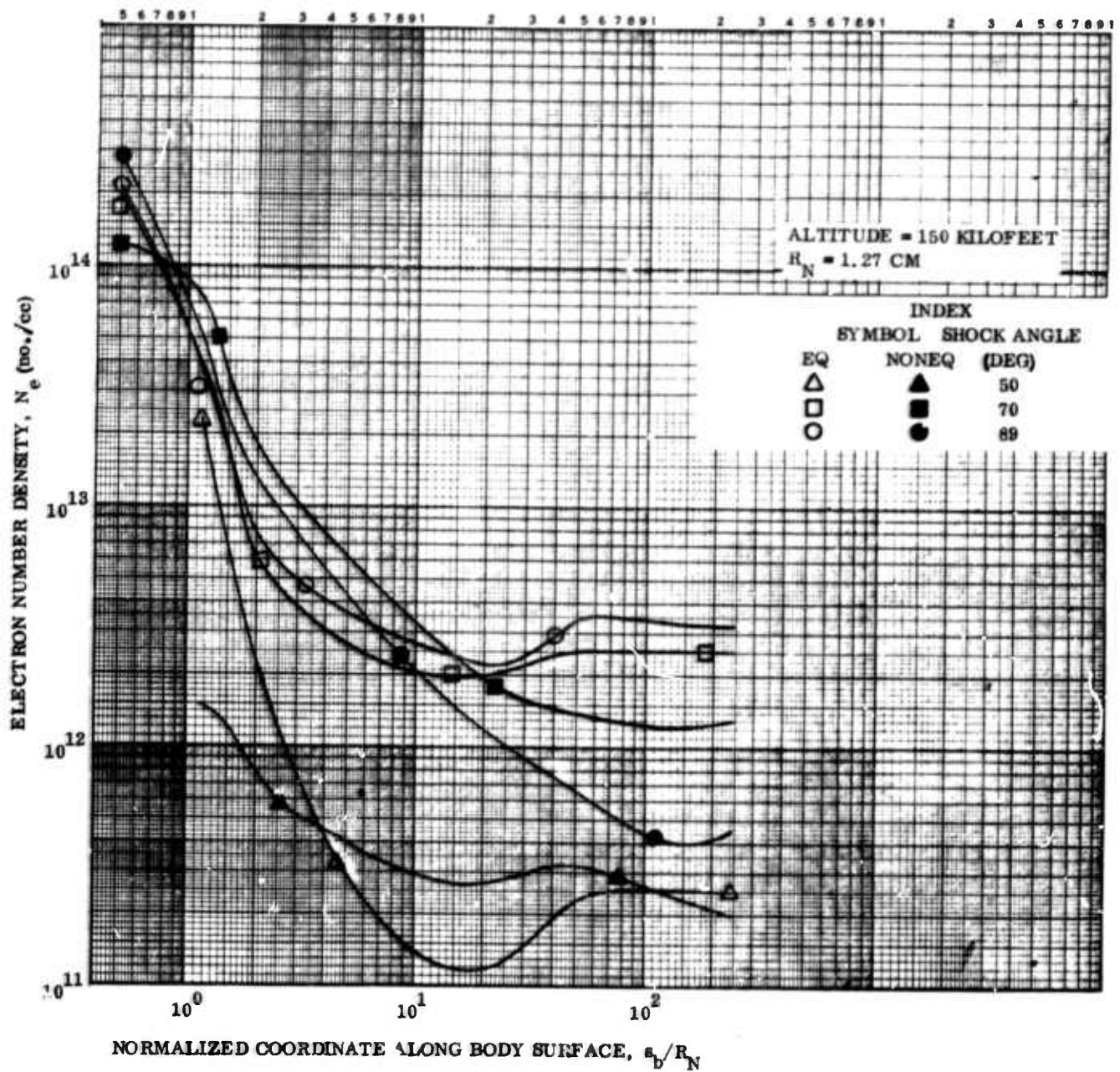


Figure 3-10. Streamwise Variation of Electron Number Density vs. Normalized Coordinate Along Body Surface

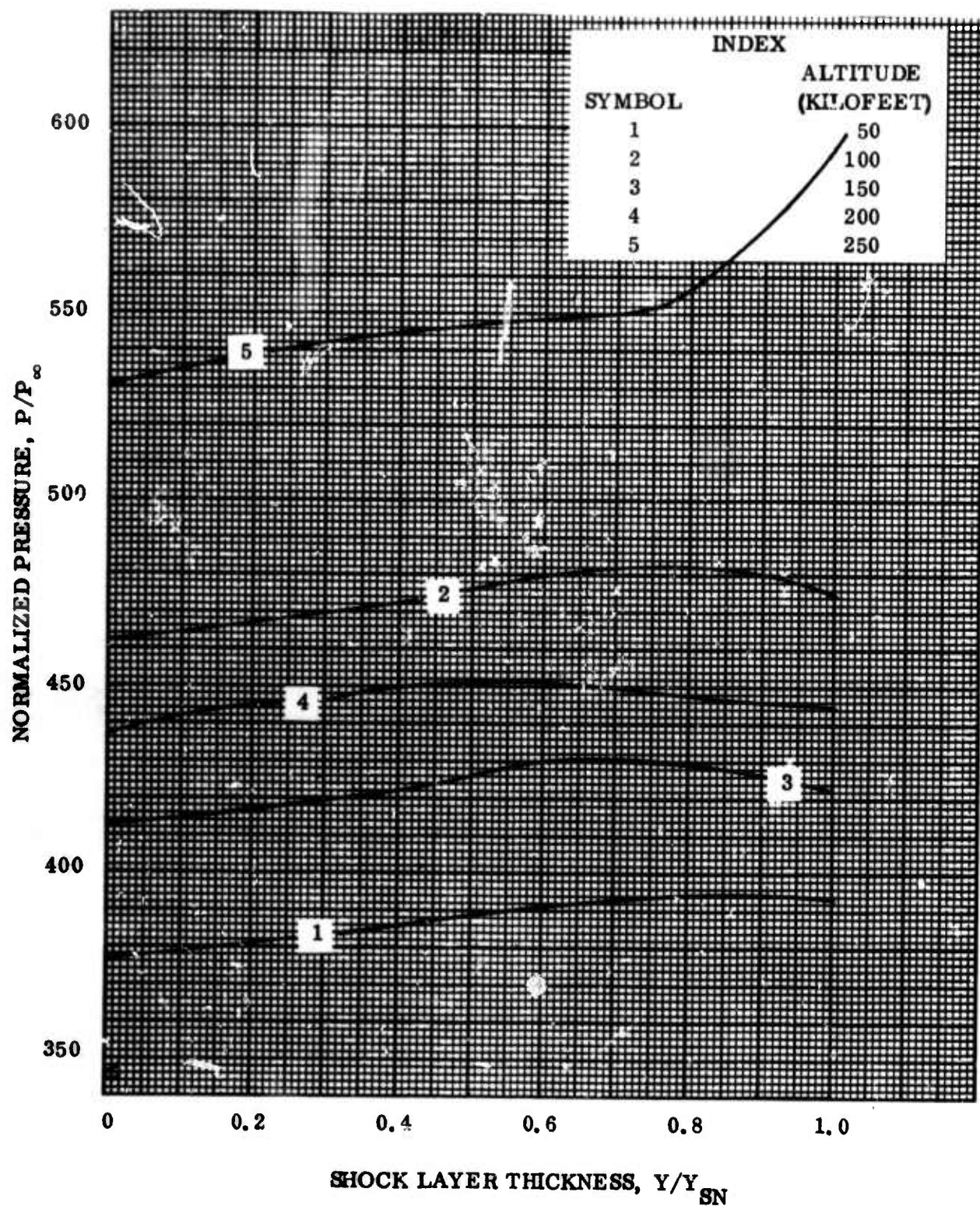


Figure 3-11. Normalized Pressure vs. Shock Layer Thickness;  $s_b/R_N = 4.962^{-1}$ ; Nonequilibrium

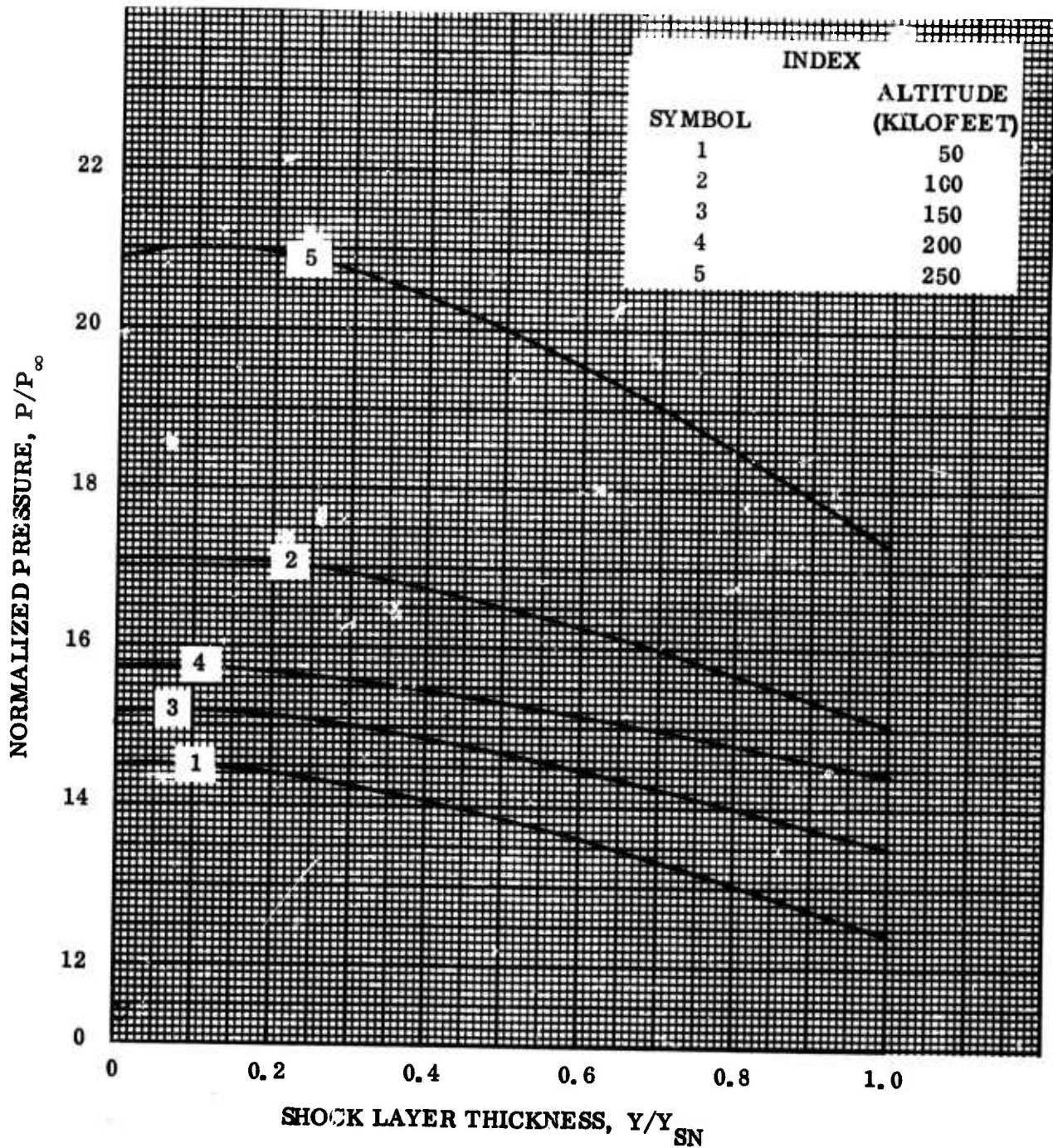


Figure 3-12. Normalized Pressure vs. Shock Layer Thickness;  $s_b/R_N = 6.125^{1/2}$ ; Nonequilibrium

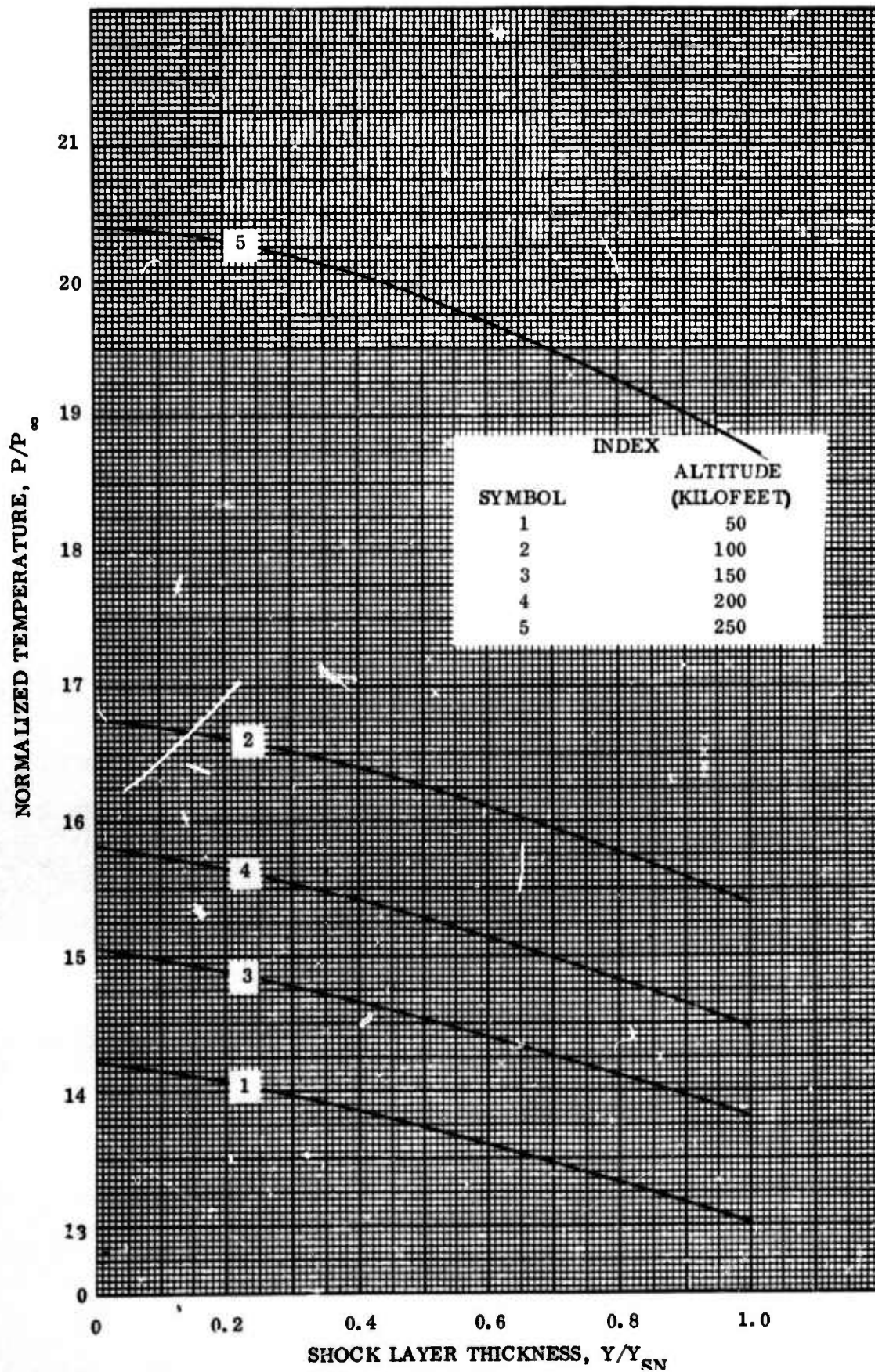


Figure 3-13. Normalized Pressure vs. Shock Layer Thickness;  $s_b/R_N = 2.433^{1/2}$ ; Nonequilibrium

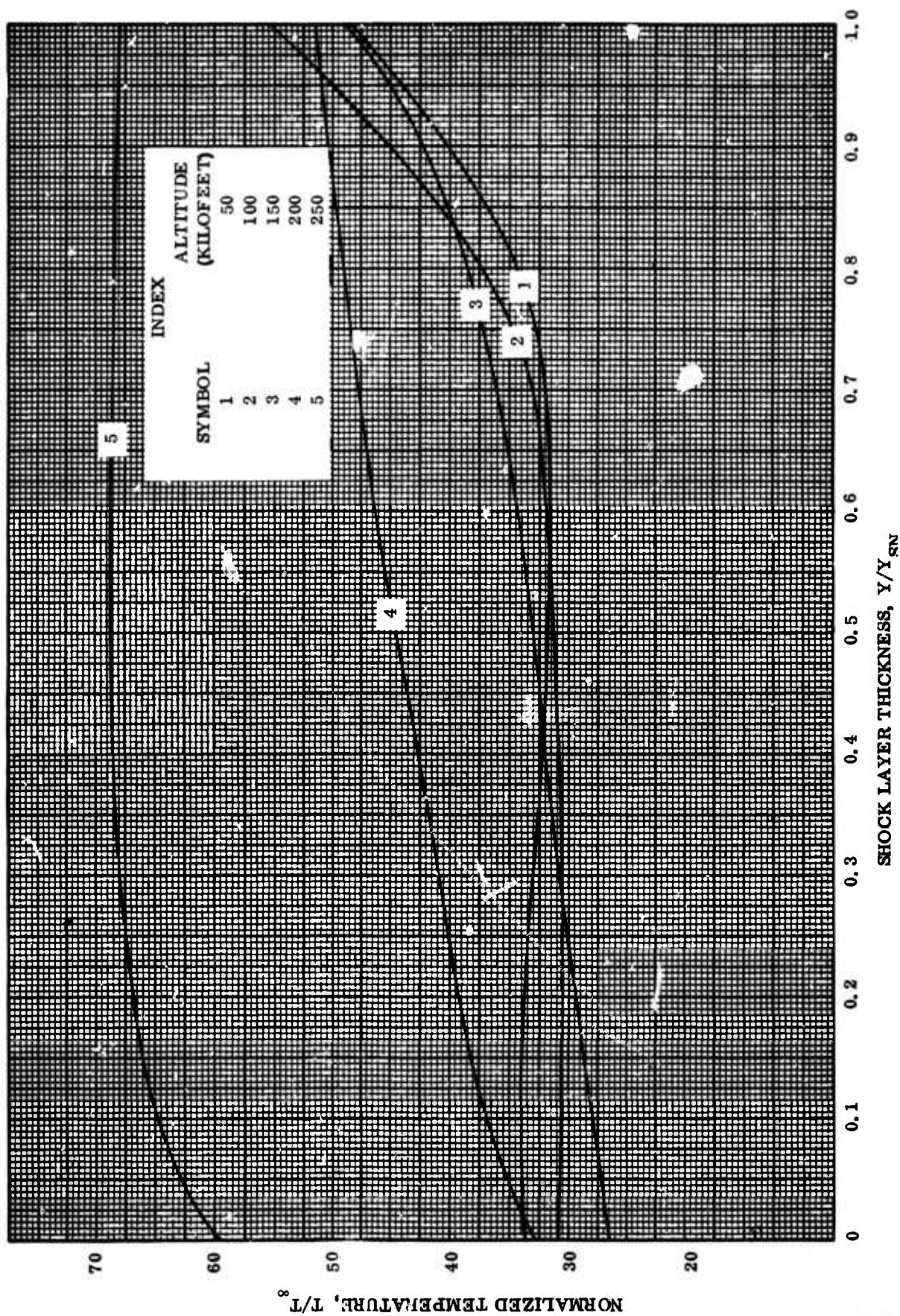


Figure 3-14. Normalized Temperature vs. Shock Layer Thickness;  $s_b/R_N = 4.962 \times 10^{-1}$ ;  
Norequilibrium

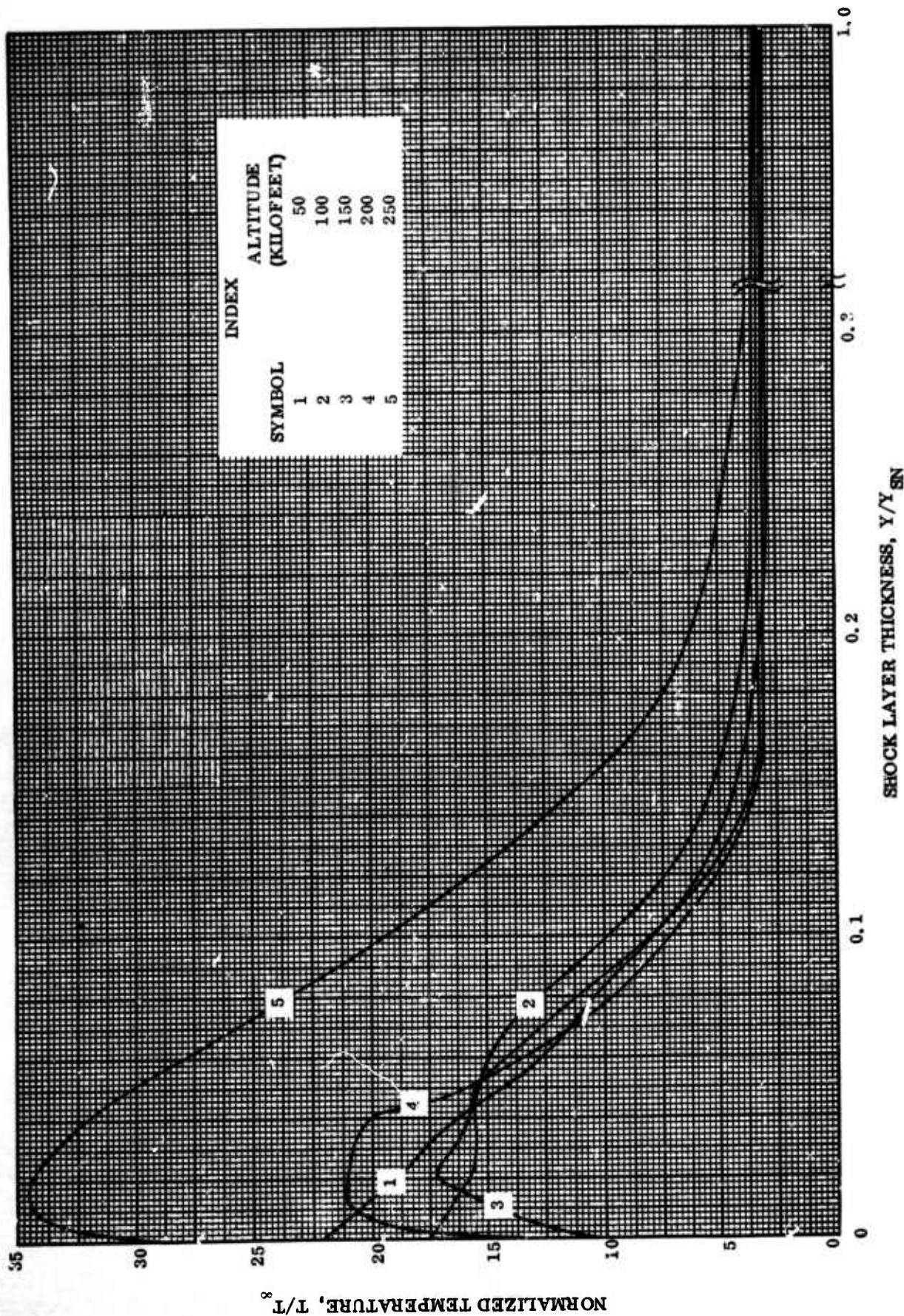


Figure 3-15. Normalized Temperature vs. Shock Layer Thickness;  $s_b/R_N = 6.125 \sqrt{1}$ ; Nonequilibrium

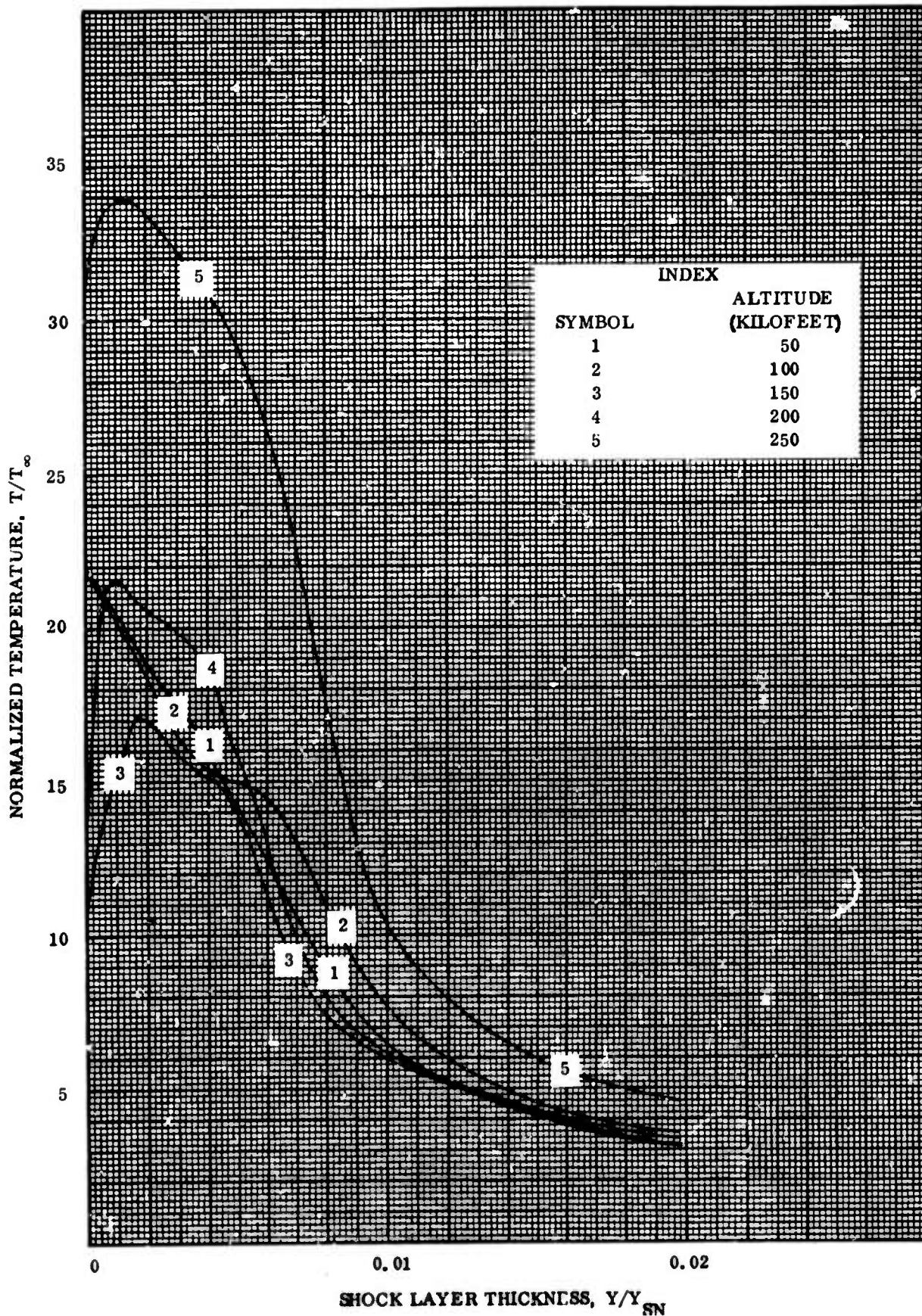


Figure 3-16. Normalized Temperature vs. Shock Layer Thickness;  $s_b/R_N = 2.433^{1/2}$ ; Nonequilibrium

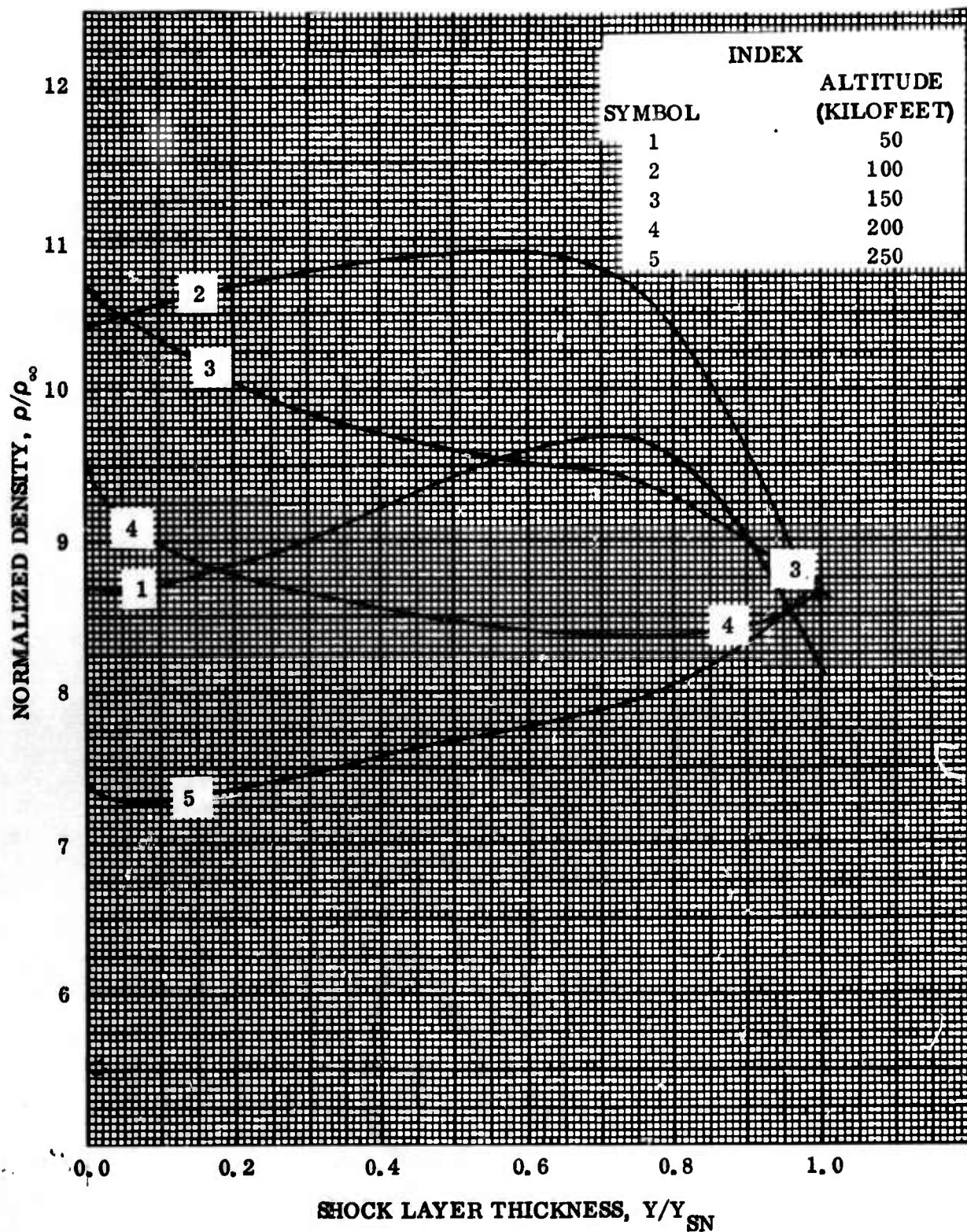


Figure 3-17. Normalized Density vs. Shock Layer Thickness;  $s_b/R_N = 4.962 \times 10^{-1}$

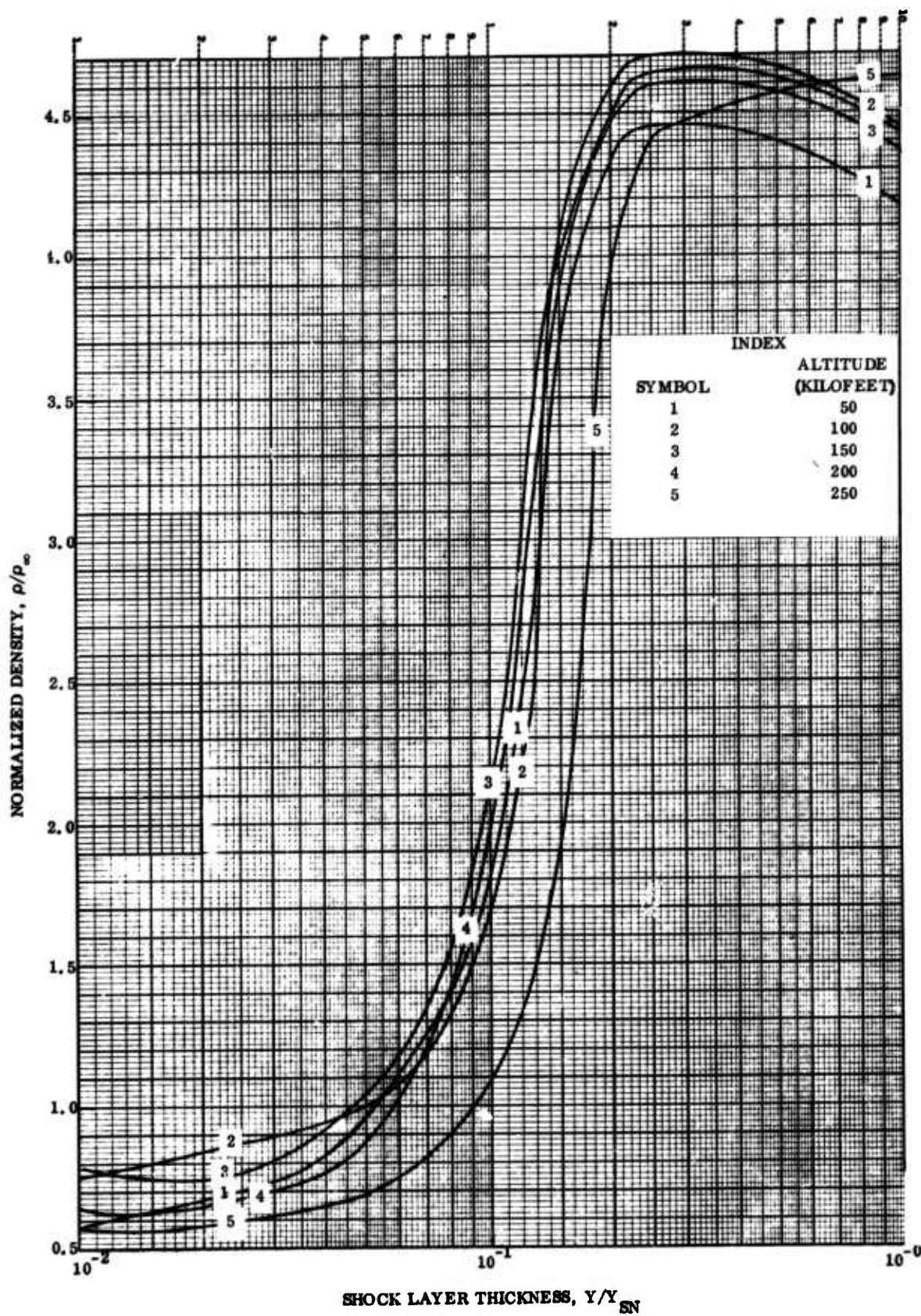


Figure 3-18. Normalized Density vs. Shock Layer Thickness;  $s_b/R_N = 6.125$

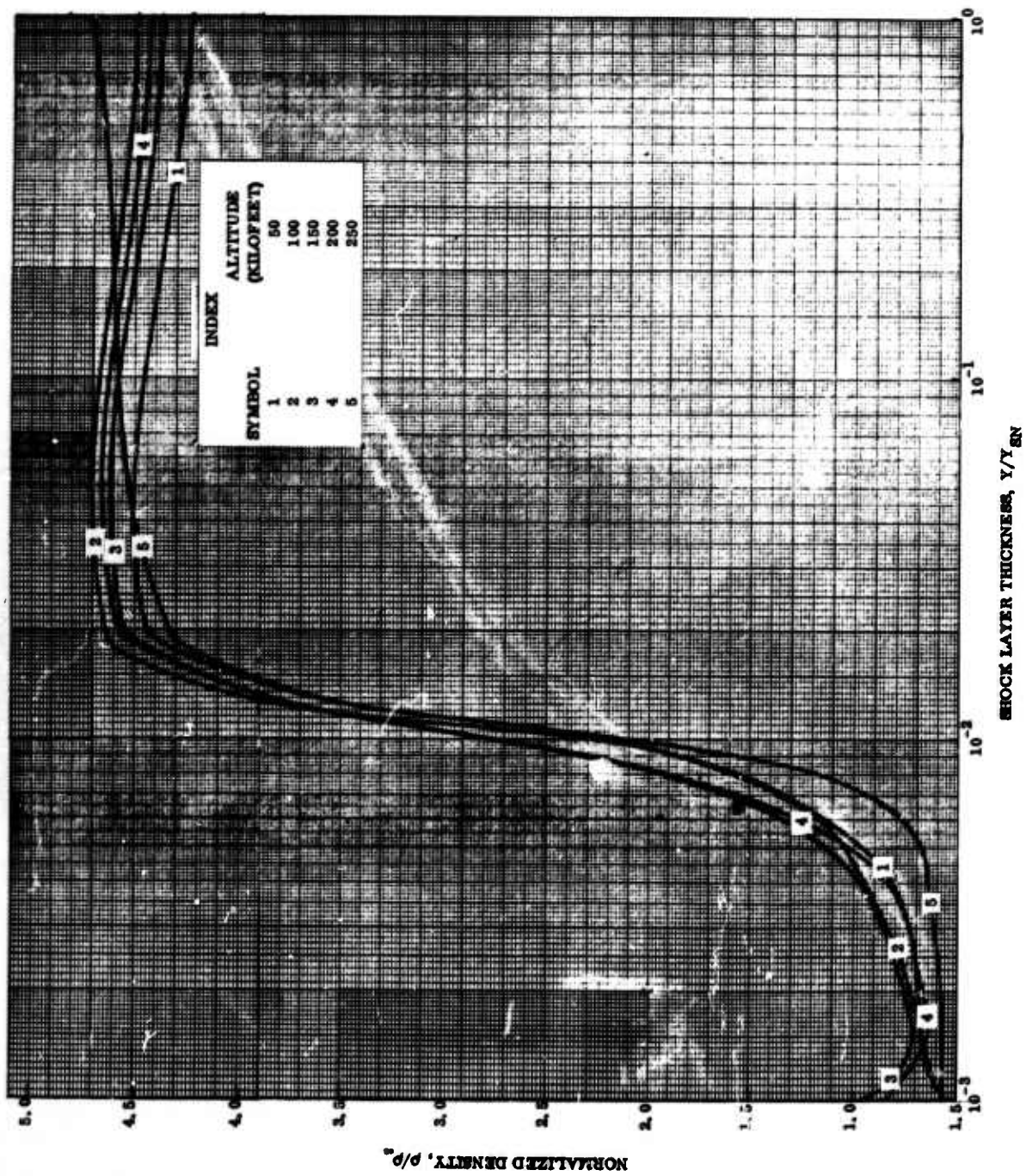


Figure 3-19. Normalized Density vs. Shock Layer Thickness;  $s_b/R_N = 2.433/2$

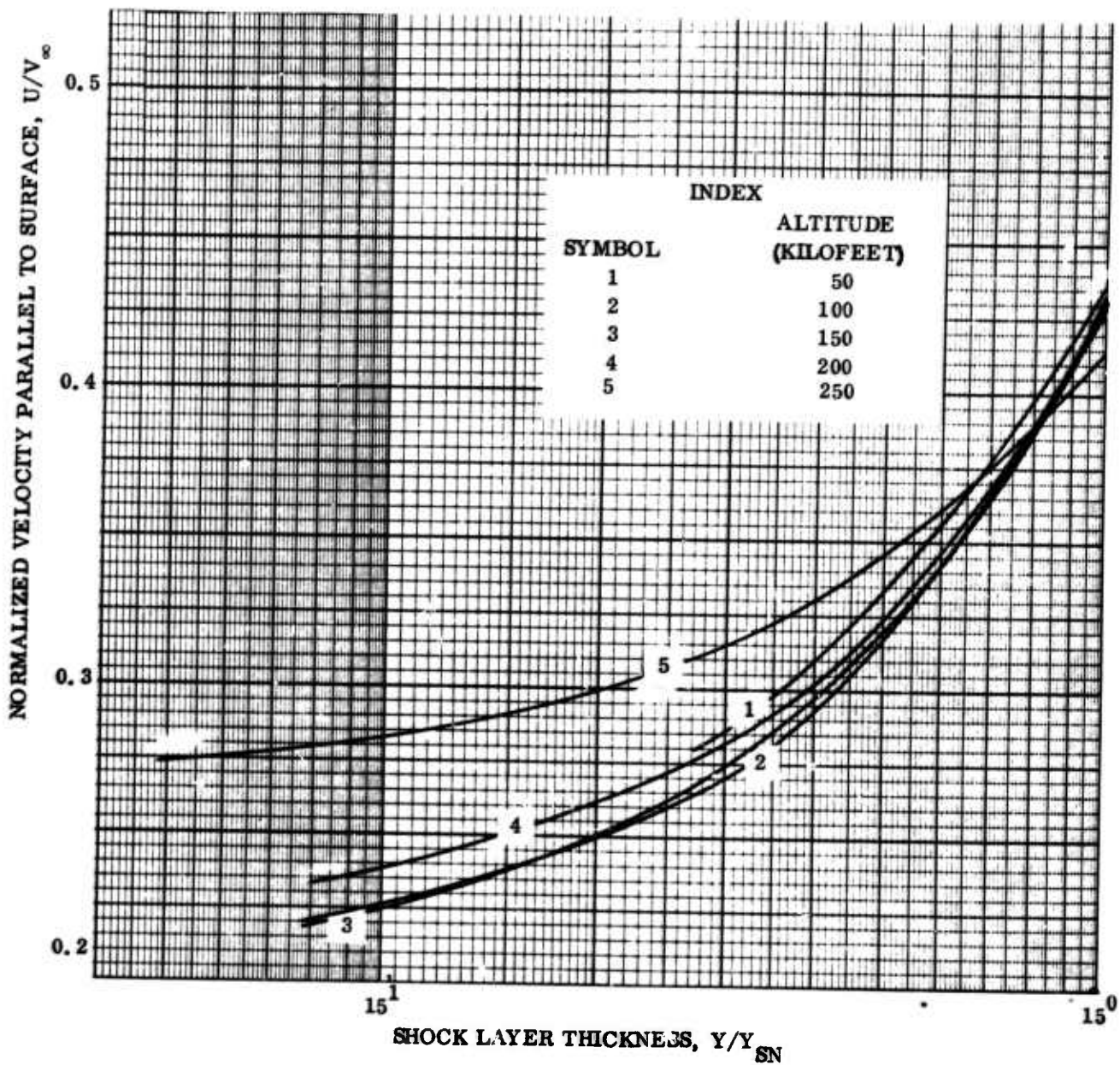


Figure 3-20. Normalized Velocity Parallel to Surface vs. Shock Layer Thickness;  
 $s_b/R_N = 4.962 \times 10^{-1}$

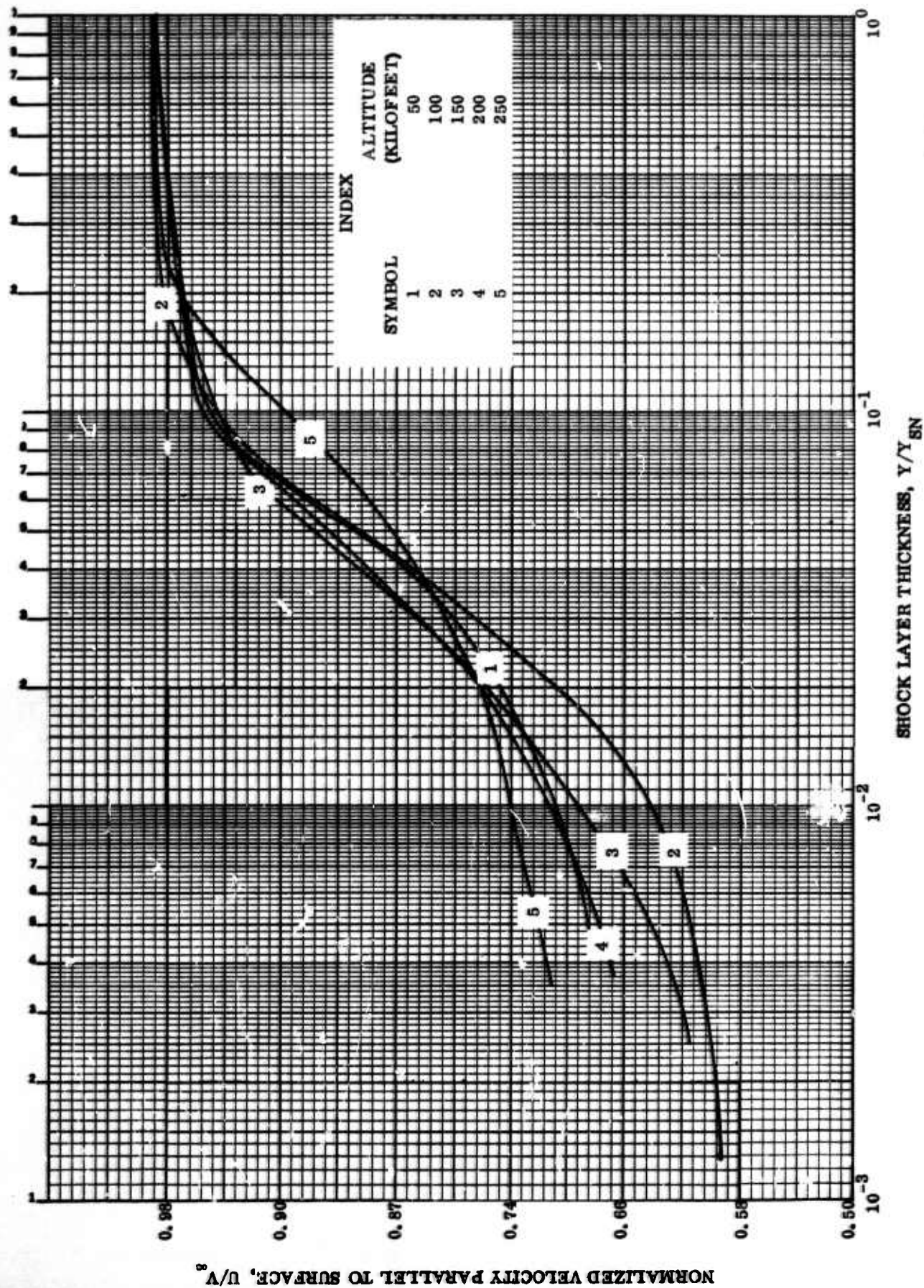
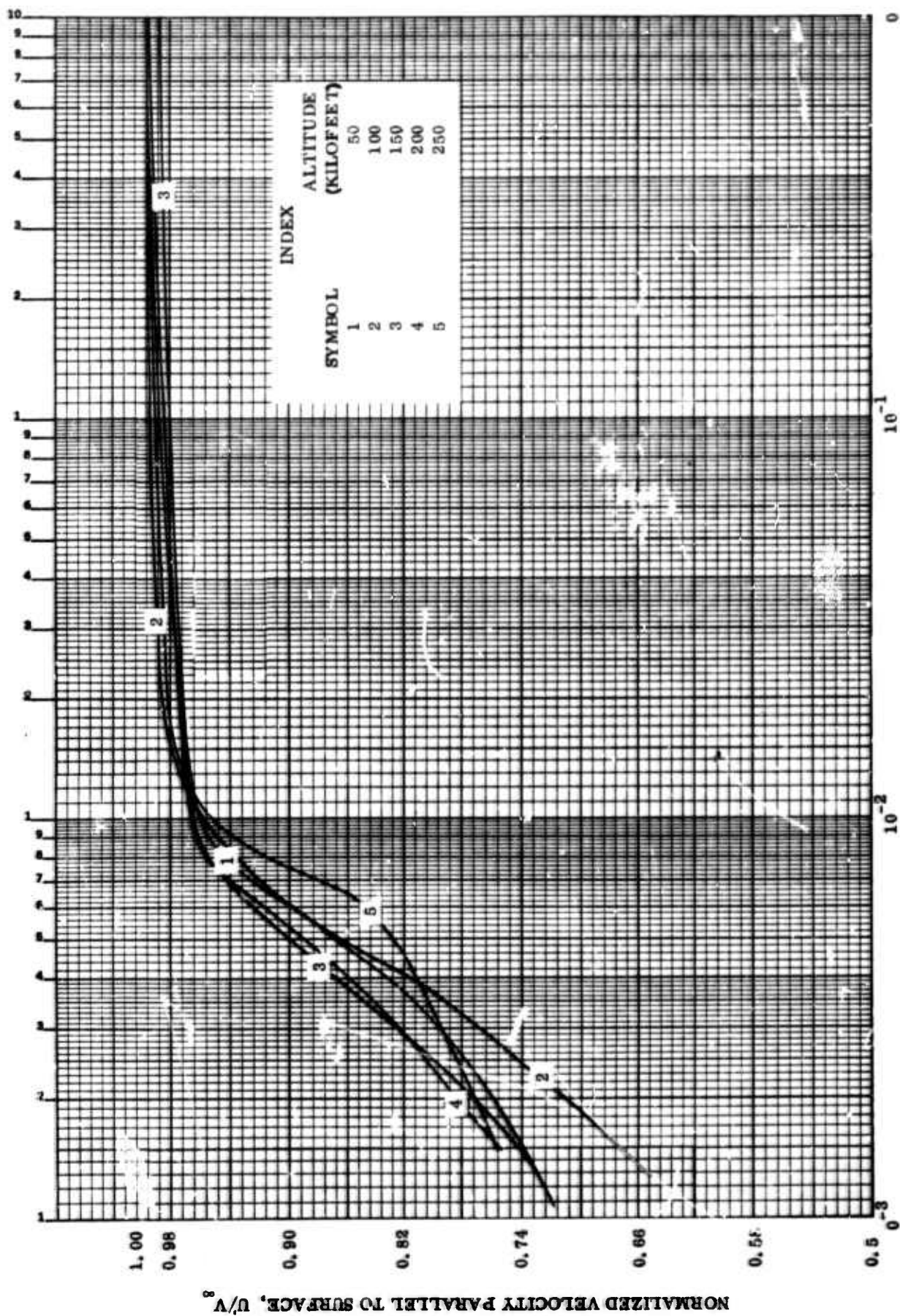


Figure 3-21. Normalized Velocity Parallel to Surface vs. Shock Layer Thickness;  $s_b/R_N = 6.125$



SHOCK LAYER THICKNESS,  $Y/Y_{SN}$   
 Figure 3-22. Normalized Velocity Parallel to Surface vs. Shock Layer Thickness;  $s_b/R_N = 2.433/2$

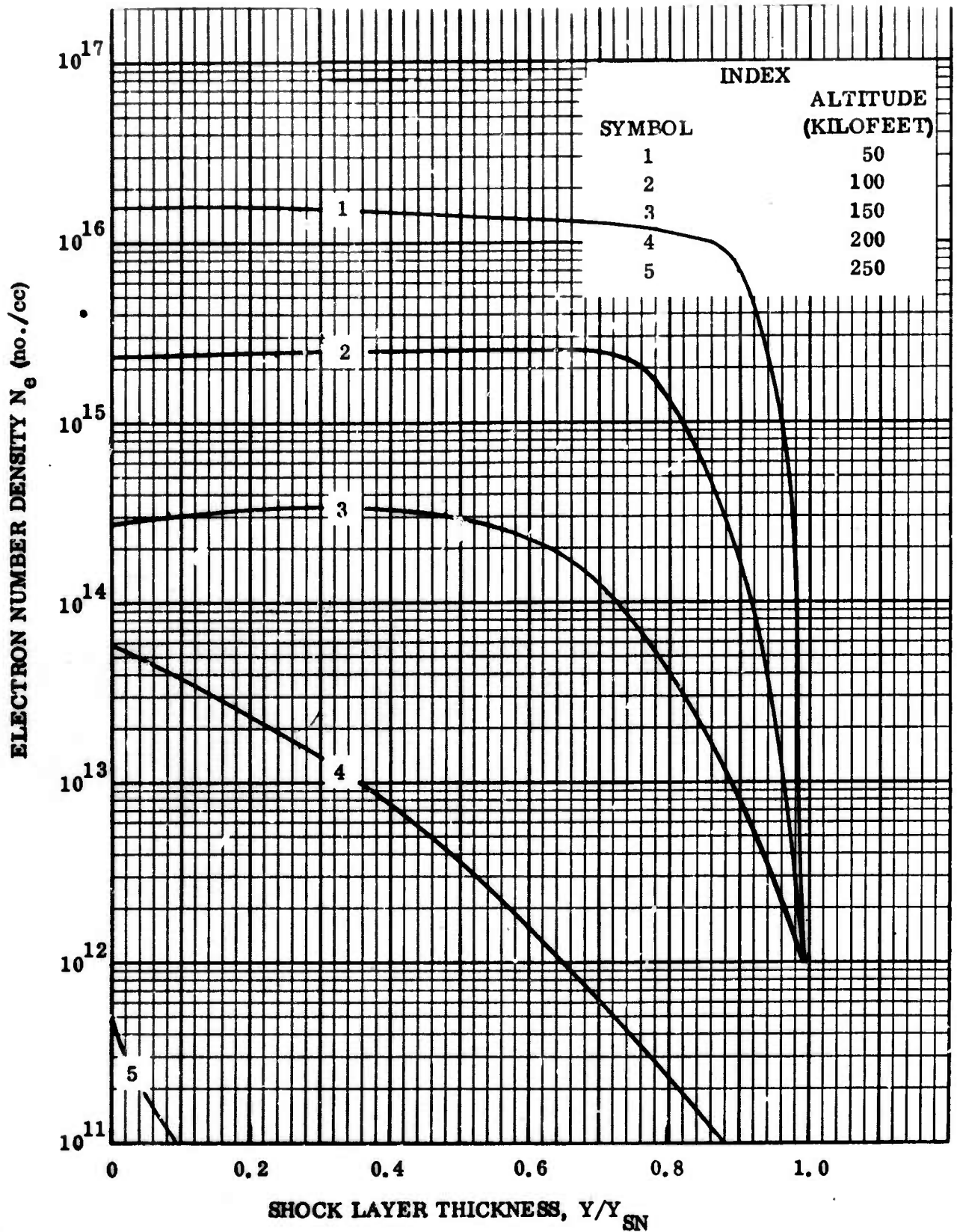


Figure 3-23. Electron Number Density vs. Shock Layer Thickness;  $s_b/R_N = 4.962^{-1}$

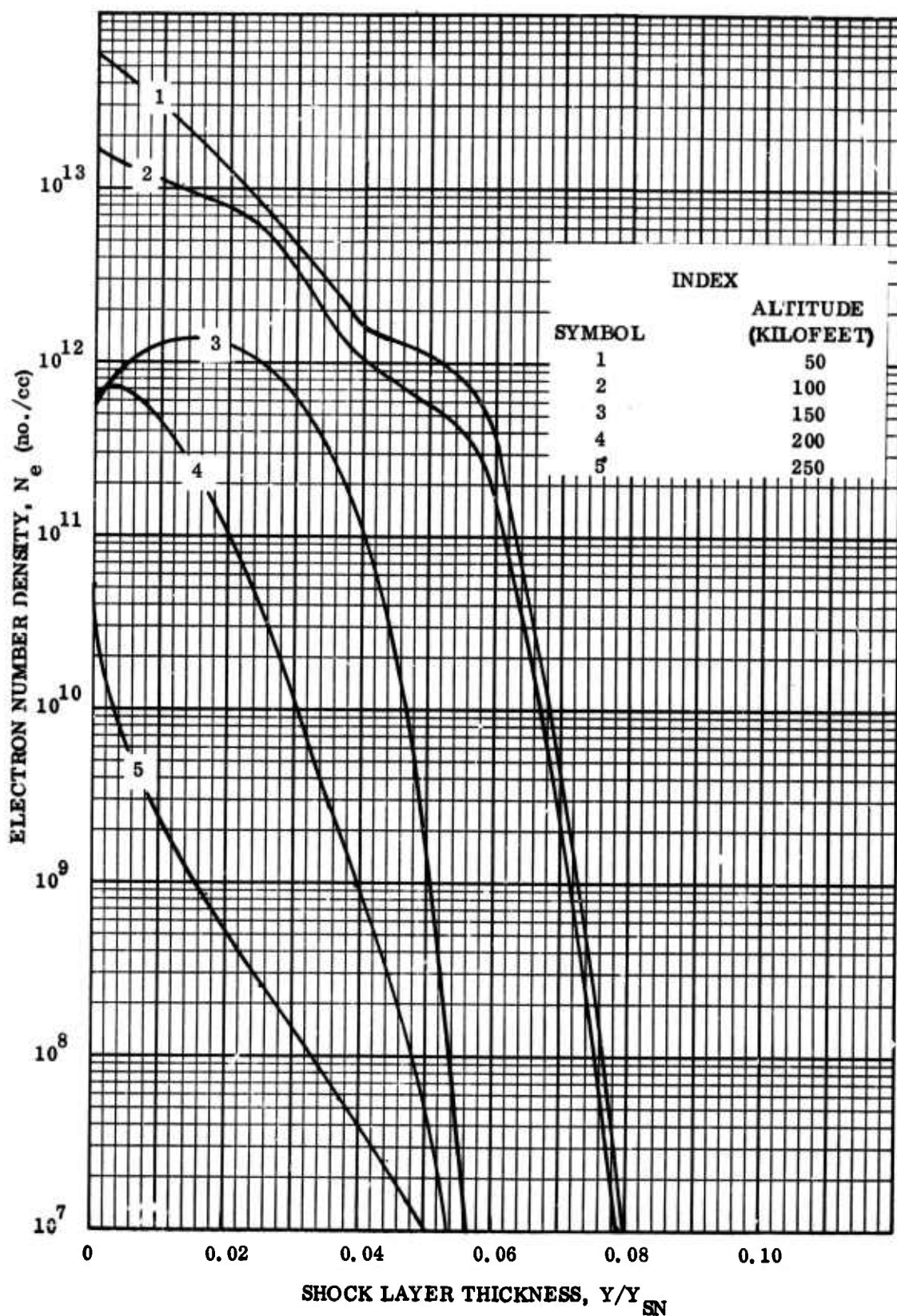


Figure 3-24. Electron Number Density vs. Shock Layer Thickness;  $s_b/R_N = 6.125^{1/2}$

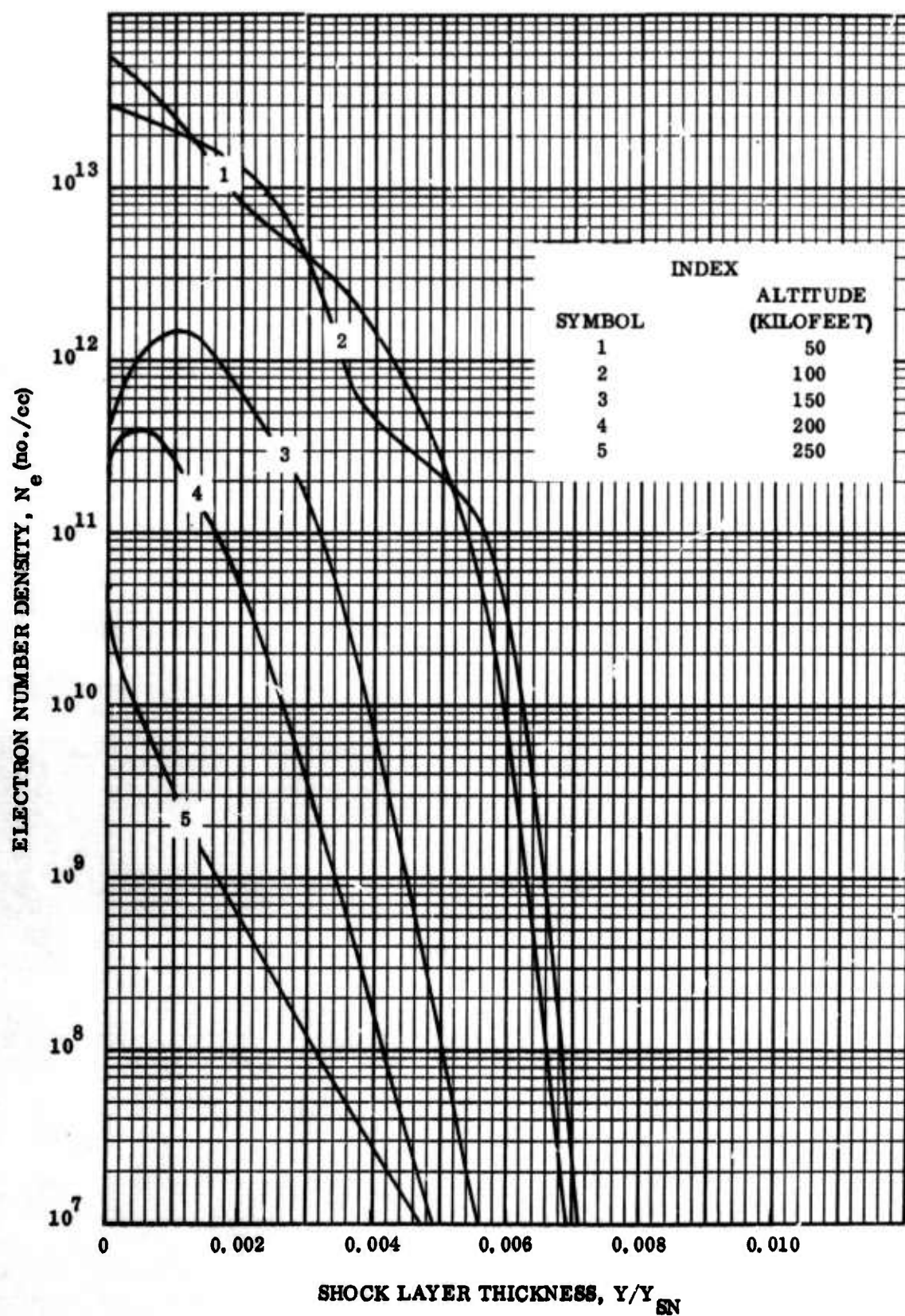


Figure 3-25. Electron Number Density vs. Shock Layer Thickness;  $s_b/R_N = 2.433 \sqrt{2}$

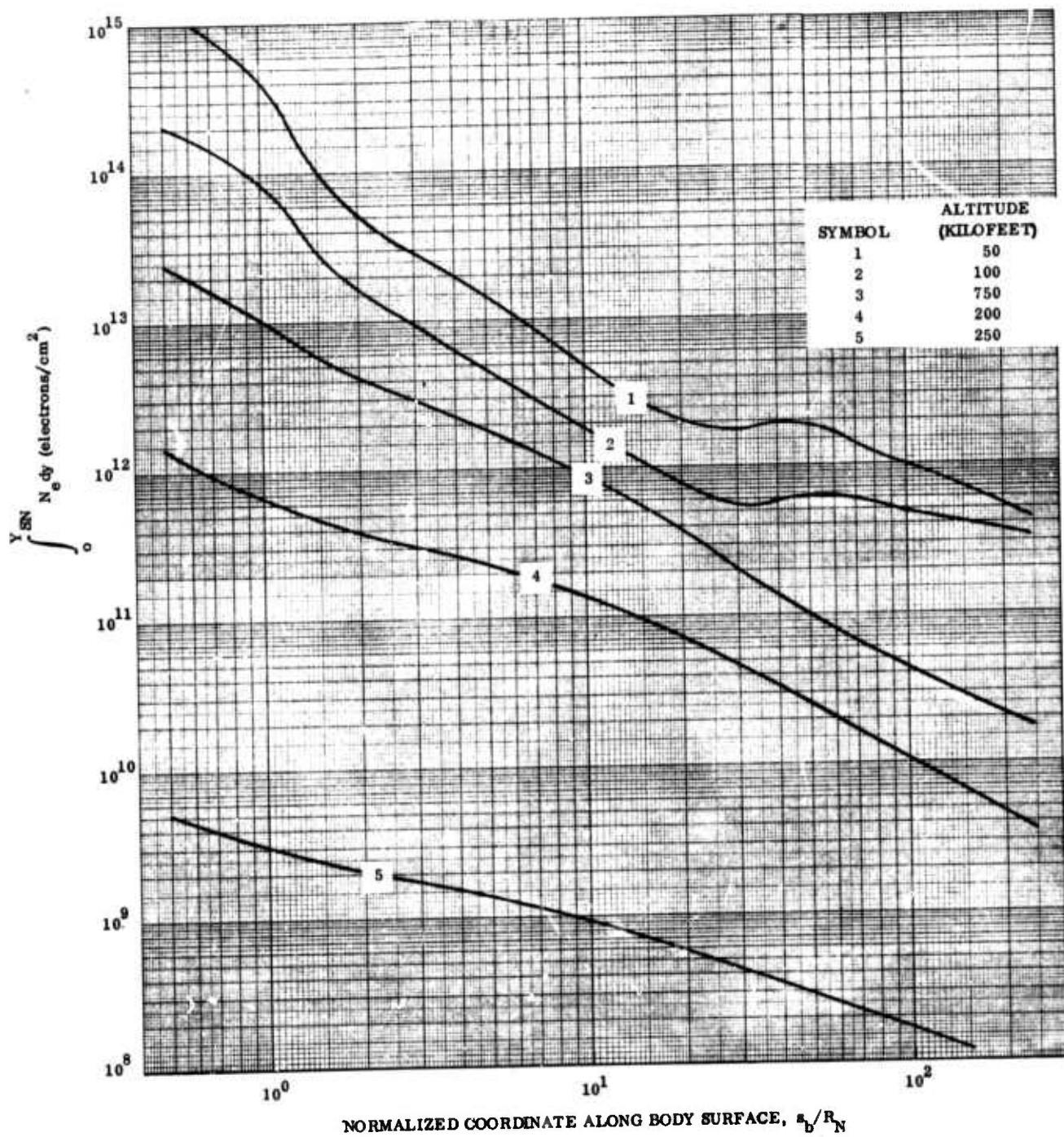


Figure 3-26.  $\int_0^{y_{SN}} N_e dy$  vs. Normalized Coordinate Along Body Surface; Nonequilibrium

Table 3-4. Altitude Dependence of the Species Number Density Normal Profiles,  
 $s_b/R_N = 4.962 \backslash^{-1}$

Species Number Density (particles per cc)						
Altitude (kilo feet)	Y/Y <sub>sn</sub>	O <sub>2</sub>	N <sub>2</sub>	N	O	NO
50	0	5.701 \16	2.2.81 \19	6.785 \18	1.296 \19	1.121 \18
	2.723 \-1	6.520	2.375	6.405	1.329	1.203
	7.128	9.689	2.651	5.228	1.418	1.476
	1.000 \0	6.662 \18	2.509	0	0	0
100	0	8.290 \14	2.056 \18	1.1714 \18	1.515 \18	3.810 \16
	7.742 \-2	8.742	2.080	1.707	1.526	3.867
	2.429 \-1	9.556	2.1584	1.660	1.553	4.161
	4.838	1.374 \15	2.279	1.503	1.566	5.293
	7.005	3.100	2.384	1.195	1.510	8.962
	1.000 \0	6.399 \17	2.410	0	0	0
150	0	7.407 \13	2.097 \17	2.013 \17	1.617 \17	3.753 \15
	8.064 \-2	1.126 \14	2.090	1.838	1.562	4.945
	2.393 \-1	2.655	2.127	1.484	1.452	8.684
	4.780	7.244	2.187	1.103	1.313	1.693 \16
	7.044	1.910 \15	2.238	7.386 \16	1.113	3.174
	1.000 \0	6.717 \16	2.530	0	0	0
200	0	5.316 \13	3.072 \16	2.194 \16	2.080 \16	1.624 \15
	7.989 \-2	1.226 \14	3.040	1.707	1.828	2.878
	2.706 \-1	2.772	3.068	1.145	1.541	4.567
	4.782	1.087 \15	3.220	6.543 \15	1.324	4.656
	7.098	4.637	3.463	2.973	8.002 \15	2.588
	1.000 \0	1.027 \16	3.867	0	0	0
250	0	1.519 \14	3.731 \15	8.299 \14	1.522 \15	5.107 \14
	4.899 \-2	3.244	3.845	5.944	1.252	4.070
	1.975 \-1	6.774	4.101	3.517	7.516 \14	2.238
	4.612	9.954	4.412	1.807	3.348	8.846 \13
	7.594	1.192 \15	4.693	6.529 \13	1.062	2.459
	1.000	1.384	5.211	0	0	0

Table 3-5. Altitude Dependence of the Species Number Density Normal Profiles,  
 $s_b / R_N = 6.125 \times 10^{-1}$

Species Number Density (particles per cc)						
Altitude (kiloft)	Y/Y <sub>sn</sub>	O <sub>2</sub>	N <sub>2</sub>	N	O	NO
50	0	1.617 <sup>-16</sup>	1.647 <sup>-18</sup>	2.962 <sup>-16</sup>	7.956 <sup>-17</sup>	7.437 <sup>-16</sup>
	4.213 <sup>-3</sup>	2.259	1.699	2.214	8.009	8.426 <sup>-17</sup>
	1.247 <sup>-2</sup>	5.303 <sup>17</sup>	1.844	9.882 <sup>-15</sup>	7.917	1.144 <sup>-17</sup>
	2.416	1.366	2.018	3.102 <sup>-14</sup>	6.872	1.523
	4.088	2.873	2.469	7.620 <sup>-13</sup>	6.238	1.535
	5.726	5.636 <sup>-18</sup>	3.169	8.651 <sup>-10</sup>	3.738 <sup>-15</sup>	2.473 <sup>-15</sup>
	7.875 <sup>-1</sup>	1.094	4.138	1.614 <sup>-1</sup>	4.946 <sup>-9</sup>	5.603 <sup>-9</sup>
	1.145 <sup>-0</sup>	1.847	6.955 <sup>-19</sup>	2.339 <sup>-1</sup>	1.399 <sup>-9</sup>	1.362 <sup>-9</sup>
	1.000 <sup>-0</sup>	3.413	1.285 <sup>-19</sup>	0	0	0
100	0	1.105 <sup>-12</sup>	1.573 <sup>-17</sup>	8.295 <sup>-16</sup>	1.062 <sup>-17</sup>	7.680 <sup>-13</sup>
	3.832	1.206	1.636	8.057	1.082	7.306
	8.272	1.351	1.739	7.733	1.128	6.396
	1.279 <sup>-2</sup>	1.706	1.853	6.865	1.166	6.684
	1.904	2.582	2.048	5.433	1.231	7.097
	2.439	4.354	2.231	3.844 <sup>-14</sup>	1.286	9.189 <sup>-15</sup>
	4.013	5.815 <sup>-16</sup>	2.558	3.992 <sup>-13</sup>	1.184 <sup>-16</sup>	8.132 <sup>-16</sup>
	5.907	4.500 <sup>-16</sup>	2.898	4.402 <sup>-10</sup>	4.184 <sup>-14</sup>	3.001 <sup>-14</sup>
	8.275 <sup>-1</sup>	9.934 <sup>-17</sup>	3.763	2.417 <sup>-2</sup>	6.729 <sup>-10</sup>	6.632 <sup>-10</sup>
	1.166 <sup>-1</sup>	1.615 <sup>-17</sup>	6.082 <sup>-18</sup>	5.249 <sup>-15</sup>	1.733 <sup>-8</sup>	1.936 <sup>-9</sup>
	2.214	3.493	1.315 <sup>-18</sup>	1.7518 <sup>-15</sup>	1.005 <sup>-8</sup>	1.493 <sup>-9</sup>
	1.000	3.330	1.254	0	0	0
150	0	2.516 <sup>-10</sup>	1.998 <sup>-16</sup>	1.843 <sup>-16</sup>	1.550 <sup>-16</sup>	4.343 <sup>-11</sup>
	7.858 <sup>-4</sup>	2.190	1.931	1.624	1.457	4.315
	2.501 <sup>-3</sup>	1.809	1.912	1.270	1.352	7.737 <sup>-12</sup>
	5.777	2.169	1.924	9.210 <sup>-15</sup>	1.266	2.341 <sup>-12</sup>
	9.369	5.688 <sup>-11</sup>	1.945	6.289	1.199	7.363 <sup>-13</sup>
	1.484 <sup>-2</sup>	6.291 <sup>-13</sup>	1.984	2.900 <sup>-14</sup>	1.128	3.648 <sup>-14</sup>
	2.002	2.907 <sup>-15</sup>	2.008	7.161 <sup>-13</sup>	1.057 <sup>-15</sup>	3.083 <sup>-15</sup>
	3.479	1.645 <sup>-15</sup>	2.262	4.191 <sup>-12</sup>	6.532 <sup>-15</sup>	2.999 <sup>-14</sup>
	5.117	6.374 <sup>-16</sup>	2.721	1.633 <sup>-8</sup>	1.148 <sup>-13</sup>	7.510 <sup>-13</sup>
	7.224 <sup>-1</sup>	1.032 <sup>-16</sup>	3.890	5.873 <sup>-0</sup>	1.324 <sup>-8</sup>	1.199 <sup>-8</sup>
	1.036 <sup>-0</sup>	1.674	6.306 <sup>-17</sup>	4.821 <sup>-0</sup>	1.793 <sup>-8</sup>	2.006 <sup>-8</sup>
	1.000 <sup>-0</sup>	3.381	1.273 <sup>-17</sup>	0	0	0

Table 3-5. Altitude Dependence of the Species Number Density Normal Profiles,  
 $s_b/R_N = 6.125 \times 10^{-1}$  (Cont)

Species Number Density (particles per cc)						
Altitude (kilofeet)	Y/Y <sub>sn</sub>	O <sub>2</sub>	N <sub>2</sub>	N	O	NO
200	0	1.379 <sup>9</sup>	2.789 <sup>15</sup>	1.780 <sup>15</sup>	1.953 <sup>15</sup>	2.712 <sup>11</sup>
	9.506 <sup>-4</sup>	2.141 <sup>10</sup>	2.655	1.205	1.728	2.111 <sup>12</sup>
	3.690 <sup>-3</sup>	4.829 <sup>11</sup>	2.559	6.763 <sup>14</sup>	1.523	1.886 <sup>13</sup>
	7.235	3.251 <sup>12</sup>	2.543	3.753	1.393	6.783 <sup>14</sup>
	1.176 <sup>-2</sup>	1.569 <sup>13</sup>	2.557	2.199	1.239	1.982 <sup>14</sup>
	1.821	8.078	2.674	7.925 <sup>13</sup>	1.043	3.214
	2.381	2.284 <sup>14</sup>	2.809	2.821	8.013 <sup>14</sup>	3.279
	3.932	7.121	3.288	1.830 <sup>12</sup>	2.365	1.164 <sup>13</sup>
	5.796	1.126 <sup>15</sup>	4.305	2.864 <sup>10</sup>	2.317 <sup>13</sup>	1.435 <sup>11</sup>
	7.596	1.568	5.908	5.450 <sup>7</sup>	4.089 <sup>11</sup>	3.617 <sup>11</sup>
	1.076 <sup>-1</sup>	2.695	1.015 <sup>16</sup>	2.168 <sup>-1</sup>	3.471 <sup>6</sup>	3.877 <sup>6</sup>
	1.000 <sup>0</sup>	5.256	1.980	0	0	0
250	0	5.390 <sup>12</sup>	2.712 <sup>14</sup>	5.617 <sup>13</sup>	1.223 <sup>14</sup>	3.509 <sup>13</sup>
	8.088 <sup>-4</sup>	1.155 <sup>13</sup>	2.719	3.993	1.068	3.411
	3.543 <sup>-3</sup>	2.575	2.711	2.228	7.805 <sup>13</sup>	2.764
	9.200	4.199	2.769	1.209	5.188	1.959
	1.668 <sup>-2</sup>	5.486	2.869	6.996 <sup>12</sup>	3.460	1.347 <sup>12</sup>
	2.511	6.556	3.010	4.101	2.309	9.121 <sup>12</sup>
	3.639	7.713	3.234	2.060	1.394	5.583
	4.668	9.840	3.971	9.455 <sup>11</sup>	1.086	4.720
	7.038	1.286 <sup>14</sup>	4.902	9.069 <sup>10</sup>	2.382 <sup>12</sup>	1.163 <sup>11</sup>
	9.495	1.631	6.149	2.478 <sup>8</sup>	2.902 <sup>11</sup>	1.852 <sup>11</sup>
	1.411 <sup>-1</sup>	2.745	1.034 <sup>15</sup>	3.099 <sup>3</sup>	1.696 <sup>8</sup>	1.805 <sup>8</sup>
	2.495	6.982	2.622	6.678 <sup>-15</sup>	1.179 <sup>-10</sup>	2.969 <sup>-11</sup>
	1.000 <sup>0</sup>	7.302	2.750	0	0	0

Table 3-6. Altitude Dependence of the Species Number Density Normal Profiles,  
 $s_b/R_N = 2.433 \sqrt{2}$

Species Number Density (particles per cc)						
Altitude (kilofeet)	Y/Y <sub>sn</sub>	O <sub>2</sub>	N <sub>2</sub>	N	O	NO
50	0	1.577 <sup>16</sup>	1.624 <sup>18</sup>	2.858 <sup>16</sup>	7.853 <sup>17</sup>	7.204 <sup>16</sup>
	3.638 <sup>-4</sup>	2.205	1.675	2.132	7.910	8.163
	1.077 <sup>-2</sup>	5.254	1.818	9.445 <sup>15</sup>	7.812	1.115 <sup>17</sup>
	2.092	1.367 <sup>17</sup>	2.030	3.154	6.929	1.532
	3.575	3.003	2.327	8.382 <sup>14</sup>	4.986	1.864
	5.073	6.048	2.982	7.207 <sup>13</sup>	2.577	1.583
	7.011	1.100 <sup>18</sup>	4.162	1.668 <sup>10</sup>	4.990 <sup>15</sup>	5.729 <sup>15</sup>
	1.013 <sup>-2</sup>	1.847	6.955	2.341 <sup>-1</sup>	1.400 <sup>9</sup>	1.363 <sup>9</sup>
	1.000 <sup>0</sup>	3.467	1.306 <sup>19</sup>	0	0	0
100	0	7.503 <sup>12</sup>	1.362 <sup>17</sup>	5.191 <sup>16</sup>	8.570 <sup>16</sup>	4.821 <sup>14</sup>
	1.181 <sup>-4</sup>	7.409	1.373	5.150	8.621	4.758
	3.755	7.253	1.415	4.980	8.801	4.600
	8.123	6.793	1.497	4.681	9.160	4.224
	1.253 <sup>-3</sup>	6.877	1.609	4.173	9.618	3.984
	1.852	7.504	1.806	3.293	1.044 <sup>17</sup>	3.626
	2.349	1.049 <sup>13</sup>	2.009	2.313	1.126	3.696
	3.710	6.429 <sup>15</sup>	2.499	3.757 <sup>14</sup>	1.137	8.444 <sup>15</sup>
	5.265	4.653 <sup>16</sup>	2.866	3.930 <sup>13</sup>	4.199 <sup>16</sup>	2.334 <sup>16</sup>
	7.216	1.005 <sup>17</sup>	3.808	2.694 <sup>10</sup>	7.180 <sup>14</sup>	7.368 <sup>14</sup>
	1.001 <sup>-2</sup>	1.625	6.120	5.739 <sup>2</sup>	1.765 <sup>10</sup>	1.968 <sup>10</sup>
	1.871	3.449	1.299 <sup>18</sup>	4.914 <sup>-20</sup>	7.574 <sup>-8</sup>	1.109 <sup>-8</sup>
	1.000 <sup>0</sup>	3.357	1.264	0	0	0
150	0	2.125 <sup>10</sup>	1.927 <sup>16</sup>	1.728 <sup>16</sup>	1.482 <sup>16</sup>	4.386 <sup>11</sup>
	6.892 <sup>-5</sup>	1.960	1.929	1.580	1.444	5.525
	2.177 <sup>-4</sup>	1.914	1.934	1.264	1.363	1.031 <sup>12</sup>
	4.986	2.544	1.960	9.300 <sup>15</sup>	1.288	3.102
	8.056	7.945	1.989	6.397	1.226	9.555
	1.272 <sup>-3</sup>	1.030 <sup>12</sup>	2.034	2.978	1.155	4.937 <sup>13</sup>
	1.713	3.146 <sup>13</sup>	2.064	7.684 <sup>14</sup>	1.086	3.290 <sup>14</sup>
	2.973	1.866 <sup>15</sup>	2.351	4.604 <sup>13</sup>	6.937 <sup>15</sup>	2.487 <sup>15</sup>
	4.366	6.355	2.814	2.271 <sup>12</sup>	1.379	1.166
	6.160	1.063 <sup>16</sup>	4.009	8.016 <sup>8</sup>	1.499 <sup>13</sup>	1.399 <sup>13</sup>
	8.868	1.749	6.587	8.923 <sup>0</sup>	1.969 <sup>8</sup>	2.189 <sup>8</sup>
	1.000 <sup>0</sup>	3.405	1.282 <sup>17</sup>	0	0	0

Table 3-6. Altitude Dependence of the Species Number Density Normal Profiles,  
 $s_b/R_N = 2.433 \sqrt{2}$  (Cont)

Species Number Density (particles per cc)						
Altitude (kiloft)	Y/Y <sub>sn</sub>	O <sub>2</sub>	N <sub>2</sub>	N	O	NO
200	0	9.286 <sup>8</sup>	2.793 <sup>15</sup>	1.782 <sup>15</sup>	1.956 <sup>15</sup>	2.599 <sup>11</sup>
	7.827 <sup>-5</sup>	9.822 <sup>9</sup>	2.659	1.206	1.731	1.525 <sup>12</sup>
	3.059 <sup>-4</sup>	1.740 <sup>11</sup>	2.562	6.651 <sup>14</sup>	1.529	9.520 <sup>13</sup>
	6.022	1.600 <sup>12</sup>	2.544	3.375	1.411	3.545 <sup>14</sup>
	9.835 <sup>-3</sup>	1.277 <sup>13</sup>	2.590	1.370 <sup>13</sup>	1.304	1.117 <sup>14</sup>
	1.524 <sup>-3</sup>	7.330 <sup>14</sup>	2.726	4.590 <sup>13</sup>	1.110	2.763
	1.987	1.064 <sup>14</sup>	2.868	2.094 <sup>12</sup>	8.794 <sup>14</sup>	3.758
	3.255	6.715 <sup>15</sup>	3.355	2.185 <sup>10</sup>	2.977 <sup>13</sup>	1.029 <sup>13</sup>
	4.795	1.126 <sup>15</sup>	4.320	3.440 <sup>7</sup>	2.802 <sup>11</sup>	1.971 <sup>11</sup>
	6.298	1.593	6.002 <sup>16</sup>	2.960 <sup>-1</sup>	4.602 <sup>6</sup>	4.180 <sup>6</sup>
	8.955 <sup>0</sup>	2.702	1.017 <sup>16</sup>	1.305 <sup>-1</sup>	3.619 <sup>6</sup>	4.020 <sup>6</sup>
	1.000 <sup>0</sup>	5.259	1.981	0	0	0
250	0	1.914 <sup>12</sup>	3.062 <sup>14</sup>	3.896 <sup>13</sup>	1.516 <sup>14</sup>	2.379 <sup>13</sup>
	7.526 <sup>-5</sup>	4.776 <sup>13</sup>	3.023	2.435	1.338	3.218
	3.225 <sup>-4</sup>	1.518 <sup>13</sup>	3.014	1.070	1.037 <sup>13</sup>	3.920
	8.234 <sup>-3</sup>	3.244	3.092	4.622 <sup>12</sup>	7.464 <sup>13</sup>	3.525
	1.480 <sup>-3</sup>	4.892	3.220	2.261	5.362	2.738
	2.217	6.404	3.389	1.137	3.767	1.979
	3.206	8.080	3.649	4.733 <sup>11</sup>	2.319	1.236 <sup>12</sup>
	4.115	9.277 <sup>14</sup>	3.881	2.202 <sup>10</sup>	1.476 <sup>12</sup>	7.957 <sup>12</sup>
	6.308	1.241 <sup>14</sup>	4.758 <sup>15</sup>	1.595 <sup>3</sup>	3.015 <sup>8</sup>	1.741 <sup>8</sup>
	9.209 <sup>-2</sup>	2.670	1.005 <sup>15</sup>	1.328 <sup>-15</sup>	1.716 <sup>-10</sup>	1.831 <sup>-10</sup>
	1.909 <sup>0</sup>	6.824	2.570	5.798 <sup>-15</sup>	7.851 <sup>-10</sup>	1.857 <sup>-10</sup>
	1.000 <sup>0</sup>	7.469	2.813	0	0	0

It is worth noting in Figures 3-11, and 3-13 that the pressure profiles obtained from the perfect gas or equilibrium flow fields actually follow the free stream Mach number variation rather than the altitude variation. Also, for these pressure profiles, which are derived from the perfect gas or equilibrium streamwise pressure distributions and reproduced during the construction of the approximate nonequilibrium flow field, the pressure behind the shock is replaced by the value from the thermal equilibrium frozen shock flow solution. This change at  $Y/Y_{SN} = 1$  is particularly noticeable on the first normal, where the result is a lower value for the equilibrium cases and a higher value for the perfect gas case.

Some attention should also be directed to the development of an off-wall peak in the temperature profiles back on the conical surface (Figures 3-15 and 3-16) as the altitude is increased. This trend is unquestionably one of the more marked effects of nonequilibrium flow, inasmuch as the temperature for equilibrium flow decreases monotonically from the wall to the shock (except in the region where the streamlines have traversed that portion of the shock where the minimum shock angle occurs as a result of the overexpansion).

### 3.2.2 VIBRATIONAL NONEQUILIBRIUM CALCULATIONS

The relative importance of vibrational nonequilibrium on the shock layer flow properties has been investigated by applying the following superpositional method. Landau and Teller<sup>207</sup> have shown that the Master Equation for a system of harmonic oscillators reduces to the familiar vibrational relaxation equation:

$$\frac{d\epsilon_v}{dt} = \frac{1}{\gamma} (\epsilon_{v\infty} - \epsilon_v) \quad (3-3)$$

where  $\gamma$  denotes the relaxation time of the system;  $\epsilon_{v\infty}$  the equilibrium vibrational energy; and  $\epsilon_v$  the vibrational energy at time  $t$ . For the harmonic oscillator

$$\epsilon_v = R\theta_v / (e^{\theta_v/T_v} - 1) \quad (3-4)$$

$$\epsilon_{v\infty} = R\theta_v / (e^{\theta_v/T} - 1) \quad (3-5)$$

in which  $R$  is the universal gas constant;  $\theta_v$  is the characteristic vibrational temperature;  $T$ , the kinetic or gas temperature; and  $T_v$ , the vibrational temperature. For applications in which the relaxation time and the equilibrium vibrational energy are implicit functions of time, the general solution for equation 1 is:

$$\epsilon_v = \left[ \int_0^t \frac{\epsilon_{v\infty}}{\gamma} \exp \int_0^{t^*} \frac{dt^{**}}{\gamma} dt^* + \text{const} \right] \exp - \int_0^t \frac{dt^*}{\gamma} \quad (3-6)$$

$$\epsilon_v = \left[ \int_0^t \frac{\epsilon_{v\infty} - \epsilon_{v0}}{\gamma} \exp \int_0^{t^*} \frac{dt^{**}}{\gamma} dt^* \right] \exp - \int_0^t \frac{dt^*}{\gamma} + \epsilon_{v0} \quad (3-7)$$

in which  $t^*$  and  $t^{**}$  are dummy variables for time. The second equation is obtained from applying the boundary conditions at  $t = 0$ ,  $\epsilon_v = \epsilon_{v0}$ .

For steady flow, the distance along a streamline,  $s$ , and the ordered velocity,  $V$ , are related by

$$\frac{ds}{dt} = V \quad (3-8)$$

so that the integrals in Equation 3-7 may be transformed into:

$$\epsilon_v = \left[ \int_0^s \frac{\epsilon_{v\infty} - \epsilon_{v0}}{V\gamma} \exp \left( \int_0^{s^*} \frac{ds^{**}}{V\gamma} \right) ds^* \right] \exp - \int_0^s \frac{ds^*}{V\gamma} + \epsilon_{v0} \quad (3-9)$$

Using Equations 3-4 and 3-5 the vibrational energy may be rewritten as:

$$\frac{\epsilon_v}{R\theta_v} = \left\{ \int_0^s \frac{1}{V\gamma} \left( \frac{1}{\exp(\theta_v/T) - 1} - \frac{1}{\exp(\theta_v/T_v) - 1} \right) \exp \int_0^{s^*} \frac{ds^{**}}{V\gamma} \right\} \exp - \int_0^s \frac{ds^*}{V\gamma} + \frac{1}{\exp(\theta_v/T_{v0}) - 1} \quad (3-10)$$

and the local vibrational temperature along the streamline is given by

$$T_v = \theta_v / \ln(1 + R \theta_v / \epsilon_v) \quad (3-11)$$

By superimposing the solution of Equations 3-10 and 3-11 over the thermal equilibrium calculations for the inviscid flow field at 250 kilofeet, the relative importance of the vibrational nonequilibrium problem can be assessed. The highest altitude flow field was selected for investigation because, since vibrational relaxation times vary inversely with pressure, conditions for vibrational nonequilibrium are most favorable at higher altitudes. Based on this simplified, order-of-magnitude analysis it is concluded that vibrational nonequilibrium can cause substantial changes in the flow properties, particularly the gas temperature and density, and consequently must be taken into account to accurately predict the shock layer properties at higher altitudes. The analysis and the results which form the basis for this conclusion are discussed below.

The superpositional method used in this investigation consists of solving the uncoupled streamwise vibrational relaxation equation using superposition with the thermal equilibrium chemical nonequilibrium inviscid flow field to provide the values of the gas pressure and temperature required to calculate the local relaxation time and vibrational equilibrium energy. Only the primary molecular constituents  $N_2$  and  $O_2$  were considered and the relaxation times for each of these species were obtained from Millikan and White<sup>208</sup>:

$$\gamma_{O_2} = \frac{1}{p} e^{(129T^{-1/3} - 22.3)} \quad (3-12)$$

$$\gamma_{N_2} = \frac{1}{p} e^{(220T^{-1/3} - 24.8)} \quad (3-13)$$

where the relaxation times  $\gamma_{O_2}$  and  $\gamma_{N_2}$  are in seconds,  $p$  is the gas pressure in atmospheres, and  $T$  is the gas temperature in degrees Kelvin. The harmonic oscillator model is used to define the vibrational temperature corresponding to the vibrational energy obtained from the solution of the relaxation equation and, therefore, is given by

$$T_v = \theta_v / \ln(1 + R\theta_v / \epsilon_v) \quad (3-14)$$

In the above expression  $T_v$  and  $\epsilon_v$  are the vibrational temperature and energy,  $R$  is the universal gas constant and  $\theta_v$  is the characteristic vibrational temperature which has a value of 2239°K for oxygen and 3395°K for nitrogen.

Some typical results of the analysis are shown in Figures 3-27, 3-28, and 3-29 for streamlines which intersect the bow shock at shock angles of 89, 70, and 46 degrees, respectively. In these figures the streamwise variation of the vibrational temperatures of  $O_2$  and  $N_2$  as well as the gas temperatures obtained from solutions for thermal equilibrium chemical nonequilibrium and for perfect gas with  $\gamma = 7/5$  (undissociated air with no vibrational excitation) are given as functions of the normalized distance along the body surface. In all cases the vibrational temperatures of both oxygen and nitrogen are characterized by an initial rapid rise from the free stream value at the shock. However, as the streamline continues to expand around the body, the drop in the gas pressure and temperature causes a rapid increase in the local relaxation time with a corresponding rapid leveling off ("freezing") of the vibrational temperature. If at this point the vibrational temperature is less than the equilibrium temperature it will continue to rise gradually until the two are equal, which for this application, particularly for nitrogen, requires a considerable distance along the body. If the vibration temperature at the leveling off point is greater than the equilibrium temperature it will decrease gradually until the two are equal. It can be seen that this latter situation is the case for the 89 degree shock angle streamline, whereas the former situation applies for the other two streamlines. Also for the 89 degree streamline it may be noticed that the difference between the no vibrational excitation temperature and the thermal equilibrium temperature back on the conical portion of the body is about 2500°K or about 45 percent of the equilibrium temperature. In this case, however, this temperature difference should not be interpreted as indicative of the extent of vibrational nonequilibrium effects because both the oxygen and nitrogen vibrational temperatures are above the thermal equilibrium temperature. As a result of this, if, in the solution of the coupled problem, gas temperature changes from

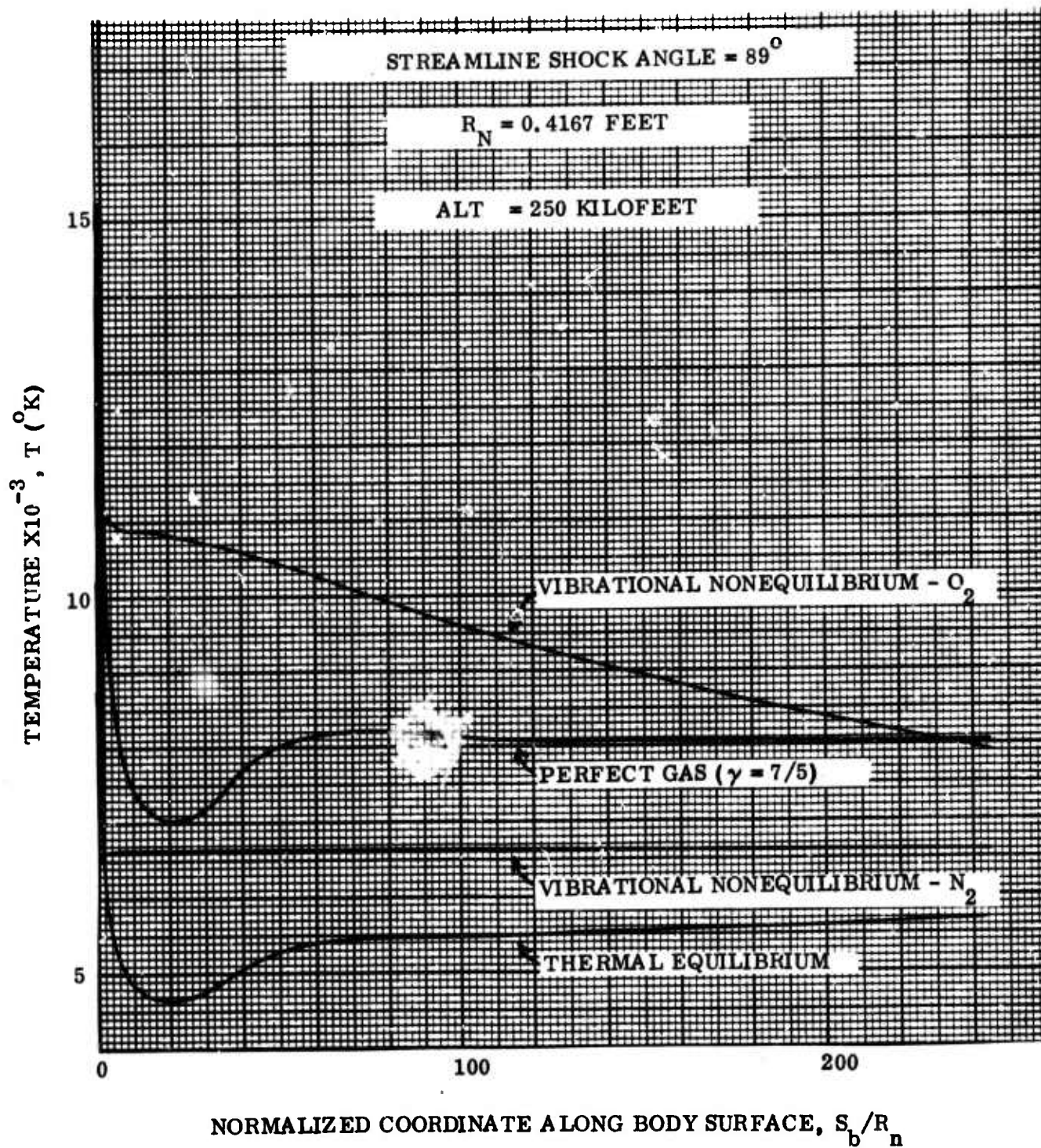


Figure 3-27. Vibrational Nonequilibrium; Streamwise Variation of Temperature vs. Normalized Coordinate Along Body Surface

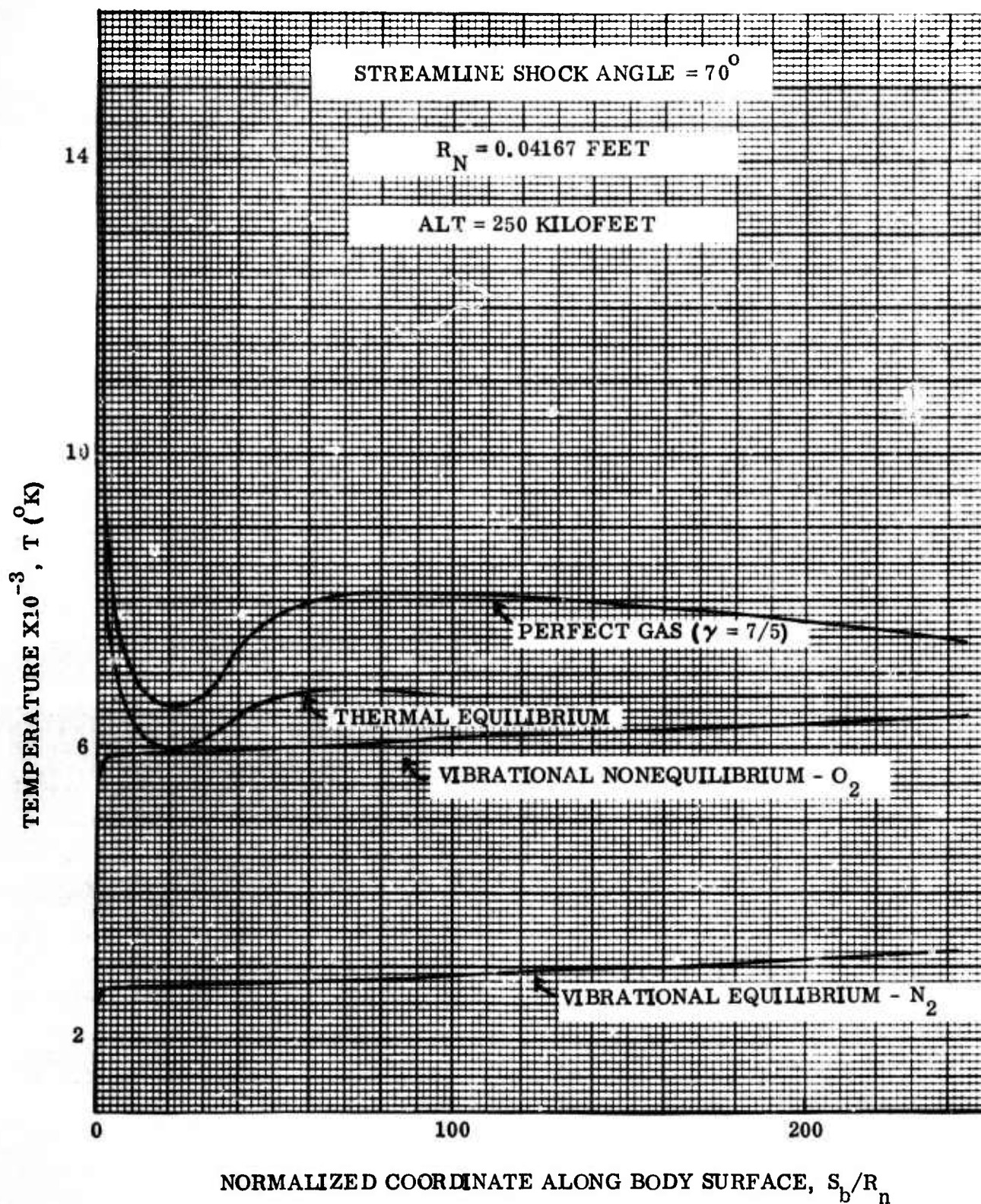


Figure 3-28. Vibrational Nonequilibrium; Streamwise Variation of Temperature vs. Normalized Coordinate Along Body Surface

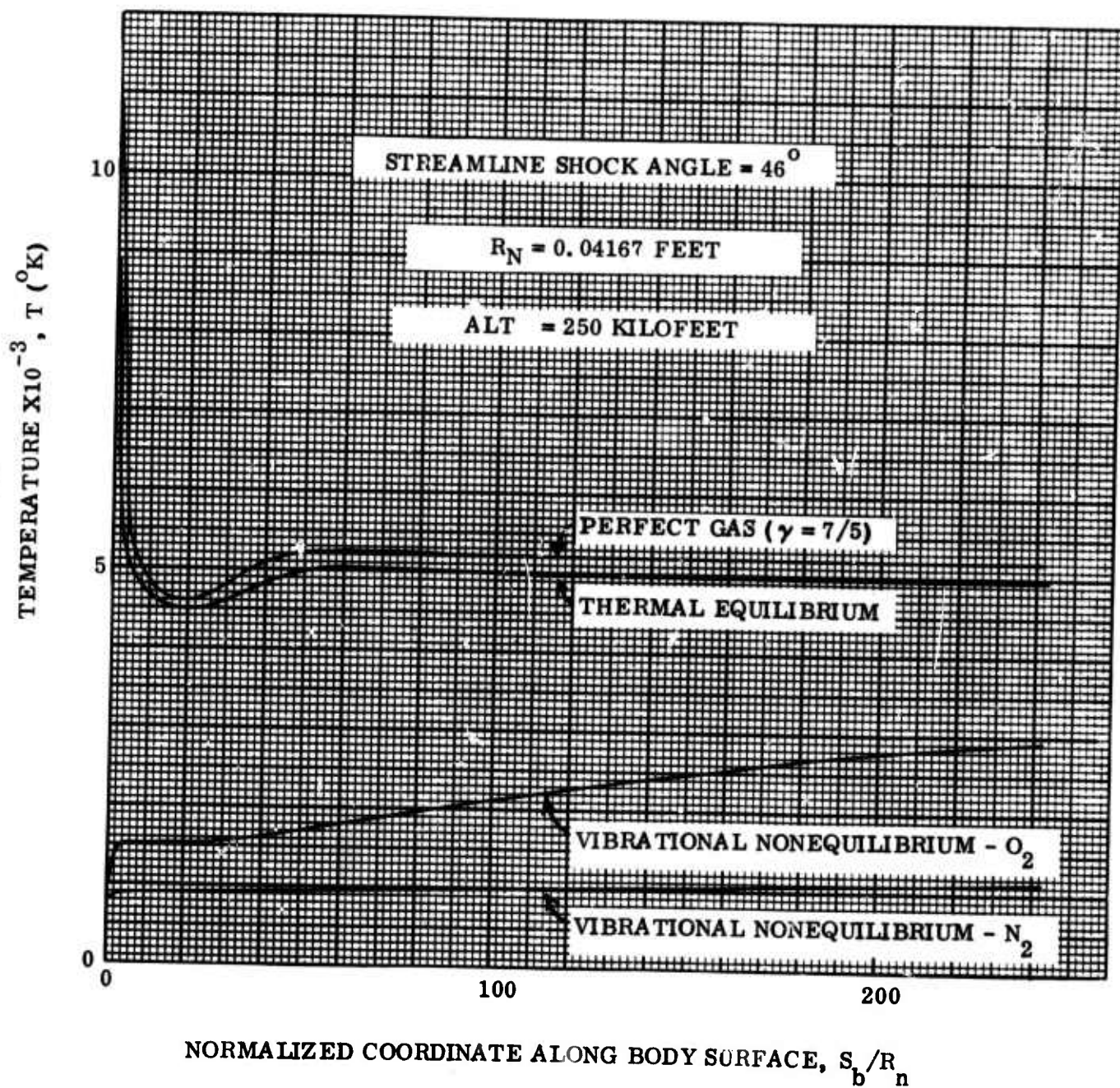


Figure 3-29. Vibrational Nonequilibrium; Streamwise Variation of Temperature vs. Normalized Coordinate Along Body Surface

thermal equilibrium do not significantly affect the chemical activity, the gas temperature from the coupled solution would be below the equilibrium temperature shown in Figure 3-27. To evaluate the extent of vibrational nonequilibrium effects in this case would require a comparison with the gas temperature from a perfect gas solution with  $\gamma = 9/7$  (full vibrational excitation). In the other two cases, however, where the vibrational temperatures are below the thermal equilibrium temperature, the gas temperature from the coupled solution would be between the  $\gamma = 7/5$  curve and thermal equilibrium curve and, consequently, the difference between these two curves would indicate the extent of the vibrational nonequilibrium effects.

### 3.2.3 STAGNATION POINT MATCHED INVISCID-BOUNDARY LAYER CALCULATIONS

Profiles of the flow properties along the stagnation streamline within the shock layer have been obtained from matched inviscid - boundary layer chemical nonequilibrium pure air solutions for altitudes of 200 and 150 kilofeet. These profiles are required as initial conditions for the nonequilibrium boundary layers which are presented in Paragraph 3.2.4; they are, however, of considerable interest in themselves and as such are presented separately from the boundary layer solutions.

In shock layer applications, the stagnation line matched inviscid-boundary layer problem is coupled, i. e., the inviscid solution must be used to provide edge conditions for the boundary layer solution which in turn must be known to locate the bow shock as influenced by boundary layer displacement. The matched solution must, therefore, be obtained by iteration. The procedure used herein is to first assume the boundary layer profiles necessary to locate the edge at which the inviscid solution is terminated thereby supplying the necessary edge conditions. The boundary layer solution with these edge conditions is obtained, these profiles are then used to relocate the edge, and the process is repeated until the change in the edge is less than a specified small tolerance after which the solutions are considered matched.

Before proceeding to a description of both the inviscid and boundary layer solutions it is appropriate to point out that both solutions have identical thermodynamic and nonequilibrium chemical reaction systems and both assume the condition of thermal equilibrium.

### 3.2.3.1 The Inviscid Layer Solution

In the inviscid region of the shock layer, the solution is provided by the streamtube method of McMenamin and O'Brien<sup>118</sup> which was described in detail in Paragraph 3.2.1.2. The governing variable used with the streamtube method is the streamwise velocity which is obtained from a correlation of data from Burke, Curtis, and Boyer<sup>209</sup> which are the result of the inverse shock nonequilibrium inviscid shock layer solution of Cornell Aeronautical Laboratory<sup>97</sup>. The correlation which reproduces the data of reference to within  $\pm 8$  percent is given by:

$$v = v_s (1 - s/\Delta)^b \quad (3-15)$$

in which  $v$  is the streamwise velocity,  $v_s$  is the velocity behind the shock wave,  $\Delta$  is the shock detachment distance and the exponent is given by:

$$\begin{array}{ll} b = 1 & \text{for } v_s \leq 1670 \text{ ft/sec} \\ b = 0.000596 v_s & \text{for } v_s \geq 1670 \text{ ft/sec} \end{array}$$

The nonequilibrium shock detachment distance required for the inviscid shock layer solution is obtained in the following manner. By examining a multitude of shock detachment distances from equilibrium air and perfect gas ( $1 \leq \gamma \leq 5/3$ ) flow field solutions for spherical noses, Storer<sup>210</sup> found that all cases could be correlated with excellent agreement by the formula

$$\frac{\Delta}{R_N} = 0.75 \left( \frac{\rho_\infty}{\rho_s} \right) + 1.543 \left( \frac{\rho_\infty}{\rho_s} \right)^{3.571} \quad (3-16)$$

in which  $R_N$  is the sphere radius,  $\rho_\infty$  is the free stream density, and  $\rho_s$  is the density behind a normal shock wave corresponding to either the equilibrium air or perfect gas shock solution as the case may be. Insofar as the gas density in the stagnation region for either equilibrium air or a perfect gas is nearly constant, it might be expected that the shock detachment distance could be essentially specified by the density behind the normal shock. This cannot be true for the nonequilibrium flow, however, because the density varies from the frozen value ( $\gamma = 7/5$ ) at the shock wave to the equilibrium value at the stagnation point. Nevertheless, because Storer's formula applies equally well to both of the extremes of nonequilibrium flow, it might be expected to apply also in the nonequilibrium case if the density behind the shock were replaced by a suitable average density along the stagnation streamline. Indeed, this has been found to be the case and good agreement with the nonequilibrium shock detachment data of reference<sup>92</sup> has been obtained when  $\rho_s$  in Storer's formula is replaced by

$$\bar{\rho} = \frac{1}{\Delta_{\text{FROZ}}} \int_0^{\Delta_{\text{FROZ}}} \rho \, ds \quad (3-17)$$

in which  $\Delta_{\text{FROZ}}$  is the frozen shock detachment distance, and  $\rho$  is the density from the nonequilibrium streamtube solution which is obtained using the velocity correlation with  $\Delta = \Delta_{\text{FROZ}}$ .

### 3.2.3.2 Boundary Layer Solution

In the boundary layer region of the shock layer the solution is provided by the implicit finite difference method of Blottner<sup>182</sup>. At the stagnation point the boundary layer equations degenerate to a set of ordinary nonlinear differential equations with two-point boundary conditions. After a transformation to the Howarth-Dorodnitsyn coordinates system, Blottner solves the linearized set of governing equations by an implicit finite difference scheme which requires the successive inversions of a tridiagonal matrix. The governing equations which must be solved are of the form

$$\frac{d^2 H}{d\eta^2} + \alpha_1 \frac{dH}{d\eta} + \alpha_2 H + \alpha_3 = 0 \quad (3-18)$$

in which  $\eta$  is the transverse Howarth-Dorodnitsyn coordinate and  $H$  represents the longitudinal velocity ratio  $u/u_e$ , the temperature ratio  $T/T_e$ , the species mass fractions  $C_i$ , or the element mass fractions  $C^j$  depending on whether the momentum, energy, species continuity, or element conservation equation is being considered. Because of the linearization process the coefficients  $\alpha_1$ ,  $\alpha_2$ ,  $\alpha_3$  and  $\alpha_4$  depend on the unknown variables  $H$ . Thus, to start the solution, initial profiles of the dependent variables must be provided from which to calculate the coefficients. The set of governing finite difference equations forms a tridiagonal matrix which yields the solution of the dependent variables after inversion. Based on these values of the dependent variables, the coefficients are recalculated and the process repeated until the change in the dependent variables for successive iterations is less than a specified small tolerance.

Calculations for a 0.5 inch nose radius body at velocities of 22.0 and 21.95 kilofeet/sec at altitudes of 200 and 150 kilofeet respectively have been done. The results of the matched inviscid-boundary layer stagnation line solutions are presented in Figures 3-30 through 3-36 where successfully in groups of two, the inviscid and boundary layer solutions are compared at altitudes of 200 and 150 kilofeet for the gas temperature, density, electron density, and pressure. In both cases the boundary layer edge was arbitrarily defined as the point where the derivative of the longitudinal velocity ratios equaled 1/10 i. e., at the point where

$$\frac{du}{d\eta} \frac{u_e}{u} = 1/10 \quad (3-19)$$

In both cases the boundary layer displacement thickness is negative due to the cold wall condition and, it is so small as to be unnoticeable in the results. Also, in both cases the catalytic wall condition (thermodynamic equilibrium) is imposed.

It should be noted that the rapid decrease in temperature and corresponding increase in density for the inviscid solution near the wall is caused by the equilibrium condition which is intrinsically required by reacting inviscid flows at a stagnation point.

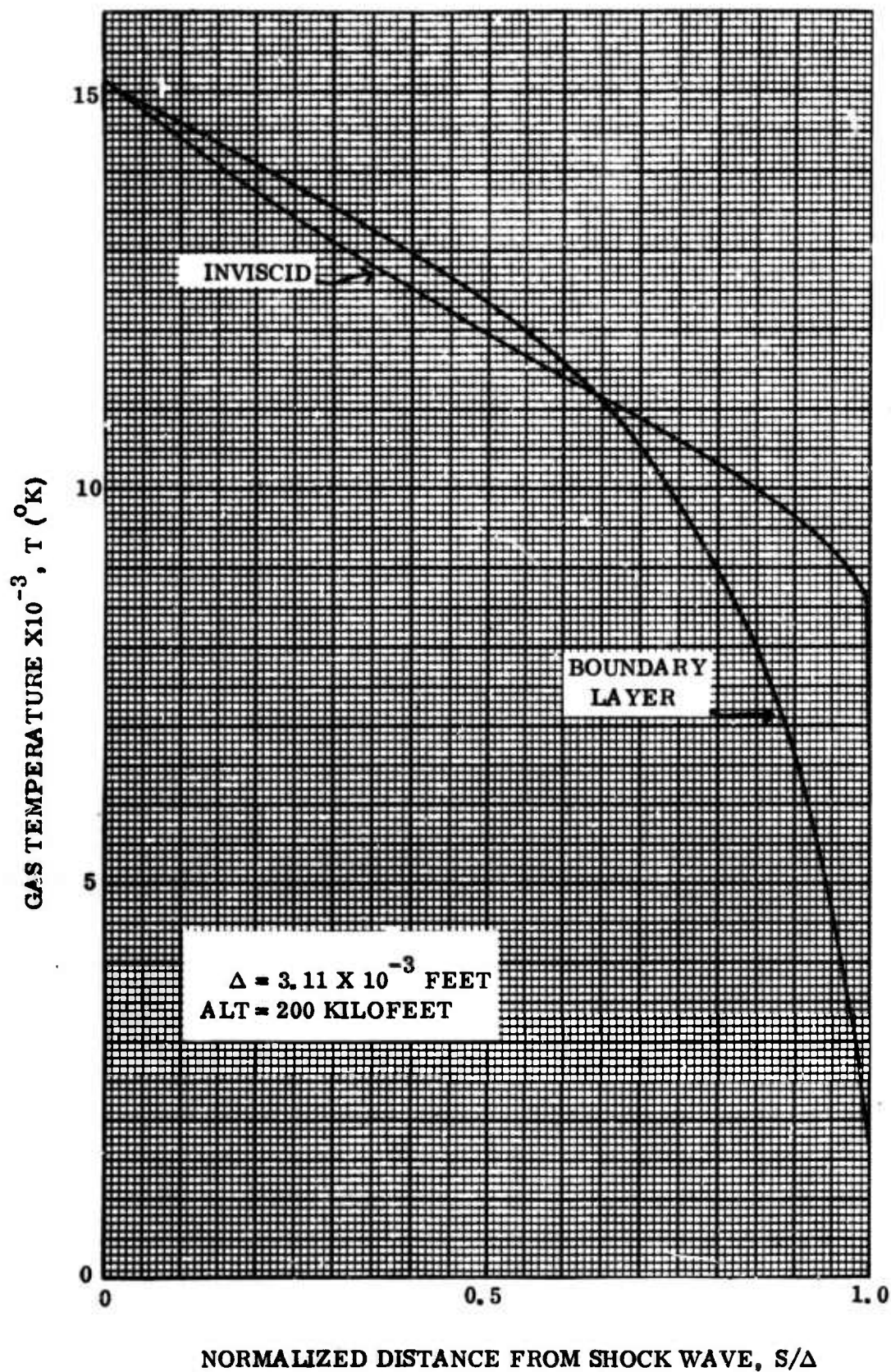


Figure 3-30. Matched Inviscid - Boundary Layer Solutions; Gas Temperature vs. Normalized Distance from Shock Wave

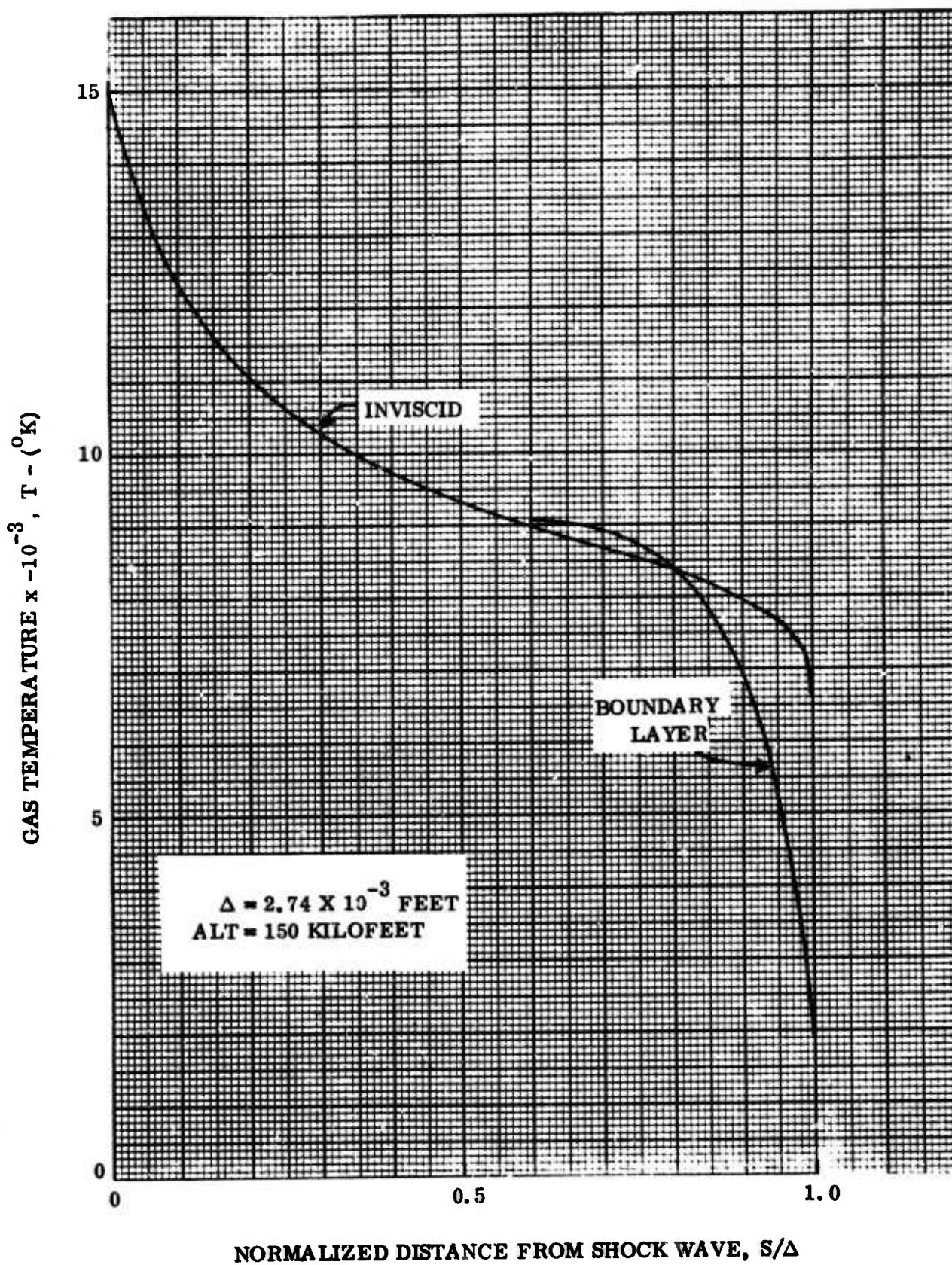


Figure 3-31. Matched Inviscid - Boundary Layer Solutions; Gas Temperature vs. Normalized Distance from Shock Wave

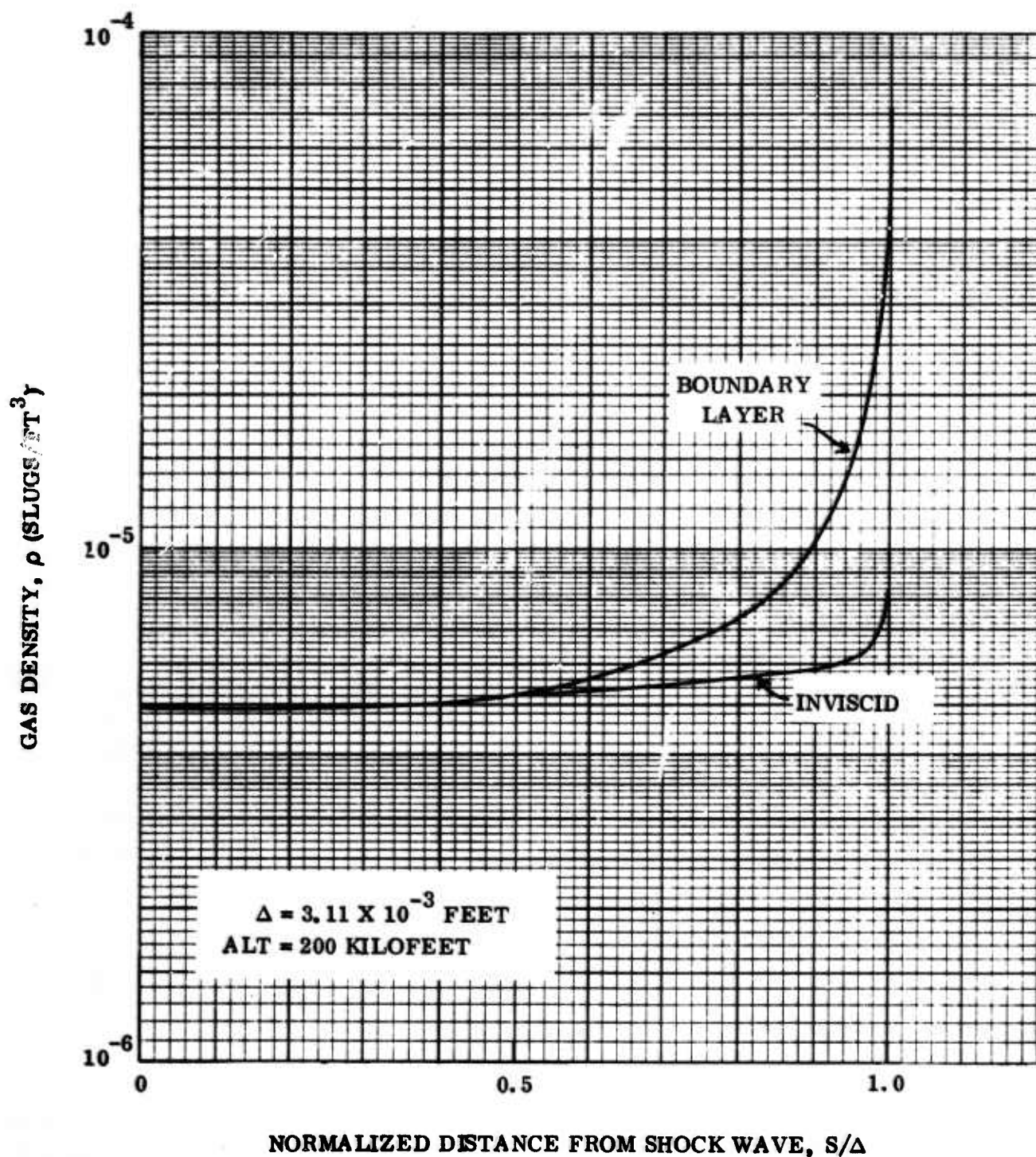


Figure 3-32. Matched Inviscid - Boundary Layer Solutions; Gas Density vs. Normalized Distance from Shock Wave

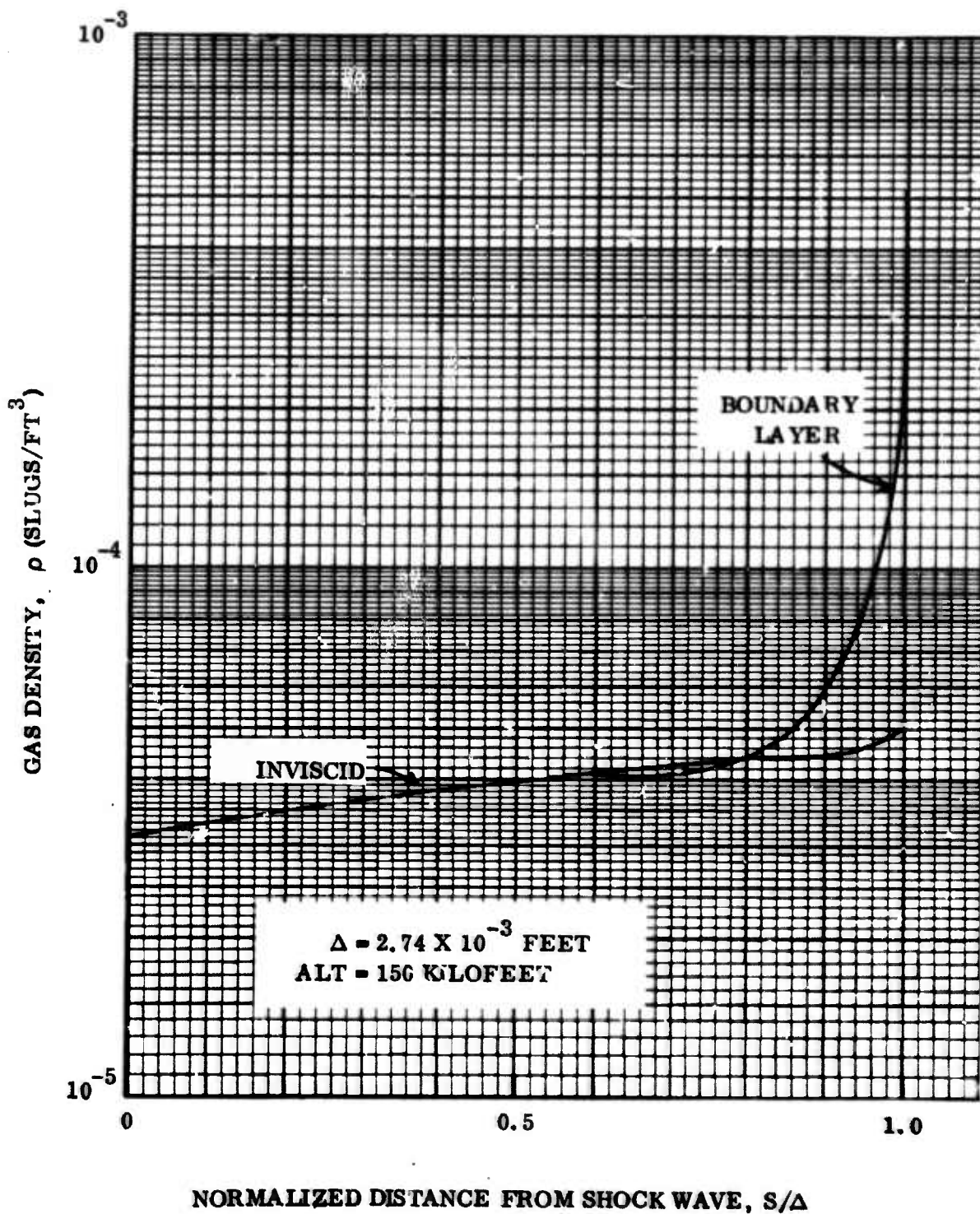


Figure 3-33. Matched Inviscid - Boundary Layer Solutions; Gas Density vs. Normalized Distance from Shock Wave

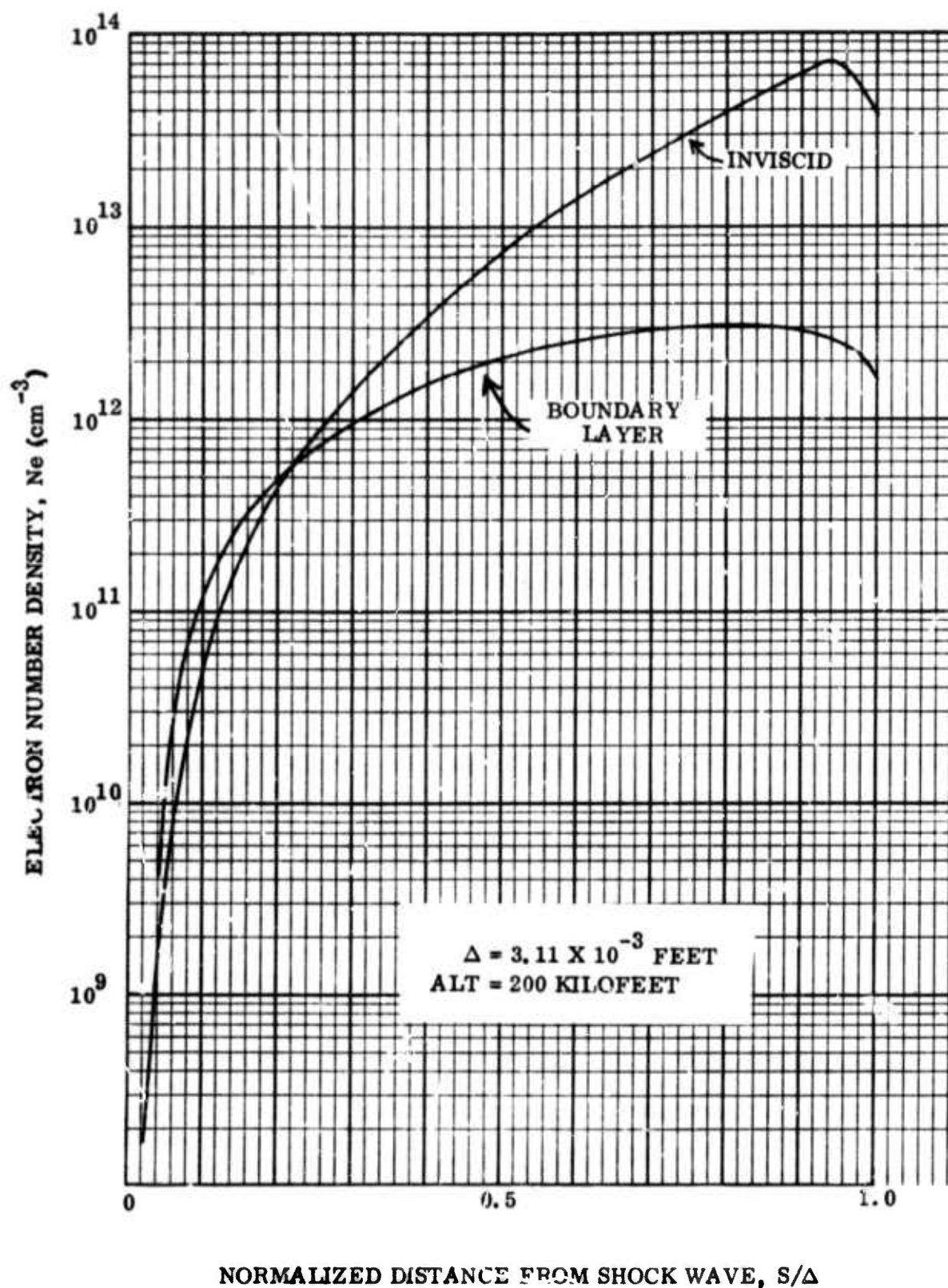


Figure 3-34. Matched Inviscid - Boundary Layer Solutions; Electron Density vs. Normalized Distance from Shock Wave

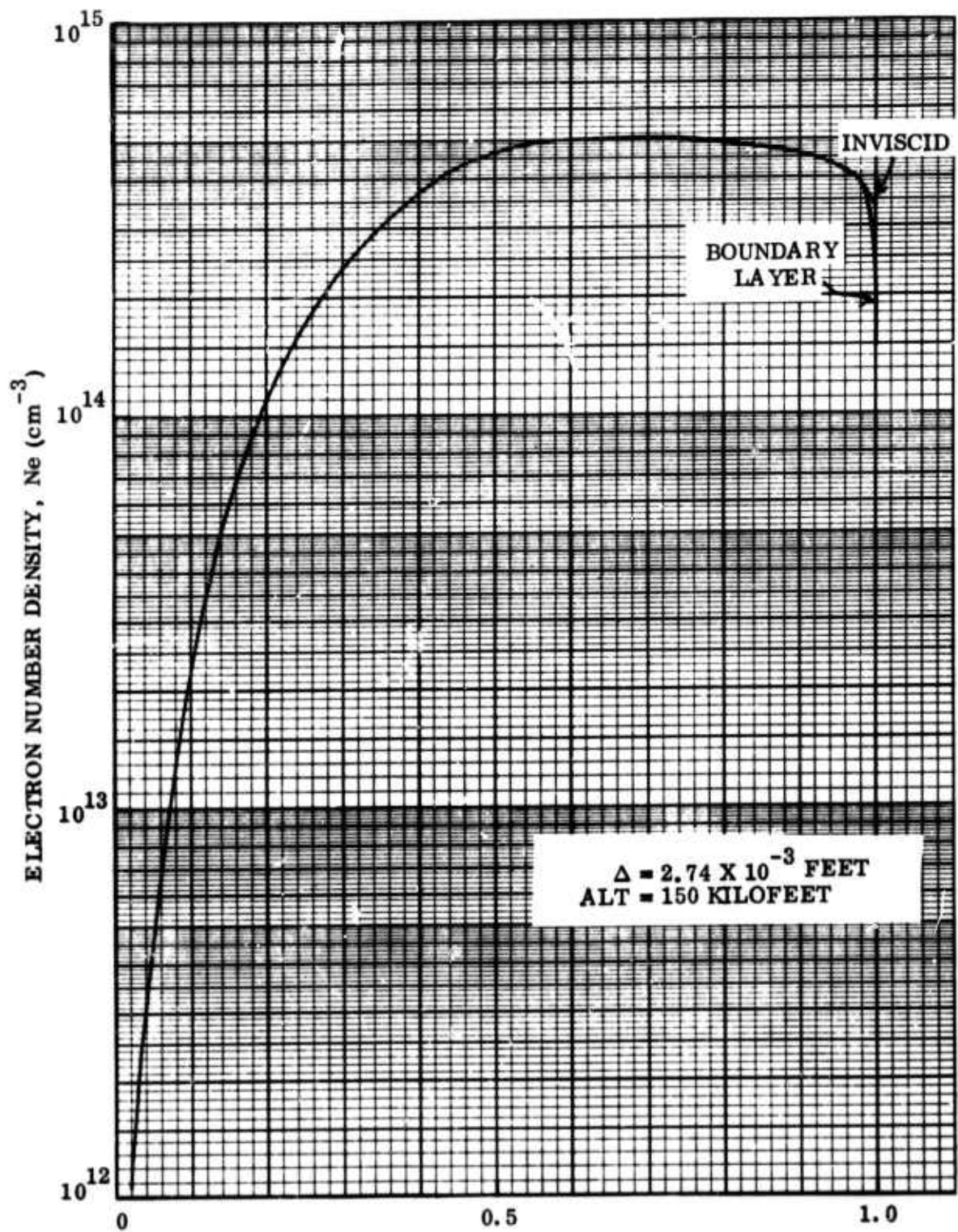


Figure 3-35. Matched Inviscid - Boundary Layer Solutions; Electron Density vs. Normalized Distance from Shock Wave

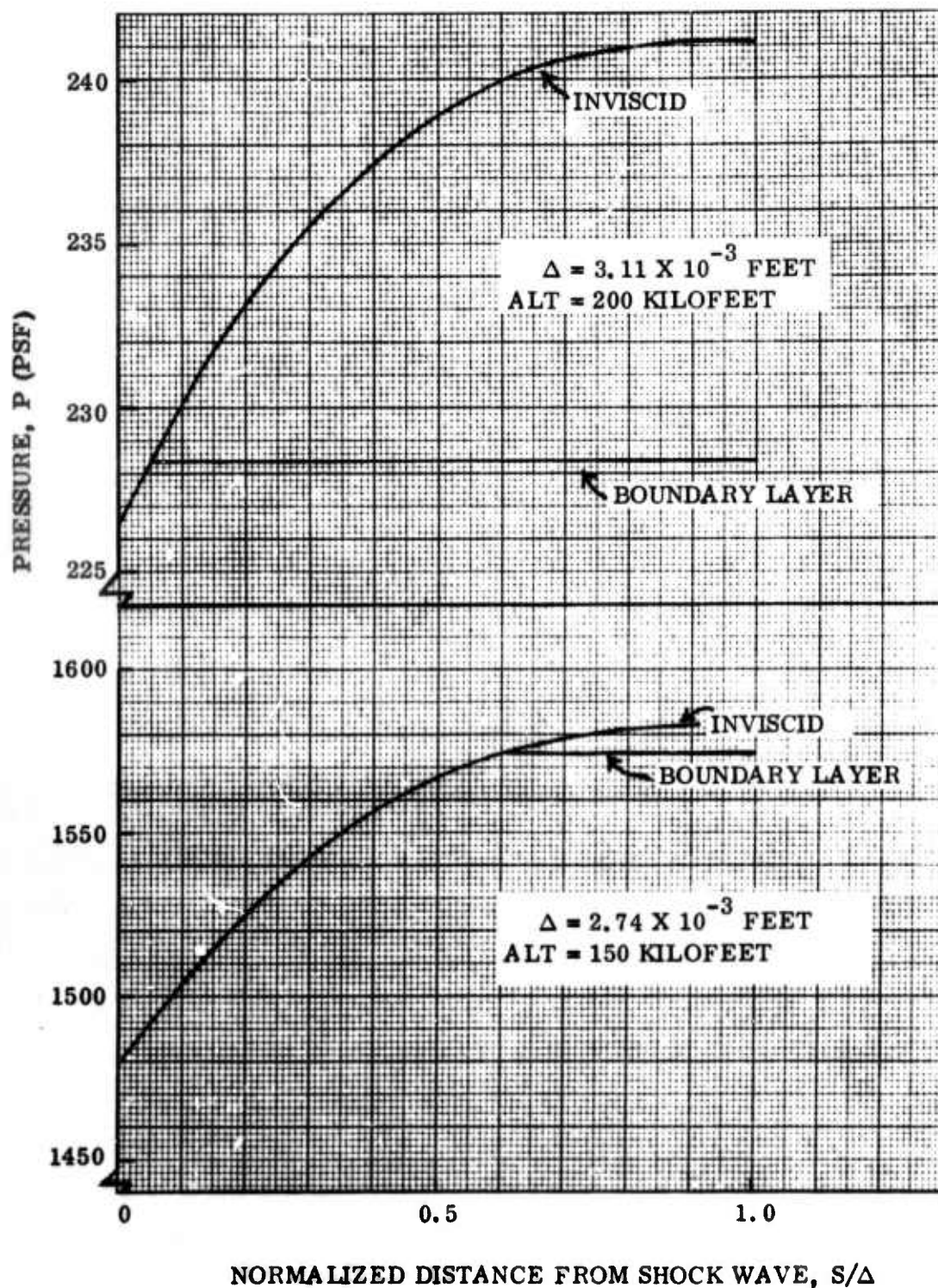


Figure 3-36. Matched Inviscid - Boundary Layer Solutions; Gas Pressure vs. Normalized Distance from Shock Wave

### 3.2.4 INVISCID LAYER-BOUNDARY LAYER CALCULATIONS

Profiles of the nonequilibrium flow properties (temperature, velocity, density, and electron density) at body stations corresponding to  $s_b/R_N = 0.4962, 61.25, \text{ and } 243.3$  are shown in Figures 3-37 to 3-48. In each of these figures the dashed lines represent the results of a pointed cone teflon-air boundary layer calculation with simulated nose bluntness and a noncatalytic wall. Nose bluntness effects on electron production were simulated in the pointed cone calculation by adding electrons at the boundary layer edge in the tip region so that the integrated electron mass flow at a station farther back on the body matches that of a corresponding blunt cone. This procedure was necessary for the teflon calculations because the teflon chemistry has not yet been incorporated into the blunt body boundary layer. The integrated electron mass flows were obtained from the blunt body pure air calculation at 150 kilofeet and scaled for the two higher altitudes. The matching station was taken at  $2\frac{1}{2}$  nose radii back on the conical section. From the matching station to the end of the body, teflon was injected at a rate inversely proportional to the square root of the distance along the surface, and the wall temperature was equal to  $1800^\circ\text{R}$ . Also, at the present time, the noncatalytic wall option is the only one available with mass addition other than air.

The broken dashed lines in each of the figures represent the results of pure air blunt body boundary layer calculation with no mass transfer and a catalytic wall at a temperature of  $1800^\circ\text{R}$ . Based on Probst's<sup>2</sup> criterion, the solution at altitudes of 150 and 200 kilofeet are in the boundary layer - inviscid layer and the viscous layer regimes, respectively, and for these two altitudes the inviscid layer solutions are shown as solid lines. However, at an altitude 250 kilofeet, the flow is in the merged layer regime and in this instance the results were obtained using the boundary layer solutions with the shock layer increased to include the shock transition zone and the edge conditions obtained from the adiabatic Rankine-Hugoniot relations. The results at this altitude are, therefore, only approximate because the effects of transverse curvature, normal pressure gradient, and temperature and velocity jump at the edge have not been properly accounted for.

At the two lower altitudes the first iteration in matching mass flows of the inviscid and boundary layer solutions, to determine the proper boundary layer edge conditions, has been done. It is significant to note that, although the two solutions have not been matched exactly, a smooth joining could be accomplished by additional iterations without apparent difficulty. This plainly indicates that in vorticity interaction problems, the only real difficulty lies in determining at what finite distance the boundary layer edge is located. For the two cases presented here, the boundary layer edge is arbitrarily prescribed at the same value of the transformed normal coordinate determined as the edge in the stagnation point solutions of Paragraph 3.2.3. It is also interesting to note that back on the cone surface the entropy layer is contained within the boundary layer.

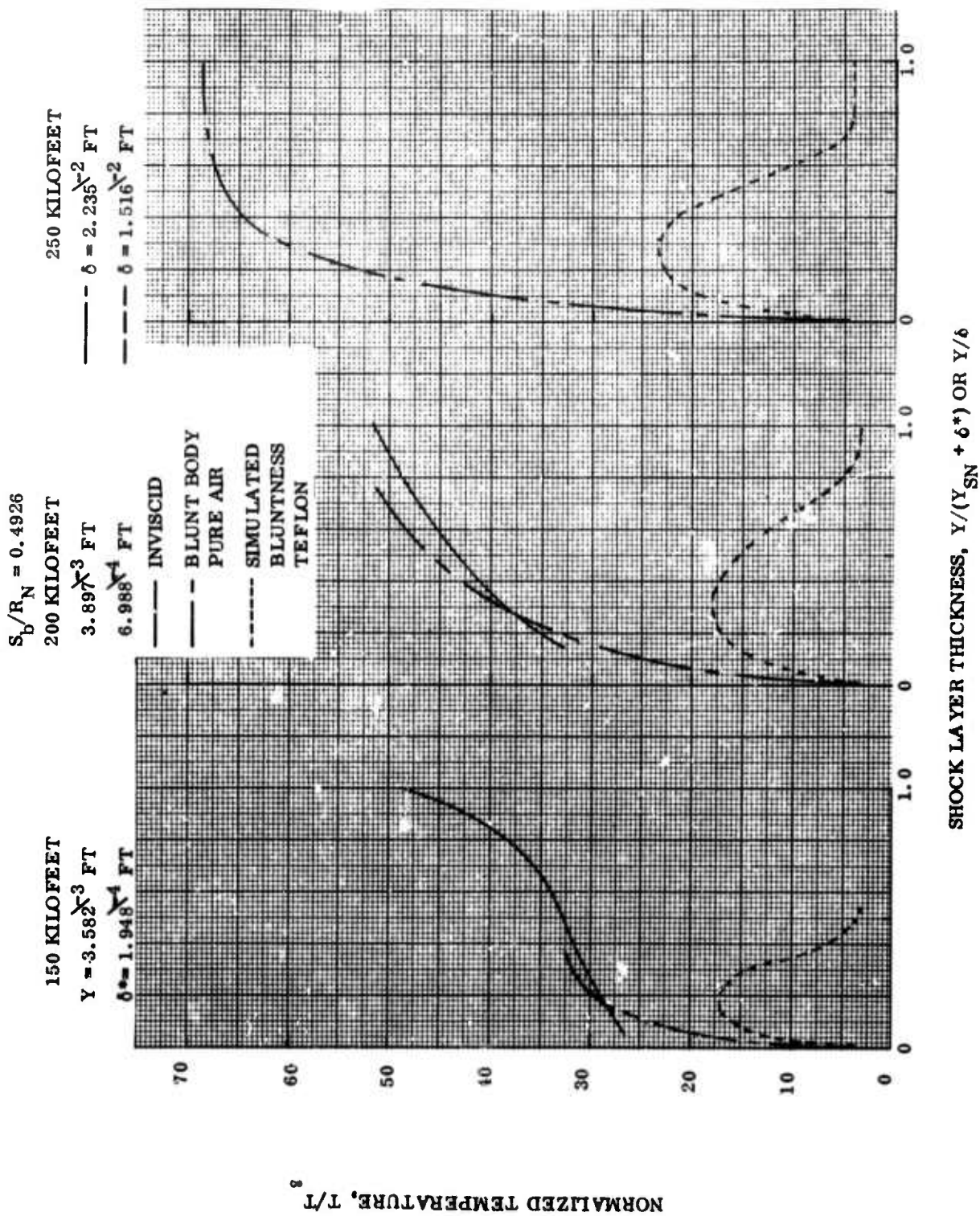


Figure 3-37. Normalized Temperature vs. Shock Layer Thickness

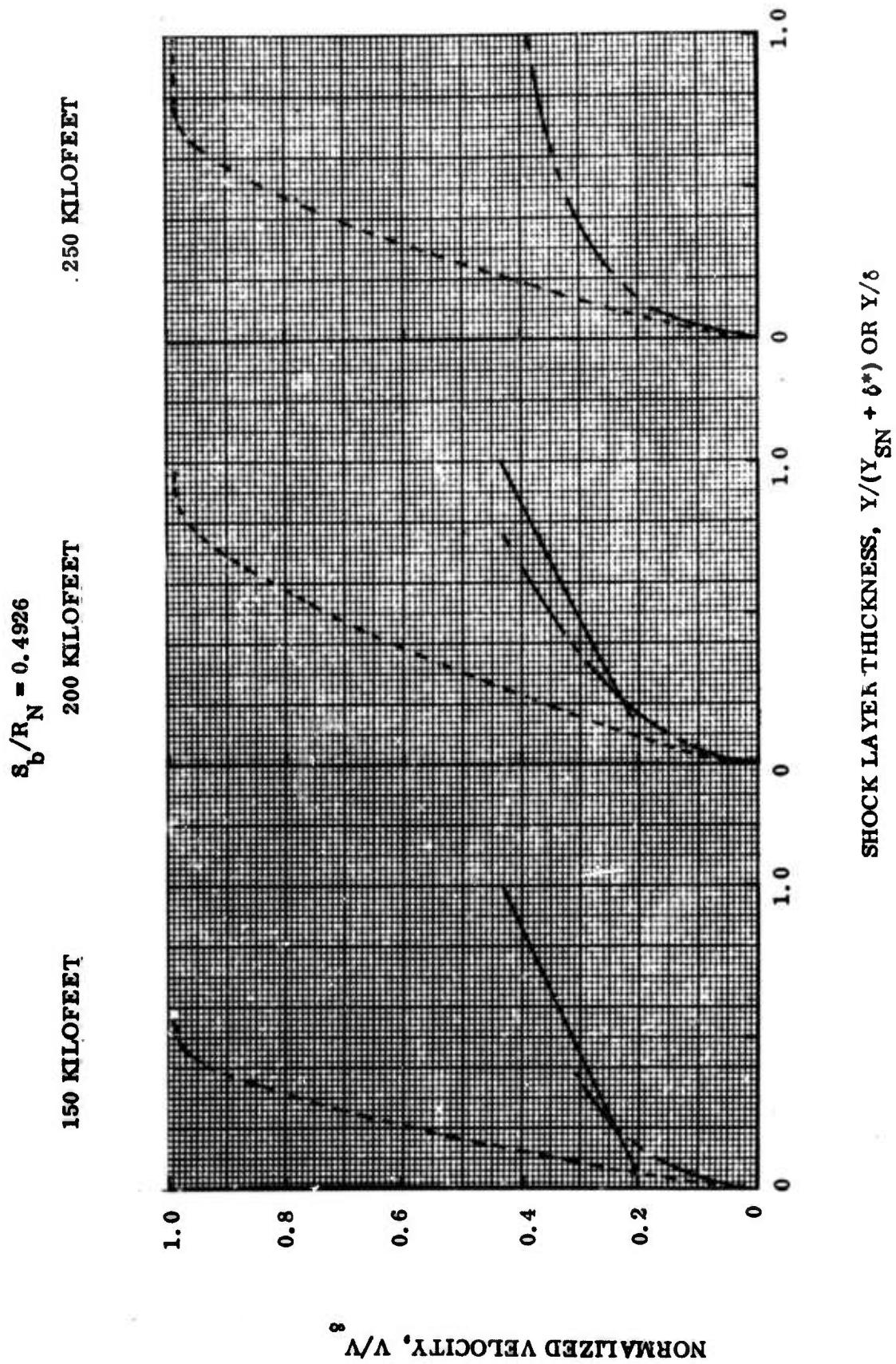


Figure 3-38. Normalized Velocity Parallel to Surface vs. Shock Layer Thickness

$$S_b/R_N = 0.4926$$

150 KILOFEET

200 KILOFEET

250 KILOFEET

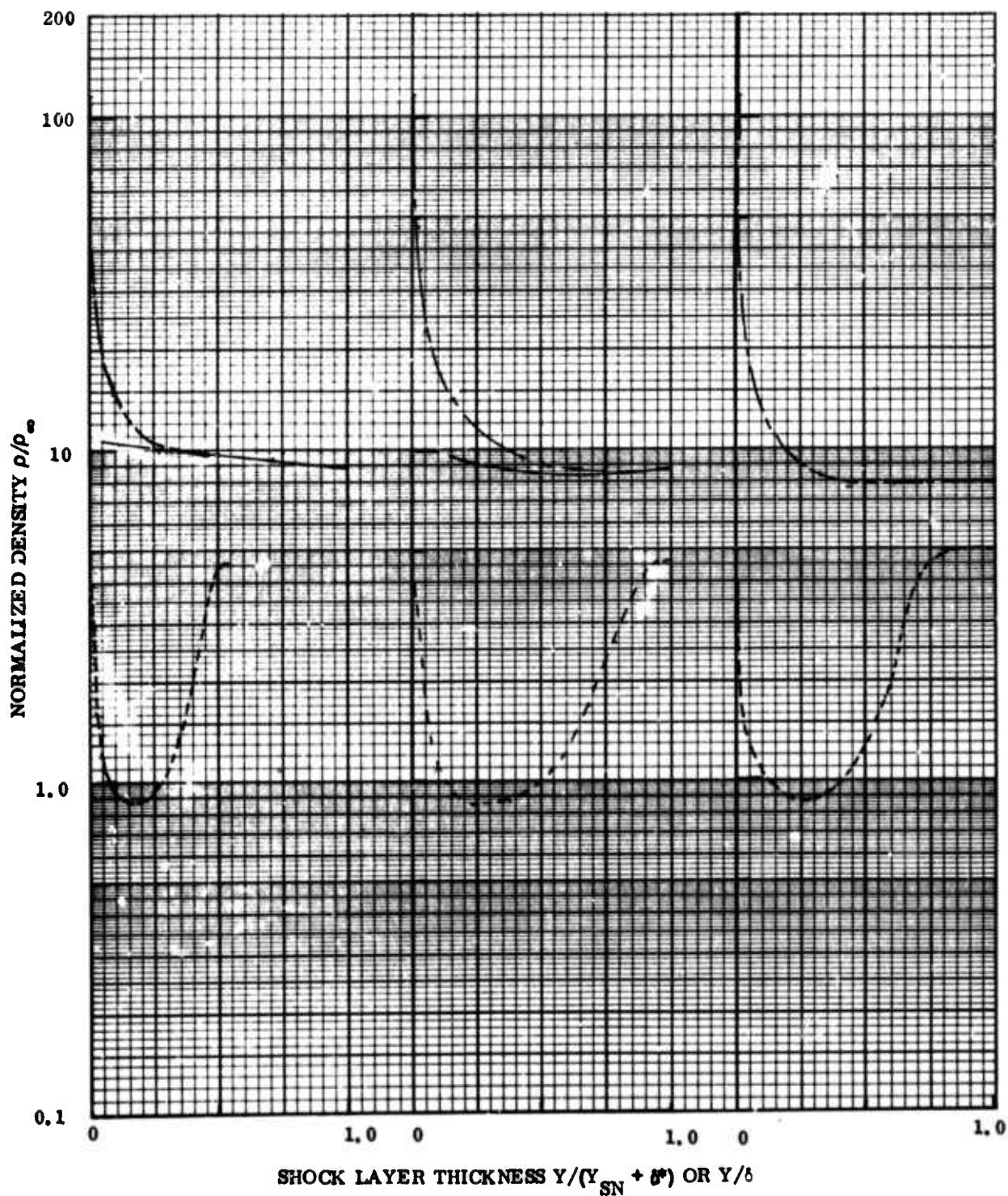


Figure 3-39. Normalized Density vs. Shock Layer Thickness

$$S_b/R_N = 0.4926$$

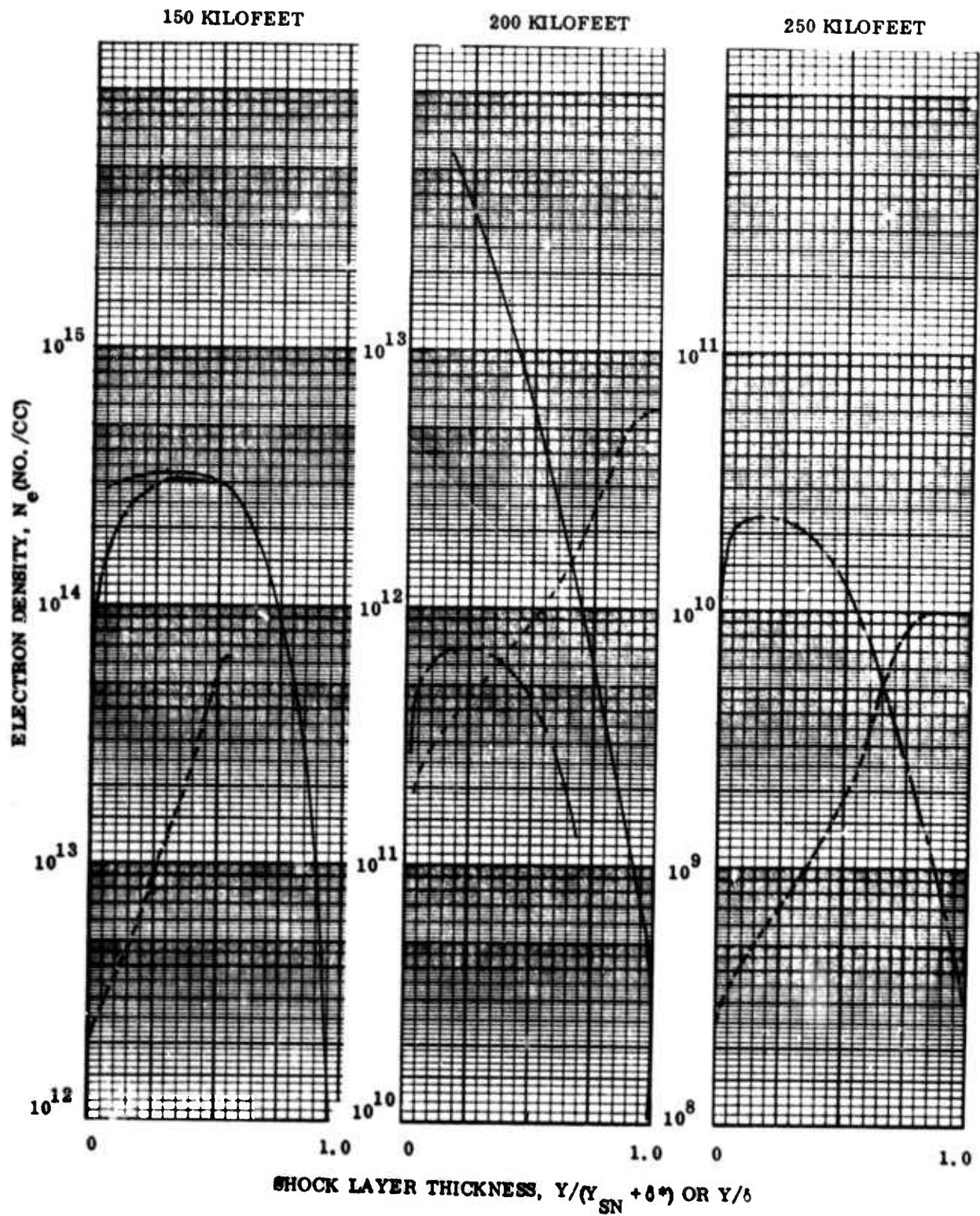


Figure 3-40. Electron Density vs. Shock Layer Thickness

$$S_b/R_N = 61.25$$

200 KILOFEET

$$\delta = 6.659 \sqrt{-2} \text{ FT.}$$

$$\delta^* = 4.341 \sqrt{-2} \text{ FT.}$$

250 KILOFEET

$$\delta = 2.752 \sqrt{-1} \text{ FT.}$$

$$\delta^* = 2.036 \sqrt{-1} \text{ FT.}$$

150 KILOFEET

$$Y_{SN} = 6.770 \sqrt{-2} \text{ FT.}$$

$$\delta^* = 1.752 \sqrt{-2} \text{ FT.}$$

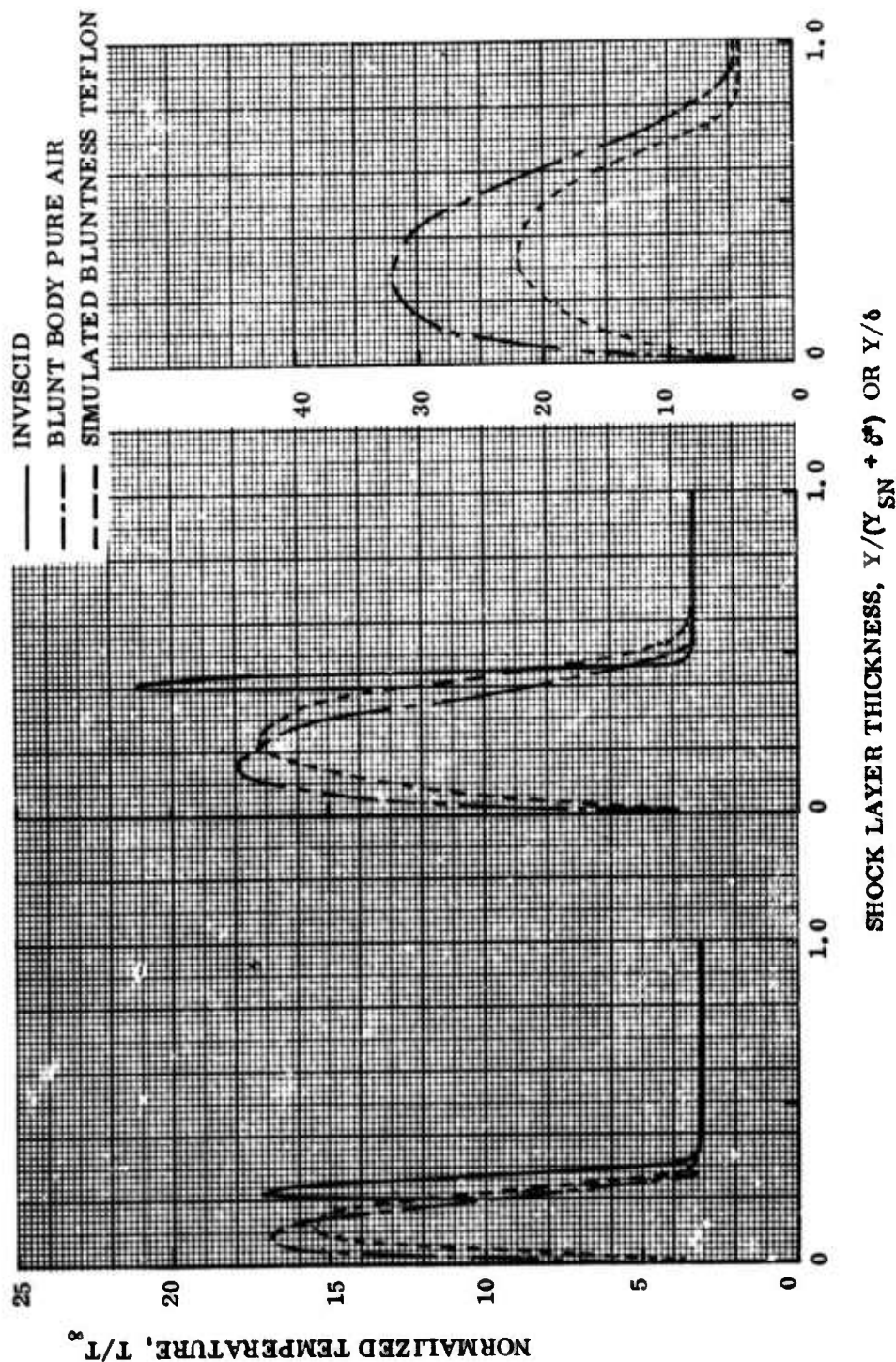


Figure 3-41. Normalized Temperature vs. Shock Layer Thickness

$$S_b/R_N = 61.25$$

3-110

150 KILOFEET

200 KILOFEET

250 KILOFEET

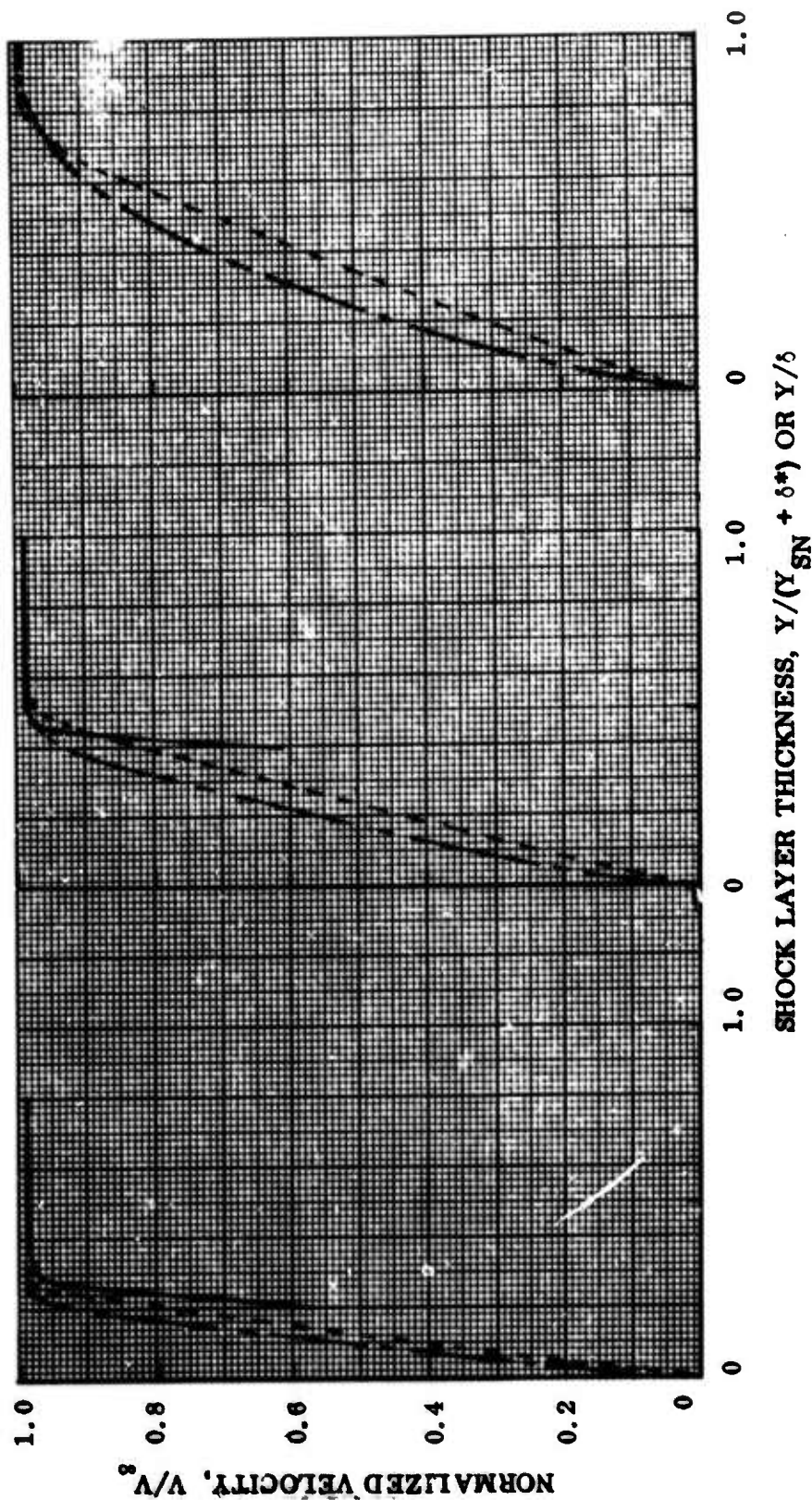


Figure 3-42. Normalized Velocity Parallel to Surface vs. Shock Layer Thickness

$$S_b/R_N = 61.25$$

150 KILOFEET

200 KILOFEET

250 KILOFEET

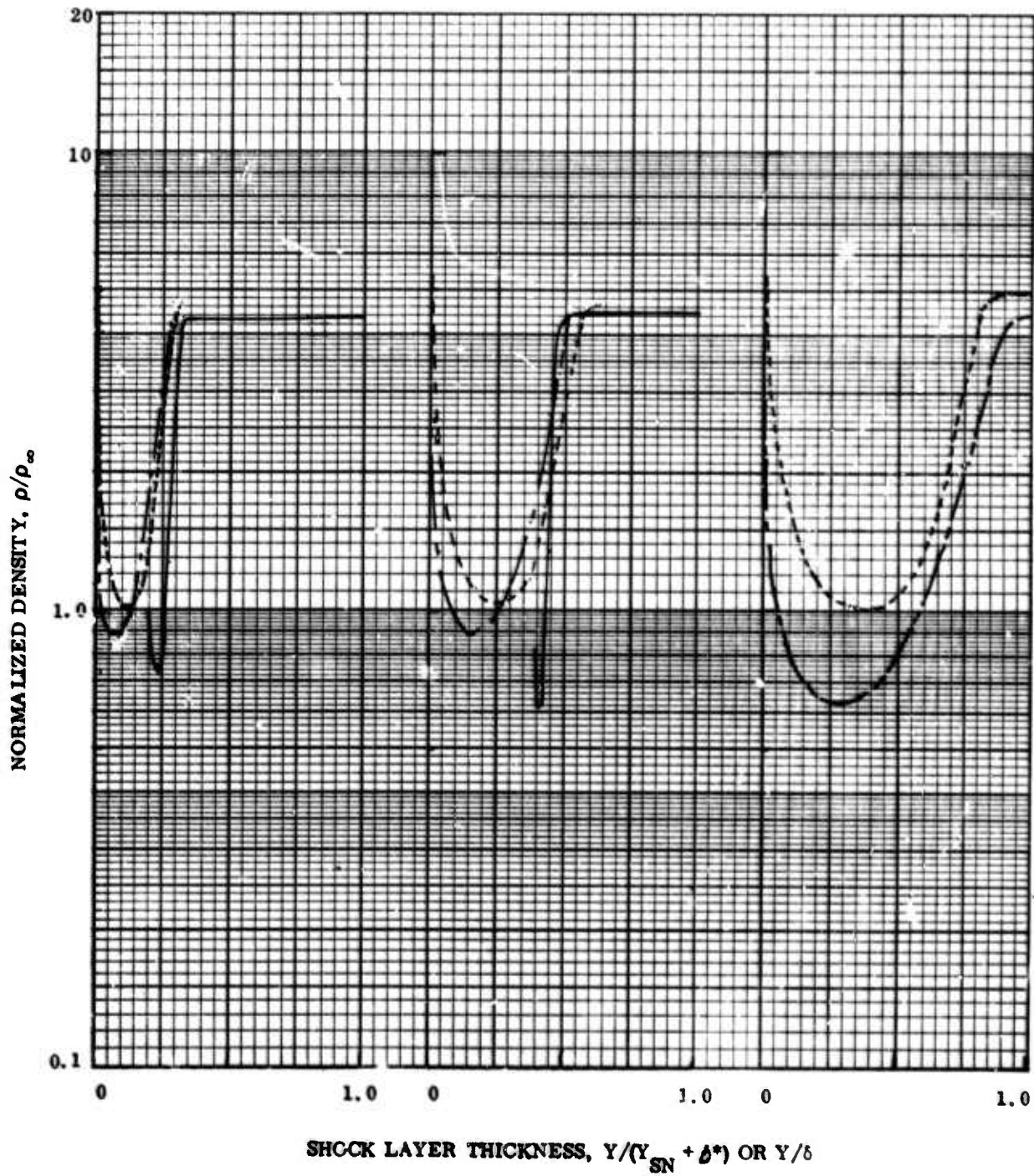


Figure 3-43. Normalized Density vs. Shock Layer Thickness

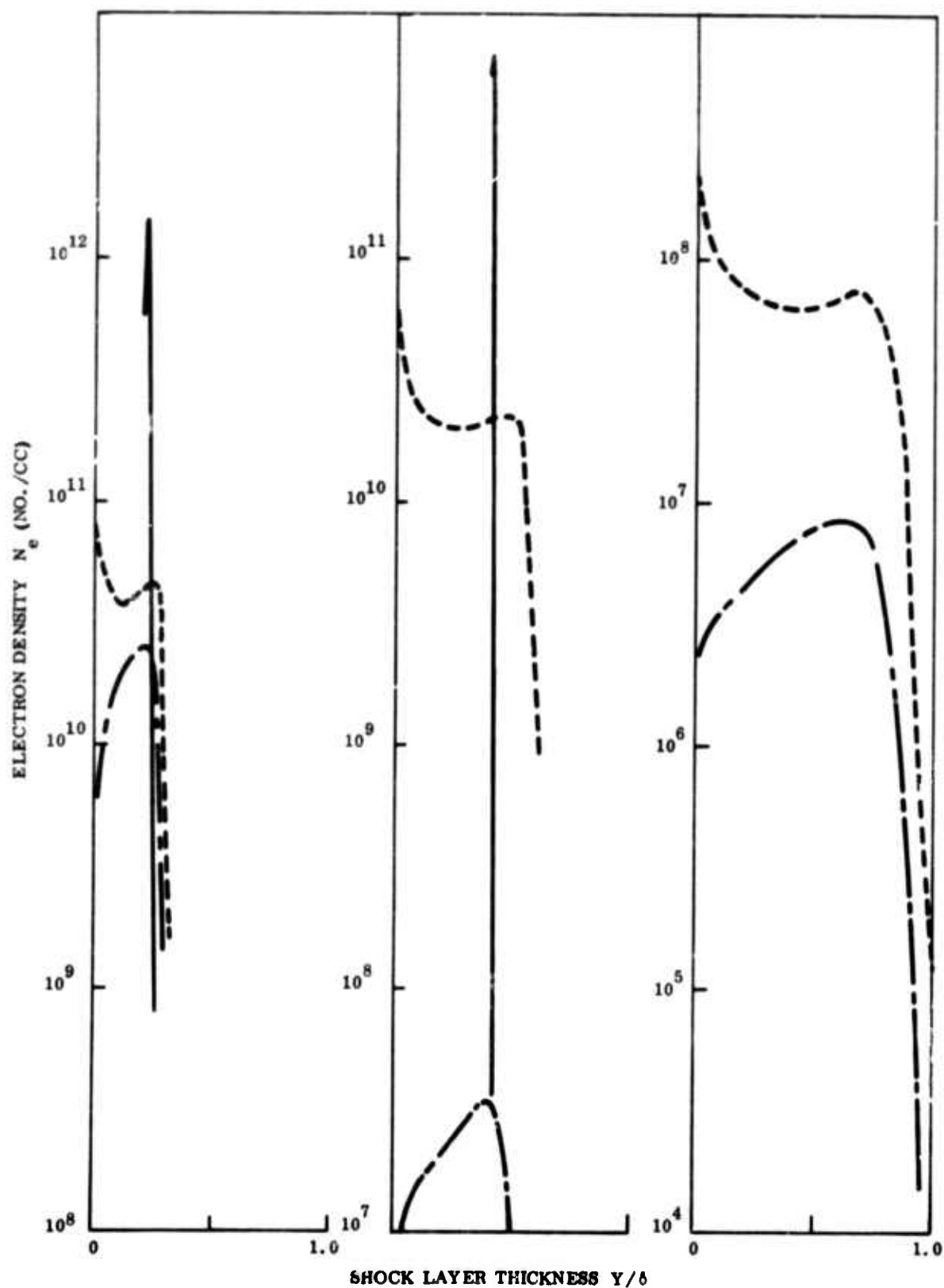


Figure 3-44. Electron Density vs Shock Layer Thickness  $s_b/R_n = 243.3$

$$S_u/R_N = 243.3$$

150 KILOFEET

$$Y_{SN} = 2.142 \sqrt[3]{K^1} \text{ FT}$$

$$\delta^* = 3.215 \sqrt[3]{K^1} \text{ FT}$$

200 KILOFEET

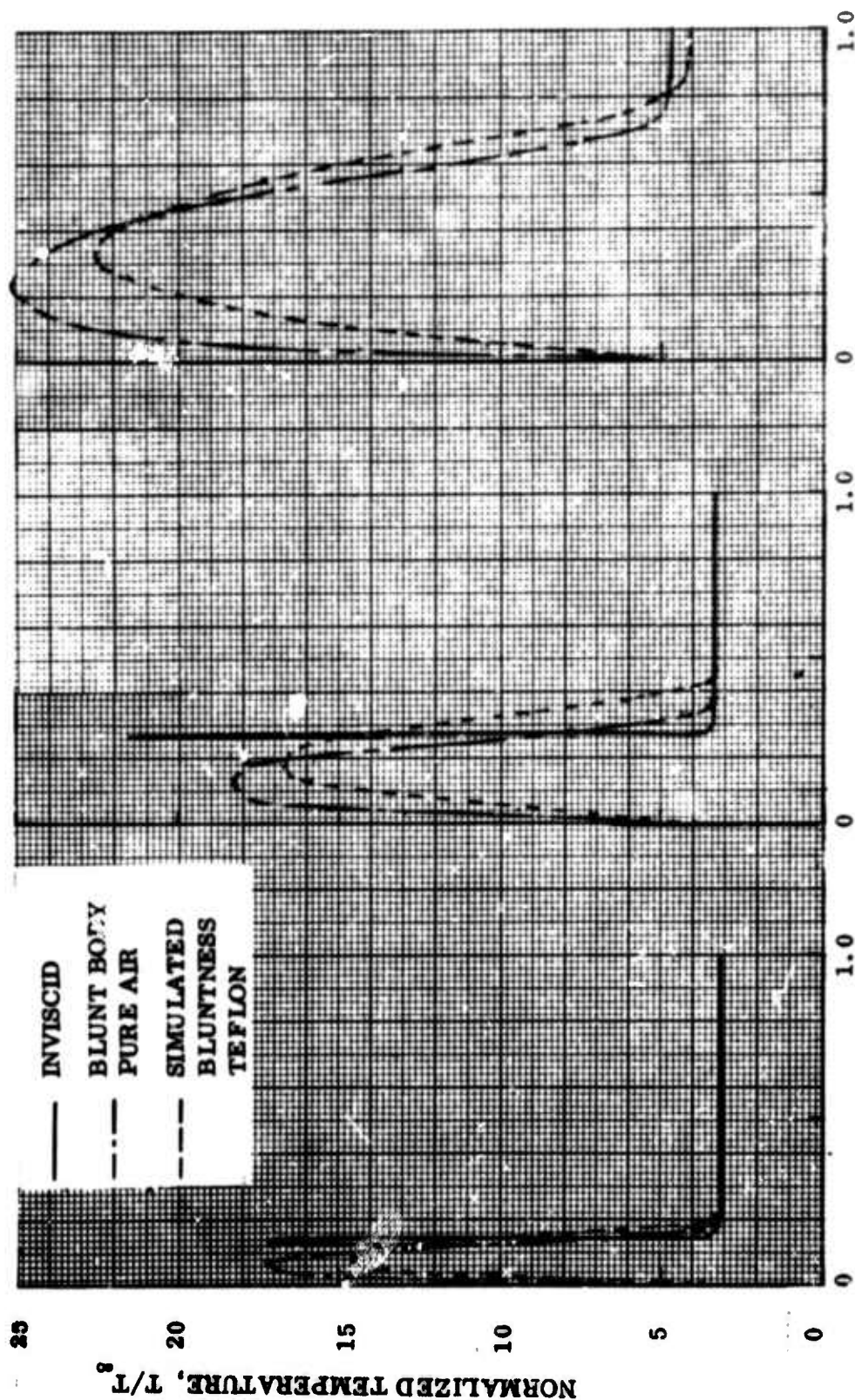
$$2.148 \sqrt[3]{K^1} \text{ FT}$$

$$7.715 \sqrt[3]{K^2} \text{ FT}$$

250 KILOFEET

$$--- = 64.16 \sqrt[3]{K^1} \text{ FT}$$

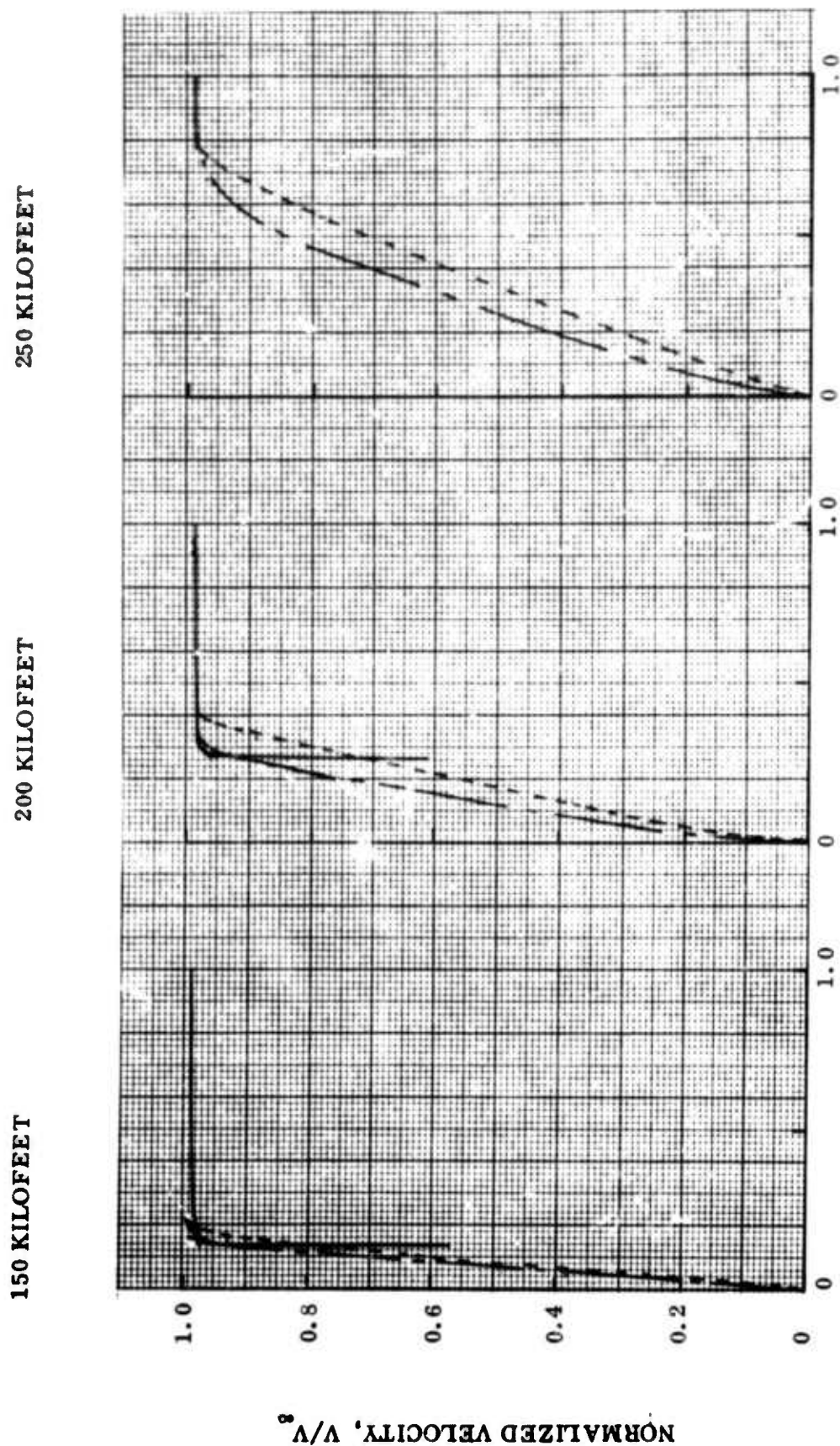
$$--- = 64.085 \sqrt[3]{K^1} \text{ FT}$$



SHOCK LAYER THICKNESS,  $Y/(Y_{SN} + \delta^*)$  OR  $Y/\delta$

Figure 3-45. Normalized Temperature vs. Shock Layer Thickness

$$S_b/R_N = 243.3$$



SHOCK LAYER THICKNESS,  $Y/(Y_{SN} + \delta^*)$  OR  $Y/\delta$

Figure 3-46. Normalized Velocity Parallel to Surface vs. Shock Layer Thickness

$$S_b/R_N = 243.3$$

150 KILOFEET

200 KILOFEET

250 KILOFEET

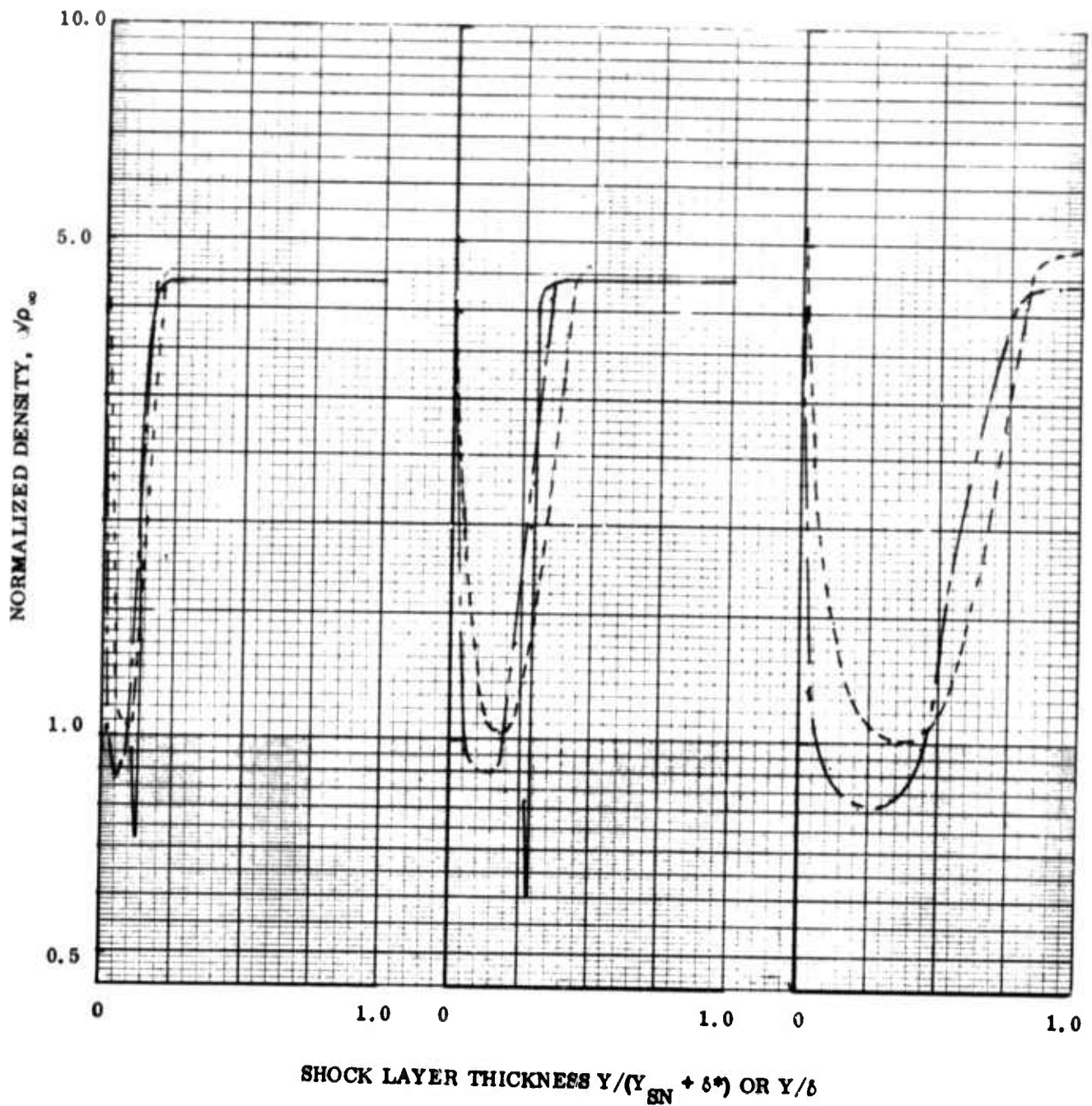


Figure 3-47. Normalized Density vs. Shock Layer Thickness

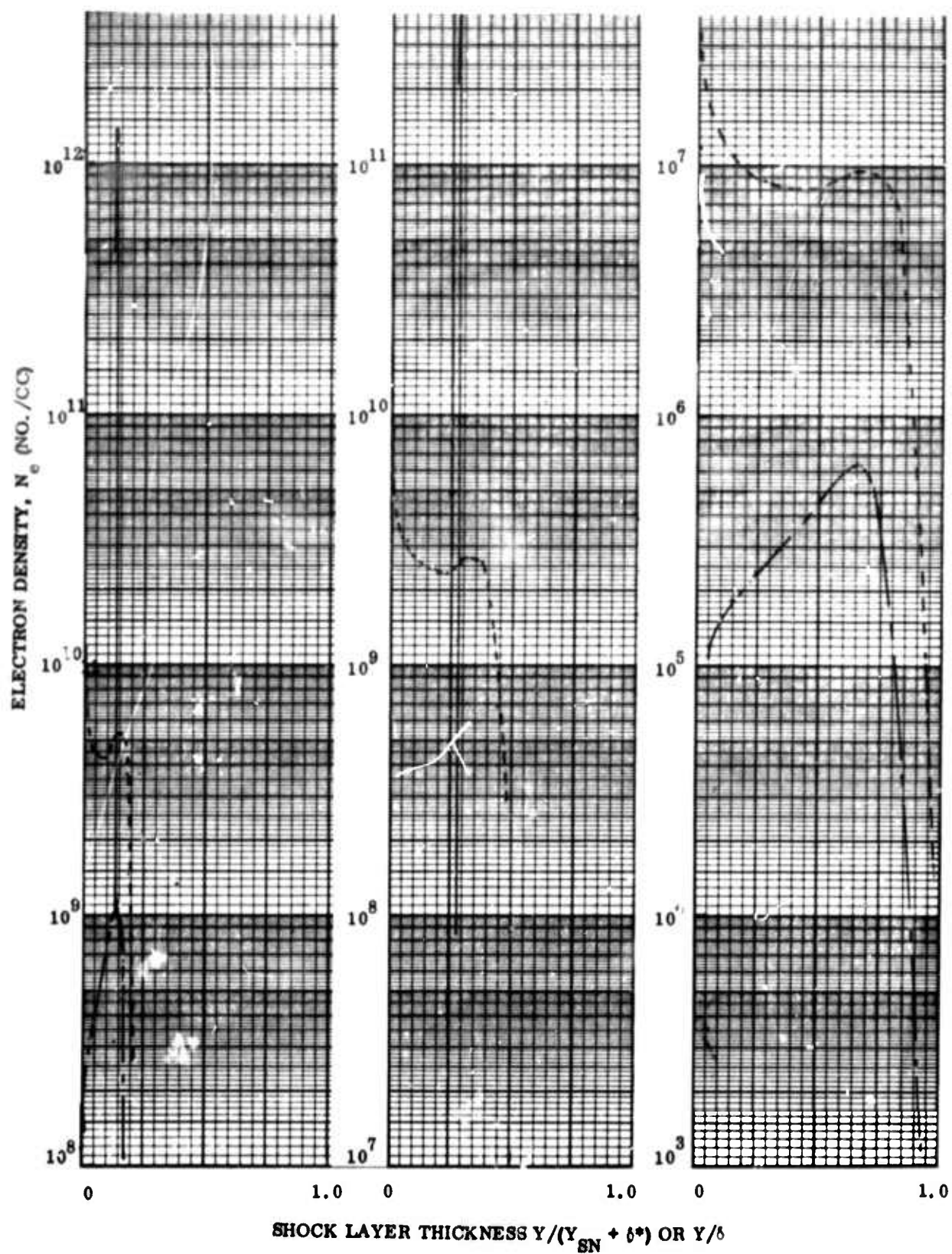


Figure 3-48. Electron Density vs Shock Layer Thickness  $s_b/R_n = 61.25$

## SECTION 4

### ANTENNAS

The importance of the antenna in a reentry transmission system goes beyond the usual factors associated with electrical performance, radiation pattern, and efficiency. The antenna near-field distribution has an intimate effect on the form and magnitude of the influence of the reentry induced environment on the antenna performance. That this is true is fairly obvious for both linear and nonlinear plasma effects, since the reentry plasma is formed in the immediate vicinity of the antenna. But it is especially true in the case of antenna breakdown effects.

The near-field distribution affects the breakdown characteristics of an antenna in various ways. The effect on the characteristic diffusion length is the most important, even in the static environment inside a vacuum chamber. In the reentry environment the near-field distribution is partially responsible for determining which flow field region will breakdown, (i. e. the region having the highest field intensity). Also the near-field distribution affects the antenna impedance and thus it controls the relationship between the input power at breakdown, which is significant to the transmitting system, and the breakdown field strength, which is predicted by the theory.

This section is devoted to a survey of the problem of antenna near-field calculation and the derivation of simple estimates of the ratio of the characteristic diffusion length to the wavelength of the RF signal.

#### 4.1 SURVEY OF FIELD DISTRIBUTIONS

The distribution of radiated fields of an antenna can in principle be determined from a solution of Maxwell's equations with appropriate boundary conditions. If the distribution of currents and charges on a given antenna is known, then the field determination reduces to the evaluation of definite integrals involving these currents and charges. The difficult part of the problem lies in determining the distributions of the source currents and charges.

These source distributions are often assumed in order to make the problem tractable, and in the calculation of far-field patterns and total radiated power this assumption is not very critical. But in the determination of the near field and the antenna impedance, the assumption of a source distribution may lead to serious errors.

The current distribution on an antenna which consists of good conductors is often solved for by integral equation techniques. Such integral equations are based on the requirement that the tangential electric field at the surface of the antenna must vanish, where the field at a given point is determined by an integral over the current distribution at all other points.

King<sup>211</sup> and Hallen<sup>212</sup> have made extensive calculations of currents and fields on finite cylindrical antennas, and Harrington<sup>213</sup> has studied thin wire antennas in detail. While many variations on the techniques of solution of these equations, such as variational and perturbation methods, have been studied; it is possible to place them all on a common ground in terms of numerical methods of solution of integral equations. Unfortunately the numerical analysis nature of the theory makes it difficult to generalize, except when the form of the antenna is restricted to a very simple type.

The electric field  $E$ , caused by a source current density distribution  $J$ , is given by (MKS units)

$$\vec{E}(\vec{r}) = \frac{j\mu_0\omega}{4\pi} \int \vec{J}(\vec{r}') \frac{e^{ik|\vec{r}-\vec{r}'|}}{|\vec{r}-\vec{r}'|} dv' \quad (4-1)$$

where  $\mu_0$  is the permeability of free space,  $\omega$  is the radian frequency,  $k$  is the wave number,  $\vec{r}'$  is the radius vector in the source coordinates,  $\vec{r}$  is in the field coordinates, and  $dv'$  is the source volume element. This equation is useful in deriving an integral equation for the unknown current distribution, as well as in calculating the field distribution for an assumed source current distribution.

## 4.2 ILLUSTRATIVE CALCULATIONS

The main concern in this section is the derivation of simple estimates of the effective diffusion length for the prediction of antenna breakdown. As discussed in Section 6.1, the diffusion length in classical breakdown theory comes from the solution of the equation,

$$\nabla^2 \Psi + (\nu/D) \Psi = 0 \quad (4-2)$$

where  $\nu$  is the high frequency ionization coefficient, and  $D$  is the diffusion coefficient. In the uniform field theory of cavity breakdown, the boundary conditions on the unknown function  $\Psi$  determine the solution to this equation. If the function  $\Psi$  is made to vanish at the walls, the operator  $\nabla^2$  has an eigenvalue  $(-1/\Lambda^2)$ , where  $\Lambda$  is the diffusion length. This result leads to the breakdown condition  $\nu = D/\Lambda^2$ .

In antenna breakdown theory, it is artificial to appeal to boundary conditions on the vanishing of  $\Psi$  in Equation (4-2), since the fields are not confined within a vessel with electron-absorbing walls. In this case the coefficient  $\nu/D$  is not constant, since it depends on the electric field intensity. No eigenvalue exists, except by analogy with the constant coefficient case in terms of the value of the Laplacian at a given point. The proper boundary conditions are that  $\Psi$  be continuous and have a continuous gradient and that it vanish at great distances and at the surface of the antenna.

A useful connection between the uniform field theory and antenna breakdown theory may be found in the results of Herlin and Brown<sup>214,215</sup> and MacDonald<sup>216</sup>. These authors studied the effects of nonuniform fields on the diffusion lengths of cavities, using a power law dependence of  $\nu/D$  on  $E$ . The results show that an effective diffusion length can be assigned at the peak field point, depending on the field intensity distribution. The effective diffusion length for cylindrical cavities depends on the geometry, especially at small cavity radius. The effective diffusion length in spherical cavities can be a factor of the order of one-half the geometrical diffusion length. Assuming that the field distribution is the controlling

factor, in light of the fact that the ionization frequency is a very strong function of field intensity, then the width of the high field region of an antenna should be related to its diffusion length. By analogy with the geometrical diffusion length, the antenna diffusion length should be on the order of  $1/\pi$  times the width of the high field region.

A simple illustrative case for microwave antennas is the waveguide opening into a ground plane. Assuming that the waveguide is operated in the dominant mode near cutoff, the wavelength  $\lambda$  is related to the guide dimensions  $a$  and  $b$  by

$$1/\lambda^2 = (1/2a)^2 + (1/2b)^2 \quad (4-3)$$

But the field distribution in the vicinity of the aperture will be dependent on  $a$  and  $b$  such that the following is approximately true for the geometrical diffusion length.

$$1/\Lambda^2 \cong (\pi/a)^2 + (\pi/b)^2 \quad (4-4)$$

Thus, for a slot fed by an open ended waveguide

$$\lambda \cong 2\pi\Lambda \quad (4-5)$$

Whether the above approximate value of the ratio  $\lambda/\Lambda$  is valid for antennas operated over the entire radar spectrum is open to some question. At the long wavelength end of the spectrum, there is considerable payoff in vehicle design to miniaturize antennas to be mounted on reentry vehicles. The antenna dimensions may be forced to be small compared to the wavelength, by utilizing special techniques such as end-fire design. As an example of such an antenna on which much data have been obtained, consider the conical equiangular spiral or log spiral antenna. This antenna has been analyzed theoretically by integral equation techniques<sup>217,218</sup> and the radiation patterns and near fields have been measured by Dyson<sup>219,220</sup>. This antenna consists of conducting arms spiraling around the surface of

a cone. The logarithm of the distance of the arms from the apex, measured along the cone surface, is proportional to the angle of rotation of the arm about the axis. Figure 4-1 shows results of near field measurements for a typical log spiral antenna of cone half-angle 10 degrees and 80 degrees pitch. The graph shows electric field amplitude at a distance of  $0.03 \lambda$  from the cone surface versus distance from the apex. In this figure it is clear that the antenna has an active region of finite extent, which for the example shown is  $0.23 \lambda$  wide at the 3 db points. If this active region is assumed equivalent to a slot of the same width, then

$$\lambda \cong 14 \Lambda \quad (4-6)$$

Based on the results of this section it is probably reasonable to assume that the ratio  $\lambda/\Lambda$  takes values from  $2\pi$  to about 14 for most types of antennas. The larger values are applicable to complicated antennas, such as periodic structures, and the smaller values apply to simple slot antennas.

An interesting example of a fairly rigorous calculation of near-field and diffusion length of a spheroidal monopole is provided by Cullen and Dobson<sup>221</sup>, who use the power law approximation to  $\nu/D$ .

$$\nu/D = (\nu/D)_0 (E/E_0)^\beta \quad (4-7)$$

Their result is

$$\Lambda = R/a(\beta+1) \quad (4-8)$$

where  $R$  is the radius of the antenna tip and  $a$  is the root of the Bessel function.

$$\frac{J_1}{2(\beta+1)}(a) = 0 \quad (4-9)$$

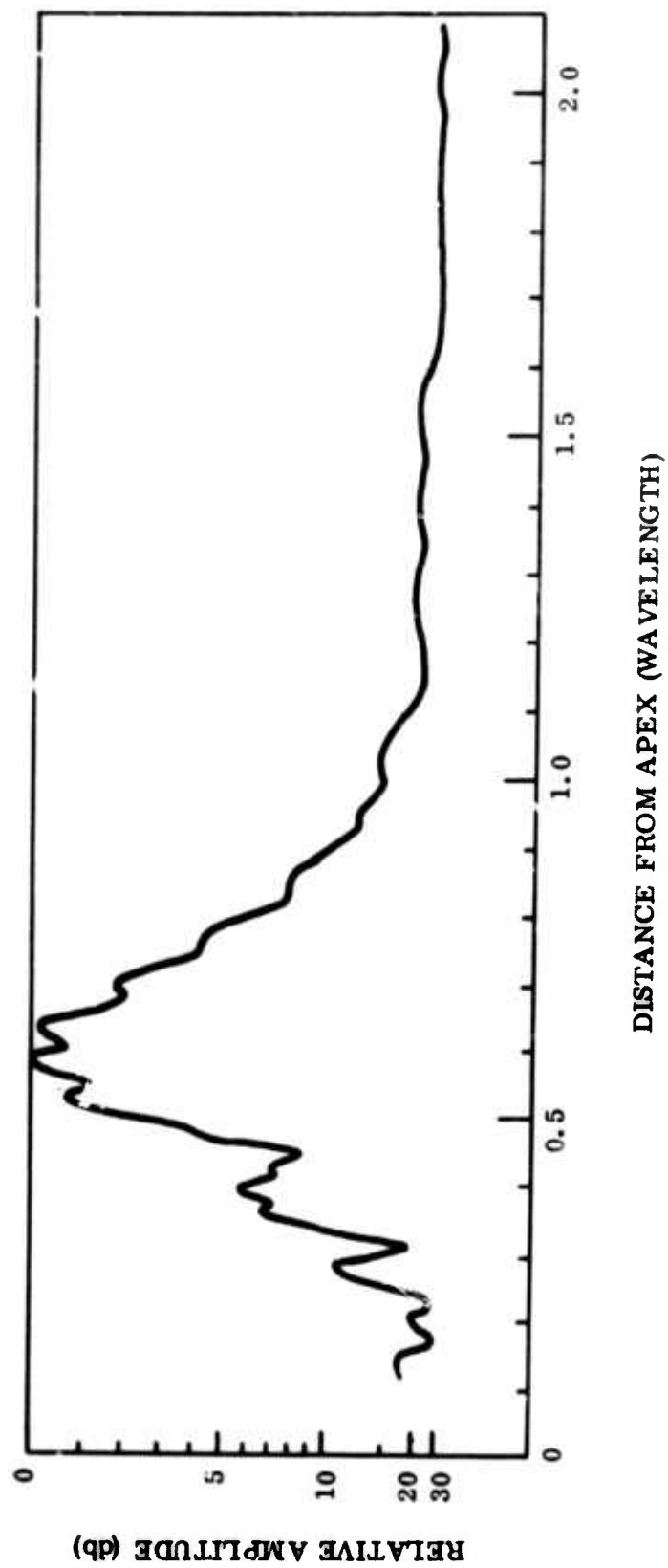


Figure 4-1. Amplitude of Near Fields of a Conical Spiral Antenna Measured at  $0.03\lambda$  from Surface

## SECTION 5

### LINEAR PLASMA EFFECTS

An antenna radiating through the reentry induced body plasma will be subject to certain effects regardless of how low the power level input to the antenna is made. These effects which tend not to depend on the magnitude of the local electromagnetic field strength are termed linear plasma effects. Such effects may take various forms. Absorption and reflection of electromagnetic waves by the plasma results in attenuation of the transmitted signals. Antenna pattern distortion causes the apparent attenuation to depend on the direction and polarization of the receiver. The energy reflected by the plasma couples into the antenna and causes its input impedance to change from the value it would have in free space. The change in input impedance can cause a mismatch to the device which feeds the antenna and a reduction in the power delivered to it. Severe mismatch may even create nonlinear circuit effects in the transmitter.

The theoretical analysis of linear plasma effects is made tractable by simplified description of the plasma constitutive parameters, which work well in the types of plasmas created by reentry phenomena. The propagation of transverse electromagnetic waves through such plasmas can be analyzed fairly rigorously with comparative ease, for simple plasma geometries. Such analyses are obviously correct for the radiation, or far zone, fields of an antenna; but the presence of the reentry plasma in the antenna near-field complicates the problem. Thus, although the wave propagation theory is capable at times of giving fairly correct results, the near-field problem of antenna-plasma interaction should actually be treated in any mathematical analysis. For example, reactive near fields can be made dissipative by the plasma.

#### 5.1 SURVEY OF THEORY

A recent book by Shkarofsky, Johnston, and Bachynski<sup>222</sup> gives a fairly thorough treatment of the theory of plasma interaction with electromagnetic fields. Basic to all linear plasma effects theory is the cold plasma approximation, in which all effects of thermal motion of

the electrons are ignored. This approximation is well justified, since the thermal velocity is much less than the phase velocity of electromagnetic waves.

The electromagnetic field interaction is determined by the plasma conductivity  $\sigma$ , which has the following form in sufficiently weak magnetic fields.

$$\sigma = \epsilon_0 \omega_p^2 / (\nu_c - i\omega) \quad (5-1)$$

where  $\epsilon_0$  is the permittivity of free space,  $\omega_p$  is the radian plasma frequency,  $\nu_c$  is the momentum transfer collision frequency\*, and  $\omega$  is the radian frequency of the wave which is assumed to have  $\exp(-i\omega t)$  time dependence.

$$\omega_p = \sqrt{ne^2 / (\epsilon_0 m)} = 5.646 \times 10^4 \sqrt{n} \quad (5-2)$$

where  $n$  is the electron density,  $e$  is the electron charge,  $m$  is the electron mass, and the numerical constant applies when  $n$  is expressed in  $\text{cm}^{-3}$ . The electric field vector  $E$  in a plasma satisfies the wave equation.

$$\nabla \times \nabla \times E = k^2 \left( 1 - i\sigma / \epsilon_0 \omega \right) E \quad (5-3)$$

where  $k = \omega/c$ , and  $c$  is the speed of light. Thus propagation in a given plasma can be analyzed in terms of the parameters electron density, collision frequency, and signal frequency.

---

\* The use of collision frequency as a constant in the expression for the electrical conductivity is not rigorously possible, but an effective constant collision frequency is reasonably accurate in most cases. See Section 7.

The fact that the reentry plasma around a slender cone vehicle is confined to a relatively thin boundary layer can be used to advantage in solving the propagation problem. The boundary conditions may be simplified to the requirements that the tangential electric field be continuous and the discontinuity in the tangential magnetic field be equal to the surface current density in the sheath. For example, Poeverlein<sup>223</sup> has solved the problem of a plane wave incident on a plane thin-plasma sheath. His results are a function of the surface density  $N$  of electrons, and their form depends on the wave polarization. For polarization in the plane of incidence ( $E$  and the plasma normal are coplanar with the direction of propagation), the voltage reflection and transmission coefficients  $R$  and  $T$  are

$$R = \frac{-T r_o N \lambda \cos \theta}{\nu_c / \omega - 1} \quad (5-4)$$

$$T = \frac{1}{1 + \frac{r_o N \lambda \cos \theta}{\nu_c / \omega - 1}} \quad (5-5)$$

where the classical electron radius  $r_o = e^2 / (4\pi \epsilon_o m c^2) = 2.82 \times 10^{-13}$  cm,  $\lambda$  is the wavelength, and  $\theta$  is the angle of incidence with respect to the normal. For perpendicular polarization,

$$R = \frac{-T r_o N \lambda}{(\nu_c / \omega - 1) \cos \theta} \quad (5-6)$$

$$T = \frac{1}{1 + \frac{r_o N \lambda}{(\nu_c / \omega - 1) \cos \theta}} \quad (5-7)$$

Even in the simplification of the thin plasma approximation, which is valid when the surface electron density divided by the peak volume electron density is less than  $1/k$ , the geometry of the reentry plasma presents difficulties in terms of orthogonal coordinate systems. But it is necessary to bring into play the geometry of either the plasma or the antenna in order

to go beyond the simple attenuation and reflection effect. The above results are very unrealistic with regard to predicting antenna pattern distortion, and they are only qualitatively useful in the estimation of antenna impedance changes. The major advantage of these equations is in terms of estimating the relative importance of a given electron density level or in terms of defining the level of electron density at which plasma effects become important. Thus the surface density of electrons at which plasma effects are significant is  $N = (r_0 \lambda)^{-1}$ . Of course in a thick plasma the criterion is  $\omega_p = \omega$ .

A higher level of sophistication involving the effects of the plasma geometry on antenna pattern distortion is provided by the work of Baños, et al.<sup>224</sup>. These authors solved the problem of a thin conical plasma sheath surrounding a point dipole, by transformation of the normal mode solutions to the form of a residue series. The roots of the dispersion relation which is obtained indicate the contributions of surface waves to the radiated fields and the pattern distortion. These calculations also have been generalized to include the effects of collisions, by Jordan and Pinski<sup>225</sup>. The results show that the effects of the conical plasma sheath are significant at nearly the same values of surface plasma density as predicted by the above plane geometry theory, but that in the range when the plasma has an intermediate effect on attenuation it may have a large effect on antenna radiation pattern. When either the electron density or the collision frequency becomes large, the pattern distortion is again minimum. At very large collision frequencies the patterns show very little attenuation or distortion, in qualitative agreement with the plane geometry theory.

It is physically feasible for the effect of the plasma on antenna pattern distortion to be calculated fairly accurately without including near field effects, since the far field pattern can be significantly affected by surface waves in the plasma at relatively large distances from the antenna. The radiation from these surface wave modes can dominate the far field, while the source of primary waves is localized to the antenna's effective aperture and may not appreciably change the radiation field geometry in some cases. In fact the effects of plasma geometry and various other obstacles remotely located can have predominant effects. For this reason also, the pattern distortion is not a good diagnostic indication of the plasma density over the antenna.

Near-field effects must be taken into account in the theory of plasma effects on antenna impedance. In this area of the problem, the major subject of study has been the slot antenna. The infinite slotted cylinder has been studied by Smith and Golden<sup>226</sup>, Swift<sup>227</sup>, and Rusch<sup>228</sup> and it represents a convenient model for mathematical analysis because of the separability of the wave equation in cylindrical coordinates. Much work has been done recently on finite slots in ground planes covered by plasma layers. Villeneuve<sup>229</sup> has computed the effective input impedance of a rectangular waveguide terminated in an infinite ground plane, where the ground plane is covered by a dielectric slab of finite thickness. For a plasma slab, his results show the impedance or its reciprocal, admittance, to be relatively insensitive to the plasma thickness, when the thickness is greater than 0.625 times the larger waveguide or aperture dimension. This analysis does not include the overdense plasma case, where  $\omega_p/\omega > 1$ .

Croswell, et al,<sup>230, 231</sup> have considered the admittance of a rectangular waveguide terminated in an infinite ground plane covered with an inhomogeneous plasma, both theoretically and experimentally. The experimental data is that of Taylor, obtained at Stanford Research Institute. The derivation of the admittance follows essentially the same method of Villeneuve but is extended to electron densities greater than the critical density, i. e.,  $\omega_p/\omega > 1$ . The experimental data was obtained using both shock-heated and rf generated plasmas flowing past the aperture in a ground plane. Various boundary layer thicknesses or electron density gradients were assumed for the calculations and the results show that the susceptance is strongly dependent on the electron density gradients at the aperture. Reflection coefficient measurements for the rf-generated plasma agreed quite well with the computed values up to about critical density, but showed a wide disagreement above critical. This was due to the conductance not approaching zero above critical electron density, as predicted.

The admittance of a rectangular aperture radiating into plasma slab has also been extensively considered by Galejs<sup>232</sup> and Galejs and Mentzoni<sup>233</sup>. This analysis differs from those of Villeneuve and Croswell in that the waveguide radiates into a larger rectangular waveguide instead of free space. The computed admittance was compared with measurements using the afterglow of a capacitor discharge as the plasma, and relatively good agreement

resulted. It is apparent that antenna admittance (or impedance) is more readily related to the properties of the plasma in the immediate vicinity of the antenna than are the parameters of the radiation field. This fact is the reason for the relative success of plasma diagnostics by impedance measurement.

An additional effect, that of mutual coupling between antennas, has been investigated by Galejs<sup>232</sup> and Galejs and Mentzoni<sup>233</sup>. Generally speaking the presence of a plasma sheath tends to decrease the mutual coupling between slot antennas in a ground plane.

## 5.2 ILLUSTRATIVE CALCULATIONS

The discussion above indicates that the major impact of antenna near-field/linear plasma interactions is obtained in terms of the electrical performance of the antenna as a circuit element. The antenna/transmitter system design thus has a significant effect on the importance of the near-field effects. Assuming that the system is designed to account for such effects, by the use of broadband components and sufficient antenna isolation, then the radiated field characteristics are of primary concern. Parametric representation of near-field effects on antenna impedance is difficult to accomplish, at any rate, because of its dependence on a multitude of parameters.

Radiation pattern distortion is also difficult to treat parametrically, but it is generally comparable in importance to the attenuation effect as an indication of electron density levels which have an appreciable effect on received signals. Thus the simple attenuation calculation, which includes losses due to both absorption and reflection, provides a fairly useful illustrative calculation. Figures 5-1 and 5-2 show the total attenuation ( $A = 10 \log |1/T|^2$ ) given by Equation (5-5), for normal incidence. At small values of the collision frequency, the attenuation depends on the parameter  $N\lambda$ , while at large values of collision frequency, the parameter  $N\lambda_c$  enters, where  $\lambda_c = 2\pi c/\nu_c$ . These curves may be used to represent either polarization at arbitrary incidence angle by properly normalizing to  $\cos \theta$  or  $\sec \theta$ ; however the application of this theory to antenna pattern distortion is not realistic.

The collision frequency  $\nu_c$  generally increases with decreasing altitude, at a rate dependent on the flow field properties. A typical situation for a 9 degree half-angle cone reentering with a velocity of 22,500 ft/sec is shown in Figure 5-3. These results were obtained using Musal's<sup>234</sup> tables for equilibrium air collision frequency, and they show that the collision frequency traverses the microwave region in the same range of altitudes as that in which the electron density becomes significant on a slender cone vehicle.

These results show that the linear plasma effects on signal transmission from a slender cone vehicle become independent of signal frequency and tend to decrease (provided the electron density does not increase) as the altitude decreases, once the altitude is less than that at which the collision frequency equals the signal frequency.

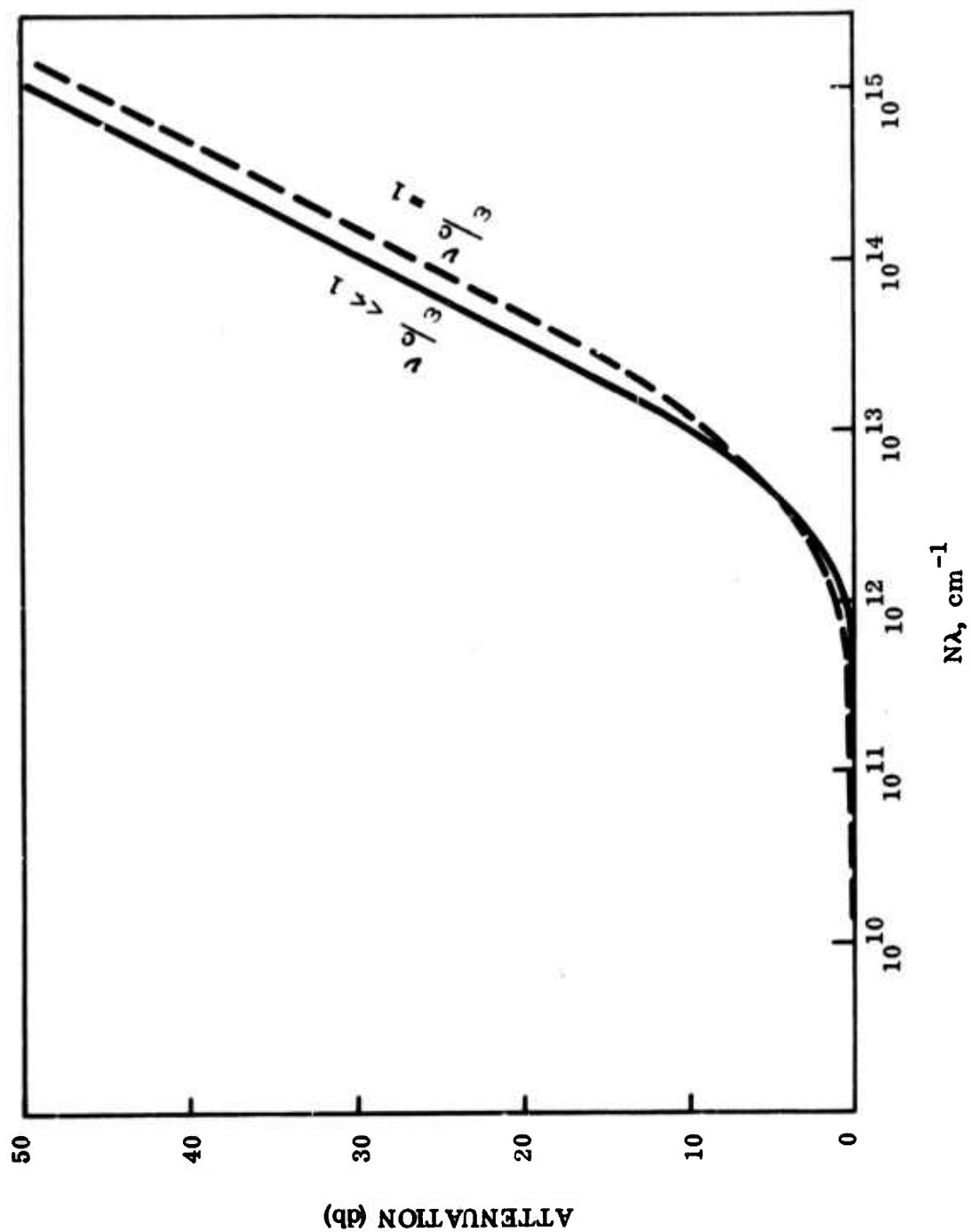


Figure 5-1. Thin Plasma Attenuation

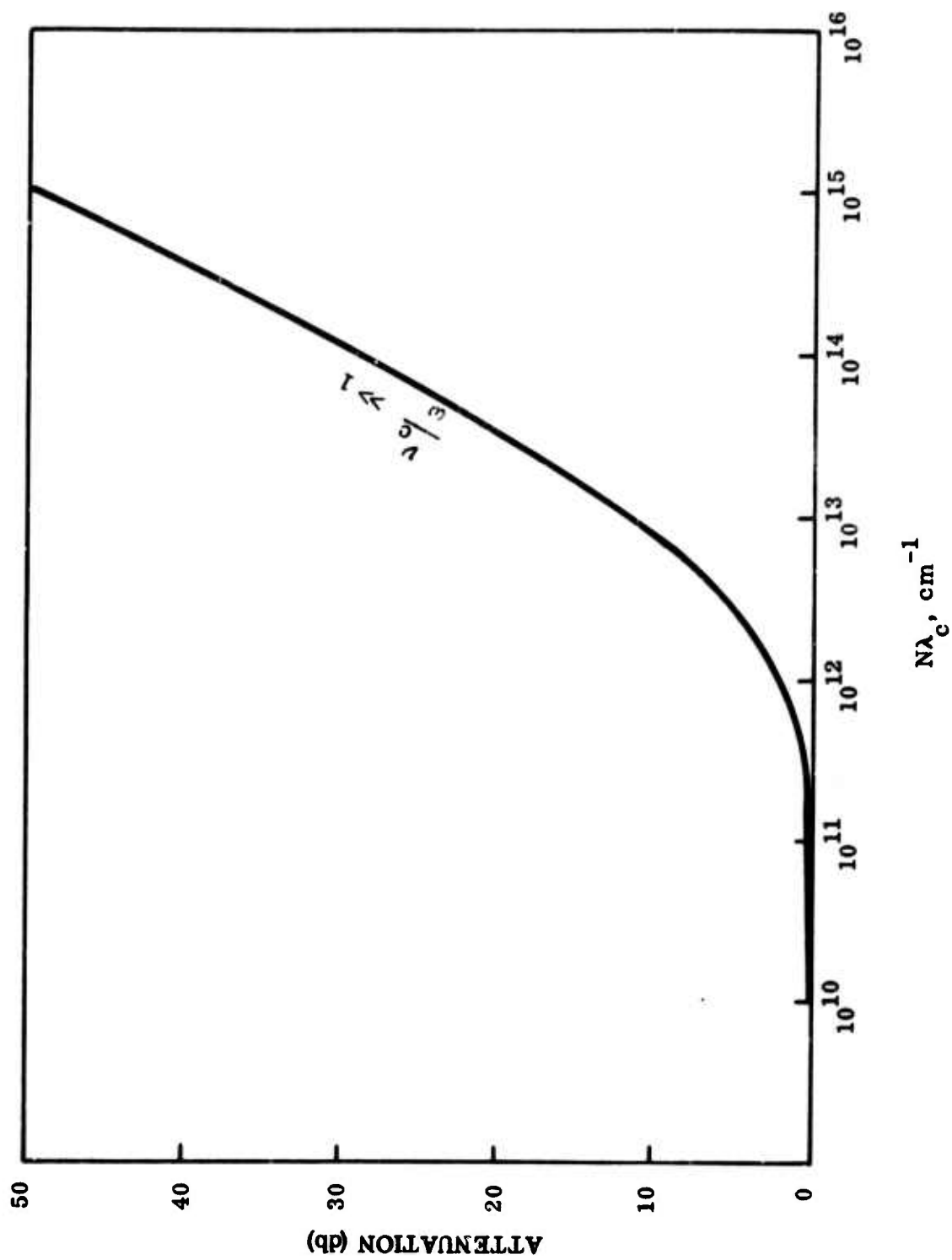


Figure 5-2. Thin Plasma Attenuation at Large Values of Collision Frequency

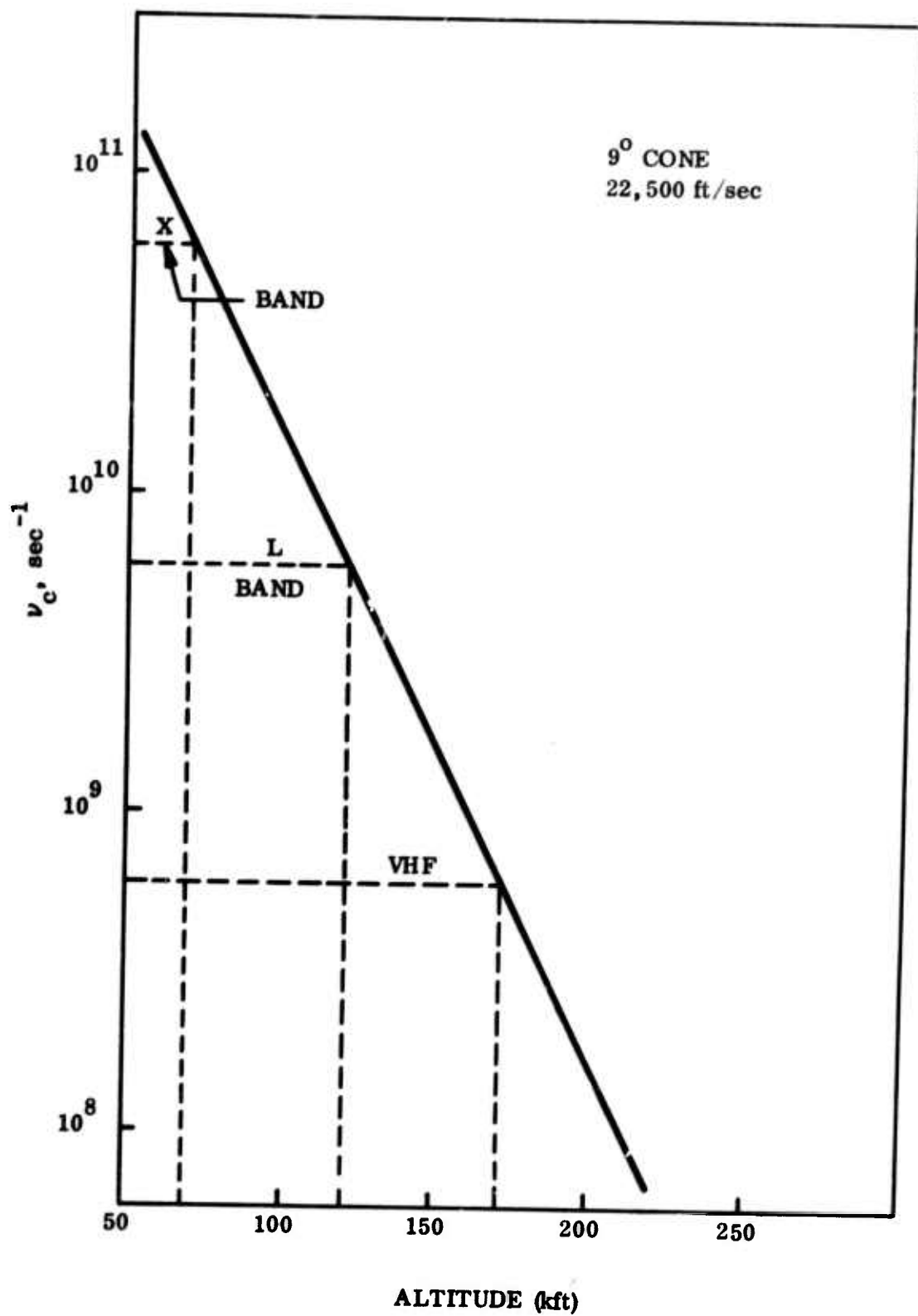


Figure 5-3. Typical Variation of Collision Frequency for a Slender Vehicle

## SECTION 6

### ANTENNA BREAKDOWN

The phenomenon of antenna voltage breakdown becomes an important consideration whenever relatively high power levels are to be transmitted, especially when the atmosphere surrounding the antenna is reduced to pressures on the order of one Torr. If the power input to an antenna is increased from low levels, the output power initially increases proportionately, but eventually a sudden decrease in output power will result from breakdown of the air surrounding the antenna. The strong electric fields near the antenna create ionization in the air at a greater rate than the loss processes can remove the electrons from this high field region. This field-induced plasma reflects and absorbs the incident electromagnetic energy so that very little power is transmitted. The value of input power at which breakdown takes place is called the breakdown power, and it is obtained reproducibly for a given antenna at a given pressure under the proper conditions, including the presence of initiating electrons.

Breakdown power generally varies with pressure in such a way as to undergo a minimum at a particular pressure. At low pressure, the electrons diffuse rapidly away from the high field region, causing the breakdown power to increase. At high pressure, the increased rate of collisions of electrons with neutral particles reduces the energy gained by the electrons from the field, also causing the breakdown power to increase. (The high pressure region in air is often referred to as the attachment controlled region, since attachment to neutral molecules is the dominant electron loss mechanism.) Both the minimum breakdown power and the pressure at the minimum tend to increase as the signal frequency is increased.

The subject of antenna breakdown can be related to the subject of high frequency gas discharges or microwave cavity breakdown, for general theoretical description of the processes involved. The advantages of this approach derive from the extensive study of the latter field which has been carried out during the past twenty years. The terms and equations used in microwave breakdown theory will be employed in the discussion of antenna breakdown.

The matter of principal concern in this report is the effect of the reentry environment. Indeed there would be no need to discuss the subject of antenna breakdown were it not for the effects of reentry. One can most reliably determine the breakdown characteristics of an antenna experimentally, except for the effects of a given reentry environment. The important question then is how to predict the change in the breakdown characteristics of an antenna in the reentry environment. Before providing the solution to this problem, we review the classical theory.

### 6.1 SURVEY OF CLASSICAL BREAKDOWN THEORY

The subject of microwave breakdown in gases has been thoroughly surveyed by MacDonald in a recent book<sup>235</sup>. This book presents practically all of the basic theory of high frequency gas discharge. Moreover, it indicates how breakdown field strengths can be calculated reliably. The book is thus useful in providing the basic physical theories on the subject as well as the practical tools needed for applications. In addition, a whole chapter is devoted to experimental methods.

It is instructive to begin the discussion of breakdown theory with a qualitative description of the breakdown process. The impressed electromagnetic field exerts force on any free electrons which may be present in the gas. Through the process of collisions of electrons with neutral gas particles, the field does work on the electrons, raising their average temperature well above that of the gas. Ionization of neutral particles by impact of high-energy electrons competes with electron attachment to neutral particles to give a net rate of electron population gain. This net ionization rate competes with losses by diffusion until the point is reached where the ionization builds up at a very rapid rate and the gas becomes conducting. The various collision processes are very important in determining breakdown, in that they control the energy distribution as well as the number density of electrons.

Generally speaking there are two methods of analysis which can be used to predict breakdown, the kinetic theory method and the phenomenological theory.

The kinetic theory approach to breakdown prediction treats the electron distribution function  $F(v, r, t)$ , which represents the number of electrons with velocities close to  $v$ , in a small volume of space at the point  $r$ , and at the time  $t$ . This distribution function obeys the Boltzmann equation<sup>236</sup> where  $\nabla$  is the gradient in configuration space,  $\nabla_v$  is the gradient in velocity space,  $\vec{a}$  is the acceleration, and  $C$  represents the effects of collisions.

$$\frac{\partial F}{\partial t} + \vec{V} \cdot \nabla F + \vec{a} \cdot \nabla_v F = C \quad (6-1)$$

The collision term  $C$  may be written as an integral involving the distribution function and the collision cross section<sup>237</sup>, and hence knowledge of collision cross section as a function of electron velocity is sufficient in principle to solve the Boltzmann equation. However, the difficulties involved are so great that accurate results are possible in only a few cases.

Hydrogen and helium have practically constant collision frequencies above an energy of about 3 or 4 electron volts, and this fact has been used by MacDonald and Brown<sup>238, 239</sup> and Reder and Brown<sup>240</sup> to calculate breakdown fields for these two gases and for admixtures of mercury. The results agree very well with experiment, especially for the case of helium containing a small amount of mercury. The presence of mercury serves to convert the metastable excitation level of helium to ionization of mercury by an exchange reaction. This has the effect that the gas has no excitation levels below the effective ionization level, greatly simplifying the analysis. The theoretical results for neon and neon-argon mixtures, for which the collision frequency is approximately proportional to the square root of the electron energy, do not agree with experimental data quite as well as for constant collision frequency gases. Of course the use of simple collision frequency relationships for predicting atmospheric breakdown by kinetic theory does not work.\*

\* Lenander and Epstein<sup>241</sup> have reported recently on the successful prediction of breakdown fields of air, using a computer program of Carelton and Megill,<sup>242</sup> with detailed collisional data.

The phenomenological method of predicting breakdown has been widely used by various authors in classical breakdown theory. Essentially this method is a collection of extrapolation formulas based on the best fit of reasonable phenomenological ideas to existing basic data. This method starts with the electron continuity equation, which can be derived from the Boltzmann equation. The various terms in this equation are then treated as simple functions of the proper variables of the problem, and experimental data are used to determine the arbitrary constants in these equations.

The electron continuity equation is written as

$$\nabla \cdot \vec{\Gamma} + \frac{\partial n}{\partial t} = \frac{dn}{dt} \quad (6-2)$$

where  $n$  is the electron density,  $\vec{\Gamma}$  is the electron flux, and  $dn/dt$  is the net effect of all sources and sinks. Electron diffusion leads to the electron flux

$$\vec{\Gamma} = -\nabla (Dn) \quad (6-3)$$

where  $D$  is the diffusion coefficient. When the net ionization rate per electron is represented by the symbol  $\nu$ , the continuity equation may be written as

$$\frac{\partial n}{\partial t} = \nabla^2 (Dn) + n\nu \quad (6-4)$$

This equation is generally solved by assuming separability, using

$$\nabla^2 (Dn) = -Dn/\Lambda^2 \quad (6-5)$$

where  $\Lambda$  is the characteristic diffusion length. Thus

$$\frac{\partial n}{\partial t} = \nu - D/\Lambda^2 n \quad (6-6)$$

The Townsend criterion, carried over from the theory of direct current discharges, has been shown by Herlin and Brown<sup>243</sup> to apply to microwave discharges. According to this criterion, the breakdown point is reached when the right-hand side of Equation 6-6 is zero, since a slightly higher electric field would cause the runaway production of electrons.

When either the electric field or the electron mobility is not uniform in space, as would be the case in antenna breakdown, the diffusion equation must be solved in the form of Equation 6-4, with the left-hand side set equal to zero. However, it is possible to use an effective diffusion length which can be derived from the solution of the diffusion equation. For example, Herlin and Brown<sup>215</sup> derived the solution for a TM<sub>010</sub>-mode cylindrical cavity and MacDonald and Brown<sup>216</sup> derived the results for a spherical cavity. (See Section 4 for a discussion of methods of estimating the diffusion length for antennas.)

It can be shown<sup>235</sup>, through certain considerations in the kinetic theory, that the important parameter with respect to electric field  $E$  and the microwave radian frequency  $\omega$  is

$$E_e^2 = \nu_c^2 E^2 / (\nu_c^2 + \omega^2) \quad (6-7)$$

where  $E_e$  is the effective field and  $\nu_c$  is the collision frequency for momentum transfer. The effective field concept is useful in the phenomenological theory of breakdown, as in the analysis of Brown<sup>244</sup>, Rose and Brown<sup>245</sup>, and Gould and Roberts<sup>246</sup>. The Townsend criterion is written as

$$\nu_i = \nu_a + D/\Lambda^2 \quad (6-8)$$

where  $\nu_i$  and  $\nu_a$  are the ionization and attachment frequencies, respectively. The first Townsend coefficient  $\alpha$  is used in place of  $\nu_i$  according to the equation

$$\nu_i = \alpha \mu E_e \quad (6-9)$$

where  $\mu$  is the dc mobility. The ratio of diffusion coefficient to mobility is invoked to give the relation

$$\frac{\alpha}{p} = \frac{\beta}{p} + \frac{2}{3} \frac{u}{(p\Lambda) (E_e \Lambda)} \quad (6-10)$$

where  $p$  is pressure,  $u$  is average electron energy, and  $\beta$  is the number of attachments per centimeter of path length. Data exist for  $\alpha/p$ ,  $\beta/p$ , and  $u$  as functions of  $E/p$  in air<sup>244, 247</sup>. Hence, Equation 6-10 may be used to give  $E_e/p$  as a function of  $p\Lambda$ , provided  $E_e$  can be calculated.

The difficulty connected with the phenomenological theory is that the effective field is not a sound concept, since the collision frequency is not constant. Brown<sup>244</sup> obviates this difficulty by calculating an effective constant collision frequency from the measured ac mobility, using

$$\mu_{ac} = (e/m) \nu_c / (\nu_c^2 + \omega^2) \quad (6-11)$$

where  $e/m$  is the ratio of charge to mass for the electron. He gets a value of  $\nu_c$  equal to  $4.3 \times 10^9$  p. The results of breakdown calculations then agree with experimental data fairly well over a limited range of pressures.

It appears that the most reliable and generally useful method of calculating breakdown is that given by MacDonald. This method uses the effective field concept in a way which is much less sensitive to the specific form of collision frequency assumed than is the above method. The

diffusion coefficient can be calculated from the variation of collision frequency with electron energy, if the electron energy distribution is assumed; however, it can be shown that the form of the distribution function has little effect on the result. Hence the approximation of MacDonald, Gaskell, and Gitterman<sup>248</sup> works well.

$$D_p = (29 + 0.9E_e/p) 10^4 \text{ cm}^2 \text{ -Torr/sec} \quad (6-12)$$

This equation was derived from assuming a linear dependence of  $D_p$  on average electron energy in terms of the latter's experimentally determined dependence on  $E/p$ . Equation 6-12 is equivalent to

$$D\lambda/\Lambda^2 = 10^4 \left( \frac{\lambda}{\Lambda} \right)^2 S \quad (6-13)$$

where  $\lambda$  is the wavelength and

$$S = (1/p\lambda) \left[ 29 + \frac{0.9 E\lambda}{[(p\lambda)^2 + (35.6)^2]^{1/2}} \right] \quad (6-14)$$

where  $E\lambda$  is in volts and  $p\lambda$  is in Torr/cm.

The net ionization rate  $\nu$  may be related to the electric field and the pressure by using experimental breakdown data. The result is shown in Figure 8-18 of Reference 235 in terms of  $\nu\lambda$  versus  $p\lambda$  for fixed values of  $E\lambda$ . Figure 8-19 in Reference 235 shows a plot of Equation 6-14. The solution to a given problem in continuous wave breakdown in air is found by the points of intersection of these two sets of curves, as shown in Figure 8-20 in Reference 235, since at breakdown,  $\nu\lambda$  is equal to  $D\lambda/\Lambda^2$ . Figure 6-1 shows curves of  $E\lambda$  versus  $p\lambda$  for three different values of  $\lambda/\Lambda$ , derived from MacDonald's curves.

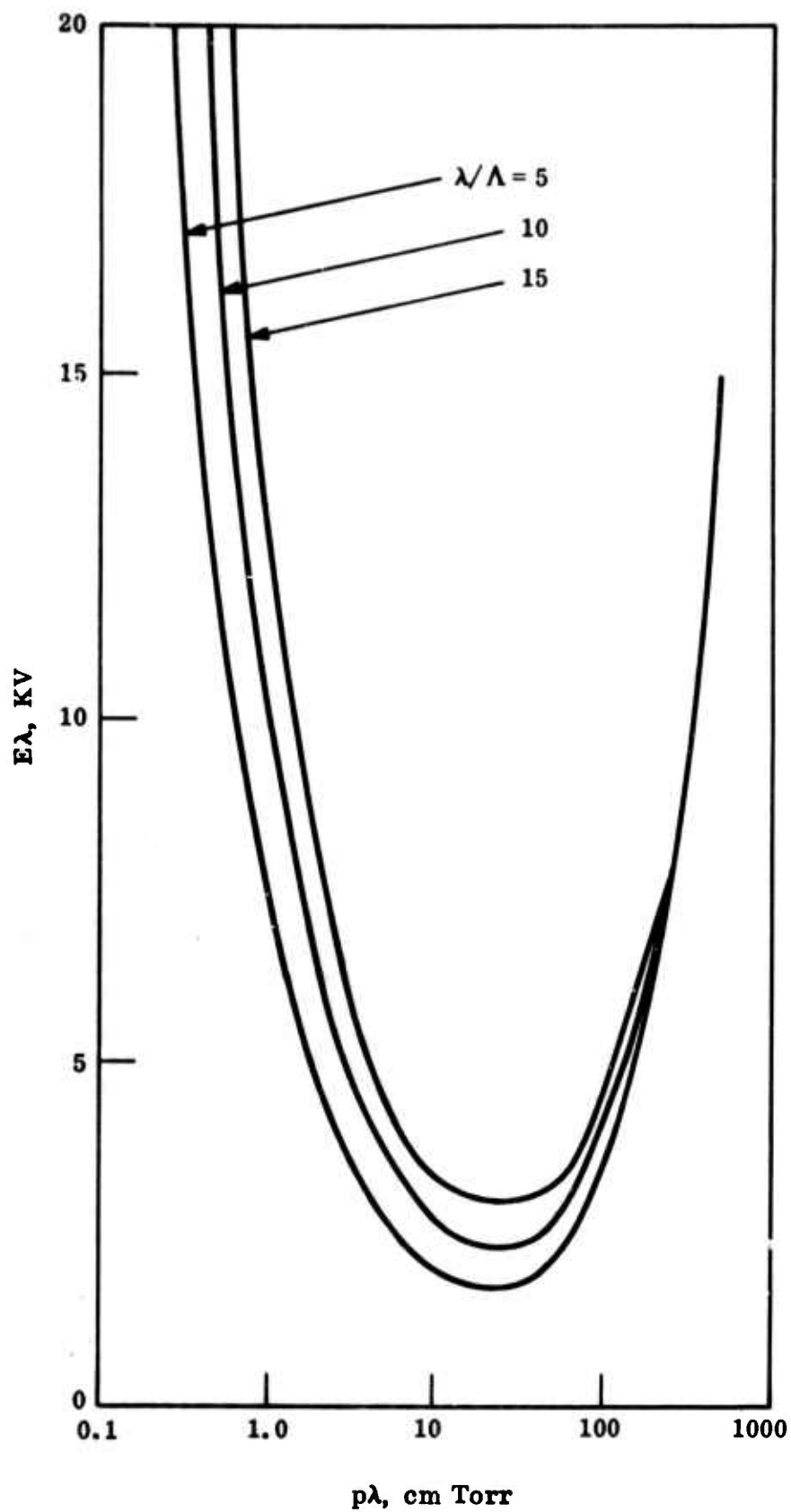


Figure 6-1. Breakdown Field as a Function of Pressure in Terms of Proper Variables

The above method of calculating continuous wave breakdown can be generalized to include pulse (or finite time) effects, following the approach of Gould and Roberts<sup>246</sup>. For example, for pulsed breakdown at low pulse repetition rate, the net ionization frequency is determined by

$$\nu_b \tau = \ell_n (n_b/n_o) \quad (6-15)$$

where  $\tau$  is the pulse length,  $n_b$  is the electron density required for breakdown, and  $n_o$  is the initial electron density. The value of  $n_b$  is usually taken as the critical value,  $10^{13}/\lambda^2$ , (where  $\lambda$  is in cm and  $n_b$  is  $\text{cm}^{-3}$ ), and  $n_o$  is a fairly small number. For a given pulse length, Equation 6-15 determines  $\nu_b$ , which is actually related to  $\nu$  of the CW analysis by

$$\nu \lambda = D\lambda/\Lambda^2 + \nu_b \lambda \quad (6-16)$$

The procedure is to start with  $E\lambda$  as a function of  $p\lambda$  from continuous wave theory and to determine  $D\lambda/\Lambda^2$  from Equation 6-13. Then  $\nu \lambda$  is determined from Equation 6-16. This gives  $E\lambda$  from MacDonald's curves, and the process can be iterated to determine  $E\lambda$  more accurately. In the case of rapid pulse repetition rates, the decay time of the afterglow between pulses must be taken into account. Then the breakdown criterion is that the buildup of ionization during the pulse is just equal to the decay between pulses. A slightly greater net ionization rate during the pulse would give a runaway condition. As the pulse repetition rate is increased, the breakdown field approaches the continuous wave case.

It remains for us to show the limits of validity of the above phenomenological theory, referred to as the diffusion theory of microwave breakdown. Brown and MacDonald<sup>249</sup> have studied this question for hydrogen, and their approach can be applied to air with relatively insignificant changes in numerical results. Briefly, the principal physical limitations on the validity of the theory have to do with the fact that the electrons must remain in the high field region for more than a single collision or a single cycle of the alternating field. When the mean free path

equals the diffusion length, ( $p \Lambda \cong 0.03$  cm Torr), we have the mean free-path limit. At lower pressures the diffusion theory is inapplicable. When the amplitude of the oscillatory motion of an electron in the field exceeds the diffusion length, we have the oscillation amplitude limit ( $\lambda / \Lambda$  is on the order of  $10^3$  or greater), beyond which the theory is also inapplicable. The uniform field limit ( $\lambda = 2 \pi \Lambda$ ) need not be considered as a boundary of the region of validity, provided the field distribution is accounted for in the diffusion length.

## 6.2 SURVEY OF REENTRY EFFECTS

The subject of this section is the effects of reentry on antenna breakdown, with emphasis on the reentry environment associated with slender cone bodies at hypersonic speeds. The discussion will depend on ideas and data taken from written reports and verbal communications with a number of researchers in the field, in the manner of a survey of present knowledge.

For conical vehicle reentry, three distinct flow-field regions may be important in antenna breakdown: the ambient free stream, the inviscid shock layer, and the boundary layer. With the exception of relatively high altitudes where these regions are not necessarily distinct, the reentry environmental effects on breakdown will be different for each of the three regions. In fact, most workers assume that a convenient separation can be made such that the effects of each region can be treated independently. At any rate, the different basic processes which control breakdown can be identified for each of the three flowfield regions, for example, as done by Reilly<sup>250</sup> and numerous other authors.

The free stream ahead of the shock layer is characterized essentially only by the fact that the air is moving relative to the transmitting antenna. The effects of altitude on the state or composition of the ambient air probably are not significant in breakdown; and even if they were, it would be a relatively simple task to account for them. Hence, the only important effect in the free stream is convection.

The inviscid flow region is characterized by a state of elevated temperature and increased molecular number density relative to the free stream. On a slender conical vehicle, ionization is probably insignificant in this region, but the detailed thermodynamic state and chemical composition of the shock-heated air may be quite important. At any rate, the effects of the inviscid flow region are felt in terms of convection, increased air density, and elevated temperature.

The boundary layer is characterized by even higher temperatures produced by viscous dissipation. The presence of significant levels of thermal ionization is thus probable. Particle number density and convection are not so easy to generalize because of the strong gradients of these quantities which exist here. In addition, the presence of chemical contamination of the air by products of ablation will be important. Thus, convection, gas density, temperature, ionization, and chemical additives, all in the context of strong gradients, must be considered in the boundary layer.

In summary, there can be distinguished six phenomena of hypersonic reentry flow fields which can affect antenna breakdown in one or more of the regions of the flow field. The following six subsections treat each of these in varying detail, depending on the extent of present knowledge.

#### 6.2.1 GAS DENSITY

The classical theory of microwave breakdown is developed in terms of proper variables such as  $\nu/p$  and  $D_p$ , where  $p$  is the pressure in Torr. These quantities generally normalize in this way because of the dependence of collision frequencies on number density of gas particles. In voltage breakdown experiments under standard laboratory conditions, the practice is to express the state of the gas being tested in terms of pressure, since this is a directly measurable quantity. However, pressures in the reentry induced shock layer are often orders of magnitude higher than in the free stream. Also, because of increased gas temperature, shock-layer density is not generally the same as in the free stream. Whitmer and

MacDonald<sup>251</sup> have noted that the physically important parameter for breakdown is the gas density rather than pressure, since it is the number of gas particles per unit volume which determines the rates for all the processes which control breakdown. Thus the use of either the free-stream pressure or the shock-layer pressure in predicting breakdown at a given altitude would give erroneous results. The distribution of gas density in the high field intensity region is the correct determining factor.

In order to give a quantity which is commensurable with the classically used parameter of pressure, most authors define a reduced pressure as  $p^*$ . Reilly defines the reduced pressure in Torr in terms of the gas number density  $N$  in particles per cubic centimeter.

$$p^* = 2.9 \times 10^{-17} N \quad (6-17)$$

Light and Taylor<sup>252</sup> define the reduced pressure in an equivalent way in terms of temperature,  $T$ , in  $^{\circ}\text{K}$ :

$$p^* = 273 p/T \quad (6-18)$$

These corrections have the effect of shifting the curve of breakdown field versus altitude about 30,000 feet higher in altitude at velocities on the order of 22,000 ft/sec, according to Whitmer and MacDonald<sup>251</sup>.

Gas density effects have been observed in reentry flight experiments. Bisbing<sup>253</sup> showed that the observed period of breakdown of a slot antenna on a conical vehicle agreed with laboratory data in cold air when the air density corresponding to the inviscid flow region was used as the independent variable. Nanevicz<sup>254</sup> also showed that when the VHF breakdown data from Nike-Cajun flights is corrected for local density, it agrees roughly with laboratory measurements in cold air.

The gas density affects all the terms of the continuity equation in their proper variables form in terms of the reduced pressure  $p^*$  in place of the pressure  $p$ .

### 6.2.2 IONIZATION

An appreciable electron density probably exists in the flow field of a reentry body at all altitudes of interest for antenna breakdown. This is true even at altitudes too high for thermal ionization of the air, because the ionosphere provides ambient electrons. This initial ionization has various effects on breakdown. One effect of some practical importance is that the breakdown threshold will be obtained fairly often for a given set of reentry conditions. There will always be sufficient ionization to initiate breakdown, which requires at least one free electron before it can proceed.

The most important effect of flow-field ionization is to change diffusion from free to ambipolar, or at least to create transitional diffusion. That is, with the buildup of a sizable electron space charge, the electron and molecular diffusion processes become inextricably linked. The result is to slow down the diffusion of electrons to the molecular rate and thereby correspondingly reduce diffusion as an electron loss mechanism. Allis and Rose<sup>255</sup> have indicated that the transition from free to ambipolar diffusion begins where the Debye length becomes comparable to the diffusion length. The magnitude of the transitional diffusion coefficient  $D_s$  can be calculated only by solving the boundary value problem constituting the separate electron and ion continuity equations, with space charge, and Poisson's equation. The result depends on the geometry of the boundaries as well as on the ionization level.

Allis and Rose<sup>255</sup> have performed calculations for hydrogen and found that the transition from free to ambipolar diffusion takes place over five orders of magnitude of electron density. Moreover their results indicate that the constant ratio approximation is nearly correct if the electron density used in this approximation is decreased from its actual value by a constant factor. (The constant ratio approximation consists of assuming that the ratio of electron and ion densities is constant throughout the discharge.) From Figure 4 of their paper it appears that this factor should be about 20, but Allis<sup>256</sup> indicates a factor of five in another calculation. A factor of ten may be reasonable. Allis<sup>256</sup> has derived an expression for the transitional diffusion coefficient which follows.

$$\frac{D_s}{D_- D_a} = \frac{\ell_D^2 + \Lambda^2 \left(1 + \frac{\mu_- n_+}{\mu_+ n_-}\right)}{D_a \ell_D^2 + D_- \Lambda^2 \left(1 + \frac{\mu_+ n_-}{\mu_- n_+}\right)} \quad (6-19)$$

where  $\Lambda$  is the diffusion length,  $\ell_D$  is the Debye length,  $\mu$  is mobility,  $n$  is particle density (+ refers to ions and - to electrons),  $D_-$  is the electron free diffusion coefficient, and  $D_a$  is the ambipolar diffusion coefficient.

$$D_a = \frac{\mu_+ D_- + \mu_- D_+}{\mu_+ + \mu_-} \quad (6-20)$$

$$\ell_D^2 = \frac{\epsilon_0 D_-}{r_- e \mu_-} \quad (6-21)$$

where  $\epsilon_0$  is the permittivity of free space and  $e$  is the electronic charge. In practice, the ratio  $\mu_+ n_+ / (\mu_- n_-)$  is generally small compared with unity, except possibly when the Debye length is very large, in which case the ratio is not important. Thus, a good approximation which depends only on the electron density is the following equation:

$$\frac{D_s}{D_- D_a} = \frac{\ell_D^2 + \Lambda^2}{D_a \ell_D^2 + D_- \Lambda^2} \quad (6-22)$$

In the limits of low and high electron density, the value of  $D_s$  approaches  $D_-$  and  $D_a$  respectively. In order to allow the above constant ratio approximation formula to reproduce approximately the actual transition situation, apply the factor of ten recommended above.

$$\frac{D_s}{D_- D_a} = \frac{10 \ell_D^2 + \Lambda^2}{10 D_a \ell_D^2 + D_- \Lambda^2} \quad (6-23)$$

Thus the transition from free to ambipolar diffusion in this approximation occurs when the Debye length is about one third of the diffusion length.

Two simplified approximations to the ambipolar diffusion coefficient are possible, considering the fact that  $\mu_-$  is much greater than  $\mu_+$ . In an active discharge,  $D_- \mu_+$  is much greater than  $D_+ \mu_-$ , so that the ambipolar diffusion coefficient is given approximately by the following equation:

$$D_a = (\mu_+ / \mu_-) D_- \quad (6-24)$$

But in the case of an isothermal plasma,  $D_- \mu_+$  is equal to  $D_+ \mu_-$ .

$$D_a = (2\mu_+ / \mu_-) D_- = 2D_+ \quad (6-25)$$

It is important to note that the latter result applies only to the afterglow plasma, for example, the decaying plasma which exists between pulses in multiple pulse breakdown. Also, there is not actually a factor of two difference between these two results, because  $D_- / \mu_-$  is much greater in the active discharge than in the isothermal plasma, while  $\mu_+$  is practically constant.

It is apparent that one needs values for the parameters  $D_-$  and  $\mu_+ / \mu_-$  to apply these equations, and also one needs a value of  $D_- / \mu_-$  in order to calculate the Debye length for Equation 6-23. The latter problem is accurately enough handled for the purposes of transitional diffusion in the constant ratio approximation by casting Equation 6-21 in the following form:

$$\lambda_D^2 = \epsilon_0 k T_e / n e^2 \quad (6-26)$$

where  $k$  is Boltzmann's constant and  $T_e$  is the electron temperature. In the isothermal afterglow plasma  $T_e$  is equal to the gas temperature, and in an active discharge in air  $kT_e$  is on the order of a few electron volts. At breakdown in air, a commonly used value of  $D_-$  is given by Kelly and Margenau<sup>257</sup>.

$$D_{-p} = 1.6 \times 10^6 \text{ cm}^2 \text{ Torr sec}^{-1} \quad (6-27)$$

But MacDonald<sup>248</sup> prefers to use a value which depends on the microwave field intensity E.

$$10^{-4} D_p = 29 + 0.9 E_e / p \text{ cm}^2 \text{ Torr sec}^{-1} \quad (6-28)$$

Various values of  $\mu_-/\mu_+$  (or  $D_-/D_+$ ) for breakdown in air have appeared in the literature, including Kelly and Margenau's<sup>257</sup> value of 100 and Whitmer and MacDonald's<sup>251</sup> value of 40. But these are not actually inconsistent, since the latter authors applied Equation 6-25 to the data on mobilities for nonisothermal plasmas. Thus the value of 40 is actually 80 and it seems reasonable to assume that for breakdown of air,

$$\frac{D_-}{D_+} = \frac{\mu_-}{\mu_+} \cong 100 \quad (6-29)$$

Flow-field ionization can also affect pulsed-signal breakdown in terms of the initial electron density in the pulsed-signal breakdown criterion. The relative importance of this effect is somewhat difficult to define, since it depends on a somewhat arbitrary parameter, the final electron density. The final electron density level usually used in the pulsed breakdown criterion is the critical electron density, which in units of  $\text{cm}^{-3}$  is approximately equal to  $10^{-8}$  times the square of the microwave frequency (for example see References 250 and 251). Most authors generally state that when the initial ionization from the flow field is already equal to or greater than the critical value, then the breakdown field is essentially zero, since the gas may already be considered to be broken down and there can be no penetration of the microwave field through the plasma. On the other hand, the CW breakdown criterion normally used does not depend on the electron density level, but only on the rate of increase of electron density from the microwave field. Thus, no such critical electron density effect as described above appears. But the two physical situations cannot be this different merely because one is for pulsed signals and the other is for CW. The difficulty is obviously a result of the two arbitrary criteria used in defining breakdown.

In the case of the reentry induced flow field of a slender cone body, it is possible to have greater than critical electron density in a thin layer, such that total signal blackout does not occur. Thus there will be a significant transmission of power through the plasma which will increase linearly with input power until breakdown is approached, when the transmitted power will attenuate nonlinearly due to the thickening of the plasma layer by the breakdown process. This indicates that the only physically meaningful way to calculate breakdown in the presence of strong flow-field ionization is to calculate signal transmission as a function of input power level, taking into account the increased level of ionization induced by the field, as has been suggested by Epstein<sup>258</sup>.

A careful consideration of the form of the breakdown criterion is not only necessary for pulsed signal breakdown in the presence of ionization, but also for breakdown with convection, as discussed in greater detail below. A meaningful prediction of breakdown in the presence of flow-field ionization with convection requires one to calculate the electron density distribution over the antenna and the power transmitted through this plasma as functions of the input power. The importance of this consideration lies mainly in its effect on the breakdown criterion and not so much in the phenomenon of alteration of the antenna near-field and impedance by the plasma, although the latter may be important considerations if the electron density is initially very high.

### 6.2.3 HIGH GAS TEMPERATURE

It has been recognized for some time that the flow-field gas temperatures produced by hypersonic reentry would have a significant effect on antenna breakdown. This effect is known to be separate from and additional to the effects of ionization and gas density, which both accompany high temperature, but it is the least understood effect theoretically.

Direct current breakdown at high temperature has been investigated experimentally at a relatively early date<sup>259</sup>. It was found that up to temperatures of 1400°K no deviation from cold gas results could be observed<sup>260</sup>. The investigation of this phenomenon by the use of a shock tube in order to produce higher temperatures was carried out by Sharbaugh et al.

for nitrogen<sup>261</sup>. These investigators found that significant departures from cold gas breakdown occur at temperatures of 2000°K and that at 4000°K the breakdown potential is one-half the cold gas value. Their analysis of this effect was based on a theory<sup>262</sup> of space-charge alteration of the field by ionization in the shock tube, although certain anomalies were present, which they ascribed to ionization relaxation in the shock tube. The same investigators carried out further experiments in both nitrogen and air, in which the electron density was also measured<sup>263</sup>. These data showed an apparent correlation between the reduction in breakdown voltage and the electron density.

Although dc breakdown is affected by surface phenomena and space-charge effects, it may be that the above results provide an indication of effects of temperature on basic processes of gaseous breakdown. In fact, it is apparent that they are in qualitative agreement with more recent shock tube experiments on microwave breakdown<sup>264, 265, 252</sup>. Taylor<sup>264</sup> and Light<sup>252</sup> have found significant effects at temperatures above 3000°K in the constituents of air. Their data are plotted in Figure 6-2 in terms of the deduced values of net ionization frequency as a function of the effective field. The cold air data of Scharfman<sup>266</sup>, as well as data of various other experimenters reduced by Scharfman to this form, are plotted in this same figure for comparison. It is apparent that for the shock tube conditions there is a significant increase in ionization frequency over the cold air values, corresponding to a lowering of the breakdown field by a factor of the order of two.

Some attempts<sup>267</sup> have been made to predict theoretically high temperature air effects, but the results of these fail to agree with the experimental data of Figure 6-2. Both experimenters apparently have eliminated shock-induced ionization effects in their experiments. Also the effects of attachment cannot be important, since the cold air attachment frequency is orders of magnitude lower than the values of ionization frequency obtained in the experiments. Thus the observed effects are true gas temperature effects, except for the possible air composition effects of shock-induced dissociation.\* It is apparent that excitation of air species at high

\* In an attempt to explain the data, Light suggested a simple model, which depends on the dissociation of air molecules to a significant extent. This model is based on the effect of vibrationally excited molecules in changing the energy-loss rates of electrons in inelastic collisions.

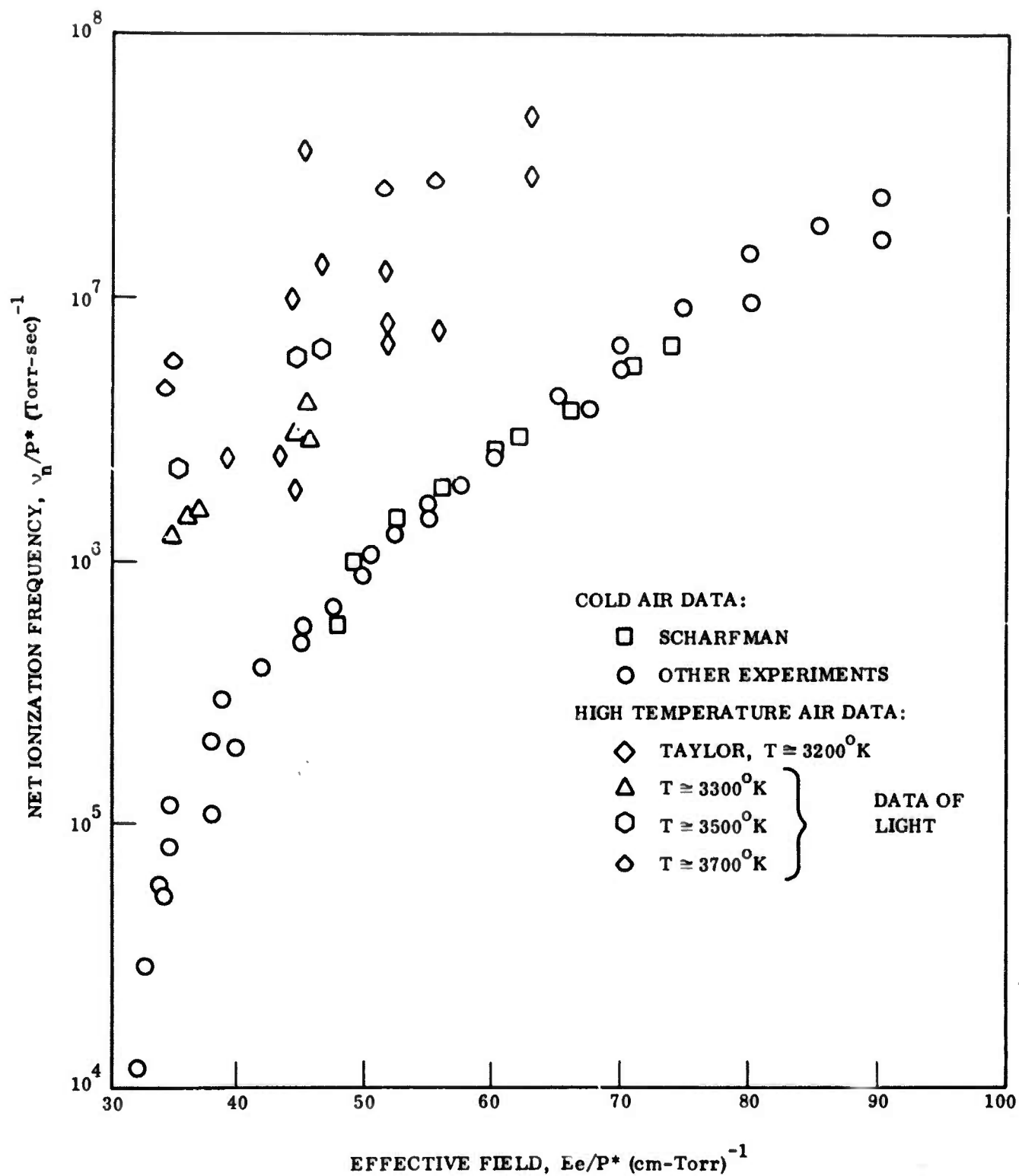


Figure 6-2. High Gas Temperature Effects on Ionization Frequency

temperature is an important factor in changing the electron energy distribution (and hence the ionization frequency) through the effect on the inelastic collision frequencies of electrons with neutral particles, but the theoretical prediction of this effect is impossible without solving the Boltzmann equation for breakdown of high temperature air.

As an alternative to the difficult task of rigorous theoretical prediction, a simple curve fit of the breakdown data has been obtained in the form of a power law, as follows:

$$\nu/p^* = 4 \times 10^7 \left[ \frac{(E_e/100 p^*)^2}{1 - e^{-(3000/T)^5}} \right]^{2.67} - 6.4 \times 10^4 \quad (6-30)$$

This function has been plotted in Figure 6-3 in comparison with Light's high temperature data and the cold air data. It can be seen to be a good fit, considering the probable accuracy of the data of Light, who used theoretical calculations of thermochemical relaxation behind the shock to deduce the air temperatures in his experiments. (Note that there is only 200°K difference between each set of points.)

It should be pointed out at this point that the cold air data of Scharfman and Morita<sup>266</sup> used in these figures represents a departure from the theory of MacDonald at low pressure (see Paragraph 6.1), which does not permit  $\nu/p$  versus  $E_e/p$  to collapse into a single curve independent of  $p\lambda$ . The Scharfman method is similar in this regard to the Brown<sup>244</sup> theory, which preceded the MacDonald theory. MacDonald's theory would appear to be the best for cold air, since it has been well tested against cavity breakdown data. But it is fallacious to assume that it gives the true values of ionization frequency in air. Epstein<sup>268</sup> and Lenander<sup>241</sup> recently have concluded from numerical solutions of the Boltzmann equation that the use of the effective field concept and the neglect of nonuniform field effects may lead to inaccurate inferences of ionization frequency at low pressure. The Scharfman data were obtained with short pulse techniques, as were all of the high temperature data, and the results were not dependent on the calculation of diffusion losses, so that they possibly could be more reliable.

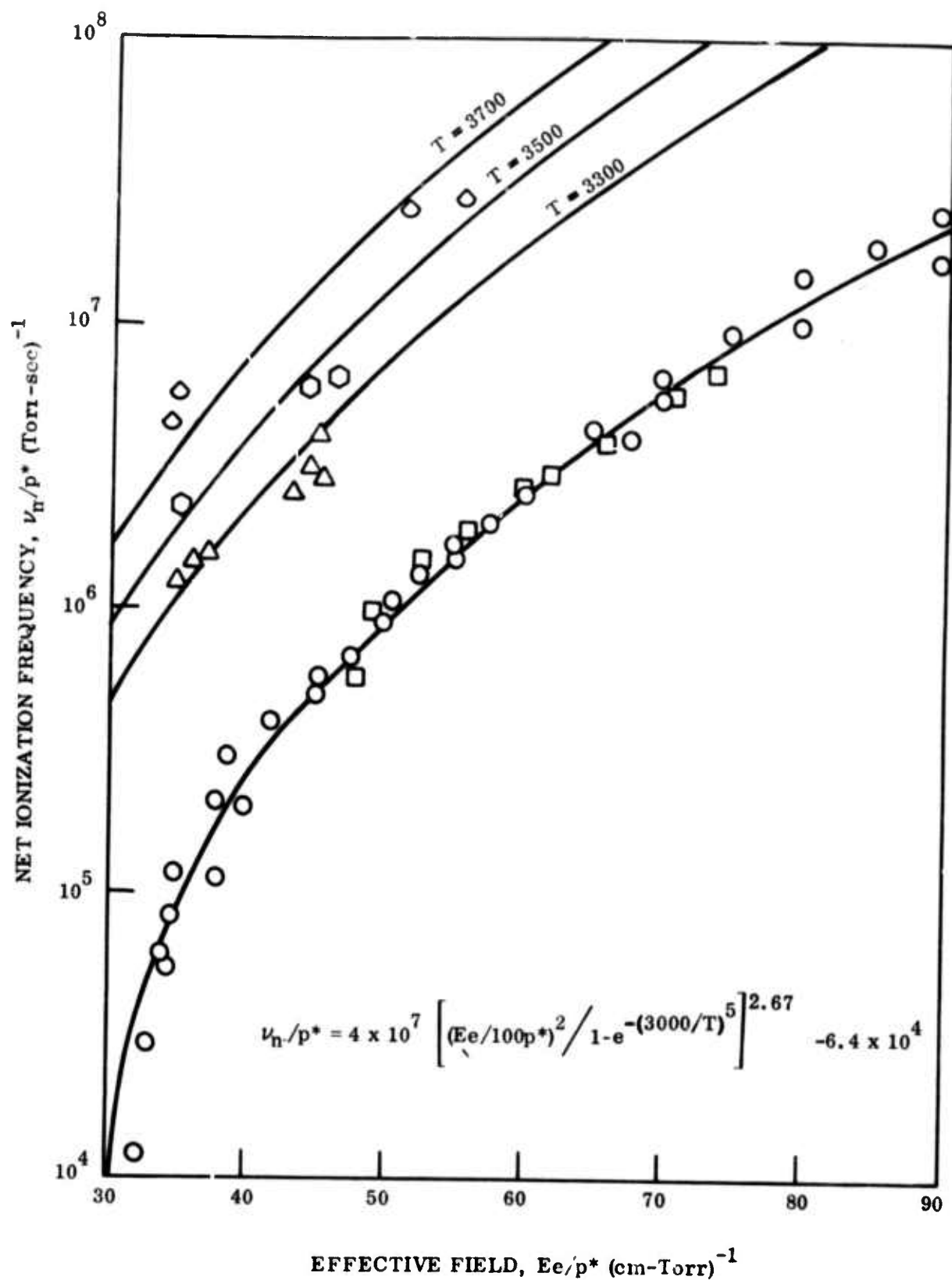


Figure 6-3. Curve Fit to Ionization Frequency

Unfortunately the ionization frequency has never been measured directly except for hydrogen, by Cottingham and Buchsbaum<sup>269</sup>, using an optical method.

In conclusion, the format of Scharfman, shown in the figures of this section, is recommended in predictions of gas temperature effects. It has the advantage of simplicity in terms of an excellent algebraic curve fit within the accuracy of the data. The high temperature data could be converted to the MacDonald format ( $\lambda = 3.21$  cm in the shock tube experiment); but the data would become much too meager because of the additional parameter involved. The data are too meager even in the economical format used.

#### 6.2.4 CONVECTION

The period of time in which a given volume element of air comes under the influence of the field of an antenna mounted on a reentry vehicle is on the order of other characteristic times for breakdown. Hence, the convection effect can be important. However, many alternative theoretical analyses of this effect have appeared, and the most important aspect of the theoretical prediction problem is to resolve which theory applies.

Three theoretical formulations of the effect of convection on breakdown are presently known, and in fact four are possible logically. These theories derive from the combination of two alternative views of the electron flux in a moving plasma and two views of the effects of the electron flux on breakdown. The contribution of convection to the electron flux in a plasma can be assumed to be equal to the product of the electron density and the flow velocity (free convection), or one can take into account space-charge effects by which there is an additional "force" on the electrons caused by the convection of the ions. The convective flux can be coupled to the diffusive flux in the continuity equation, or the convective flux can be treated as an electron loss term whereby the electrons are present in the microwave field for a finite time. The possible combinations of these assumptions give four theories, of which only the combination of space charge enhanced flux in the finite time theory has not been reported. Romig<sup>270</sup> and later Fante<sup>271</sup> used free convection coupled to diffusion, Kelly and Margenau<sup>257</sup> used free convection in the finite time theory, and Cottingham<sup>272</sup> used space-

charge enhanced convection coupled to diffusion.

Each of the four convection theories adds a term to the breakdown criterion for the ionization frequency.

$$\nu = \nu_0 + \nu_v \quad (6-31)$$

where  $\nu_0$  is the ionization frequency for breakdown in the absence of convection and  $\nu_v$  is the added effect of convection. Table 6-1 gives the form of the contribution  $\nu_v$  for each of the four theories.

Table 6-1. Contribution of Convection to the Breakdown Criterion for  $\nu$

	Coupled to Diffusion	Finite Time
Free Convection	$\frac{v^2}{4D}$	$(v/L) \ln(n_b/n_0)$
Space Charge Enhanced	$\frac{v^2 D}{4D_a^2}$	$(vD/LD_a) \ln(n_b/n_0)$

In this table  $v$  is the flow velocity,  $L$  is the length of the microwave field region parallel to the flow,  $D_a$  is the ambipolar diffusion coefficient, and  $D$  is the diffusion coefficient (which may be free, ambipolar, or transitional, depending on the plasma density).

The derivation of these theories begins with the electron continuity equation in the form

$$\nabla \cdot \Gamma + \frac{\partial n}{\partial t} = \nu_n \quad (6-32)$$

where the electron flux  $\Gamma$  is given by either of two alternative formulas. In the free convection theory it is assumed that

$$\Gamma = nv - \nabla \cdot (Dn) \quad (6-33)$$

Thus, neglecting  $\nabla \cdot (v/D)$

$$\nabla^2 (Dn) - v/D \cdot \nabla (Dn) + \nu_n = \frac{\partial n}{\partial t} \quad (6-34)$$

In the finite time theory, the coupling between diffusion and convection is neglected. Then the eigenvalues of the two differential operators can be assigned independently.

$$\nabla^2 (Dn) = -Dn/\Lambda^2 \quad (6-35)$$

$$v \cdot \nabla (Dn)/Dn = \alpha \quad (6-36)$$

where  $\alpha$  is a separation constant. Integration over a region of length  $L$  gives

$$n = n_0 \exp (\alpha L/v) \quad (6-37)$$

Defining breakdown in terms of electron density  $n_b$  and substitution back into Equation 6-34 gives the breakdown criterion.

$$\nu = D/\Lambda^2 + v/L \ln \frac{n_b}{n_0} + 1/n \frac{\partial n}{\partial t} \quad (6-38)$$

The other alternative in the free convection theory is to couple the diffusion and convection together. A change of variables then transforms Equation 6-34 to canonical form. Let

$$\psi = Dn \exp \left( -\int [v/2D] dx \right) \quad (6-39)$$

where  $\psi$  is distance along the streamline. The equation for  $\psi$  is, again ignoring  $(\nabla \cdot \mathbf{v}/2D)$ ,

$$\nabla^2 \psi + \left[ \nu/D - 1/Dn \frac{\partial n}{\partial t} - (\mathbf{v}/2D)^2 \right] \psi = 0 \quad (6-40)$$

Now if the eigenvalue of  $\nabla^2$  is  $-1/\Lambda^2$ , then the breakdown criterion is

$$\nu = D/\Lambda^2 + V^2/4D + 1/n \frac{\partial n}{\partial t} \quad (6-41)$$

The other theory of convective flux recognizes the possibility of space-charge coupling by treating ions (+) and electrons (-) separately.

$$\Gamma_- = n_- v - \nabla (D_- n_-) - \mu_- E n_- \quad (6-42)$$

$$\Gamma_+ = n_+ v - \nabla (D_+ n_+) + \mu_+ E n_+ \quad (6-43)$$

where  $\mu$  is the mobility and  $E$  is the space-charge field. In the steady state the electron and ion fluxes are equal, giving

$$\Gamma = \Gamma_- = \frac{(\mu_- + \mu_+) n_- n_+ v - \mu_+ n_+ \nabla (D_- n_-) - \mu_- n_- \nabla (D_+ n_+)}{\mu_- n_- + \mu_+ n_+} \quad (6-44)$$

Two limiting forms of this result may be applied. At low electron densities  $D_+ n_+ = D_- n_-$ , giving

$$\begin{aligned} \Gamma &= \left[ \frac{\mu_- + \mu_+}{\mu_- D_+ + \mu_+ D_-} \right] D_- n_- v - \nabla (D_- n_-) \\ &= (D_-/D_a) n_- v - \nabla (D_- n_-) \end{aligned} \quad (6-45)$$

Also, at high electron density  $n_+ = n_-$ , giving

$$\Gamma = n_- v - \left( \frac{\mu_+}{\mu_- + \mu_+} \right) \nabla (D_- n_-) - \left( \frac{\mu_-}{\mu_- + \mu_+} \right) \nabla (D_+ n_+) \quad (6-46)$$

Under the reasonable assumption that the ratio of mobilities is independent of position, this gives

$$\Gamma = n_- v - \nabla (D_a n_-) \quad (6-47)$$

Now since  $D = D_-$  at low electron density and  $D = D_a$  at high electron density, we may infer the following approximation during transitional diffusion ( $D = D_s$ ).

$$\Gamma = (v/D_a) D_s n - \nabla (D_s n) \quad (6-48)$$

The velocity is thus enhanced by the ratio  $D_s/D_a$ , giving the results shown in the second row of Table 6-1.

It is presently possible to resolve the discrepancies presented by the above four theories, to the extent that they can all be shown to be special cases of the general situation. First we point out that when the initial electron density is sufficiently high, the two rows of Table 6-1 automatically become identical, because  $D = D_a$ . Thus there is no need to resolve the discrepancy between the free convection and space-charge enhanced convection theories except at low initial electron density.

The resolution of the disparity between columns of the table has been established by W. C. Taylor of Stanford Research Institute (private communication), who has pointed out that the finite-time theory is actually a special case of the diffusion-coupled theory. This is demonstrated by solving Equation 6-40 for the electron density at the downstream edge of an

aperture antenna in a gas flow of uniform velocity. We depart from Taylor's analysis and Fante's<sup>271</sup> solution to pose the following one-dimensional problem\*:

$$\frac{d^2 n}{dx^2} - \left( \nu/D_v \right) \frac{dv}{dx} + \nu/D_s n = 0 \quad (6-49)$$

where  $D_v$  is either  $D_s$  or  $D_a$ , depending on whether the free-convection theory or the space-charge enhanced convection theory is under discussion. Outside the region  $0 < x < L$ , the ionization frequency vanishes and the value of  $D_v$  is taken much smaller than its value inside this region. The values of  $n$  and its derivative are matched at the boundaries. The solution for the electron density at  $x \geq L$  is

$$n/n_0 = \frac{2\sqrt{1-A} e^B}{(1 + \sqrt{1-A}) \exp(B\sqrt{1-A}) + (\sqrt{1-A} - 1) \exp(-B\sqrt{1-A})}, \quad A < 1$$

$$= \frac{e^B}{1+B}, \quad A = 1$$

$$= \frac{\sqrt{A-1} e^B}{\sqrt{A-1} \cos(B\sqrt{A-1}) + \sin(B\sqrt{A-1})}, \quad A > 1$$

$$B = \frac{\nu L}{2D_v}, \quad A = \nu/\nu_b \left[ 1 + (\pi/B)^2 \right] \quad (6-50)$$

\* This particular problem is posed to obviate the following difficulties:

- 1) Fante solved a problem in two dimensions with uniform flow and with a constant background ionization rate, as an inhomogeneous differential equation; but unfortunately the particular solution becomes infinite when the classical breakdown criterion for parallel plate breakdown in the transverse direction is satisfied ( $\nu/D = \pi^2/L^2$ ), a fact apparently unnoticed by Fante; and
- 2) Taylor included diffusion perpendicular to the flow, which gives results which do not reproduce a constant background electron density when  $\nu$  vanishes. No sacrifice of generality is made in terms of the relative importance of convection when the problem is posed in simplified form.

where  $\nu_b$  is the breakdown value from the simple diffusion coupled theory and  $n_0$  is the electron density at negative x.

$$\nu_b = D_s \left[ (\pi/L)^2 + (\nu/2D_v)^2 \right] \quad (6-51)$$

Breakdown defined as infinite  $n/n_0$  is determined by the solution of the transcendental equation

$$\sqrt{A-1} = -\tan(B\sqrt{A-1}), \quad \pi/2 < B\sqrt{A-1} < \pi \quad (6-52)$$

In addition when  $\nu$  is much less than  $\nu_b$ , the above equations have the following simple approximate form.

$$n/n_0 = \exp \left[ \nu L L_v / \nu D_s \right], \quad \nu \ll \nu_b \quad (6-53)$$

If breakdown is defined in terms of a finite electron density  $n_b$ , at which the exponential approximation (6-50) still applies, then the breakdown criterion is

$$\nu = \left( \nu D_s / L D_v \right) \ln(n_b/n_0), \quad \nu \ll \nu_b \quad (6-54)$$

The exact solution, Equation 6-50, and the exponential approximation, Equation 6-53, are shown for certain specific cases in Figures 6-4 through 6-6, for a velocity of 20 kft/sec, assuming  $D_p = 1.6 \times 10^6 \text{ cm}^2/\text{Torr}/\text{sec}^{-1}$  and  $D_-/D_a = 100$ . Three values of  $pL$  are assumed, 1, 10, and 100 cm/Torr. The first case considered is the free-convection theory assuming free diffusion applies. Figure 6-4 shows that the simple exponential approximation does not hold, and in addition, the actual breakdown occurs at much lower values than  $\nu_b$ . Thus in the free convection theory the breakdown ionization frequency is given approximately by the smaller of the two criteria given by Equations 6-52 and 6-54, with  $D_s = D_v$ .

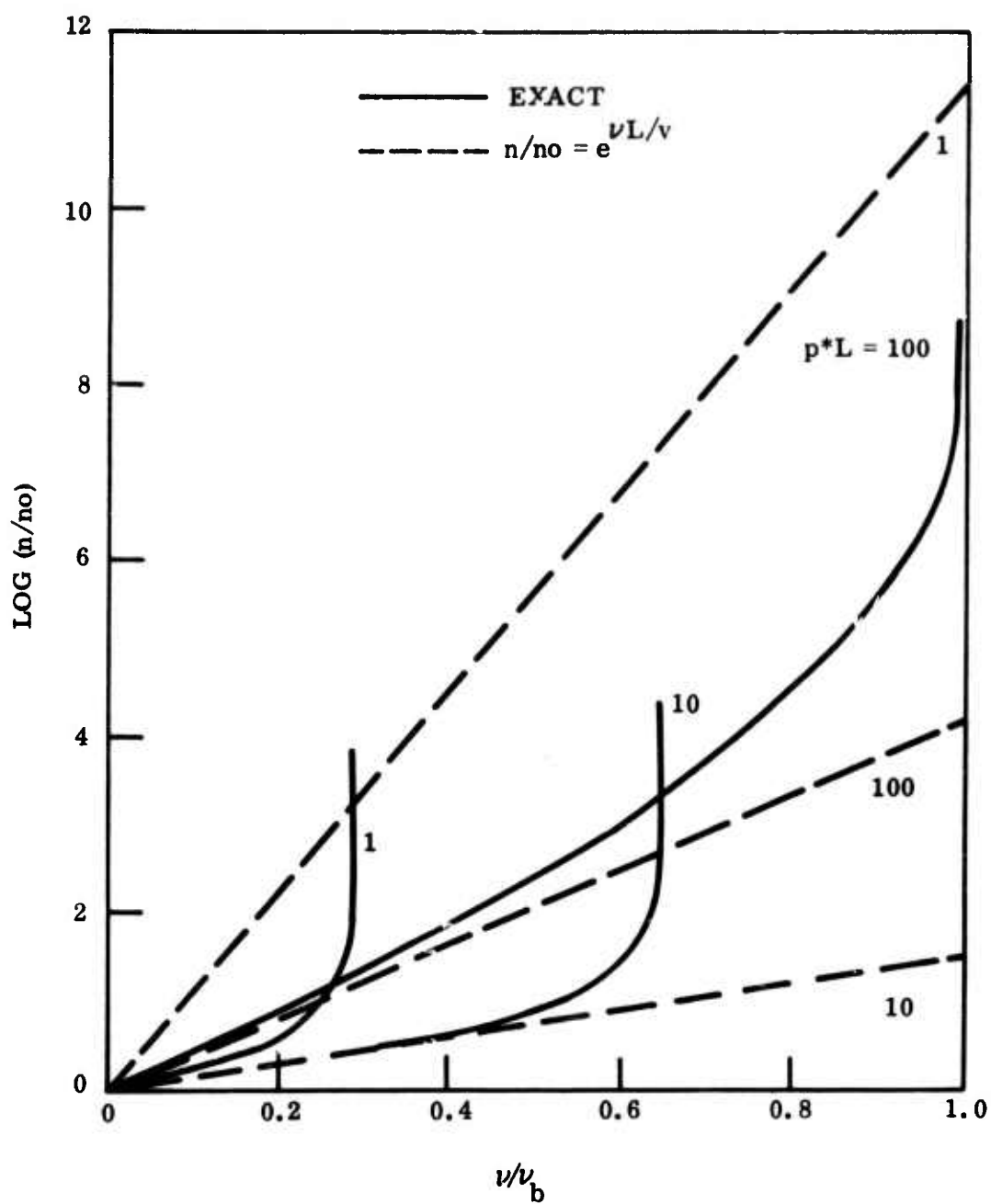


Figure 6-4. Electron Density at the Downstream Edge of a Uniform Field Region, Assuming Free Diffusion

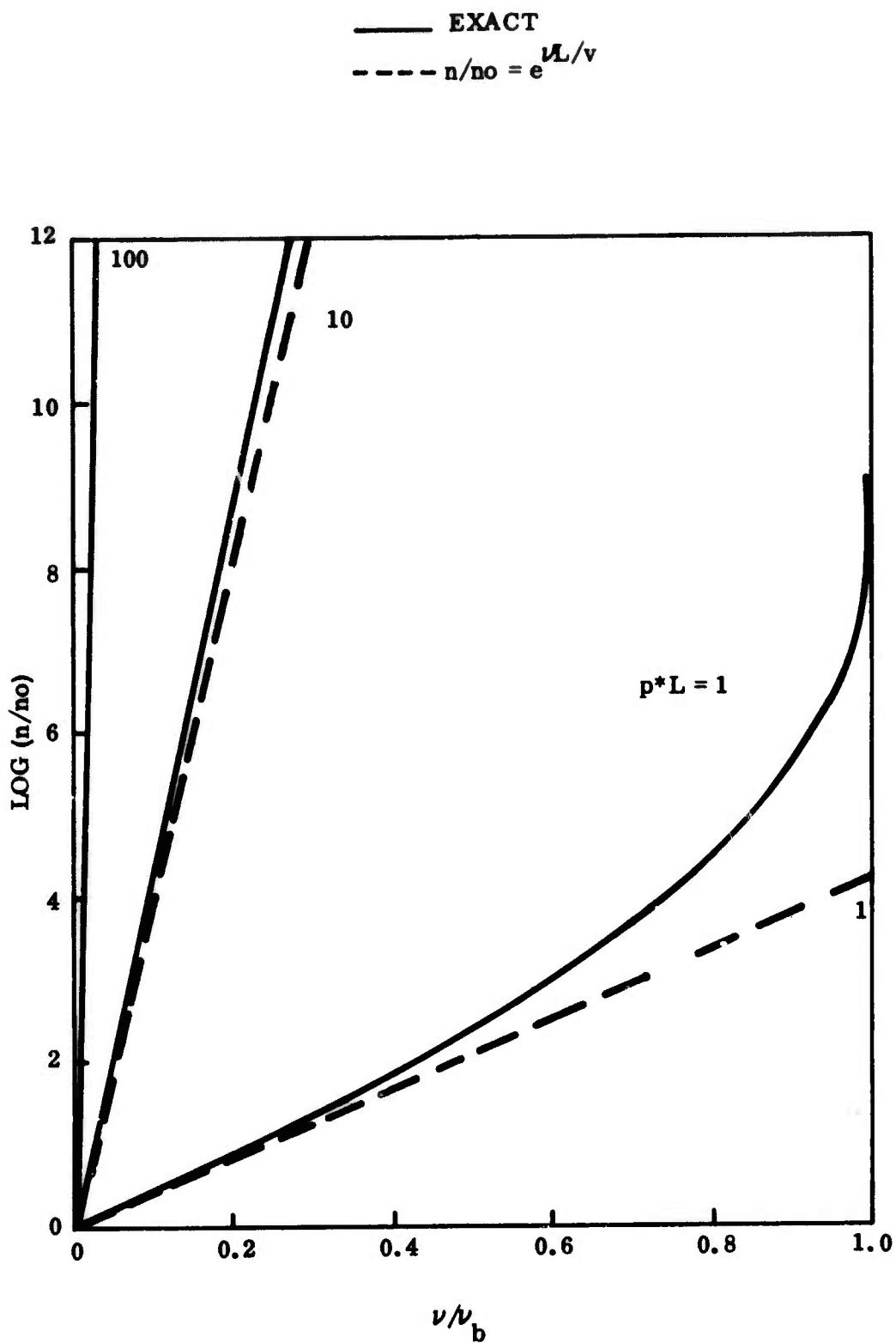


Figure 6-5. Ambipolar Diffusion Effect

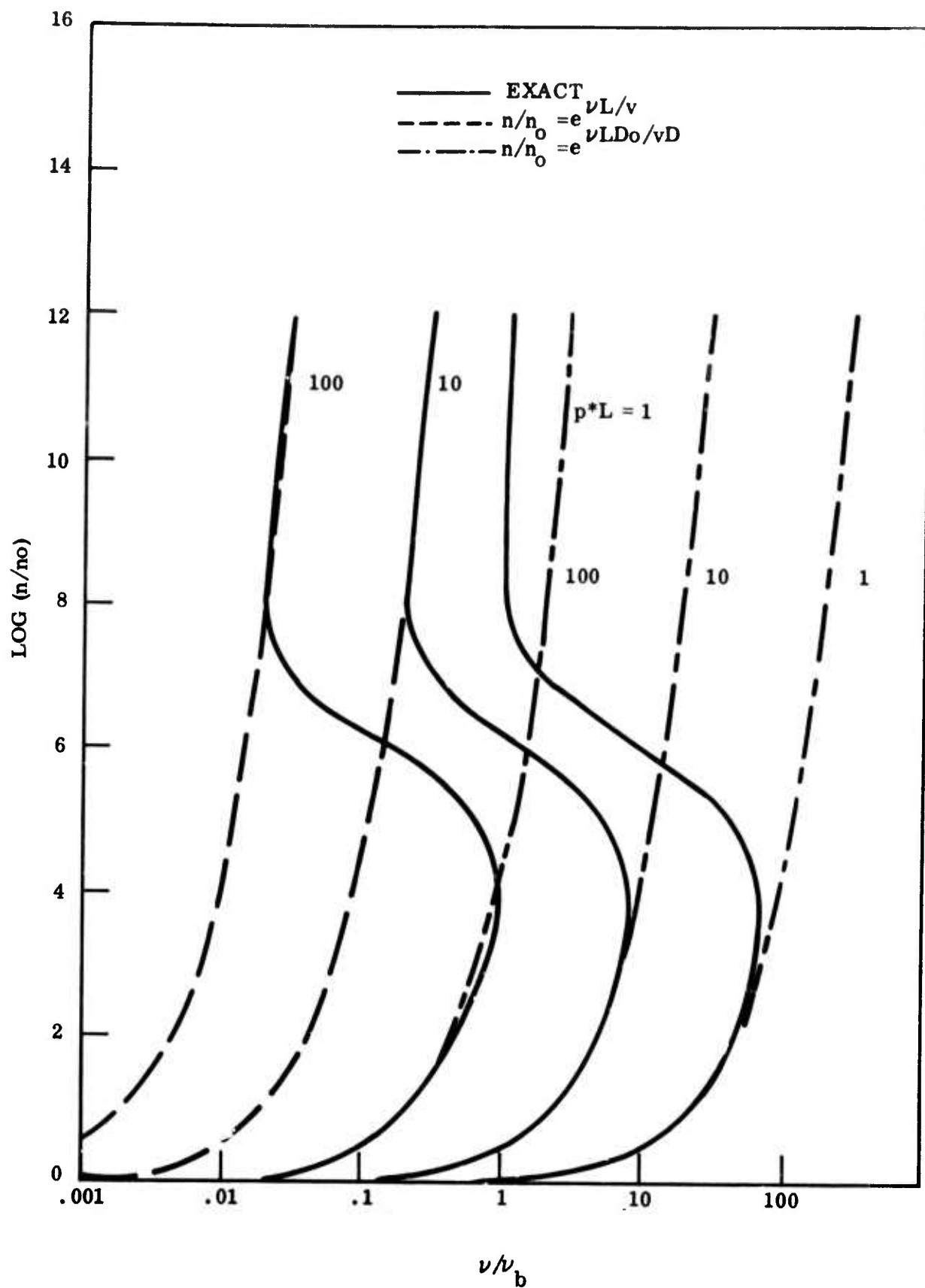


Figure 6-6. Space Charge Enhanced Convection Effect on Electron Density

Figure 6-5 shows the results assuming ambipolar diffusion applies (for either theory of convective flux). This time the exponential approximation predicts breakdown very precisely at high pressure, and the simple criterion  $\nu = \nu_b$  begins to apply at low pressure. Therefore the correct breakdown criterion is less than either  $\nu_b$  or Equation 6-54 with  $D_s = D_v$ , and a fair approximation is to take the smaller of the two.

Figure 6-6 is for the Cottingham theory, in which space-charge enhanced convection is assumed and transitional diffusion is considered. These curves were calculated applying Equation 6-23 to  $n/n_0$ , assuming  $T_e / (n_0 \Lambda^2) = 2 \times 10^4 \text{ cm}^3/\text{K}$ . Also,  $\nu_b$  in this figure has the meaning of the ambipolar value, the same as in the previous figure. Two different forms of exponential approximation are shown, that for the ordinary  $L/v$  theory, and that for the Cottingham velocity with free diffusion. The transition from free to ambipolar diffusion shows up at  $n = 10^6 n_0$ . All three curves are asymptotic to  $\nu = \nu_b$ . The interpretation of these results is confusing in light of the multi-valued electron density as a function of the ionization frequency. But if the criterion of a finite electron density is used, then the breakdown ionization frequency is single valued. The initial condition corresponds to having approximately one electron in a volume of gas equal to the extent of the field region, so that breakdown probably corresponds to the portion of the curves at which the transition is complete. Thus breakdown is determined approximately by the smaller of  $\nu_b$  or Equation 6-54 with  $D_s = D_v = D_a$ .

The conclusions from Figures 6-5 and 6-6 are essentially equivalent, and it is possible to show that the results of Figures 6-4 and 6-5 are consistent if transitional diffusion is assumed and if the difference in values of  $\nu_b$  is accounted for. Hence ambipolar diffusion always accompanies breakdown with convection, since the curves of the Figure 6-4 never reach large electron densities before  $\nu = \nu_b$ . Also the contribution of convection to the breakdown criterion is always smaller than either of the following, regardless of the initial electron density.

$$\nu_v \leq (v/L) \ln(n_b/n_0), \quad \nu_v \leq v^2/4D_a \quad (6-55)$$

### 6.2.5 GRADIENTS OF GAS PROPERTIES

As previously noted, the boundary layer surrounding a slender cone vehicle in hypersonic flight has strong gradients of density, temperature, velocity, and electron density. In addition, the entire flow field is highly nonuniform, with large changes in properties in passing from one region to another. Thus the importance of these nonuniformities must be evaluated before the breakdown analysis can be simplified.

Fante<sup>271</sup> has analyzed the situation of nonuniform media in terms of the effect of an ambipolar-diffusion layer and an outer free-diffusion layer covering an aperture antenna. The results of this calculation show that even a small ambipolar-diffusion layer can drastically reduce the breakdown field strength. In general, it can be seen from the effects of reentry that several factors contribute to spatial nonuniformity of different terms in the continuity equation. The flow velocity is obviously nonuniform in space as determined by the flow-field properties. The diffusion coefficient will have gradients due to molecular density gradients and ionization gradients (transition to ambipolar diffusion in high electron-density regions). If the effective field is included in the formula for the diffusion coefficient, gradients will also be due to field nonuniformity. The frequencies of ionization and attachment have spatial gradients contributed by variations in particle number density, field intensity, and also air temperature. Profiles of chemical species which are distributed in the flow field would conceivably contribute to gradients in both the diffusion coefficient (molecular weight effect) and the ionization and attachment frequencies. Finally, the ionization gradients would affect pulse breakdown in terms of the spatial variation of initial electron density, although this effect is probably not very important.

These effects can be accounted for in principle by solving the continuity equation as a differential equation with nonconstant coefficient, just as in the problem on nonuniform antenna fields. A fair approximation is to treat the breakdown on a slender cone vehicle separately in terms of three different regions, boundary layer, inviscid layer, and free stream. The contribution of the first two regions to the effect should be to give an effective diffusion length of the order of the thickness of the particular region in question.

The presence of high-electron density in a thin layer is not necessarily a sufficient condition for breakdown, but rather the adjacent flow-field region must also ionize to cause the plasma to thicken, leading to breakdown. This aspect of the problem is related to the general question of breakdown criteria discussed above.

#### 6.2.6 EFFECTS OF GAS CHEMICAL COMPOSITION

Two sources of chemical composition effects in the flow fields of slender reentry vehicles are dissociation of the air and ablation of gases from the heat protection shield. These effects can be accounted for in principle by reviewing the basic data on each of the species involved. However, much of the breakdown data have been obtained in terms of materials as candidates for deliberate injection into the flow as alleviants. Therefore these data are reviewed in Section 8.

#### 6.3 ILLUSTRATIVE CALCULATIONS

The breakdown power of an antenna in the reentry environment can be estimated from the results developed above. In fact, it is possible to write these results in terms of a closed form algebraic equation, utilizing the following equation for the power output of an antenna<sup>273</sup>.

$$P = 1.33 \times 10^{-3} E^2 A \quad (6-56)$$

where  $P$  is in watts,  $E$  is the maximum rms field intensity in volts/cm, and  $A$  is the effective aperture in  $\text{cm}^2$ , defined in terms of the near field and the input power.

Equations for the effects of gas density, ionization, temperature, and convection are discussed above and can be used here. The most uncertain of these equations is the high gas temperature, Equation 6-30, which is a curve fit to some very meager data and which is based on a simplified view of cold air breakdown. Before proceeding to the application of this equation to illustrative calculations, let us indicate the extent of the discrepancy between this simplified theory and that of MacDonald<sup>248</sup>. Figure 6-7 shows this comparison for three values of  $\lambda/\Lambda$ . The limitations and difficulties of the data and theories are discussed more fully above, but

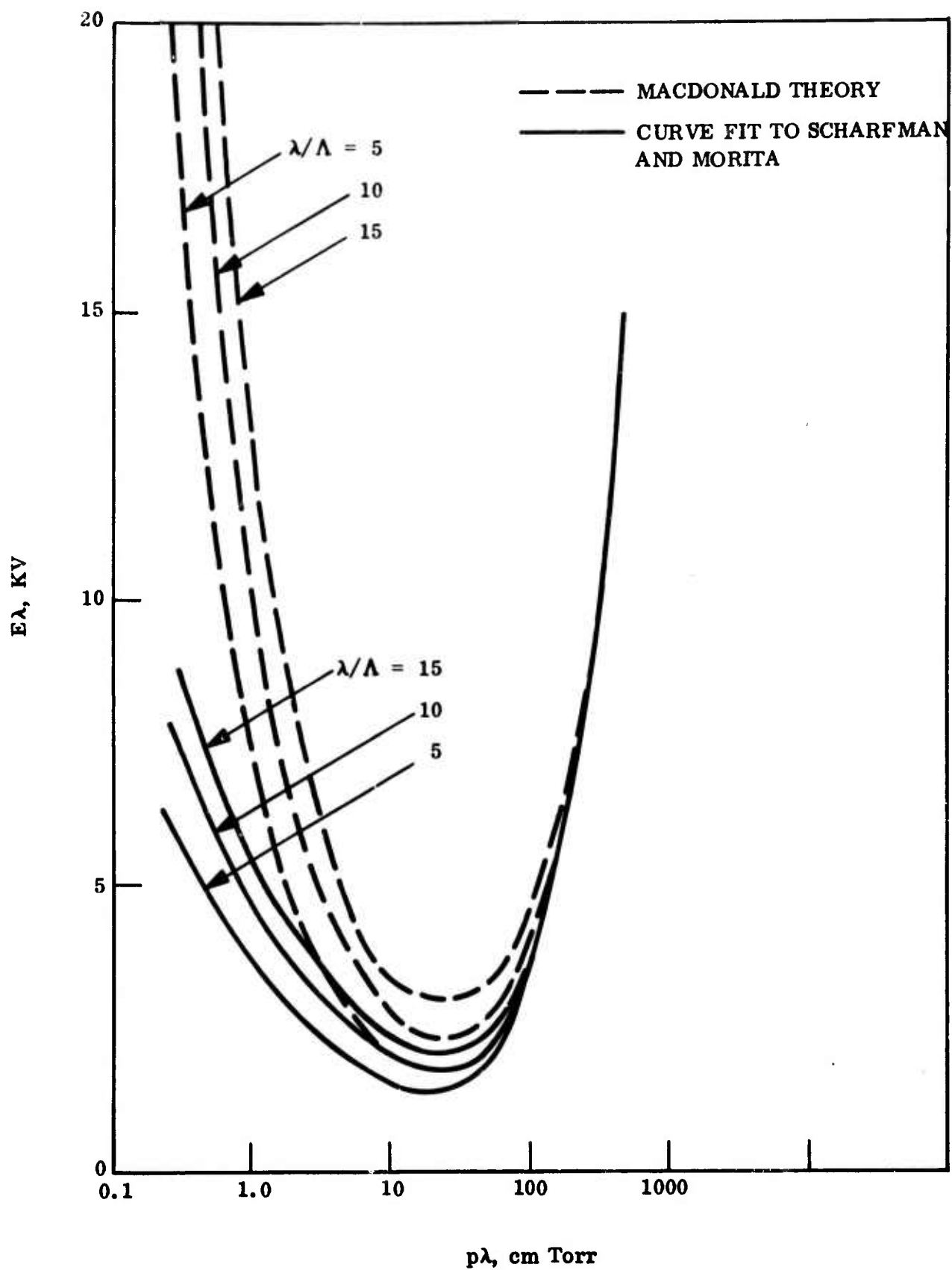


Figure 6-7. Comparison of Breakdown Field by the Theory of MacDonald and Scharfman

Figure 6-7 can be used, if desired, to correct the values of breakdown power calculated below to the values corresponding to the MacDonald theory. Of course the method used here is conservative, since it will always predict lower breakdown power than MacDonald's theory.

The resulting equation for CW breakdown power can be written in proper variable form by normalizing  $P$ .

$$P/P_o = (A/\lambda^2) \left[ 1 - e^{-(3000/T)^5} \right] = (A/\lambda^2) f(T) \quad (6-57)$$

$$P_o = 19 \left[ (p^*\lambda)^2 + (35.6)^2 \right] \left[ 6.4 \times 10^4 + \right.$$

$$\left. \frac{D_p p^*}{(p^*\lambda)^2} \left( \frac{480 T_e + n_o \Lambda^2}{480 T_e + n_o \Lambda^2 D_-/D_a} \right) + \left( 4D_a p^* + \frac{p^* L v}{\ln(n_b/n_o)} \right)^{-1} v^2 \right]^{3/8} \quad (6-58)$$

$$p^* = 273 p/T \quad (6-59)$$

$$n_b = 1.12 \times 10^{13} / \lambda^2 \quad (6-60)$$

In these equations  $P_o$  is in watts,  $T_e$  and  $T$  are in  $^{\circ}\text{K}$ ,  $p^*$  and  $p$  are in Torr, and all other quantities are in cgs units. This normalization removes the temperature effect as a simple multiplicative factor  $f(T)$  and expresses the remaining reentry effects in terms of proper variables. For fixed values of  $\lambda/\Lambda$  and  $\lambda/L$ ,  $P_o$  is a function of the proper variables  $p^*\lambda$ ,  $n_o \lambda^2$ , and  $v$ , if the electron temperature is held constant.

$P_o$  is plotted parametrically as a function of these proper variables in Figures 6-8 through 6-10 using the following constants:  $D_p p^* = 1.6 \times 10^6$ ,  $T_e = 2 \times 10^4$ ,  $D_-/D_a = 100$ .

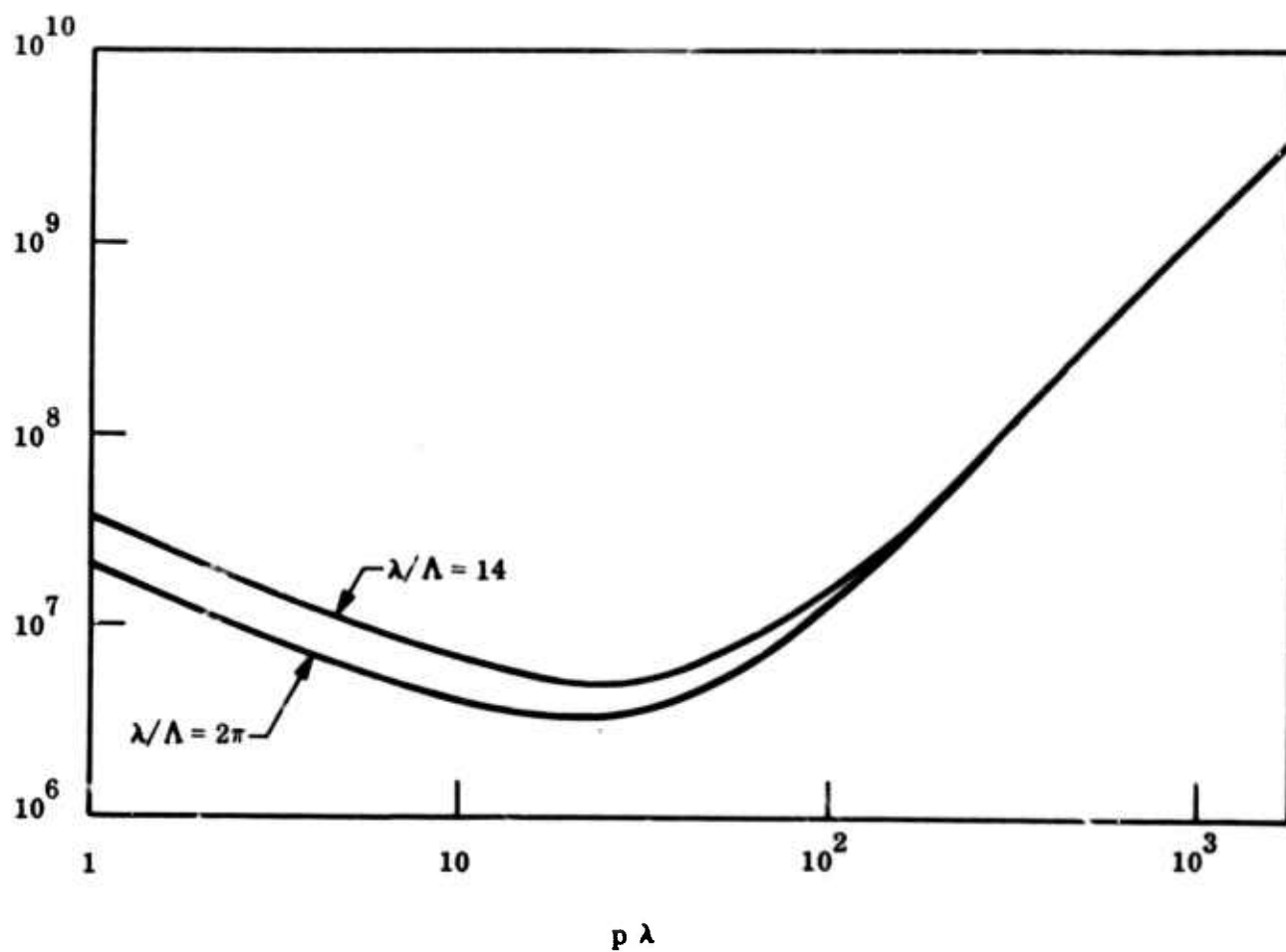


Figure 6-8. Normalized Breakdown Power Versus  $p\lambda$  Without Reentry Effects

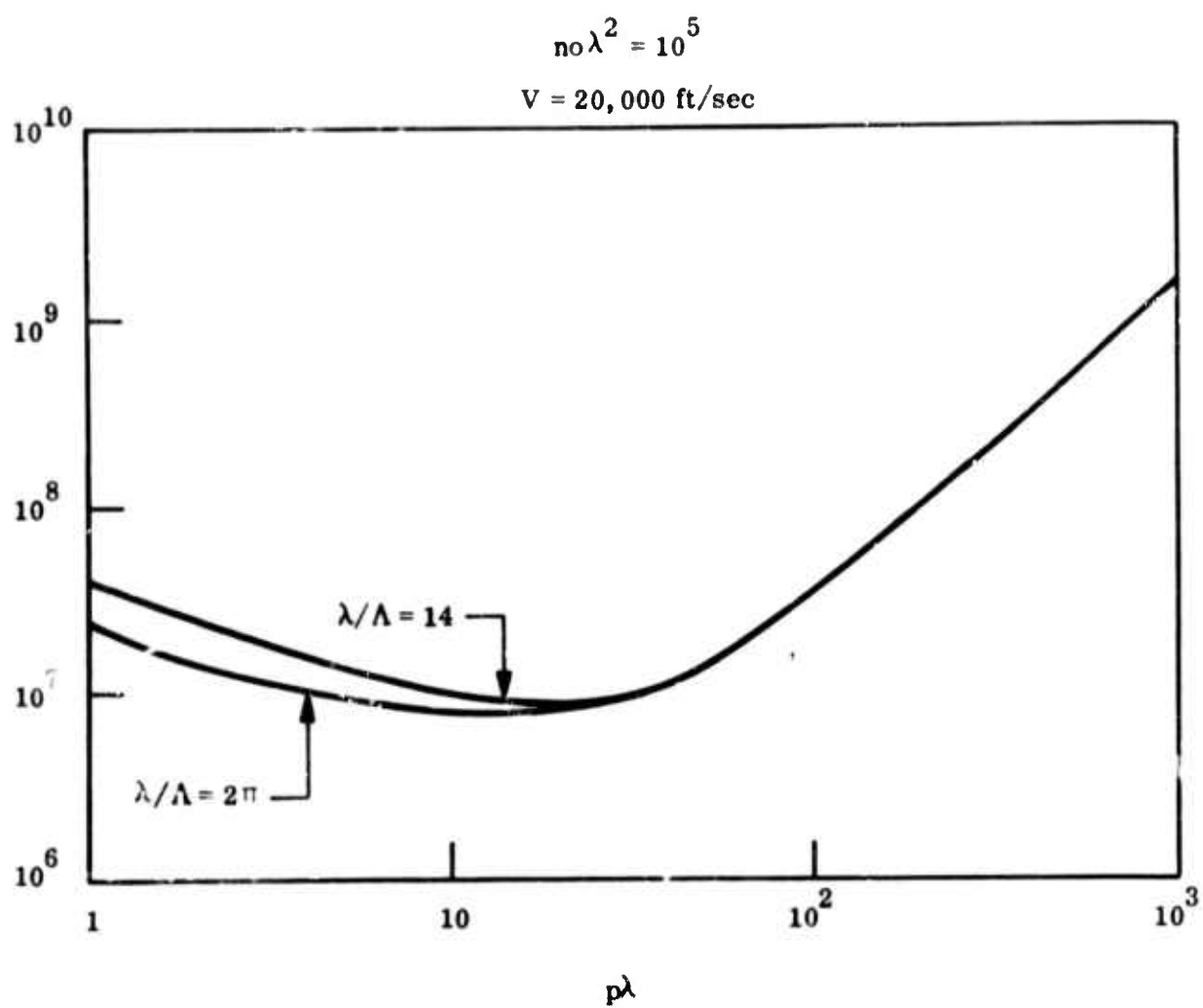


Figure 6-9. Normalized Breakdown Power Versus,  $p\lambda$  with Convection

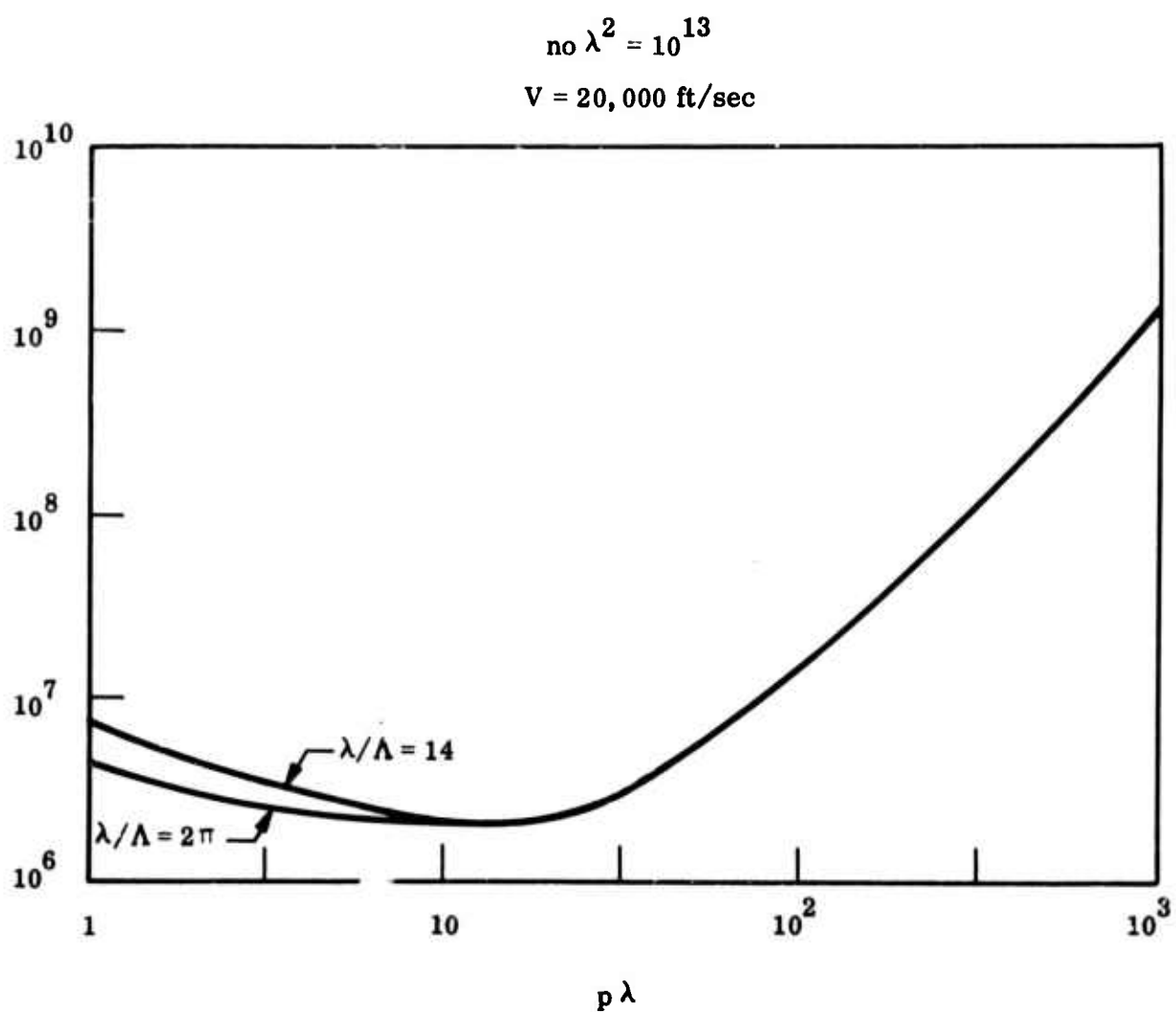


Figure 6-10. Normalized Breakdown Power Versus  $p\lambda$  with Convection and Ionization

**BLANK PAGE**

## SECTION 7

### NONLINEAR INTERACTIONS

Electromagnetic fields of sufficient intensity can induce a change in the state of a partially ionized plasma due to field energy coupling into the electron gas. As a result, the electron distribution function is altered and becomes dependent on the electric field intensity. Consequently, transport coefficients such as thermal and electrical conductivities, which are deduced from the distribution function, become dependent on the local field intensities. While various forms of nonlinearities may be exhibited from the interaction of electromagnetic radiation with a plasma, the particular class covered in this section is restricted to the case where the incident field deposits energy in the plasma and modifies the electron temperature, electron density, and effective collision frequency. The present interest is in the propagation of electromagnetic radiation in a plasma, and the conductivity coefficient is of paramount importance.

#### 7.1 SURVEY

Papa<sup>274</sup> has performed a comprehensive survey of nonlinear electromagnetic wave propagation in plasmas. His conclusions indicate that there are many kinds of nonlinear interactions possible, resulting from the fact that the physical mechanisms involved have such a large number of characteristic times, especially in terms of electronic interactions. The various possible combinations of relative magnitudes of these characteristic times lead to the definition of myriad possible situations. For example, if the electron-electron collision time is much less than the times for the relaxation of electron density and temperature and the diffusion time, then the isotropic part of the distribution function is Maxwellian. But if the electron temperature relaxation time is much shorter than all other characteristic times except the period of the electromagnetic field, then the Margenau<sup>275</sup> distribution applies.

When the power level of a signal in a plasma is increased, the first nonlinear effects to be observed are collision frequency effects, especially in plasma formed in air. The

dependence of collision frequency on electron velocity changes the effective collision frequency as the electron energy gained from the field is increased. Strictly speaking, the plasma-electromagnetic wave interaction is always nonlinear, since the electron energy depends on the field strength under all conditions. In addition, the plasma constitutive parameters depend on the signal frequency, and they are not additive in the case of mixtures of different species.

Various approaches to the definition of effective parameters for a plasma have been used. The problem is to define two parameters, which are related to the complex conductivity of the plasma. Molmud<sup>276</sup> used a complex collision frequency to obviate the difficulty of non-constant collision frequency, while Shkarofsky<sup>277</sup> used auxiliary real functions. The method of Whitmer and Herrmann<sup>278</sup>, who defined effective values of collision frequency and plasma frequency for direct use in the conductivity formula, is the most convenient to use. The latter authors give useful numerical results for actual gases in graphical form.

Bakshi et al.<sup>279</sup> have shown that all the above approaches are equivalent, and they have derived a general procedure for calculating effective parameters. The effective small signal conductivity, defined as the ratio of the current density to the electric field, in the limit of vanishing field, is defined in terms of response functions.

$$\sigma(\omega) = \epsilon_0 \pi^2 \left[ C(\omega) + iS(\omega) \right] \quad (7-1)$$

$$C(\omega) = \int_0^\infty R(y) \cos \omega y \, dy \quad (7-2)$$

$$S(\omega) = \int_0^\infty R(y) \sin \omega y \, dy \quad (7-3)$$

where  $R(y)$  is the average response of an electron in the plasma to a unit amplitude step function of electric field starting at  $y = 0$ . These authors also give graphical results for idealized forms of dependence of collision frequency on electron speed.

Haskell et al.<sup>280</sup> have considered the above theory of effective parameters for strong fields, i. e. non-Maxwellian velocity distributions. As in the case of vanishing fields considered above, each plasma parameter undergoes a transition from a low frequency value to a high frequency value in the neighborhood of the average collision frequency. However, in this case the results depend on the field strength at low frequency. But even though the low-to-high frequency transition occurs when the collision frequency is independent of velocity, it is independent of field strength in this case. Thus, for a constant electron density, all nonlinear effects must come from non-constant collision frequency effects. For collision frequency as an increasing function of velocity, both the effective plasma frequency and the effective collision frequency increase with increasing field strength at low frequency (or low altitude). Unfortunately, the ratio  $\omega_p^2/\nu_c$ , which is important in thin plasma for slender reentry vehicles at low altitudes, tends to increase with field strength.

The nonlinear collision frequency effect is absent at high altitude, so that nonlinear production of electrons, or breakdown, is the only important phenomenon. Nonlinear breakdown can take a variety of forms. If very little ambient plasma is present, very little effect will be observed until the breakdown field is reached. The ionization frequency increases too rapidly with field strength for appreciable prebreakdown nonlinear effects to occur. Subsequent increase in power level beyond breakdown causes the discharge plasma to thicken, so that output power is generally limited to a low level. When the initial electron density is high (near critical) the process of breakdown has the apparent behavior of a nonlinear effect, since the transmitted power will begin to level off as input power is increased and the plasma layer thickens. These effects have been observed experimentally by Chown et al.<sup>281, 282</sup>

## 7.2 BROADBAND SIGNAL EFFECTS

The most important aspect of nonlinear phenomena is their effects on broadband signals. In terms of prebreakdown nonlinear collision frequency effects, it appears that the most

important effects will occur in a band of frequencies near the average collision frequency. But the plasma dispersion tends to decrease as the field increases, at field strengths below breakdown, from the results of Haskell. Thus the only important broadband signal effect is breakdown. The problem of multi-frequency propagation has been considered by Mott<sup>283</sup> in conjunction with antenna breakdown in air. The breakdown depends not only on frequency but also on the envelope of the electric field. The envelope may be determined by phasor addition of the individual components. A minimum level is obtained for  $n$  equal amplitude signals by in-phase addition. The resulting envelope peaks determine breakdown by acting as a continuous wave breakdown field  $n$  times as large as the single field. The resulting breakdown power is  $1/n$  times that for one frequency. Additional work on multi-frequency signals has been carried out by Fante and Mullin<sup>284</sup>. Here an attempt is made to determine the effective electric field strength for a composite signal such as noise. For a stationary random signal  $E(t)$ , the effective field is given by

$$E_{\text{eff}} = \left[ \nu_c^2 \int_0^\infty \frac{S(f) df}{\omega^2 + \nu_c^2} \right]^{1/2}, \quad (7-4)$$

where  $\nu_c$  is the velocity-independent collision frequency, and  $S(f)$  is the spectral density. The transmission of power by the noise signal is compared to that of a single frequency component. At high collision frequencies there is no difference between the signals. However, when the collision frequency is less than the average signal frequency, the single frequency can transmit more power than the noise signal.

## SECTION 8

### ALLEVIATION TECHNIQUES

The alleviation of reentry plasma effects on signal transmission and of reentry flow field effects on antenna breakdown is generally a matter of considerable concern where these effects are apt to be serious. The solution of the problem of alleviation is dependent on gaining an understanding of the phenomena involved in terms of the causative factors and the mechanisms of interaction. Plasma effects on signal transmission depend on the flow-field ionization and collision frequency as sole causative factors; whereas the effects of reentry on breakdown are caused by a variety of phenomena. Both types of effect depend on basically the same mechanism of interaction of the antenna field with the medium. The discussion of alleviation is best organized according to the discussion of alleviation of the causative environment or the interaction, since overlap may occur between attenuation and breakdown. The environment control is discussed under the heading of plasma alleviation and the interaction is treated under electromagnetic techniques.

#### 8.1 PLASMA ALLEVIATION

It is desirable from the standpoint of both plasma attenuation and breakdown to minimize the flow field ionization in the vicinity of the antenna. Aerodynamic shaping and material injection are considered in this vein. In terms of body shape effects, the nose bluntness of a slender cone vehicle is the most important contributor to ionization. Thus, the use of a sharp nose tends to minimize shock-induced plasma. Various other aspects of body shaping are also considered in an Aerospace Corporation report,<sup>285</sup> including the communications fin and flow diverters. But these techniques have no application to slender cone vehicles, especially when the nose radius can be made sufficiently small. Various ideas for liquid or gas coolants have been suggested. Some of these techniques may possibly alleviate the high gas temperature effect on breakdown, as well as plasma effects on both attenuation and breakdown.

Chemical additives may take the form of either ablation products from the heat shield or active mass injection.

Aisenberg<sup>286</sup> has conducted analytical and experimental studies on alleviation of plasma sheath and antenna breakdown effects. They have been evaluating materials for the ability to reduce electron concentration and to increase breakdown power level in thermal plasmas. The primary alleviation mechanism studied is attachment of electrons by electronegative gases. The plasma simulation facility used in these studies is an argon arc jet. Conditions simulated include atmospheric pressure down to 13 Torr and temperatures of 3000 to 5000°K. Diagnostics are conducted by means of K-band transmission through the test section. Additives tested include  $\text{SF}_6$ ,  $\text{BF}_3$ ,  $\text{N}_2$ , Freon 116, air, and argon.

Aisenberg concluded that materials which are good attachers in glow discharges often do not work in thermal plasmas because of dissociation. A figure of merit for attachers would appear to depend on the molecular weight, the electron attachment cross section (including its energy dependence), and the resistance to thermal dissociation. Highly electronegative materials have higher attachment cross sections in the molecular form than in the atomic form. Survival lifetimes of molecular additives in thermal plasmas are thus important in determining their effectiveness as plasma alleviative substances.

The ideal additive material for alleviation of both ionization and breakdown is pictured as one made up of "giant molecules," which would actually be extremely small solid particles or liquid drops. These particles would have maximum survival times as well as providing surface recombination as a mechanism for electron removal. Refractory solids would have to be avoided because of thermionic emission and Saha-Langmuir ionization.

MIT Aerophysics Laboratory has been conducting experiments in a wind tunnel under the direction of E. E. Covert<sup>237</sup>. In this experiment a supersonic arc jet is blown over the nose of a cone model in a Mach 4 wind tunnel. Breakdown of an X-band slot on the cone was determined under conditions of injection of  $\text{SF}_6$ . They have observed that the electron

density was reduced by an order of magnitude, but that the breakdown was unaffected unless the additive was injected immediately in front of the antenna. Good results were also obtained with Teflon products. Thompson<sup>265</sup> has measured the effects of CO, CF<sub>4</sub>, and SF<sub>6</sub> on electron density and antenna breakdown in an arc channel. The first two of these materials are products of ablation for carbon and Teflon heat shields, respectively; and the last is a popular electrophilic quenchant candidate. Twenty percent by volume of each of these materials was added to the flow, and experiments were conducted at temperatures between 3000 and 5000°K. Carbon monoxide was found to have no effect on either electron density or breakdown. CF<sub>4</sub> reduced the electron density by a factor of 2 to 3 and increased the breakdown power by a factor of 3. SF<sub>6</sub> reduced the electron density by more than a factor of 3 and increased the breakdown power by a factor of 2. The authors attribute the breakdown alleviation by the fluorides to the additional electron attachment provided by fluorine and fluoride radicals.

An additional aspect of plasma alleviation is the problem of collision frequency control, which can have a payoff in both attenuation and breakdown. If the plasma is thin compared to the wavelength of the signal, as it tends to be for slender cones, then it is beneficial to make the collision frequency a maximum. Thus one should locate the antenna on a forward facing part of the body, preferably on the cone frustum. (Optimum body station on the cone from the standpoint of plasma density is a complicated question involving nose bluntness and ablation effects in a tradeoff, which is beyond the scope of this study.) This approach tends also to minimize the plasma thickness over the antenna. The effectiveness of this technique in alleviating breakdown is dependent on the desired altitude of operation of the system. It is a decided disadvantage in a high altitude ECM system, since the increase in collision frequency tends to push breakdown to higher altitudes but it is probably helpful in increasing the overall power handling capability if the breakdown minimum can be moved to an altitude where ionization and high temperature effects are weak.

## 8.2 ELECTROMAGNETIC TECHNIQUES

The most basic technique for control of the electromagnetic interaction is the antenna design. The use of a non-charring dielectric window or covering the entire antenna area with non-charring low loss ablation material, such as Teflon, reduces the near field intensity in the flow field. This can alleviate linear plasma effects by reducing the contribution of the plasma to the antenna input impedance. Breakdown is alleviated by reducing the strength of the near field and by increasing the rate of diffusion loss, as noted by Scharfman and Morita<sup>288,289</sup>. Chown et al.<sup>281</sup> point out that the alleviation of breakdown by antennas designed to maximize the breakdown field strength does not necessarily increase the power handling capability, especially if the antenna Q is increased in order to do so. High-Q antennas are characterized by the fact that there is a large amount of stored energy near the antenna in comparison with the energy radiated per cycle. This means that the field will be quite high in the vicinity of the antenna. The high-Q antenna is undesirable for several reasons--one is that the high fields imply low power-handling capability, another is that the impedance of a high-Q antenna will be more sensitive to the presence of the plasma environment. Reactive fields, upon immersion in a plasma, become dissipative, providing another means of absorbing the RF power. Also the multipactor discharge phenomenon which is possibly detrimental to the vehicle or antenna in terms of heating if not power transmission, is enhanced in high-Q antennas. Multipacting occurs when the electron mean free path exceeds the limits of validity of the diffusion theory of breakdown (see Paragraph 6.1). It tends to flatten out the curve of breakdown field versus pressure in such a way that the multipactor breakdown field remains approximately equal to the normal breakdown field at the mean free path limit.

Scharfman and Morita<sup>288, 289</sup> also have measured the effect of a dc bias voltage on antenna breakdown, to determine if it would perform the function of sweeping the electrons out of the high field region. However, this technique is much less effective for well designed antennas which have low near-field intensity than for those which already have a low power-handling

capability. The technique does not work when the antenna is covered by dielectric material since the electrons attracted to the dielectric surface cancel the biasing field in the plasma.

Static magnetic fields can, in principle, be used to alleviate plasma attenuation. Attenuation for right-hand circularly polarized waves propagating normal to a plasma layer will be reduced in the presence of a magnetic field in the direction of propagation. This is because the Lorentz force checks the ability of the electron generated field to cancel the imposed field. Rothman and Morita<sup>290</sup> consider the problem analytically for rectangular coordinates. The conditions for enhancement are that the electron cyclotron frequency be greater than the signal frequency, and that the square of the collision frequency be much less than the square of the difference between the cyclotron frequency and the imposed angular frequency. Rothman and Morita carried out experimental laboratory work using an RF discharge which demonstrated qualitative enhancement and polarization in the presence of a magnetic field.

Samaddar<sup>291, 292</sup> considers magnetic window effects in special cases of nonrectangular geometries. In particular, he considers cylindrical and conical geometries which approximate vehicle shapes. His method utilized calculating the dielectric tensor as a function of the applied magnetic field, and the plasma and collision frequencies. To gain effective control over attenuation, mutual orientation of the antenna and imposed magnetic field must be chosen so that the field components are independent of components of the dielectric tensor parallel to the imposed magnetic field. This approach has been analyzed<sup>285</sup> in terms of weight requirements and found to be feasible only if a greater system loss figure, than with the other alleviants (20 db rather than 10 db), could be tolerated. The use of superconducting magnet has some promise for short flights, but cooling equipment becomes a limiting factor.

Lax et al<sup>293</sup> have studied breakdown in transverse magnetic fields, which tend to worsen the problem through two mechanisms. The magnetic field enhances the transfer of energy to the electrons and it decreases the diffusion losses perpendicular to the field.

The breakdown field is reduced by very significant amounts in the neighborhood of the cyclotron resonance (2.8 MHz/Gauss), although it is slightly increased at much higher values of magnetic field. These conclusions are based on studies of well behaved noble gases and there are only qualitative indications that they would still hold for air, in which static magnetic fields can create serious nonlinear behavior. But static fields are probably not feasible alleviation techniques for slender body reentry effects at any rate.

## SECTION 9

### RECOMMENDATIONS

The present state of knowledge of reentry effects on signal transmission is sufficiently incomplete to warrant further work on this subject. In order to arrive at research recommendations which are best suited to the systems problems to which the technology is applied, it is necessary to evaluate the results of this study from the standpoint of certain criteria. Accordingly, three criteria are applied to assessing the importance of a given effect, as follows:

- a. The effect must be severe.
- b. It must be relatively difficult to predict.
- c. It must be difficult to control or alleviate.

#### 9.1 EVALUATION

Linear plasma effects are wholly dependent on the presence of flow-field ionization. At low altitudes, collision frequency effects become important in such a way on slender vehicles as to make increased collision frequency desirable. While these effects are potentially very severe, it is also possible to alleviate them by body shaping and materials selection. The predictability of these effects is relatively poor, but it is possible to estimate the electron density levels below which they are alleviated.

Nonlinear plasma effects are unimportant. These effects deviate from linear effects as a function of the collision frequency. Thus they are present only at low altitudes, when the collision frequency exceeds the signal radian frequency, and they are not very severe, especially on a slender cone vehicle. The theoretical prediction of these effects is very difficult, but they may be alleviated in the same way as linear plasma effects.

Antenna breakdown effects are the most important. They score high on all three evaluation criteria of severity, unpredictability, and uncontrollability. The six phenomena which have been identified as important influences on breakdown have varying degrees of predictability

and controllability, not only in terms of the breakdown mechanism but also as a function of the flow-field prediction and control. For example, little is presently known about the high gas temperature effect on the breakdown mechanism, and available techniques for describing the thermal nonequilibrium effect have not been applied to the flow field properties of a slender cone at high altitudes.

Table 9-1 summarizes the evaluation of reentry effects on antenna breakdown. The items marked "1" are the most important, and the phenomena are listed in the order of importance based on these criteria. Temperature is most important because so little is known about it. Gradients effects can be predicted by solving simple boundary value problems and using the resulting effective diffusion length, but the breakdown prediction should be performed in the context of the actual flow-field profiles. The convection effect requires more careful consideration of the mathematical criterion for breakdown.

Table 9-1. Evaluation of Flow-Field Effects on Breakdown

Phenomenon	Severity	Predictability	Controllability
Temperature	1	1	1
Gradients	2	2	1
Convection	2	2	1
Ionization	1	3	2
Density	1	3	2
Chemical Composition	3	2	2
1 = most severe, least predictable, or least controllable			

Ionization effects on breakdown correspond to lower electron densities than for linear plasma effects, so that they are not so easily controlled. Density effects are well understood and somewhat controllable by antenna placement on the vehicle. Chemical composition effects are severe only with heavy mass injection and then only in the boundary layer.

In addition to the consideration of the importance of a given flow-field effect, it is necessary to consider the importance of the flow-field prediction and control problems. Breakdown generally occurs at much higher altitudes than linear plasma effects on slender vehicles, and this fact leads to difficulties in the flow field prediction, especially if the vibrational and electronic excited states of the gas are important in antenna breakdown. In addition, the best way to account for flow-field gradients effects is to couple the breakdown theory to the flow-field computation.

## 9.2 RESEARCH RECOMMENDATIONS

Recommendations for needed research to improve the predictability and controllability of reentry effects on breakdown can be derived from the above evaluation. Three topics are recommended for further study; gas temperature, convection, and gradients effects on breakdown.

### 9.2.1 HIGH GAS TEMPERATURE

More research is needed in order to extend and validate the data already obtained, for which the range of conditions of pressure and temperature is too narrow to permit a good empirical formula to be derived. The formula derived in this study represents a very great extrapolation, which does not correspond fully in the cold air limit to the best available theory. Data at lower pressures and higher temperatures are required to fill this gap. The following tasks should be performed in order to obtain a reliable phenomenological model:

- a. Measure microwave breakdown in air in a shock tube at various values of pressure, shock velocity, pulse duration, and station behind the shock.
- b. Measure the air properties for the above conditions, including gas temperature, pressure, density, and electron density.
- c. Calculate the gas properties in the above experiment, using the best techniques available and including coupled vibration-dissociation-vibration (CVDV) effects and allowing for arbitrary preferred dissociation from the upper vibrational energy levels.

- d. Compare the calculated and measured gas properties and adjust the probability for preferred dissociation to match the experimental data.
- e. Reduce the breakdown data to give curves of normalized ionization frequency versus normalized electric field as a function of the gas properties, including vibrational and electronic temperatures, if necessary.
- f. Derive a phenomenological theory for the gas temperature effect on ionization frequency, using the above data to determine the values of arbitrary parameters.

### 9.2.2 CONVECTION

A set of experiments on microwave breakdown in flowing gases at a wide range of conditions of pressure, velocity, and ionization level is needed to verify the theories and show their regions of validity.

A further study of convection theory is needed to resolve the discrepancies among the various theories, and to interpret the results of experiments. The basic problem is to solve the coupling among diffusion, convection, and space charge. The analysis which was done in this study neglected to do this, using instead simplified formulas for the transitional parameters without explicitly accounting for space charge. Results would be compared with experiments.

### 9.2.3 GRADIENTS AND BREAKDOWN CRITERIA

The effects of flow-field gradients on breakdown need to be studied by solving the breakdown equations for typical flow-field profiles of gas velocity, density, temperature, and ionization, using realistic antenna-field distributions. This work should be done in conjunction with a study of breakdown criteria for slender body flow-field effects. In other words, the antenna impedance and radiated power should be calculated as a function of input power in conjunction with the breakdown equations. To do this properly may mean coupling the flow-field, the breakdown, and the propagation equations together into a single computer program.

#### 9.2.4 FLIGHT EXPERIMENTS

Flight experiments are needed to provide realistic results on reentry effects on antenna breakdown. Two types of experiments can be fruitful. Systems tests would be useful in testing the breakdown behavior of a given particular antenna system, and basic data experiments would be designed to show the importance of one or another of the six basic reentry phenomena. Recommendations for flight experiments are given in detail in Volume 2 of this report.

## SECTION 10

### CONCLUSION

The most important effect of slender cone vehicle reentry on signal transmission is the perturbation of the breakdown characteristics of the antenna. The breakdown phenomenon is important in terms of the severity, unpredictability, and uncontrollability of reentry effects. Not all of the six presently identifiable phenomena of the reentry environment are equally important, but the fact that there are so many factors contributing to the effects adds to their unpredictability and the lack of ability to control them. Linear plasma effects are controllable and relatively predictable on a slender cone vehicle, so that their importance is less than reentry antenna breakdown effects. Nonlinear effects are unimportant, because they are not very severe, although they are the least predictable.

Signal transmission systems for reentry vehicles can be designed to anticipate the reentry effects, to a certain extent. Slender cone vehicles which reenter the atmosphere at ICBM velocity can be designed to eliminate linear (and nonlinear) plasma effects under the proper design constraints. The designer must have the freedom to select the vehicle shape, materials, and antenna location. A good broadband antenna design should be used also. Of course the plasma effects cannot be alleviated by these means below the altitude of reentry to which the vehicle shape and materials survive, unless the vehicle velocity is sufficiently low when the shape or materials advantage is lost.

No such situation exists in the case of reentry effects on antenna breakdown. Here the alleviation of flow field plasma, as shown above, has some beneficial effect, but not enough is known about various other environmental influences on breakdown to permit their reliable alleviation, especially in the high altitude portion of reentry. More research in flow-field effects and antenna breakdown phenomenology is needed.

SECTION 11  
REFERENCES

1. Gruszczynski, J.S. and Warren, W.R., Jr.: "Study of Equilibrium Air Total Radiation," AIAA Paper No. 66-103, January 1966; also AIAA Journal Vol. 5, No. 3, pp. 517-525, March 1967.
2. Probst, R.F.: "Shock Wave and Flow Field Development in Hypersonic Re-Entry," ARS Journal Vol. 31, No. 2, pp. 185-194, February 1961.
3. Shapiro, A.H.: The Dynamics and Thermodynamics of Compressible Fluid Flow, Vol. I, pp. 532-534, The Ronald Press Co., New York, 1953.
4. Crocco, L.: "A Suggestion for the Numerical Solution of the Steady Navier-Stokes Equations," AIAA Paper No. 65-1, January 1965.
5. Scala, S.M. and Gordon, P.: "Solution of the Time-Dependent Navier-Stokes Equations for the Flow around a Circulation Cylinder," AIAA Paper No. 67-221, January 1967.
6. Scala, S.M. and Gordon, P.: "Solution of the Time-Dependent Navier-Stokes Equations for the Flow of Dissociating Gas Over a Circular Cylinder," General Electric Co., TIS R67SD56, May 1967.
7. Shapiro, A.H.: The Dynamics and Thermodynamics of Compressible Fluid Flow, Vol. II, pp. 653-663 and 676-684, The Ronald Press Co., New York, 1953.
8. Kopal, Z.: "Tables of Supersonic Flow Around Cones," Massachusetts Institute of Technology, TR No. 1, 1947.

9. Wang, C. J., Goebel, T. P. and Farnell, A. B.: "Conical Flow Tables," North American Aviation Inc., Rpt. No. NA-55-671, June 1955.
10. Dalley, C. L. and Wood, F. C.: Computation Curves for Compressible Fluid Problems, John Wiley and Sons, Inc., New York, 1949.
11. Ames Research Staff: "Equations, Tables and Charts for Compressible Flow," NACA Rpt. No. 1135, 1952.
12. Johnson, C.: "The Flow Field About a Right Circular Cone at Zero Yaw," General Electric Co., TIS 62SD211, November 1962.
13. Ferri, A.: "The Method of Characteristics," General Theory of High Speed Aerodynamics (W. R. Sears, ed.) Sect. 6, pp. 583-669, Princeton Univ. Press, Princeton, 1954.
14. Isenberg, J. S. and Lin, C. C.: "The Method of Characteristics in Compressible Flow," Part I Steady Supersonic Flow, Wright-Patterson Air Force Base Air Material Command, Rpt. No. F-TR-1173A-ND, December 1947.
15. Powers, S. A.: "Hypersonic Studies - Equilibrium Real Gas Flow Fields for Blunt Bodies," Northrop Corp., NB-62-14, January 1962.
16. Dresser, H. S.: "Method of Characteristics Program for Real Gas Equilibrium Flow," North American Aviation Inc. SID64-633, March 1964.
17. Edsall, R. H.: "A Modified Method of Characteristics for Calculating Inviscid Flow Fields," General Electric Co., FM-101, March 1963.

18. Gravalos, F.G., Brong, E. and Edelfelt, I.H.: "The Calculation of Flow Fields with Secondary Shocks for Real Gases at Chemical Equilibrium," General Electric Co., TIS R59SD419, May 1960.
19. Davis, R.S.: "Analysis and Programming of Supersonic Field with Shock Intersection," General Electric Co., TIS 62SD105, April 1962.
20. Ferri, A.: "The Method of Characteristics for the Determination of Supersonic Flow Over Bodies of Revolution at Small Angles of Attack," NACA Rpt. 1044, 1951.
21. Witham, G.B.: "Steady High Speed Flow Past an Axisymmetric Body at Incidence to the Stream," General Applied Sciences Laboratories Inc., Rpt. TR 41, November 1957.
22. Stone, A.H.: "On Supersonic Flow Past a Slightly Yawing Cone," Journal of Mathematics and Physics, Vol. XXVII, No. 1, pp. 67-81, April 1948.
23. Rakich, J.V.: "Numerical Calculation of Supersonic Flows of a Perfect Gas Over Bodies of Revolution at Small Angles of Yaw," NASA TN D-2390, July 1964.
24. Ferri, A.: "The Linearized Characteristics Method and Its Application to Practical Nonlinear Supersonic Problems," NACA Rpt. 1102, 1952.
25. Brong, E.A. and Edelfelt, I.H.: "The Flow Field about a Slightly Yawed Blunt Body of Revolution in a Supersonic Stream," General Electric Co., TIS R62SD111, March 1962.
26. Rakich, J.V.: "Calculation of Hypersonic Flow over Bodies of Revolution at Small Angles of Attack," AIAA Journal, Vol. 3, No. 3, pp. 458-464, March 1965.

27. Holt, M.: "The Method of Characteristics for Steady Supersonic Rotational Flow in Three-Dimensions," *Journal of Fluid Mechanics*, Vol. 1, pp. 409-423, 1956.
28. Coburn, N.: "Intrinsic Form of the Characteristic Relations in the Steady Supersonic Flow of a Compressible Fluid," *Quarterly of Applied Mathematics*, Vol. 15, pp. 237-248, 1957.
29. Moretti, G., Sanlorenzo, E.A., Magnus, D.E. and Weiberstein, G.: "Flow Field Analysis of Re-entry Configurations by a General Three-Dimensional Method of Characteristics," Air Force Systems Command, A.S. Div. TR-61-727, Vol. III, February 1962.
30. Pridmore-Brown, B.N. and Frank, W.J.: "A Method of Characteristics Solution in Three Independent Variables," *Aerospace Research Laboratories*, ARL 65-124, June 1965.
31. Chu, C.W.: "Compatibility Relations and a Generalized Finite-Difference Approximation for Three-Dimensional Steady Supersonic Flow," *AIAA Journal* Vol. 5, No. 3, pp. 493-501, March 1967.
32. Strom, C.R.: "The Method of Characteristics for Three-Dimensional Real Gas Flows," *Air Force Flight Dynamics Laboratory*, TR-67-47, July 1967.
33. Thommen, H.U., and D'Attorre, L.: "Calculation of Steady Three-Dimensional Supersonic Flow Fields by a Finite Difference Method," *AIAA Paper No. 65-26*, January 1965.
34. Van Dyke, M.D.: "The Supersonic Blunt Body Problem - Review and Extension," *Journal of Aerospace Sciences*, Vol. 25, No. 8, pp. 485-496, August 1958.
35. Hayes, W.D. and Probstein, R.F.: Hypersonic Flow Theory, pp. 210-252, Academic Press Inc., New York, 1959.

36. Swigart, R.J.: "The Direct Asymmetric Hypersonic Blunt Body Problem," AIAA Paper No. 66-411, June 1966.
37. Maslen, S.H. and Moeckel, W.E.: "Inviscid Hypersonic Flow Past Blunt Bodies," Journal of Aerospace Sciences, Volume 24, No. 9, pp. 683-693, September 1957.
38. Uchida, S. and Yasuhara, M.: "The Rotational Field Behind a Curved Shock Wave Calculated by the Method of Flux Analysis," Journal of Aeronautical Sciences, Vol. 23, No. 9, pp. 830-845, September 1956.
39. Mitchell, A.R.: "Application of Relaxation to the Rotational Field of Flow Behind a Bow Shock Wave," Quarterly Journal of Mechanics and Applied Mathematics, Vol. 4, pp. 371-383, 1951.
40. Lin, C.C. and Rubinov, S.I.: "On the Flow Behind Curved Shocks," Journal of Mathematics and Physics, Vol. 27, No. 2, pp. 105-129, July 1948.
41. Lin, C.C. and Shen, S.F.: "An Analytic Determination of the Flow Behind a Symmetrical Curved Shock in a Uniform Stream," NACA TN-2506, 1951.
42. Zlotnick, M. and Newman, D.J.: "Theoretical Calculation of the Flow on Blunt-Nosed Axisymmetric Bodies in a Hypersonic Stream," AVCO Manufacturing Co., Rpt. RAD-TR-2-57-29, September 1957.
43. Garabedian, P.R. and Lieberstein, H.M.: "On the Numerical Calculation of Detached Bow Shock Waves in Hypersonic Flow," Journal of Aeronautical Sciences, Vol. 25, No. 2, pp. 109-118, February 1958.

44. Vaglio-Laurin, R. and Ferri, A.: "Theoretical Investigation of the Flow Field about Blunt-Nosed Bodies in Supersonic Flight," *Journal of Aerospace Sciences*, Vol. 25, No. 12, pp. 761-770, December 1958.
45. Swigart, R.J.: "A Theory of Asymmetric Hypersonic Blunt-Body Flows," *AIAA Journal*, Vol. 1, No. 5, pp. 1034-1042, May 1963; also Stanford University, Rpt. No. 120, AFOSR-TN-62-2232, 1962; also preprint 62-98, 1962.
46. Vaglio-Laurin, R.: "On the PLK Method and the Supersonic Blunt Body Problem," *Journal of Aerospace Sciences*, Vol. 29, No. 2, pp. 185-206, February 1962.
47. Waldman, G.D.: "Integral Approach to the Yawed Blunt Body Problem," *AIAA Paper* No. 65-28, January 1965.
48. Bohachevsky, I.O. and Rubin, E.I.: "A Direct Method for Computation of Nonequilibrium Flows with Detached Shock Waves," *AIAA Journal*, Vol. 4, No. 4, pp. 600-607, April 1966; also *AIAA Paper* No. 65-24, January 1965.
49. Bohachevsky, I.O. and Mates, R.E.: "A Direct Method for Calculation of the Flow about an Axisymmetric Blunt Body at Angle of Attack," *AIAA Journal*, Vol. 4, No. 5, pp. 776-782, May 1966; also *AIAA Paper* No. 65-24, January 1965.
50. Yeh, H. and Doby, R.: "On Detached Shocks for Blunt Bodies at Small Angles of Attack," *ASME Paper* No. 65-APM-7, 1965.
51. Garabedian, P.R.: "Numerical Construction of Detached Shock Waves," *Journal of Mathematics and Physics*, Vol. 36, No. 3, pp. 192-205, 1957.
52. Van Dyke, M.D. and Gordon, H.D.: "Supersonic Flow Past a Family of Blunt Axisymmetric Bodies," *NASA TR R-1*, 1959.

53. Fuller, F.B.: "Numerical Solutions for Supersonic Flow of an Ideal Gas Around Blunt Two-Dimensional Bodies," NASA TND-791, July 1961.
54. Maslen, S.H.: "Inviscid Hypersonic Flow Past Smooth Symmetric Bodies," AIAA Journal, Vol. 2, No. 6, pp. 1055-1061, June 1964.
55. Cheng, H.K. and Gaitatzes, G.A.: "Use of the Shock-Layer Approximation in the Inverse Hypersonic Blunt Body Problem," AIAA Journal, Vol. 4, No. 3, pp. 406-413, March 1966.
56. Van Tuyl, A.H.: "Use of Rational Approximations in the Calculation of Flows Past Blunt Bodies," AIAA Journal, Vol. 5, No. 2, pp. 218-225, February 1967; also U.S. Naval Ordnance Laboratory, NOLTR 66-14, February 1966.
57. Kao, H.C.: "An Analytic Approach to the Method of Series Truncation for the Supersonic Blunt Body Problem," Journal of Fluid Mechanics, Vol. 27, pt. 4, pp. 789-813, 1967.
58. Lomax, H. and Inouye, M.: "Numerical Analysis of Flow Properties about Blunt Bodies Moving at Supersonic Speeds in an Equilibrium Gas," NASA TR R-204, July 1964.
59. Inouye, M., Rakich, J.V. and Lomax, H.: "A Description of Numerical Methods and Computer Programs for Two-Dimensional and Axisymmetric Supersonic Flow over Blunt Nosed and Flared Bodies," NASA TN D-2970, August 1965.
60. Dresser, H.S. and Anderson, R.B.: "Inverse Blunt Body Computer Program for Axisymmetric Body Shapes at Zero Angle of Attack," North American Aviation Inc., SID66-1541, October 1966.

61. Joss, W.W.: "Application of the Inverse Technique to Flow over a Blunt Body at Angle of Attack," Cornell Aeronautical Laboratories Inc., Rpt. No. AG-1729-A-6, December 1965.
62. Webb, H.G., Jr., Dresser, H.S., Adler, B.K. and Walter, S.A.: "An Inverse Solution for the Determination of Flow Fields about Axisymmetric Blunt Bodies at Large Angle of Attack," AIAA Paper No. 66-413, June 1966; also AIAA Journal, Vol. 5, No. 6, June 1967.
63. Traugott, S.C.: "An Approximate Solution of the Direct Supersonic Blunt Body Problem for Arbitrary Axisymmetric Shapes," Journal of Aerospace Sciences, Vol. 27, No. 5, pp. 361-370, May 1960.
64. Traugott, S.C.: "Some Features of Supersonic and Hypersonic Flow About Blunted Cones," Journal of Aerospace Sciences, Vol. 29, No. 4, pp. 395-399, April 1962.
65. Feldman, S.: "Numerical Comparison Between Exact and Approximate Theories of Hypersonic Inviscid Flow Past Slender Blunt Nosed Bodies," ARS Journal, Vol. 30, No. 5, pp. 463-468, May 1960.
66. Kuby, W., Foster, R.M., Byron, S.R. and Holt, M.: "Symmetrical Equilibrium Flow Past a Blunt Body at Superorbital Re-Entry Speeds," AIAA Journal, Vol. 5, No. 4, pp. 610-617, April 1967.
67. Vaglio-Laurin, R.: "Inviscid Supersonic Flow About General Three-Dimensional Blunt Bodies," Flight Dynamics Laboratory, TR ASD-TR-61-727, October 1962.
68. Leigh, D.C. and Rothrock, D.A.: "The Method of Integral Relations and Blunt Body Flows," General Electric Co., TIS 65SD227, April 1965.

69. Gravalos, F.G., Edelfelt, I.H. and Emmons, H.W.: "The Supersonic Flow About a Blunt Body of Revolution for Cases at Chemical Equilibrium," General Electric Co., TIS R58SD245, June 1958.
70. Waiter, S.A. and Anderson, R.B.: "Determination of the Transonic Flow Field Around a Blunt Body," North American Aviation Inc. SID64-634, February 1964.
71. Abbett, M. and Moretti, G.: "A Fast, Direct, and Accurate Technique for the Blunt Body Problem Part I - Analysis," General Applied Sciences Laboratory Inc., TR-583, January 1966; also AD-478119L.
72. Moretti, G. and Abbett, M.: "A Time-Dependent Computational Method for Blunt Body Flows," AIAA Journal, Vol. 4, No. 12, pp. 2136-2141, December 1966.
73. Moretti, G. and Bleich, G.: "Three-Dimensional Flow around Blunt Bodies," AIAA Journal, Vol. 5, No. 9, pp. 1557-1562, September 1967.
74. Webb, H.G., Jr. and Dresser, H.S.: "Unsteady Flow over Axisymmetric Blunt Bodies at Zero Angle of Attack," North American Rockwell Corp., SD67-881, September 1967.
75. Sauerwein, H.: "A General Numerical Method of Characteristics," AIAA Paper No. 65-25, January 1965.
76. Sauerwein, H.: "Numerical Calculations of Arbitrary Multidimensional and Unsteady Flows by the Method of Characteristics," Aerospace Rpt. TR-669 (S6815-71)-2, May 1966; also AD633 958; also AIAA Paper No. 66-412, June 1966.
77. Boericke, R.R. and Brong, E.A.: "A Method of Characteristics for Three-Dimensional Unsteady Flow Fields," General Electric Co., TIS 67SD362, November 1967.

78. Wood, W.W. and Kirkwood, J.G.: "Hydrodynamics of a Reacting and Relaxing Fluid," Journal of Applied Physics, Vol. 28, No. 4, pp. 395-398, April 1957.
79. Wood, W.W. and Kirkwood, J.G.: "Characteristic Equations for Reactive Flow," Journal of Chemical Physics, Vol. 27, No. 2, p. 596, August 1957.
80. Chu, B.T.: "Wave Propagation and the Method of Characteristics in Reacting Gas Mixtures with Applications to Hypersonic Flow," Wright Air Development Center, TN 57-213, May 1957; also AD 118 350.
81. Sedney, R.: "Some Aspects of Nonequilibrium Flows," Journal of Aerospace Sciences, Vol. 28, No. 3, pp. 189-196, March 1961.
82. Sedney, R., South, J.C. and Gerber, N.: "Characteristic Calculations of Nonequilibrium Flows," AGARD Monograph 68 (High Temperature Aspects of Hypersonic Flow), April 1962.
83. Sedney, R. and Gerber, N.: "Nonequilibrium Flow over a Cone," Ballistic Research Laboratories, Rpt. No. 1203, May 1963; also AIAA Journal, Vol. 1, No. 11, pp. 2482-2486, November 1963.
84. Sedney, R. and Gerber, N.: "Shock Curvature and Gradients at the Tip of Pointed Axisymmetric Bodies in Nonequilibrium Flow," Journal of Fluid Mechanics, Vol. 29, pt. 4, pp. 765-779, 1967; also Ballistic Research Laboratories, Rpt. No. 1350, December 1966.
85. Spurk, J.H., Gerber, N. and Sedney, R.: "Characteristic Calculation of Flow Fields with Chemical Reactions," AIAA Journal, Vol. 4, No. 1, pp. 30-37, January 1966.

86. Spurk, J.H., Knauss, D.T. and Bartos, J.M.: "Interferometric Measurement of Nonequilibrium Flow Fields around Cones and Comparison with Characteristics Calculations," AGARD Conference Proceedings No. 12 (Recent Advances in Aerothermochemistry), Vol. 2, 1967.
87. Gravalos, F.G.: "The Flow of a Chemically Reacting Gas Mixture," General Electric Co., TIS 63SD200, Vol. I and II, February 1963.
88. Gravalos, F.G.: "Analytical Foundations of Aerothermochemistry," General Electric Co., TIS 66SD259, September 1966.
89. Gravalos, F.G., Studerus, C.J. and Edelfelt, I.H.: "The Hypersonic Flow of a Chemically Reacting Gas Mixture about a Cone with an Expansion Corner," General Electric Co., TIS 67SD345, November 1967.
90. Wood, A.D., Springfield, J.F. and Pallone, A.J.: "Chemical and Vibrational Relaxation of an Inviscid Hypersonic Flow," AIAA Journal, Vol. 2, No. 10, pp. 1697-1705, October 1964; also AIAA Paper No. 63-441.
91. Kliegel, J.R., Peters, R.L. and Lee, J.T. Jr.: "Characteristics Solution for Nonequilibrium Flow Fields about Axisymmetric Bodies, Vol. 1 Analysis and Results," Thompson Ramo Wooldridge Inc., Rpt. No. 6453-6001-KU-000, July 1964.
92. South, J.C., Jr.: "Application of Dorodnitsyn's Integral Method to Nonequilibrium Flows Over Pointed Bodies," NASA TND-1942, 1963.
93. South, J.C., Jr.: "Applications of the Method of Integral Relations to Supersonic Nonequilibrium Flow Past Wedges and Cones," NASA TR R-205, 1964.

94. South, J.C. and Newman, P.A.: "Application of the Method of Integral Relations to Real-Gas Flows Past Pointed Bodies," AIAA Journal, Vol. 3, No. 9, pp. 1645-1652, September 1965.
95. Lick, W.: "Inviscid Flow Around a Blunt Body of a Reacting Mixture of Gases, Part A - General Analysis," Rensselaer Polytechnic Institute, TR AE 5810, May 1958; also AD 158 335.
96. Lick, W.: "Inviscid Flow Around Blunt Body of a Reacting Mixture of Gases, Part B - Numerical Solutions," Rensselaer Polytechnic Institute, TR AE 5814, December 1958; also AD 207 833.
97. Hall, J., Eschenroeder, A. and Marrone, P.: "Blunt Body Nose Inviscid Airflows with Coupled Nonequilibrium Processes," Journal of Aerospace Sciences, Vol. 29, No. 9, pp. 1038-1051, September 1962.
98. Gibson, W.E. and Marrone, P.V.: "A Similitude for Nonequilibrium Phenomena in Hypersonic Flight," Paper presented at AGARD Conference on High Temperature Aspects of Hypersonic Flow, Brussels, Belgium, April 1962.
99. Gibson, M.E. and Marrone, P.V.: "Nonequilibrium Scaling Criterion for Inviscid Hypersonic Airflows," Cornell Aeronautical Laboratories, Rpt. No. QM-1626-A-8, November 1967.
100. Gibson, W.E. and Marrone, P.V.: "Correspondence Between Normal Shock and Blunt Body Flows," Physics of Fluids, Vol. 5, No. 12, December 1962.
101. Wurster, W.K. and Marrone, P.V.: "Study of Infrared Emission in Heated Air," Cornell Aeronautical Laboratories, Rpt. No. QM-1373-A-2, June 1960.

102. Wurster, W.H. and Marrone, P.V.: "Study of Infrared Emission in Heated Air," Cornell Aeronautical Laboratories, Rpt. No. QM-1373-A-A, July 1961.
103. Treanor, C.E. and Marrone, P.V.: "Vibration and Dissociation Coupling Behind Strong Shock Waves," Paper presented at AFOSR-GE Symposium on Dynamics of Manned Lifting Planetary Entry, Philadelphia, Pa., October 1962.
104. Treanor, C.E. and Marrone, P.V.: "Effect of Dissociation on the Rate of Vibrational Relaxation," Physics of Fluids, Vol. 5, No. 9, September 1962.
105. Marrone, P.V. and Treanor, C.E.: "Chemical Relaxation with Preferential Dissociation from Excited Vibrational Levels," Cornell Aeronautical Laboratories, Rpt. No. QM-1626-A-10, February 1963.
106. Marrone, P.V.: "Inviscid Nonequilibrium Flow Behind Bow and Normal Shock Waves, Part I - General Analysis and Numerical Examples," Cornell Aeronautical Laboratories, Rpt. No. QM-1626-A-12 (I), May 1963.
107. Lee, R.H. and Chu, S.T.: "Nonequilibrium Inviscid Flow about Blunt Bodies," Aerospace Corp., Rpt. No. TDR-269 (4560-10)-2, January 1964.
108. Shih, W.C.L., Baron, J.R., Krupp, R.S. and Towle, W.J.: "Nonequilibrium Blunt Body Flow Using the Method of Integral Relations," Massachusetts Institute of Technology, TR-66, May 1966.
109. Shih, W.C.L. and Baron, J.R.: "Nonequilibrium Blunt Body Flow Using the Method of Integral Relations," AIAA Journal, Vol. 2, No. 6, pp. 1062-1071, June 1964.
110. Bloom, M.H. and Ting, L.: "On Near Equilibrium and Near Frozen Behavior of One-Dimensional Flow," Polytechnic Institute of Brooklyn, PIBAL R-525, July 1960.

111. Bloom, M.H. and Steiger, M.H.: "Inviscid Flow with Nonequilibrium Molecular Dissociation for Pressure Distributions Encountered in Hypersonic Flight," *Journal of Aerospace Sciences*, Vol. 27, No. 11, pp. 821-835, November 1960.
112. Vaglio-Laurin, R. and Bloom, M.H.: "Chemical Effects in External Hypersonic Flows," *Hypersonic Flow Research*, Vol. 7, pp. 205-254, Academic Press, New York, 1962.
113. Lin, S.C. and Teare, J.D.: "A Streamtube Approximation for Calculations of Reaction Rates in the Inviscid Flow Field of Hypersonic Objects," AVCO Corp. Res. Note 223, August 1961; also Proceedings of AF/Aerospace Corp. Symposium on Ballistic Missile and Aerospace Technology, 1961.
114. Eschenroeder, A.G.: "Ionization Nonequilibrium in Expanding Flows," *ARS Journal*, Vol. 32, No. 2, February 1962.
115. Eschenroeder, A.G., Boyer, D.W. and Hall, J.G.: "Nonequilibrium Expansions of Air with Coupled Chemical Reactions," Cornell Aeronautical Laboratories, Rpt. AF-1413-A-1, May 1961; also *Physics of Fluids Journal*, Vol. 5, No. 5, May 1962.
116. Hall, J.G., Eschenroeder, A.G. and Marrone, P.V.: "Inviscid Hypersonic Airflows with Coupled Nonequilibrium Processes," Cornell Aeronautical Laboratories, Rpt. AF-1413-A-2, May 1962; also IAS Paper No. 62-67, January 1962.
117. Lordi, J.A., Mates, R.E. and Moselle, J.R.: "Computer Program for the Numerical Solution of Nonequilibrium Expansions of Reacting Gas Mixtures," NASA CR-472, May 1966; Cornell Aeronautical Laboratories, Rpt. No. AD-1689-A-6, October 1965.

118. McMenamin, D. and O'Brien, M.: "The Finite Difference Solution of Multicomponent Nonequilibrium Steady Inviscid Streamtube Flows Using a Novel Stepping Technique, Part I - Analysis and Applications," General Electric Co., TIS 67SD241, April 1967.
119. Karydas, A.D.: "Computer Program for the Inviscid Flow Field about Bodies Traveling at Supersonic Speeds - Air in Chemical Equilibrium, Frozen Flow Chemistry and One-Dimensional Nonequilibrium Chemistry along Streamlines," Philco-Ford, SRS/NBO Rpt. METN 119, December 1967.
120. Chem, T. and Eschenroeder, A.G.: "A Fortran Computer Code for Inviscid Nonequilibrium Streamtube Flow," General Motors Corp., TR65-01P, December 1965; also AD 476-192.
121. Dresser, H.S., French, E.P. and Webb, H.G., Jr.: "Computer-Program for One-Dimensional Nonequilibrium Reacting Gas Flow," Air Force Flight Dynamics Laboratory, TR-67-75, June 1967.
122. Hayes, W.D. and Probstein, R.F.: Hypersonic Flow Theory, pp. 284-306, Academic Press Inc., New York. 1959.
123. Libby, P.A.: "The Homogeneous Boundary Layer at an Axisymmetric Stagnation Point with Large Rates of Injection," *Journal of Aerospace Sciences*, Vol. 29, No. 1, pp. 48-60, January 1962.
124. Weston, K.C.: "The Stagnation Point Boundary Layer with Suction and Injection in Equilibrium Dissociating Air," NASA TND-3889, March 1967.
125. Herring, T. K.: "The Boundary Layer Near the Stagnation Point in Hypersonic Flow Past a Sphere," *Journal of Fluid Mechanics*, Vol. 7, pp. 257-272, 1959.

126. Hoshizaki, H. and Smith, H. J.: "Axisymmetric Stagnation Point Mass - Transfer Cooling," Lockheed Aircraft Corp., LMSD-48379, December 1958.
127. Howe, J. T. and Mersman, W. A.: "Solutions to the Laminar Compressible Boundary Layer Equations with Transpiration which are Applicable to the Stagnation Regions of Axisymmetric Blunt Bodies," NASA TND-12, August 1959.
128. Strom, C. R.: "Heat and Mass Transfer at a Three-Dimensional Stagnation Point," General Electric Co., TIS 67SD363, December 1967.
129. Walter, S. A. and Anderson, R. B.: "Determination of the Aerodynamic Parameters in a Laminar Dissociated Boundary Layer," North American Aviation Inc., SID 64-636, February 1964.
130. Grabow, R. M.: "Boundary Layer Analysis of a Slightly Blunted Ablating Cone," Philco-Ford, SRS/NBO 4462-67-36, October 1967.
131. Brant, D. N. and Burke, A. F.: "Ablative Effects on the Turbulent Boundary Layer of Conical Bodies," Cornell Aeronautical Laboratories, Rpt. No. UB-1376-S-123, August 1965.
132. Beckwith, I. E.: "Similarity Solutions for Small Cross Flows in Laminar Compressible Boundary Layers," NASA TR R-107, 1961.
133. Beckwith, I. E. and Cohen, N. B.: "Application of Similar Solutions to Calculation of Laminar Heat Transfer on Bodies with Yaw and Large Pressure Gradient in High Speed Flow," NASA TND-625, January 1961.

134. Polak, A. and Li, T. Y.: "The Three-Dimensional Boundary Layer Flow Over a Flat Delta Wing at a Moderate Angle of Attack," AIAA Journal, Vol. 5, No. 2, pp. 233-240, February 1967.
135. Kang, S. W., Rae, W. J. and Dunn, M. G.: "Effects of Mass Injection on Compressible, Three Dimensional, Laminar Boundary Layers with Small Secondary Flow," Cornell Aeronautical Laboratories, Rpt. No. AI-2187-A-2, August 1966.
136. Kang, S. W., Rae, W. J. and Dunn, M. G.: "Effects of Mass Injection on Compressible, Three-Dimensional, Laminar Boundary Layers," AIAA Journal, Vol. 5, No. 10, pp. 1738-1745, October 1967.
137. Moran, J. P.: "Application of Coverts Approximations for the Binary Boundary Layer to a Porous Cone with a Solid Tip," Massachusetts Institute of Technology, NSL Rpt. 442, June 1960.
138. Carlson, W. O.: "Integral Solutions for Compressible Binary Gas Laminar Boundary Layers," General Electric Co. Aerophysics Laboratory, TM No. 90, July 1958.
139. Liw, S. W. and Kuby, G. H.: "Interaction of Surface Chemistry and Mass Transfer in Nonsimilar Boundary Layer Flows," AIAA Journal, Vol. 5, No. 2, pp. 527-534, March 1967.
140. Kang, S. W.: "An Integral Method for Three Dimensional Compressible Laminar Boundary Layers with Mass Injection," Cornell Aeronautical Laboratories, Rpt. No. AI-2187-A-5, May 1967.
141. Li, T. Y.: "Laminar Boundary Layer on the Frontal Portion of a Blunt Body of Revolution at Hypersonic Speeds," General Electric Co. Advanced Aerodynamics, TM No. 10, December 1956.

142. Parr, W.: "Laminar Boundary Layer Calculations by Finite Differences," U.S. Naval Ordnance Laboratory, NOLTR 63-261, March 1964.
143. Krause, E.: "On the Numerical Solution of the Boundary Layer Equations," New York University, Rpt. NYU-AA-66-57, June 1966; also AD 637-851 and AIAA Journal, Vol. 5, No. 7, pp. 1231-1237, July 1967.
144. Krause, E.: "On Investigation of the Vorticity Interaction by Perturbation Techniques," New York University, Rpt. NYU-AA-66-64, October 1966; also AD 644 026.
145. Walter, S.A. and Anderson, R.B.: "Solution of the Laminar Boundary Layer Equations by an Implicit Finite Difference Method," North American Rockwell Corp., SD 67-587, November 1967.
146. Flugge-Lotz, I. and Blottner, F.G.: "Computation of the Compressible Laminar Boundary Layer Flow Including Displacement Thickness Interaction Using Finite Difference Methods," Stanford University, Rpt. No. 131, 1962.
147. Fannelop, T.K.: "A Method of Solving the Three-Dimensional Laminar Boundary Layer Equations with Application to a Lifting Re-entry Body," AVCO Corp., AVMSD-0209-66-PM, August 1966; also AD 637 679.
148. Raetz, G.S.: "A Method of Calculating Three-Dimensional Laminar Boundary Layers of Steady Compressible Flows," Northrop Aircraft Inc., Rpt. No. NAI-58-73-BLC-114, December 1957.
149. Der, J., Jr. and Raetz, G.S.: "Solution of General Three-Dimensional Laminar Boundary Layer Problems by an Exact Numerical Method," IAS Paper No. 62-70, January 1962.

150. Crocco, L.: "Transformations of the Compressible Turbulent Boundary Layer with Heat Exchange," AIAA Journal, Vol. 1, No. 12, pp. 2723-2731, December 1963.
151. Denison, M.R.: "The Turbulent Boundary Layer on Chemically Active Ablating Surface," Journal of Aerospace Sciences, Vol. 28, No. 6, pp. 471-479, June 1961.
152. Van Dyke, M.: "Second-Order Compressible Boundary Layer Theory with Application to Blunt Bodies in Hypersonic Flow," Hypersonic Flow Research, Academic Press Inc., New York, pp. 37-76, 1962; also Stanford University, Rpt. AFOSR-TN-61-1270, July 1961.
153. Van Dyke, M.: "Higher Approximations in Boundary Layer Theory, Part I," Journal of Fluid Mechanics, Vol. 14, pp. 161-177, 1962.
154. Van Dyke, M.: "A Review and Extension of Second-Order Hypersonic Boundary Layer Theory," Rarefied Gas Dynamics Vol. II, Supplement 2, Academic Press Inc., New York, pp. 212-227, 1963.
155. Lewis, C.H.: "First and Second Order Boundary Layer Effects at Hypersonic Conditions," Presented at the AGARD Seminar on Numerical Methods for Viscous Flows, September 1967.
156. Marchand, E.O., Lewis, C.H., and Davis, R.T.: "Second-Order Boundary Layer Effects on a Slender Blunt Cone at Hypersonic Conditions," AIAA Paper No. 68-54, January 1968.
157. Adams, J.C., Jr.: "Higher Order Boundary Layer Effects on Analytical Bodies of Revolution," Presented at the AGARD Seminar on Numerical Methods for Viscous Flows, September 1967.

158. Davis, R.T. and Flugg-Lotz, I.: "Laminar Compressible Flow Past Axisymmetric Blunt Bodies (Results of Second-Order Theory)," Stanford University, TR-143, 1963.
159. Smith, A.M.O. and Clutter, D.W.: "Solution of Prandtl's Boundary Layer Equations," Douglas Aircraft Co., Paper 1530, February 1963.
160. Clutter, D.W. and Smith, A.M.O.: "Solution of the General Boundary Layer Equations for Compressible Laminar Flow, Including Transverse Curvature," Douglas Aircraft Co., Rpt. LB31088, February 1963.
161. Smith, A.M.O. and Clutter, D.W.: "Machine Calculation of Compressible Laminar Boundary Layers," AIAA Journal, Vol. 3, No. 4, pp. 639-647, April 1965.
162. Jaffe, N.A., Lind, R.C. and Smith, A.M.O.: "Solution to the Binary Diffusion Laminar Boundary Layer Equations with Second-Order Transverse Curvature," AIAA Journal, Vol. 5, No. 9, pp. 1563-1569, September 1967.
1663. Lewis, C.H. and Whitfield, J.D.: "Theoretical and Experimental Studies of Hypersonic Viscous Effects," AFARD Monograph 97 (Recent Developments in Boundary Layer Research) Part III, May 1965; also AEDC-TR-65-100, May 1965.
164. Mayne, A.W., Jr., Gilley, G.E. and Lewis, C.H.: "Binary Boundary Layers on Sharp Cones in Low Density Supersonic and Hypersonic Flow," AIAA Paper No. 68-66, January 1968.
165. Levine, J.N.: "Finite Difference Solution of the Laminar Boundary Layer Equations Including the Effects of Transverse Curvature, Vorticity and Displacement Thickness," General Electric Co., TIS 66SD349, December 1966.

166. Maslen, S.H.: "Second-Order Effects in Laminar Boundary Layers," AIAA Journal Vol. 1, No. 1, pp. 33-40, January 1963.
167. Yasuhara, M.: "Axisymmetric Viscous Flow Past Very Slender Bodies of Revolution," Journal of Aerospace Sciences, Vol. 29, No. 6, pp. 667-679, June 1962.
168. Probst, R.F. and Elliot, D.: "Transverse Curvature Effects in Compressible Axisymmetric Laminar Boundary Layer Flow," Journal of Aeronautical Sciences, Vol. 23, No. 3, pp. 208-224, March 1956.
169. Sagendorph, F.E.: "Hypersonic Flow Over a Slender Axisymmetric Body with Mass Addition," General Electric Co., ATFM 65-9, July 1965.
170. Dorrance, W.H.: Viscous Hypersonic Flow, pp. 22-38, McGraw-Hill Book Co., Inc., New York, 1962.
171. Fay, J.A. and Riddell, F.R.: "Theory of Stagnation Point Heat Transfer in Dissociated Air," Journal of Aerospace Sciences, Vol. 25, No. 2, pp. 73-85, February 1958.
172. Fay, J.A. and Kaye, H.: "A Finite-Difference Solution of Similar Nonequilibrium Boundary Layers," AIAA Journal, Vol. 5, No. 11, pp. 1949-1954, November 1967; also AIAA Paper No. 67-219.
173. Moore, J.A. and Pallone, A.: "Similar Solutions to the Laminar Boundary Layer Equations for Nonequilibrium Air," AVCO Corp., Rpt. No. RAD-TR-62-59, July 1962.
174. Libby, P.A. and Pierucci, M.: "Laminar Boundary Layer with Hydrogen Injection Including Multicomponent Diffusion," AIAA Journal, Vol. 2, No. 12, pp. 2118-2126, December 1964.

175. Libby, P.A. and Liu, T.: "Laminar Boundary Layers with Surface Catalyzed Reactions," *Physics of Fluids*, Vol. 9, No. 3, pp. 436-445, March 1966.
176. Lenard, M.: "Chemically Reacting Boundary Layers," General Electric Co., Space Sciences Lab., TIS R64SD14, March 1964.
177. Lenard, M.: "Ionization of Cesium and Sodium Contaminated Air in the Hypersonic Slender Body Boundary Layer," General Electric Co., Space Sciences Lab., TIS R64SD22, August 1964.
178. Pallone, A.J., Moore, J.A. and Erdos, J.I.: "Nonequilibrium, Nonsimilar Solutions of the Laminar Boundary Layer Equations," *AIAA Journal*, Vol. 2, No. 10, pp. 1706-1713, October 1964; also AIAA Paper No. 64-50, January 1964.
179. Smith, A.M.O. and Jaffe, N.A.: "General Method for Solving the Nonequilibrium Boundary Layer Equations of a Dissociating Gas," *AIAA Journal*, Vol. 4, No. 4, pp. 611-620, April 1966; also AIAA Paper No. 65-129.
180. Blottner, F.G.: "Nonequilibrium Laminar Boundary Layer Flow of a Binary Gas," General Electric Co., Space Sciences Lab., TIS R63SD17, June 1963; also *AIAA Journal*, Vol. 2, No. 2, pp. 232-240, February 1964.
181. Blottner, F.G.: "Nonequilibrium Laminar Boundary Layer Flow of Ionized Air," General Electric Co., Space Sciences Lab., TIS R64SD56, November 1964; also AIAA Paper No. 64-41.
182. Blottner, F.G.: "Chemically Reacting Boundary Layers with Ablation Products and Nose Bluntness Effects," General Electric Co., TIS 67SD468, June 1967 (Confidential); also AD 382-026.

183. Lew, H.G.: "The Ionized Flow Field Over Re-Entry Bodies," General Electric Co., Space Sciences Lab., TIS R67SD70, December 1967.
184. Moore, J.A. and Lee, J.T.: "Discontinuous Injection of Inert Gases into the Nonequilibrium Laminar Boundary Layer," TRW, Rp. 06388-6018-R000.
185. Fox, H.: "Laminar Boundary Layers with Chemical Reactions"; also AIAA Paper No. 65-130.
186. Hayday, A.A.: "A Generalized Asymptotic Method for the Solution of Reacting Laminar Boundary Layer Flows," U.S. Army Missile Command, Redstone Arsenal, Rpt. No. RN-TR-66-2, January 1966; also AD 630-270.
187. Lee, R.H., Levinsky, E.S.: "Binary Scaling of the Nonequilibrium Boundary Layer Over Slender Bodies," Proceedings of the 1964 Heat Transfer and Fluid Mechanics Institute, Stanford University Press, pp. 115-129, 1964.
188. Levinsky, E.S.: "Approximate Nonequilibrium Air Ionization in Hypersonic Flows Over Sharp Cones," BSD TDR 63-231, Rpt. No. TDR-269 (S4810-60)-1.
189. Lee, R.H.C., Baker, R.: "Air Ionization for Slender Cones at Small Angles of Attack," expected publication date, 24 January 1968, AIAA Fluid and Plasma Dynamics Conference, Los Angeles, California.
190. Hayes, W.D. and Probstein, R.F.: Hypersonic Flow Theory, pp. 385-395, Academic Press, New York, 1959.
191. Chen, S.Y., Aroesty, J., Mobley, R.: "The Hypersonic Viscous Shock Layer with Mass Transfer," Rand Corp., Memorandum RM-4631-PR, May 1966.

192. Goldberg, L.: "The Structure of the Viscous Hypersonic Shock Layer."
193. Goldberg, L., Scala, S.M.: "Mass Transfer in the Low Reynolds Number Viscous Layer Around the Forward Region at a Hypersonic Vehicle," General Electric Co., TIS R65SD27.
194. Kao, H.C.: "Hypersonic Viscous Flow Near the Stagnation Streamline of a Blunt Body: II. Third-Order Boundary Layer Theory and Comparison with Other Methods," AIAA Journal, Vol. 2, No. 11, pp. 1898-1906, November 1964.
195. Probstein, R.F. and Kemp, N.H.: "Viscous Aerodynamic Characteristics in Hypersonic Rarefied Gas Flow," Journal of Aerospace Sciences, Vol. 27, No. 3, pp. 174-192, March 1960.
196. Lenard, M.: "Stagnation Point Flow of a Variable Property Fluid at Low Reynolds Numbers," Ph.D. Thesis Cornell University Graduate School of Aeronautical Engineering, 1961.
197. Wei, M.H.: "Asymptotic Boundary Layer over a Slender Body of Revolution in Axial Compressible Flow," AIAA Journal, Vol. 3, No. 5, pp. 809-816, May 1965.
198. Waldron, H.F.: "Viscous Hypersonic Flow Over Pointed Cores at Low Reynolds Numbers," AIAA Journal, Vol. 5, No. 2, pp. 208-218, February 1967.
199. Cheng, H.K.: "The Blunt Body Problem in Hypersonic Flow at Low Reynolds Number," CAL Rpt. No. AF 1285-A-10, IAS Paper 63-92.
200. Shih, W.C.L. and Krupp, R.S.: "Viscous Nonequilibrium Blunt Body Flow," AIAA Journal, Vol. 5, No. 1, pp. 17-25, January 1967.

201. Chung, P. M.: "Hypersonic Viscous Shock Layer of Nonequilibrium Dissociating Gas," NASA Tech. Rpt. R-109, 1961.
202. Chung, P. M., Holt, J. F., Liu, S. W.: "Merged Stagnation Shock Layer at Nonequilibrium Dissociating Gas," Aerospace TR-0158 (3240-10)-8, 1967.
203. Lee, R. H. C., Zierden, T. A.: "Merged Layer Ionization in the Stagnation Region of a Blunt Body," Proceedings of the 1967 Heat Transfer and Fluid Mechanics Institute, pp. 452-468, June 1967.
204. Lin, S. C., Neal R. A. and Fyfe, W. I.: "Rate of Ionization Behind Shock Waves in Air. I Experimental Results," AVCO/Everett Research, Rpt. 105, September 1960.
205. Kaegi, E. M. and Chin, R.: "Stagnation Region Shock Layer Ionization Measurements in Hypersonic Air Flows," AIAA Paper No. 66-167, January 1966.
206. Gravalos, F. G. and Studerus, C. J.: "Inviscid Nonequilibrium Flow Along a Surface of a  $45^\circ$  Cone," General Electric Co., RSD PIR 8152-2127, December 1966.
207. Landau, L. and Teller, E., Physik, Z.: Sowjetunion, Vol. 10, p. 34, 1936.
208. Millekan, R. C. and White, D. R.: "The Systematics of Vibrational Relaxation," General Electric Co. Research Laboratory, Rpt. No. 63-RL- (3411C), August 1963.
209. Burke, A. F., Curtis, J. T. and Boyer, D. W.: "Nonequilibrium Flow Considerations in Hypervelocity Wind Tunnel Testing," Cornell Aeronautical Laboratories, Rpt. No. AA-1632-Y-1, May 1962.
210. Storer, E. M.: "A Simple Method for Calculating the Stagnation Point Shock Detachment of Spherical Bodies in Supersonic Flow," General Electric Co., RSD ATCFM 64-2, May 1964.

211. King, R.W.P.: Theory of Linear Antennas, Harvard University Press, 1956.
212. Hallen, E.: "Theoretical Investigations into the Transmitting and Receiving Qualities of Antennas," *Nova Acta Regiae Soc. Upsalienis*, Sec. IV, Vol. II, p. 1, 1938.
213. Harrington, R.F.: Field Computation by Moment Methods, Macmillan, New York, 1968.
214. Herlin, M.A., and Brown, S.C.: "Electrical Breakdown of a Gas between Coaxial Cylinders at Microwave Frequencies," *Phys. Rev.*, Vol. 74, No. 8, pp. 910-913, October 1948.
215. Herlin, M.A. and Brown, S.C.: "Microwave Breakdown of a Gas in a Cylindrical Cavity of Arbitrary Length," *Phys. Rev.*, Vol. 74, No. 11, pp. 1650-1656, December 1948.
216. MacDonald, A.D., and Brown, S.C.: "Electron Diffusion in a Spherical Cavity," *Can. J. Res.*, Vol. A28, pp. 168-174, 1950.
217. Chatterjee, J.S.: "Radiation Field of a Conical Helix," *J. Appl. Phys.*, Vol. 24, p. 550, May 1953.
218. Mittra, R. and Klock, P.W.: "A Theoretical Study of the Conical Spiral Antenna," *Antenna Lab., University of Illinois*, AD No. 483194.
219. Dyson, J.D.: "The Characteristics and Design of the Conical Log-Spiral Antenna," *IEEE Trans. Ant. and Prop.*, Vol. AP-13, p. 488, July 1965.

220. Dyson, J.D.: "The Unidirectional Equiangular Spiral Antenna," IEEE Trans. Ant. and Prop., Vol. AP-9, p. 329, October 1959.
221. Cullen, A. L. and Dobson, J.: "The Corona Breakdown of Aerials in Air at Low Pressured," Proc. Royal Society of London, Vol. A271, No. 1347, pp. 551-564, February 1963.
222. Shkarofsky, I. P., Johnston, T.W., and Bachynski, M.P.: The Particle Kinetics of Plasmas, Addison-Wesley, Reading, Mass., 1966.
223. Poeverlein, H.: "Low-Frequency Reflection in the Ionosphere," J. Atmos. Terr. Phys., Vol. 12, pp. 126-139, 1958.
224. Banos, A. et al: "The Radiation Field of an Electric Dipole Antenna in a Conical Sheath," J. Math. and Phys., Vol. 70, p. 189, 1965.
225. Jordan, A. K. and Pinski, G.: "The Effects of Electron Collision on Electric Dipole Radiation Through a Conical Plasma Sheath," IEEE Trans. Ant. and Prop., Vol. AP-16, No. 1, pp. 118-123, January 1968.
226. Smith, T. M. and Golden, K. E.: "Radiation Patterns from a Slotted Cylinder Surrounded by a Plasma Sheath," IEEE Trans. Ant. and Prop., Vol. AP-13, p. 775, 1965.
227. Swift, C. T.: "Radiation from Slotted Cylinder Antennas in a Reentry Plasma Environment," NASA TN D-2187, 1964.
228. Rusch, W. V. T.: "Radiation from a Plasma Clad Axially-Slotted Cylinder," USCEC, Report 82-201 (AFCRL 714), Univ. of Southern California, May 1962.

229. Villeneuve, A. T.: "Admittance of Waveguide Radiating into Plasma Environment," IEEE Trans. Ant. and Prop., AP-13, No. 1, January 1965.
230. Croswell, W. F., Rudduck, R. C., Hatcher, D. M.: "The Admittance of a Rectangular Waveguide Radiating into a Dielectric Slab," IEEE Trans. Ant. and Prop., AP-15, No. 5, September 1967.
231. Croswell, W. F., Taylor, W. C., Swift, C. T.: "The Input Admittance of a Rectangular Waveguide Fed Aperture Under an Inhomogeneous Plasma: Theory and Experiment," to be published.
232. Galejs, J.: "Admittance of a Waveguide Radiating into Stratified Plasma," IEEE Trans. Ant. and Prop., AP-13, No. 1, January 1965.
233. Galejs, J., and Mentzoni, M. H.: "Waveguide Admittance for Radiation into Plasma Layers," IEEE Trans. Ant. and Prop., AP-15, No. 3, May 1967.
234. Musal, H. M., Jr.: "Electron Collision Frequency in Equilibrium High Temperature Air," Bendix Aviation Corp., Research Note 9, May 1960.
235. MacDonald, A. D.: Microwave Breakdown in Gases, John Wiley and Sons, Inc., New York, 1966.
236. Chapman, S. and Cowling, T. G.: The Mathematical Theory of Non-Uniform Gases, Cambridge University Press, Cambridge, 1960.
237. Kihara, T.: "The Mathematical Theory of Electrical Discharges in Gases," Rev. Mod. Phys., Vol. 24, No. 1, January 1952.

238. MacDonald, A.D. and Brown, S.C.: Phys. Rev., Vol. 75, p. 411, 1949.
239. MacDonald, A.D. and Brown, S.C.: Phys. Rev., Vol. 76, p. 1634, 1949.
240. Reder, F.H. and Brown, S.C.: Phys. Rev., Vol. 95, p. 885, 1954.
241. Lenander, C.J., and Epstein, M.: "Kinetic Theory Calculations of Data for High Frequency Breakdown of Air," Bull. Amer. Phys. Soc., Series II, Vol. 13, No. 2, p. 202, February 1968 (Paper delivered at 20th Gaseous Electronics Conference).
242. Carleton, N.P., and Megill, L.R.: "Electron Energy Distribution in Slightly Ionized Air under the Influence of Electric and Magnetic Fields," Phys. Rev., Vol. 126, No. 6, pp. 2089-2099, June 1962.
243. Herlin, M.A. and Brown, S.C.: Phys. Rev., Vol. 74, p. 291, 1948.
244. Brown, S.C.: Basic Data of Plasma Physics, MIT Press, Cambridge, Mass., 1966.
245. Rose, D.J. and Brown, S.C.: J. Appl. Phys., Vol. 28, p. 561, 1957.
246. Gould, L.J. and Roberts, L.W.: J. Appl. Phys., Vol. 27, p. 1162, 1956.
247. Harrison, M.A. and Geballe, R.: Phys. Rev., Vol. 91, p. 1, 1953.
248. MacDonald, A.D., Gaskell, D.U. and Gitterman, H.N.: Phys. Rev., Vol. 130, p. 1841, 1963.
249. Brown, S.C., and MacDonald, A.D.: "Limits for the Diffusion Theory of High Frequency Gas Discharge Breakdown," Phys. Rev., Vol. 76, pp. 1629-1633, December 1949.

250. Reilly, J. P.: Microwave Breakdown of the Air Around a Conical Re-Entry Vehicle, Avco Research Report 214, BSDTR65157, April 1965.
251. Whitmer, R. F. and MacDonald, A. D.: "RF Antenna Breakdown Conditions in the Presence of the Plasma Sheath," Proceedings of the First Plasma Sheath Symposium, W. Rotman and G. Meltz, ed., Pergamon Press, 1961.
252. Light, G. C. and Taylor, E. C.: "Antenna Breakdown in High Temperature Air," Aerospace Report No. TR1001 (2220-10), SSDTR67118, June 1967.
253. Bisbing, P. E.: "Analysis of an Antenna Breakdown Experiment in a Re-Entry Environment (U)," AMRAC Proceedings, Vol. XIII, November 1965.
254. Nanevicz, J. E., Chown, J. B., Vance, E. F. and Martin, J. A.: "SRI Participation in Voltage Breakdown and Rocket Charging Experiments on Nike Cajun Rocket," AFCRL66-588, August 1966.
255. Allis, W. P. and Rose, D. J.: "The Transition from Free to Ambipolar Diffusion," Phys. Rev., Vol. 93, No. 1, January 1954.
256. Allis, W. P.: "Motions of Ions and Electrons," Handbuch der Physik, Vol. XXI, Springer Verlag, Berlin, 1956.
257. Kelly, D. and Margenau, H.: "High Frequency Breakdown of Air," Journal of Appl. Phys., Vol. 31, No. 9, pp. 1617-1620, September 1960.
258. Epstein, M.: "Antenna Breakdown in a Hypersonic Re-Entry Environment," ASTIA No. AD 473936, September 1960.

259. Bowker, H. C., "Variation of Spark-Potential with Temperature in Gases," Proc. Phys. Soc. of London, Vol. 43, pp. 96-111, 1931.
260. Alston, L. L.: "High Temperature Effects on Flashover in Air," Proc. IEE, Vol. 105, pt. A, No. 24, pp. 549-533, December 1958.
261. Sharbaugh, A. H., Watson, P. K., White, D. R., Lee, T. H. and Greenwood, A.: "An Investigation of the Breakdown Strength of Nitrogen at High Temperatures with Use of a Shock Tube," Trans. AIEE (Power Apparatus and Systems), Vol. 80, pp. 333-344, June 1961.
262. Crowe, R. W., Bragg, J. K. and Thomas, V. B.: "Space-Charge Formation and the Townsend Mechanism of Spark Breakdown in Gases," Phys. Rev., Vol. 96, p. 10, 1954.
263. Lee, T. H., Greenwood, A. N. and White, D. R.: "Electrical Breakdown of High-Temperature Gases and Its Implications in Post-Arc Phenomena in Circuit Breakers," IEEE Trans. on Power Apparatus and Systems, Vol. PAS-84, No. 12, pp. 1116-1125, December 1965.
264. Taylor, W. C., Chown, J. B. and Morita, T.: "Measurements of RF Ionization Rates in High Temperature Air," AFCRL-67-028, Stanford Research Institute, March 1967.
265. Thompson, W. P., Epstein, M. and Lenander, C. J.: "Microwave Breakdown of the Re-Entry Boundary Layer," Aerospace Corp., Report No. TR-1001 (2240-20)-11, May 1967.
266. Scharfman, W. and Morita, T.: "Focused Microwave Technique for Measurement of the Ionization Rate and Collision Frequency," J. Applied Phys., Vol. 35, No. 7, pp. 2016-2020, July 1964.

267. Hochstim, A.R.: "ECM Antenna Breakdown During Reentry (U)," Pen-X Paper 32, IDA/HQ66-4458, January 1966.
268. Epstein, M.: "High Frequency Breakdown in Nonuniform Fields," Bull. Amer. Phys. Soc., Series II, Vol. 13, No. 2, p. 202, February 1968, (Paper delivered at 20th Gaseous Electronics Conference).
269. Cottingham, W.B. and Buchsbaum, S.J.: "Electron Ionization Frequency in Hydrogen," Phys. Rev., Vol. 130, No. 3, 1002-1006, May 1963.
270. Romig, M.F.: "Steady State Solutions of the Radiofrequency Discharge with Flow," Phys. of Fluids, Vol. 3, No. 1, p. 129, January 1960.
271. Fante, R.L.: "Mathematical Analysis of Microwave Breakdown in Flowing Gases," IEEE Trans. on Antennas and Propagation, pp. 781-788, September 1965.
272. Cottingham, W.B., to be published under AFCRL sponsorship.
273. MacDonald, A.D.: "High-Frequency Breakdown in Air at High Altitudes," Proc. IRE, pp. 436-441, March 1959.
274. Papa, R.J.: "Nonlinear Electromagnetic Wave Propagation in Plasmas," AFCRL-66-347, May 1966.
275. Margenau, H.: Phys. Rev., Vol. 69, p. 508, 1946.
276. Molmud, P.: Phys. Rev., Vol. 114, p. 29, 1959.
277. Shkarofsky, I.P.: Can. J. Phys., Vol. 39, p. 1619, 1961.

278. Whitmer, R. F. and Herrmann, G. F.: Phys. Fluids, Vol. 9, p. 768, 1966.
279. Bakshi, P. M., Haskell, R. E. and Papa, R. J.: "Electrical Conductivity of Magnetoplasmas, Part I - General Theory of Effective Parameters," AFCRL-67-0527, September 1967.
280. Haskell, R. E., Papa, R. J. and Bakshi, P. M.: "Electrical Conductivity of Magnetoplasmas, Part II - Effective Parameters for Non-Maxwellian Distributions," AFCRL-67-0528, September 1967.
281. Chown, J. B., Taylor, W. C., Vance, E. F., Nanevich, J. E. and Morita, T., "Effects of Re-Entry and Space Environments on Antenna Breakdown," Proc. Third Symposium on the Plasma Sheath, AFCRL-67-0280, Vol. II, May 1967.
282. Taylor, W. C., Chown, J. B. and Morita, T.: "Effects of Reentry Vehicle Environment on Antenna Performance," Proc. Conf. on Plasma Studies (AFAL/OSU), October 1967.
283. Mott, H.: Proc. IEEE, Vol. 52, p. 1752, 1964.
284. Fante, R. L. and Mullin, C. R.: Proc. IEEE, Vol. XXX, p. 484, 1965.
285. "Lifting Re-entry Communications, Vol. I," Aerospace Report TR-669(6220-10)-3; Vol. 1, Air Force Report SSD-TR-66-73; Vol. 1, Aerospace Corporation, Re-entry and Plasma-Electromagnetics Department, May 1966.
286. Aisenberg, S.: "The Use of Chemical Additives for the Alleviation of the Plasma Sheath Problem," Proc. Conf. on Plasma Studies (AFAL/OSU), October 1967.

287. Covert, E.E. and Boedecker, L.R.: "Studies of Antenna Breakdown in the Presence of a Plasma Sheath Including the Effects of Forced Convection," MIT Aerophysics Lab Report 135, ARCRL 670190, February 1967.
288. Scharfman, W.E. and Morita, T.: "Voltage Breakdown of Antennas at High Altitude," Proc. IRE, pp. 1881-1887, November 1960.
289. Scharfman, W.E. and Morita, T.: "Power Handling Capability of Antennas at High Altitude," Planetary and Space Sciences, Vol. 6, p. 142, 1961.
290. Rothman, H., and Morita, T. (Stanford Research Institute): "Transmission Through an Ionized Medium in the Presence of a Strong Magnetic Field," Air Force Cambridge Research Laboratories, Technical Report 74, May 1961.
291. Samaddar, S.N.: "An Approach to Improve Re-entry Communications by Suitable Orientations of Antenna and Static Magnetic Field," Radio Science Journal of Research, Vol. 69D, No. 6, pp. 851-863, June 1965.
292. Samaddar, S.N.: "Principle of Blackout Communications," AIAA Journal, Vol. 3, No. 2, pp. 349-351.
293. Lax, B., Allis, W.P. and Brown, S.C.: J. Appl. Phys., Vol. 21, p. 1297-1950.

## DOCUMENT CONTROL DATA - R&amp;D

(Security classification of title, body of abstract and indexing annotation must be entered when the overall report is classified)

## 1. ORIGINATING ACTIVITY (Corporate author)

General Electric Company

Re-Entry Systems Dept. Missile &amp; Space Division

Box 8555, Philadelphia, Pennsylvania 19101

## 20. REPORT SECURITY CLASSIFICATION

Unclassified

## 21. GROUP

## 3. REPORT TITLE

STUDY TO OBTAIN DESIGN DATA FOR REENTRY ECM ANTENNA SYSTEMS

## 4. DESCRIPTIVE NOTES (Type of report and inclusive dates)

Scientific Final

## 5. AUTHOR(S) (First name, middle initial, last name)

Paul E. Bisbing, Paul M. Scherer

Daniel L. McMenamin

Arthur K. Jordan

## 6. REPORT DATE

March 1968

## 7A. TOTAL NO. OF PAGES

260

## 7B. NO. OF REFS

293

## 8. CONTRACT OR GRANT NO.

F 19(628)-67-C-0210

ARPA Order

## 9A. ORIGINATOR'S REPORT NUMBER(S)

GE Report No. 68SD591

## 9. PROJECT, TASK, WORK UNIT NOS.

8671-00-01

No. 693

Final Report

## C. DOD ELEMENT

6250301R

## 9B. OTHER REPORT NO(S) (Any other numbers that may be assigned this report)

AFCRL - 68 - 0226

## D. DOD SUBELEMENT

None

## 10. DISTRIBUTION STATEMENT

This document is subject to special export controls and each transmittal to foreign governments or foreign nationals may be made only with prior approval of AFCRL (CRDM),

L. G. Hanscom Field, Bedford, Massachusetts 01730

## 11. SUPPLEMENTARY NOTES

This research was sponsored by the Advanced Research Projects Agency.

## 12. SPONSORING MILITARY ACTIVITY

Air Force Cambridge Research Laboratories (CDR)  
L. G. Hanscom Field  
Bedford, Massachusetts 01730

## 13. ABSTRACT

This is the first volume of the final report in a study of reentry effects on signal transmission from slender cone bodies at ICBM velocities. The report gives results of state of knowledge surveys of fluid mechanics methods and electromagnetic phenomena. Results of illustrative calculations are also given in many of these areas. Antenna breakdown is found to be the most important problem in reentry transmission effects, as well as the least well understood. Recommendations for needed research are given, including high gas temperature and convection experiments and theoretical analyses of temperature, convection, and flow field gradients effects. High altitude flow field development and studies of thermal nonequilibrium effects are recommended also.

Unclassified

Security Classification

14.	KEY WORDS	LINK A		LINK B		LINK C	
		ROLE	WT	HOLE	WT	ROLE	WT
	Reentry Antenna Breakdown State of the Art Bibliography Analytical Techniques Flow Fields						

Unclassified

Security Classification